DESIGN AND SYNTHESIS OF POROUS CRYSTALLINE COVALENT ORGANIC FRAMEWORKS WITH EXCEPTIONAL CHEMICAL STABILITY

Thesis Submitted to AcSIR

For the Award of the Degree of

DOCTOR OF PHILOSOPHY

In

CHEMICAL SCIENCES

Academy of Scientific and Innovative Research

By

Sharath Kandambeth
(Registration Number: 10CC11A26008)

Under the guidance of
Dr. Rahul Banerjee

Physical & Materials Chemistry Division
CSIR-National Chemical Laboratory
Pune - 411008, MH, India.

September 2016

Dedicated to
My Parents

सीएसआईआर - राष्ट्रीय रासायनिक प्रयोगशाला
(वैज्ञानिक तथा औद्योगिक अनुसंधान परिषद)
डॉ. होमी भाभा मार्ग, पुणे - 411 008, भारत
CSIR - NATIONAL CHEMICAL LABORATORY
(Council of Scientific & Industrial Research)
Dr. Homi Bhabha Road, Pune - 411 008, India

Certificate

This is to certify that the work incorporated in this Ph.D. thesis entitled **"Design and Synthesis of Porous Crystalline Covalent Organic Frameworks with Exceptional Chemical Stability"** submitted by **Mr. Sharath Kandambeth** to **Academy of Scientific and Innovative Research (AcSIR)** in fulfillment of the requirements for the award of the Degree of Doctor of Philosophy, embodies original research work under my supervision. I further certify that this work has not been submitted to any other University or Institution in part or full for the award of any degree or diploma. Research material obtained from other sources has been duly acknowledged in the thesis. Any text, illustration, table etc., used in the thesis from other sources, have been duly cited and acknowledged.

Mr. Sharath Kandambeth
(Student)

Dr. Rahul Banerjee
(Supervisor)

Communication Channels
NCL Level DID : 2590
NCL Board No. : +91-20-25902000
EPABX : +91-20-25893300
: +91-20-25893400
FAX
Director's Office : +91-20-25902601
COA's Office : +91-20-25902660
SPO's Office : +91-20-25902664
WEBSITE
www.ncl-india.org

STATEMENT

I hereby declare that the matter embodied in this thesis entitled ***"Design and Synthesis of Porous Crystalline Covalent Organic Frameworks with Exceptional Chemical Stability"*** *is the result of investigations carried out by me in the Physical & Materials Chemistry Division, CSIR-National Chemical Laboratory, Pune, India under the supervision of Dr. Rahul Banerjee.*

In keeping with the general practice of reporting scientific observations due acknowledgements have been made wherever the work described is based on the findings of other investigators.

Pune, September 2016

Sharath Kandambeth

ACKNOWLEDGEMENT

I would take this opportunity to express my sincere gratitude to my supervisor Dr. Rahul Banerjee. My heartfelt thanks go to him for introducing me to the wonders of scientific research, for his persistent guidance, encouragement, inspiration and support during every stage of my doctoral research work. Again I warmly thank him for his precious advice, analysis, criticism and discussions on my research work. I am very much thankful to him for his pursuance for improving me as a person as well as my scientific skills. I would also like to sincerely thank my DAC committee members Dr. Suresh Bhat, Dr. Asha. S.K and Dr. Prakash P. Wadgaonkar for their constructive, innovative suggestion and comments throughout my Ph.D. work period at CSIR-NCL, Pune.

I extend my sincere thanks to the Director of CSIR-NCL Prof. Ashwani Kumar Nangia, former Directors Dr. Vijayamohanan K. Pillai and Dr. Sourav Pal, Head of Physical and Materials Chemistry Division Dr. P. A. Joy and Dr. Anil Kumar (Ex-HoD) for their kind help and encouragement during the course of this work. I must earnestly acknowledge the collaborative assistance, valuable scientific discussions and suggestions that I received from Dr. Ulhas K. Kharul and Dr. Sayam Sen Gupta. I also thank Dr. Thomas Heine, School of Engineering and Science, Jacobs University, Germany, for his help in theoretical calculations in few projects.

I am very grateful to CSIR, New Delhi for fellowship support to carry out my research work. I thank all the non-teaching staff of CSIR-NCL for their assistance on various occasions. I wish to thank all my friendly and cooperative labmates Tamas Da, Pradip Bhaya, Arijit Da, Chandan Da, Subhadeep Da, Tanay Da, Bishnu P Biswal, Divya, Harshitha, Subhash Da, Suman, Bikash, Mohitosh, Saibal, Arjun, Suvendu, Jayshri Didi, Gobinda Da, Digambar Ji, Manas Da, Shouvik Da, Sujit Da, Kaushik, Himadri, Abdul, Shebeeb, Kanhu, Harshal, Amit Da, Arghya Da, Tapan Da, Sushil Bhaya and Gargi Di for creating a cheerful and enjoyable working atmosphere in the lab. They were extremely supportive as well as helpful during my tenure. I also thank project student Anjumol, who helped in various projects.

My stay on this campus has been pleasant with the association of all the research scholars at CSIR-NCL. I am thankful to Bihag, Unnikrishnan, Anish, Prajitha, Leena, Beena, Govind, Rajesh, Jijil, Alson, Eldo, Shoy, Vijayadas, Sreekuttan, Anumon, Venugopal, Arun,

Sunil, Vyshak, Sreedala, Kiran, Anju, Lenin, Manchunath, Jaya, Jino, Ramya, Bindu, Nisha, Anjali, Suresh, Sudheesh, Manu, Rekha, Sushma, Kundan, Soumen, Joyashish, Rammy, Chaitanya, Sandip, Rajashree, Manik, Dhanya, Manoj, Sreekanth, Kshirodra, Narendra, Venkat, Prabhu, Asish, Mohan, Ashok, Anantharamaiya, Wahid, Nagesh, Pandi Raj, Vishal, Satej, Saibal, Raju, Chandan, Munmun, Basabda, Swapnil, Shekhar, Vinita, Chakadola Panda, Madhavan Nair, Loknath, Parashuram for their support, guidance, and advice.

I would also like to thankful to all my juniors Shibin, Rashid, Fayis, Zinoy, Tony, Ranjeesh, Sanoop, Vidyananth, Vipin, Munavvar, Rajith, Pranav, Sandeep, Emmanuel, Varsha, Betsy, Mariya, Maya, Jagadeesh, Kartika, Nishina, Manik, Santanu, Bittu, Sarath, Aswathy, Kuyil.

I am grateful to all my teachers and I expressed my gratitude for their encouragement in different part of my life. I thank the entire members of my family for their constant care and wishes. Last but not least, I would like to pay high regards to my parents for their constant encouragement and inspiration throughout my research work and lifting me uphill this phase of life. Dedicating this thesis to them is a minor recognition for their valuable support and encouragement.

Sharath Kandambeth

PREFACE

The future world demands the development of novel materials by taking consideration of the burst of advance technological development. Porous materials can play pivotal role in this area since they were already been tested for application such as reversible gas storage and separation, water purification etc. Covalent organic frameworks (COFs) represents emerging class of organic porous crystalline material. Since the sole compositions of COFs are lighter elements they have very low density and could be utilized as an effective gas storage media (For H_2, CO_2 and NH_3). Applications of COFs as semiconducting and photoconductive device were also been explore. Despite of these promising applications, the utilization of this porous COF material towards real life application has not reorganized yet, due to complex problems such as chemical instability and scalability.

COFs are usually synthesized by reversible organic reaction and it is believed that reversibility during synthesis is essential for the successful crystallization COFs. Since reversible back reactions can occur after the synthesis, COFs in general get completely decomposed even in presence of ambient humidity. Little improvement in water stability was achieved by pyridine doping and alkylation of COF pore walls. However these modifications always lead to decrease in the gas adsorption properties even though it enhances the hydrolytic stability to a small extent. Hence, stability problem in COFs still remain a challenge which prevents the usage of COFs for diverse practical applications.

Chapter 2 will present the synthesis of a new, highly chemically stable COFs (TpPa-1 and TpPa-2). Chemical stability of TpPa-1 and -2 arises due to the irreversible nature of the enol to keto tautomerism. TpPa-1 and -2 show exceptional resistance towards boiling water and acid treatment. Surface area of the activated COFs calculated using Brunauer-Emmett-Teller (BET) model were found to be 535 m^2/g for TpPa-1 and a 339 m^2/g for methylated TpPa-2. Hydrogen uptake of TpPa-1 and -2 were found to be 1.1 wt% and 0.89 wt%.

Chapter 3 discusses about the importance of intramolecular hydrogen bonding in improving the crystallinity, porosity, and chemical stability of the COF material. The hydrogen bond containing COF (DhaTph) display a high crystallinity and surface area (1305 m^2g^{-1}) in comparison to the non-hydroxyl analogue COF DmaTph. The H_2 uptake of DhaTph

and DmaTph was found to be 171 cm^3g^{-1} and 78 cm^3g^{-1}, respectively, at 77 K and a pressure of 1 atm.

Chapter 4 describes the synthesis of chemically stable guanidine based ionic covalent organic nanosheets (iCONs). The charged guanidine based iCONs were synthesized by Schiff base reaction. Due to the inbuilt ionic character, iCONs exhibit self-exfoliation characteristics in water. The exfoliated iCONs were comprised of few thin layers. As synthesized iCONs demonstrated high chemical stability and good antibacterial activity against both gram positive (*S. aureus*) and gram negative bacteria (*E. coli*).

In chapter 5, we have studied in detail about the morphological evolution of covalent organic framework hollow sphere. A self template approach was used for the synthesis of COF hollow spheres. The synthesized COF hollow spheres display high crystallinity and surface area (S_{BET}=1500 m^2g^{-1}). Moreover the presence of meso-pores (3.7 nm) in the COF hollow sphere walls encourages us to study the enzyme (trypsin) immobilization study. The COF hollow sphere displays a trypsin uptake of 15.5 µmol g^{-1}.

Finally, Chapter 6 will describe the conclusion of the overall work presented in this thesis. The future direction based on the understanding of this thesis work also presented in the last section of this chapter.

Sharath Kandambeth

CONTENTS **PAGE**

LIST OF FIGURES

LIST OF TABLES

CHAPTER 1

Introduction to Covalent Organic Frameworks: Synthesis, Applications and Stability issues

Abstract: *The future world demands the development of novel materials by taking consideration of the burst of advance technological development. Porous materials can play pivotal role in these area due to their potential application in the areas of reversible gas storage and separation, water purification etc. Covalent Organic Frameworks (COFs) represents emerging class of organic porous crystalline material. Since the sole compositions of COFs are lighter elements they have very low density and could be utilized as an effective gas storage media (For H_2, CO_2 and NH_3). Application of COFs as semiconducting and photoconductive device were also been explored. Despite of these promising applications, the utilization of this porous COF material towards real life application has not reorganized yet, due to complex problems such as chemical instability and scalability.*

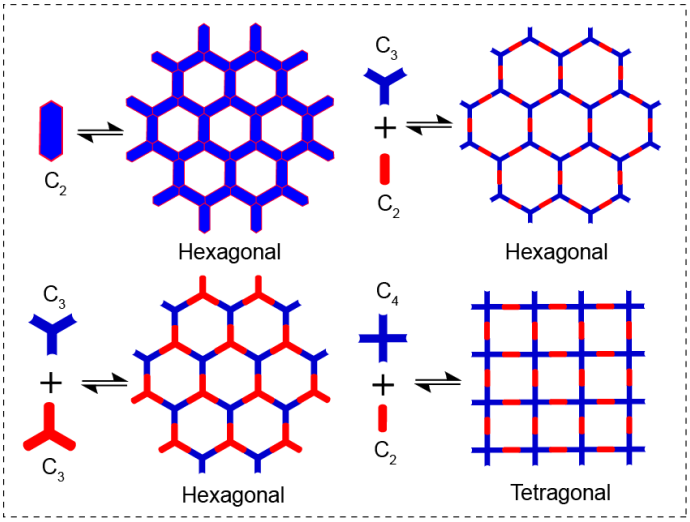

1.1 Background of porous crystalline frameworks

Scientists have designed novel porous materials by adopting ideas from nature. The common examples of porous structures found in nature includes honeycombs with hexagonal pores, hollow bamboo, diatomaceous earth, bones etc [1.1]. When the materials pore size is bring down to the micro/nanometer scale, unique properties and applications starts to originate [1.2]. Some general examples of nano-porous materials are porous carbons, mesoporous silica, zeolites, metal organic frameworks and covalent organic frame works [1.3]. The future world requires the discovery of novel porous materials by taking consideration of the burst of advance technological development. Global warming, shortening of the petroleum based fuels, environmental pollutions, nuclear accidents remind us again the importance of developing new materials which are capable of performing applications in the area of green and sustainable energy [1.2]. Porous materials can play pivotal role in the area of sustainable energy, since they were already been used for application such as reversible gas storage and separation, water purification, photocatalysis and photovoltaic's, catalysis etc [1.4]. Porous materials are open framework solids with tunable structures in the molecular scale which make them adaptable to suit for a wide variety of applications. Porous materials are now used in wide variety of applications ranging from common house hold materials to the advanced space technologies [1.5]. Porous carbon based materials were used in water purification systems, batteries, gas masks, metallurgy, supports for catalysis, etc [1.6]. While porous zeolite and silica based materials were used in molecular sieves, laundry detergents, drug delivery materials, gas storage, industrial catalyst etc. [1.7].

The first porous material used ever by the humans was activated charcoals (carbons). Ancient Indians and Egyptians utilized charcoal for the purification of water and medical applications [1.8]. As the time progressed more porous materials were discovered and applied for the development of human society. Porous hydraulic cements were used as an important building material in Roman antiquity [1.8]. The first naturally existing porous zeolite mineral (stilbite) was discovered by Swedish mineralogist Axel Fredrik Cronstedt in 1756 [1.7g]. Zeolites are a class of 'tectosilicate' minerals which are constructed from corner-sharing aluminate and silicate tetrahedral units, linked together to produce three-dimensional frameworks [1.7]. After the zeolite discovery solid state chemist has learned the

technique to synthesize porous materials artificially from naturally occurring clays and other natural minerals [1.7]. The first synthetic zeolite was made in 1862. Several other porous silicates and phosphates were invented after that, and get utilized in various industrial applications. But the difficulty in predesigning the structure and fictionalization pore channels are some of the drawbacks of the zeolites, which made the scientist to search for new ultra-porous materials[1.7]. Developing porous materials with precise control in pore size and functionality is one of the main priority since they predicted to have improved performance in the area of gas storage, energy storage, electronic properties etc [1.8]. Omar M. Yaghi and co-workers in 1998 discovered a new type of inorganic-organic hybrid porous materials, which is termed as metal organic frameworks (MOFs) [1.9]. Metal organic frameworks are porous open framework structures, which are constructed from the metal ions clusters and organic spacers. Due to the ultra high porosity and tunable pore size, MOF display improved performance in the areas of adsorption, separation, and catalysis [1.9]. But the poor chemical and thermal stability of the MOF materials limits their practical applicability [1.10]. Replacing the weak co-ordinate bonds with strong covalent bonds is one of the options to improve the chemical and thermal stability of the porous framework materials. However linking organic building blocks by strong covalent bonds to ordered frameworks is challenging task. Even though scientist were impart crystallinity in 1D polymers, attempts to build 2D or 3D organic framework structure with covalent bonds often result in the formation of amorphous cross linked polymers [1.11]. Omar M. Yaghi et al able to solve this long standing problem by synthesizing the first covalent organic framework (COF) in 2005 [1.12].

1.2 Classification of the porous materials

Porous materials are solid-state materials which contain pores or voids inside the matrix or the framework [1.2]. Most commonly these materials are classified in based on the pore diameters and framework material nature. Based on the pore diameters porous materials were categorized as follows [1.4c]. 1) Microporous materials (pore size 0.2-2 nm e.g., zeolites and metal organic frameworks). 2) Mesoporous materials (pore size 2-50 nm e.g., mesoporous silica and alumina). 3) Macroporous materials (pore size 50-1000 nm e.g., Inverse opals and metal foams). Based on their framework material nature, porous materials were also categorized in three groups. 1) Inorganic porous Frameworks, 2) Inorganic-organic

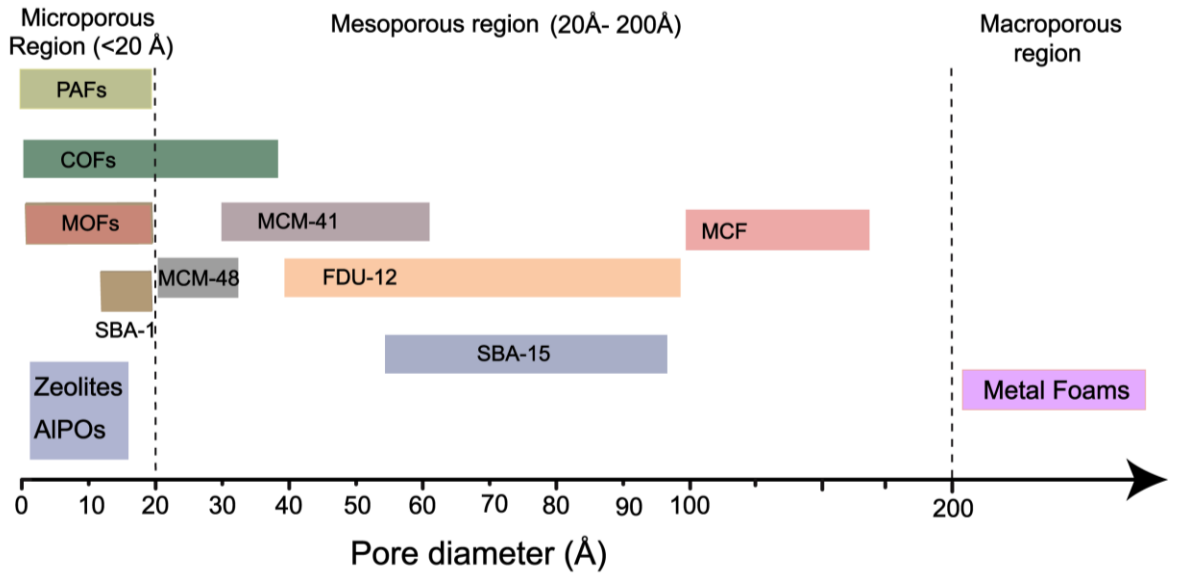

***Figure 1.1**. Classification of porous materials based on the pore diameter* [1.13].

hybrid porous frameworks, 3) Organic porous frameworks.

1.2.1 Inorganic porous Frameworks

The common examples for inorganic porous Frameworks materials are zeolites, aluminophosphates, germanosilicates, titanosilicates and metal phosphates (copper, zinc, gallium, iron phosphates, etc.). Zeolites are crystalline aluminosilicates, which are primarily constructed from the tetrahedral corner sharing TO_4 (T = Si, Al) species. The general formula for zeolites is $M_{n+x/n}$ $[(AlO_2)_x(SiO_2)_y]_x \cdot wH_2O$ (M= metal). [1.7a]. Pure silica framework is formed from SiO_4 tetrahedral units, and are electrically neutral. When some of the SiO_4 units were replaced by aluminium, a charge imbalance is created, and as a result framework becomes anionic in nature. To balance the charge, framework also occupies metal cations such as Na^{+1}, K^{+1}, Ca^{+1}. The presence of these metal cations helps to induce ion exchange characteristics to zeolites. The ratio of the silicon to aluminium (Si/Al) in zeolites varies from zero to one. Most of the zeolites are strong bronsted acid due to the presence of bridging hydroxyl group. Zeolite framework structure contains cavities or pores in the range of about 3 to 15 Å [1.7b]. Replacement of the silicon atoms in zeolites with aluminium and phosphorus results in another class of inorganic porous framework materials called aluminophosphates (AlPOs) [1.14]. Aluminophosphates are usually formed as neutral, due to the presence of octahedral aluminium sites in the framework. Replacement of aluminium

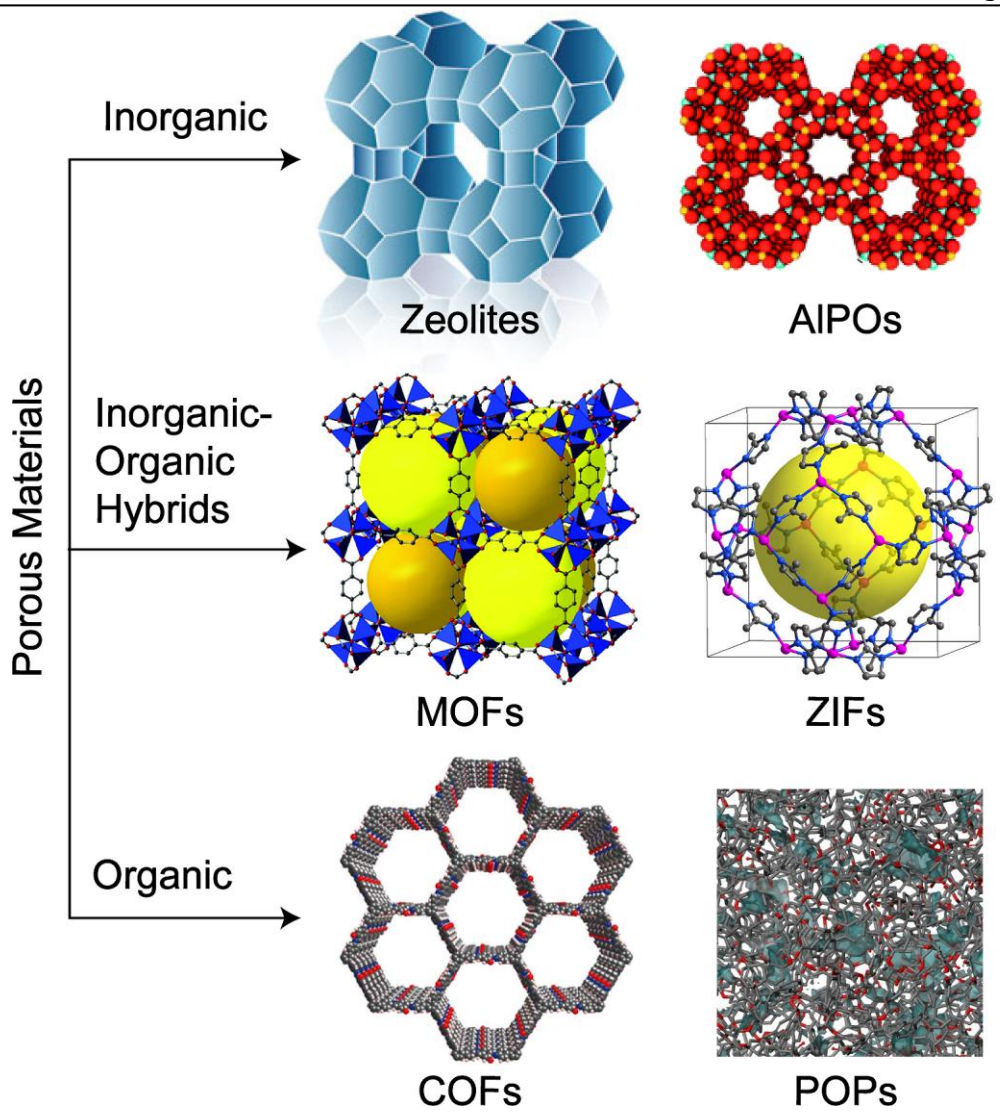

***Figure 1.2**. Classification of porous materials based on the framework material type.*

by bivalent metal ions such as copper, gallium or zinc will leaded to the formation of anionic metal phosphates frameworks [1.15]. Due to the low production costs, high chemical and thermal stability zeolites were widely employed as industrial adsorbents and catalyst. Some of the important applications of zeolites are shape selective catalysts, water purifiers or softeners, dehydrating and dehumidification agent and heat storage materials [1.16].

1.2.2 Inorganic-organic hybrid porous frameworks

Inorganic porous frameworks lack functional and structural diversity. The development of inorganic-organic hybrid porous frameworks lead to the discovery of novel unprecedented structures. The common example for the inorganic-organic porous

frameworks are metal organic frameworks (MOFs) [1.9]. MOFs posses a three dimensional framework structure with metal ion clusters at the nodes separated by organic ligands spacers. The metal ions used in MOF synthesis varies from transition metals (e.g. Cu, Zn), alkaline earth elements (e.g. Sr, Ba), p-block elements (e.g. In, Ga), actinides (e.g. U, Th) [1.17]. The commonly used organic spacers in the MOF construction are di, tri, tetra or poly carboxylate, imidazolate or phosphate anions and bipyridine ligands [1.17]. MOFs follow basic rules of reticular chemistry and it is easy to predesign the framework structure and porosity. Functional variation and pore size tuning of MOFs can be controlled by interchanging the organic spacers in iso-reticular structures. Based on the nature of the frameworks, MOFs are classified in three groups namely 1) 1^{st} generation, 2) 2^{nd} generation, 3) 3^{rd} generation [1.18]. 1^{st} generation MOF frameworks only retain their framework structure in presence of guest/ solvent molecule. After the removal of the guest molecules framework structure usually get collapsed. 2^{nd} generation MOFs are stable and robust. They retain their 3D framework structure even after the solvent removal. 3^{rd} generation MOFs are flexible and their porosity and surface area changes in a response to the external stimuli [1.18c]. MOFs are usually crystallized by solvothermal reaction, with solvents/guest molecule trapped inside pores. Removal of these solvent/guest molecules generates open frameworks structures in MOF with ultra high porosity. MOFs were tested for different gas storage application (H_2, CO_2, CH_4, acetylene etc). Selective adsorption/ separation of gas molecules were also performed in MOFs with precise pore channels. The other important applications of MOFs are catalysis, proton conductivity, drug delivery etc. [1.19]. Despite of the interesting properties, MOFs also suffers some disadvantages. It is difficult extend the porosity of MOF to mesoporous region, thus storage of bigger sized guest molecules (e.g. biomolecules) is found to be difficult. MOFs also lack sufficient chemical and thermal stability, since they are constructed from weak co-ordinate bonds [1.10].

1.2.3 Organic porous frameworks

More recently organic porous framework materials, have attracted the attention of scientists [1.20]. Organic porous framework materials are exclusively constructed from organic building blocks, with strong covalent bond connection. Due to the covalent nature, organic porous frameworks are expected to show high thermal and chemical stability. Moreover light weight elements in the building blocks can significantly reduce the

framework density, which is an advantage in vehicular gas storage application. Based on the frameworks crystallinity organic porous frameworks are classified in two categories, 1) porous polymeric frameworks (POPs) [1.20a-b] and 2) covalent organic frameworks (COFs) [1.20e-f]. Porous polymeric frameworks (POPs) are amorphous in nature while covalent organic frameworks (COFs) posses a crystalline framework structure and ordered pore channels.

Porous Polymeric Frameworks: Porous polymeric frameworks (POPs) generally posses a disordered framework structure, due to the irreversible nature in the formation reaction (***Figure 1.3***). POPs are usually synthesized by C-C coupling reaction (such as Suzuki coupling [1.21a-b], Sonogashira-Hagihara [1.21c], Yamamoto coupling [1.21d-e]), acetyl cyclotrimerisation [1.21 f], oxidative coupling reaction [1.21g-h], Friedel–Crafts reaction [1.21i] and phenazine ring fusion reaction [1.21j]. The first POP (CMP-0 and CMP-5) was reported by Andrew I. Cooper and colleagues [1.21l]. The surface areas of these networks are significantly lower than those of reported COFs, ranging from 1018 m^2 g^{-1} (CMP-0) to 512 m^2g^{-1} (CMP-5) [1.21l]. The lower surface areas of POPs are attributed to the disordered nature of the framework structure. Despite of the amorphous nature POPs posses' high chemical stability, which could be positive aspect while applying them in real life practical storage and separation application.

1.3 Covalent organic frameworks

Covalent organic frameworks are new class of crystalline organic porous materials which follows the basic rules of reticular chemistry(***Figure 1.2***). Due to the pre-designable, tunable and easy functionalizable framework structures they found to have important applications in area such as gas storage, separation, catalysis, photo conducting materials, and sensors. COFs are completely organic in nature, which is one of the main differences from predecessor porous materials such as MOF and Zeolites. COFs are constructed by the strong covalent linkage between organic building units having precise symmetry [1.22]. Due to the presence strong covalent bonds, COFs display high thermal stability. Since the COF building elements are light weight (C, N, O, H), they show very low density which is an advantage in application such as gas storage [1.23]. COFs framework can be designed in two dimensions or three dimension based on the symmetric combination of the ligands used for the formation reaction. Almost 80% of the COF reported to have 2D structure [1.22]. The

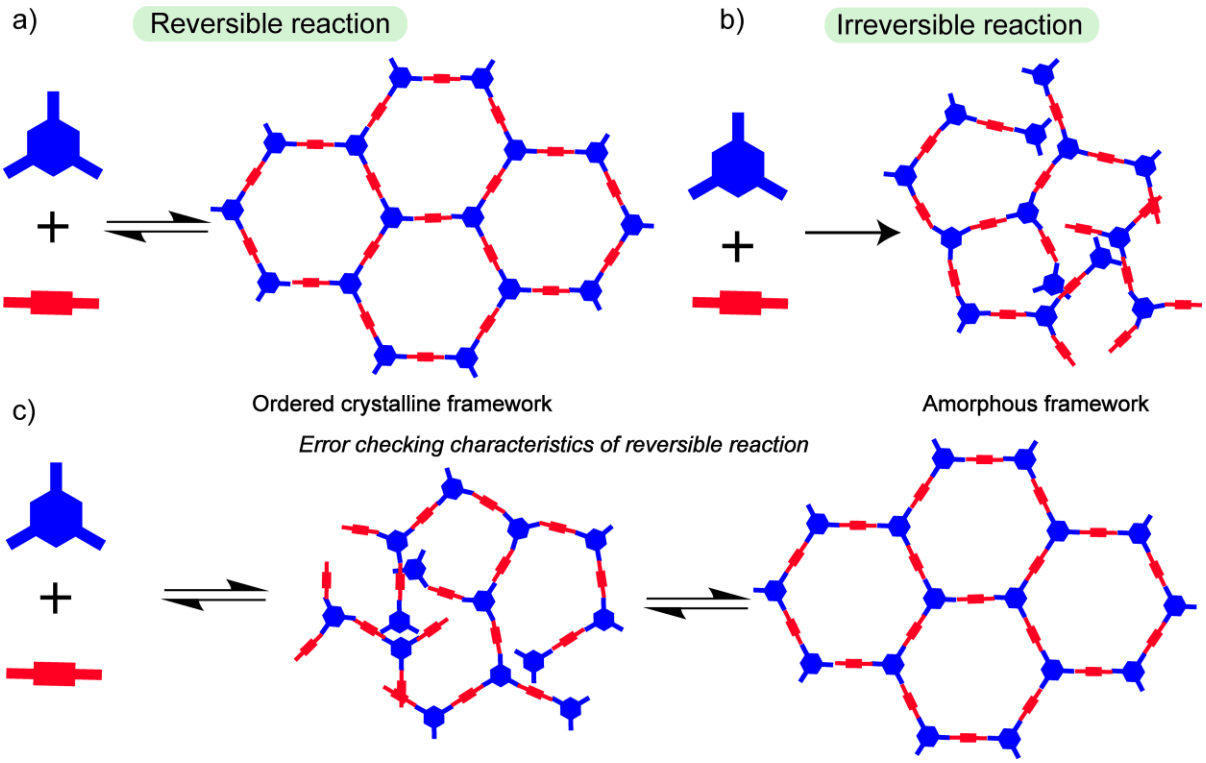

Figure 1.3. *Schematic representation of a) and c) COF formation by reversible reaction, b) PAF formation by irreversible reaction.*

non availability of higher symmetric organic building units is the main reason for the 3D COF scarcity [1.23]. Most of the 2D-COFs have stacked layer structure similar to graphite. When COFs 2D layers were uniformly stacked, it start showing unique electronic properties, due to long range overlapping of π- π orbitals of the aromatic rings [1.22a].

It is also easy to tune the pore size of the COF by varying the building unit length [1.22]. COFs are mainly synthesized as microporous materials with pore size less than 2 nm. However by following the basic rules of reticular chemistry and by the judicious selection of the building units, it is possible to extend the porosity of COFs in mesoporous region. The highest pore size reported in COFs is 4.7 nm [1.24]. COFs area mainly synthesized by reversible organic reaction. Reversibility in the COF formation reaction, imparts error checking and proof reading characteristic to the system [1.22a]. So if any disorders exist in COF crystallites, during the course of reaction, system repair these defects by multiple reversible bond formation cycles. This self repairing characteristic eventually leads to the formation of most thermodynamically stable COF structures at the end (***Figure 1.3***). Mainly

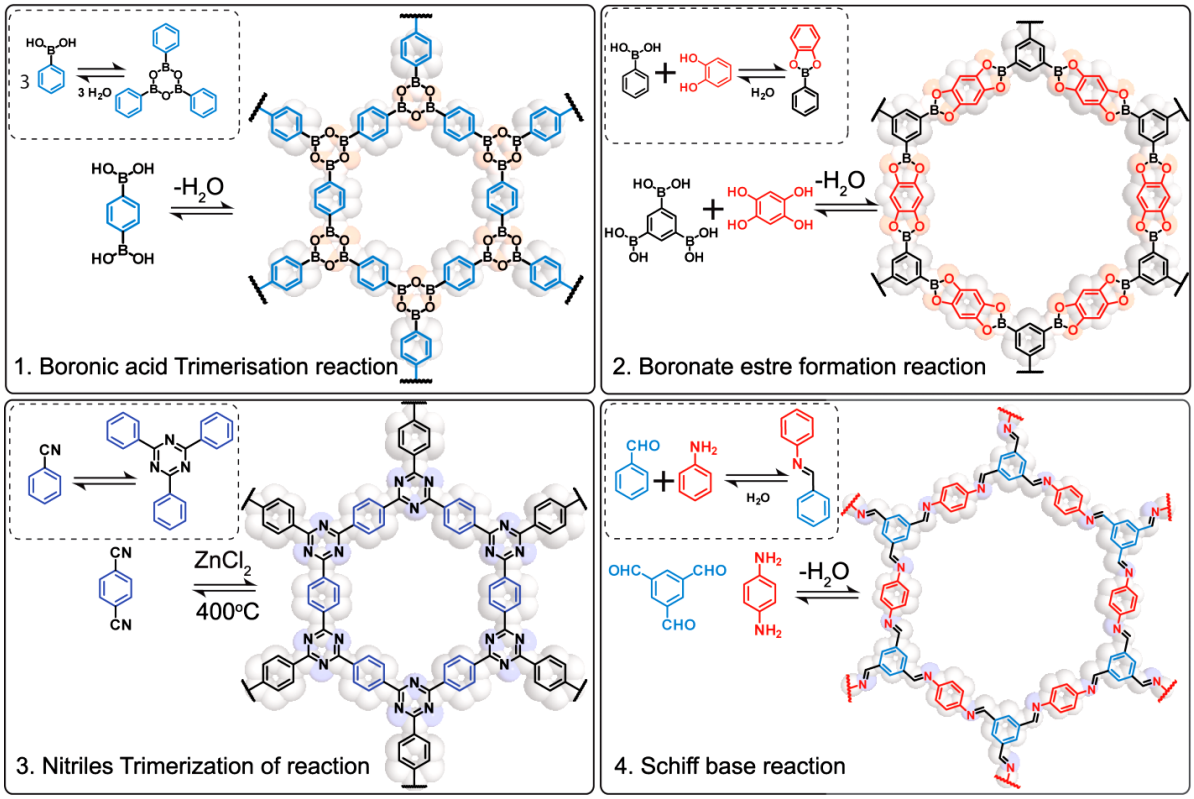

Figure 1.4*. Different reversible organic reaction used for the synthesis of COFs.*

four reversible reaction 1) boronic acid trimerisation [1.23], 2) boronate ester formation [1.25], 3) nitrile group trimerisation [1.26] and 4) Schiff base reaction [1.27], were widely used for the synthesis of COFs (***Figure 1.4***). The attempts to utilize irreversible organic reaction (such as C-C coupling reaction) always lead to the formation of amorphous framework structures, which were commonly known by porous aromatic frameworks (PAFs) or porous polymeric frameworks (POPs) [1.21].

COFs are highly porous materials, and their porosity has been exploited for storage applications such as gas storage (CO_2, H_2, NH_3 etc.) and bio-molecule storage and release (drugs and enzyme). Ordered pores also utilized for gas separation application. In addition to this, the pi-conjugated 2D COFs were tested for charge carrier mobility and photo-conducting application. The other important applications of COF include, sensing, energy storage and catalysis. Despite of these promising properties real life application of COF are yet to be realized due to complex problems such as chemical instability, processability and scalability. As discussed above COFs are usually synthesized by reversible condensation

reaction, which generally involve the evolution of water as one of the by product. Since the possibility of reversible back reaction still exists even after the COF formation, upon getting in contact with water, COFs in general get completely hydrolyzed to the starting materials [1.28]. Few attempts were done to improve the chemical stability of COF frameworks by incorporation of alkyl chains and pyridine doping in boronic acid based COFs. But these methods were only able to stabilize COFs in ambient humidity for short time duration. More over doping of these stabilizing agents in COF pores often decreases its surface area [1.28]. This thesis discusses the solution for the chemical stability problems in COFs.

1.4 Types of reversible reaction used the synthesis of COFs

1.4.1 Boronic acid trimerisation reaction*:** This reaction involves the reversible condensation of three boronic acid moiety in to planar six-membered boroxines ring (B_3O_3 ring) and water (Figure 1.4***). When 1,4-benzene diboronic acid were used reaction will happens at two ends of the molecule as result polymerization happens in two dimension and finally after infinite growth 2D framework of COF-1 were formed [1.12]. The other examples of COFs synthesized by this reaction are COF-102, COF-103 and PPy-COF [1.23]. Since the boroxines rings are planar and reaction have good reversibility the COF material synthesized by this strategy generally posses high crystallinity and porosity [1.23].

1.4.2 *Boronate ester formation reaction:* This reaction involves the reversible condensation reaction of boronic acid with aromatic diols to form five membered boronate ester rings (C_2O_2B rings) (***Figure 1.4***). Co-condensation of two or more building blocks are required for the COF formation. One the building unit will be aromatic boronic acid (usually di or tri), and the second one will be poly-hydroxy aromatic compounds like 2,3,6,7,10,11-hexahydroxytriphenylene (HHTP) (***Figure 1.4***). The common examples for COFs synthesized by this reaction are COF-5, COF-8, COF-10, HHTP-DPB COF, ZnPc-Py COF etc [1.12, 1.25]. Due to the high reversibility in the reaction COFs synthesized by boronate ester formation reaction also display high crystallinity and surface area. But poor hydrolytic stability is one of drawbacks of the COFs synthesized by this method [1.28].

1.4.3 *Schiff base reaction:* Dynamic Schiff base reaction commonly used for the synthesis of organic cages and other supra molecular structures. Omar M. Yaghi and coworkers introduces Schiff base reaction for the COF synthesis [1.27]. The first COF synthesized by

Schiff base reaction was COF-300[1.27]. This 3D COF was synthesized by the Schiff base reaction between tetra-(4-anilyl) methane (T_d) and terephthaldehyde (C_2). After this report several 2D imine based COFs were also reported by using symmetric combination such as C_3+ C_3 or C_3 + C_2. COF-42, COF-43, COF-366, COF-LZU-1 are the some of the examples for the 2D –COFs synthesized by Schiff base reaction [1.27]. As compared boronic acid trimerisation and ester formation reaction, Schiff base reaction become completely reversible under acid condition (pH=4-5). So catalytic amount of acetic were usually employed in the reaction for the successful crystallization of imine COFs [1.27]. Imine based COFs are much more hydrolytically stable in comparison to boronic acid COFs, due to its pH depended reversibility. However at lower pH imine COFs also get completely decomposed [1.27].

1.4.4 ***Trimerization of nitriles***: The reversible trimerisation of the nitrile was performed via ionothermal method at high temperature (400^{O}C) and in presence of Lewis acid ($ZnCl_2$) (***Figure 1.4***). The COFs synthesized by this reaction is known as covalent triazine-based frameworks (CTFs). This reaction methodology was developed by Arne Thomas and co-workers in 2008 and the first example for this series is CTF-1 [1.26a]. However unlike other COF formation reaction, trimerisation of the nitrile cannot be generalized to different organic building blocks. Most of the organic starting materials get decomposed at 400 °C, so this method is limited only to few frameworks. Attempts to perform nitrile trimerisation at low temperature (110 °C) in presence of trifluoromethanesulfonic acid often results in the formation of amorphous product [1.26].

1.5 Basic symmetric rules of combination

As discussed above reversibility in formation reaction is essential for the successful crystallization of COFs. Apart from the reversibility the symmetry of the building blocks also largely affects crystallinity of the COFs. A slight deviation from the basic symmetric combination rules often results in the formation of amorphous product, even though the COF formation reaction was reversible [1.22]. Rigid conformation is one of the primary criteria in selecting the COF building blocks. Building blocks with flexible core (e.g. alkyl groups) increases possibility of bond formation in multiple direction which leads to the formation of disordered frameworks. Building blocks with aromatic cores are widely employed in COF synthesis because of its high rigidity and also support π-π stacking interaction in the case of 2D COFs [1.22]. The building blocks used in COF synthesis also should follow certain

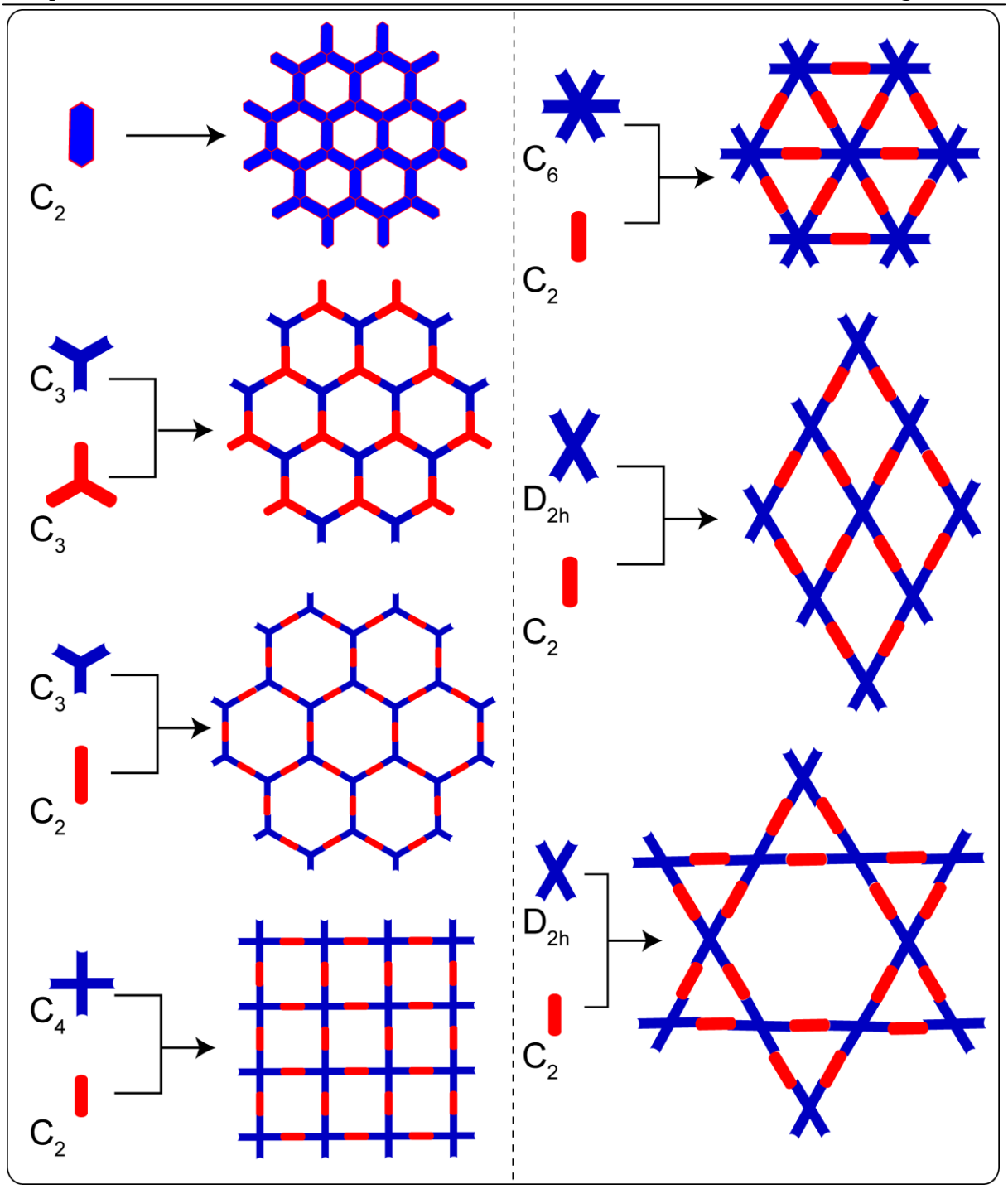

Figure 1.5. *Schematic representation of different organic symmetric combination used in COF framework construction.*

symmetric combination rules. The commonly used symmetric combinations for the 2D COF synthesis are C_3+C_2, C_3+C_3, C_4+C_2, C_4+C_4, C_6+C_2 (***Figure 1.5***) [1.20d-f,1.22]. The C_3+C_2, C_3+C_3 symmetric combination results in the formation of 2D COF with hexagonal pores

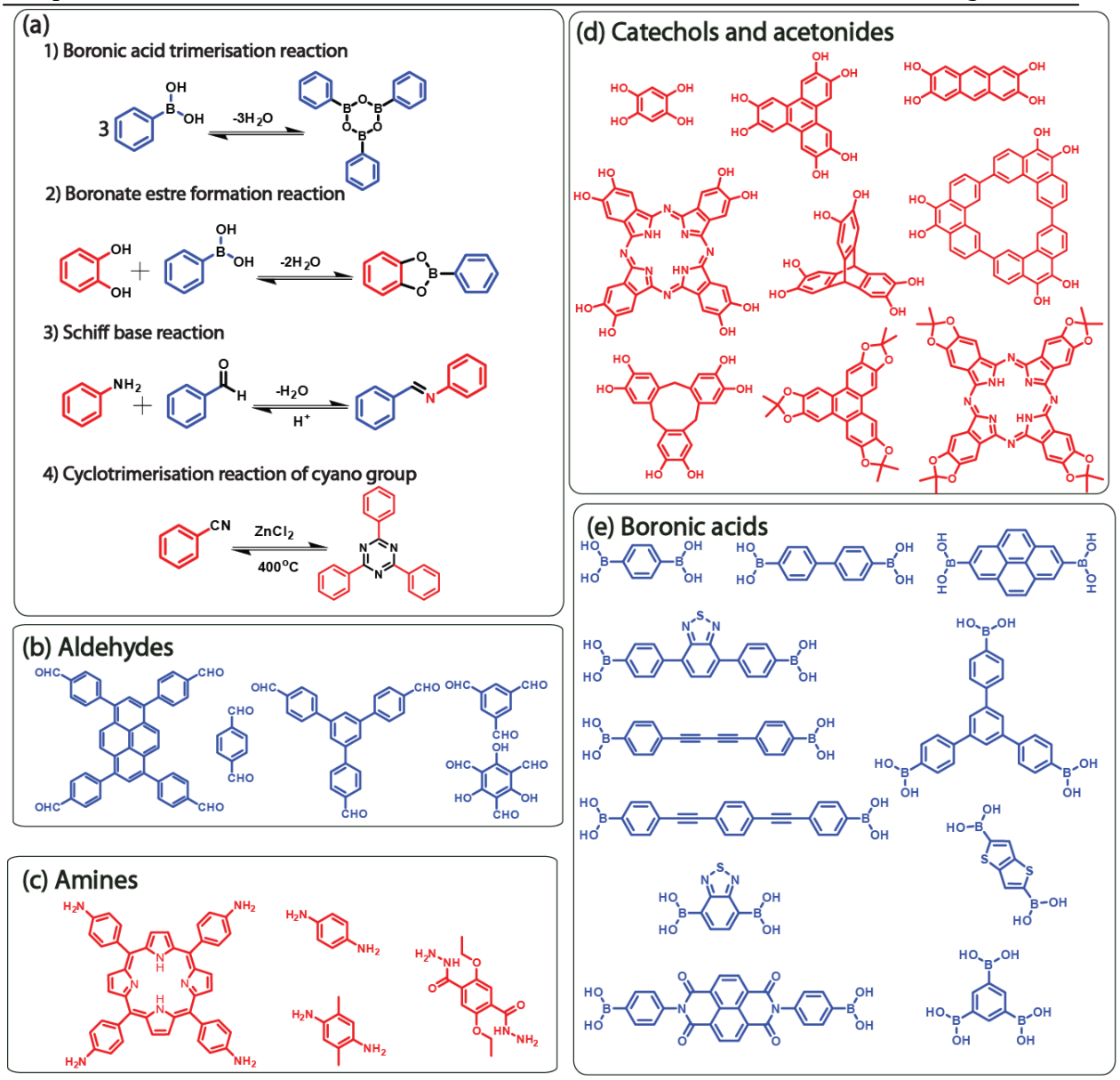

Figure 1.6.: *(a) Different type of reversible organic reactions used for COF synthesis. (b) Aldehyde building units used for the synthesis of imine based COFs. (c) Different amine linkers used. (d) Different catechol based linkers used for the synthesis of boron based COFs. (e) Boronic acid based building block used for the synthesis of boron containing COFs*.

(***Figure 1.5***). The common examples for this combination include COF-1 and COF-5 [1.12]. The COF belongs to this category usually get crystallized in hexagonal crystal system with space groups *P*6/m (eclipsed structure) and *P*6$_3$/m (staggered structure) [1.12]. The symmetric combination of C_4+C_2 and C_4+C_4 usually leads to the formation of 2D frameworks with tetragonal pores. Most of the porphyrin based COFs belongs to this

category. The examples for this particular symmetric combination are NiPc COF, COF-366, ZnPc-Py COF etc [1.27d,1.29]. Tetragonal crystal system with space group *P*4/m is commonly used to model the structures of C_4+C_2 and C_4+C_4 symmetric combinations. C_6+C_2 symmetric combinations are rarely used in COF synthesis (***Figure 1.5***) [1.30]. $[H_2N]_6$HPB and $[H_2N]_6$HBC are the only examples reported this category [1.30]. These imine COF posses' triangular topologies, having pore size in micro-porous region (1.2 and 1.8 nm). Xin Zhao and coworkers have synthesized a novel 2D-COF by using symmetric combination of D_{2h} and C_2. Interestingly authors observed that instead of forming regular tetragonal framework, the 2D-COF adopted a new type of AA-H structure (***Figure 1.5***) [1.31]. The AA-H structure posses two type of pores, one in micro pore range (7.1 Å) and the other in mesoporous region (26.9 Å). The molecular mechanics calculations showed that hexagonal AA-H has the lowest energy among the other four probable structures [1.31]. Unlike 2D COF, there are only limited examples of 3D-COFs reported in literature. The scarcity of organic building blocks having higher symmetry (eg; T_d, O_h) is the principle reason behind this problem. Most of the 3D-COFs reported in literature use building blocks with tetrahedral (T_d) symmetry [1.27a, 1.23]. The common symmetric combinations used for the construction of 3D- COFs are, T_d+ T_d, T_d+ C_2, T_d+ C_3 and T_d+ C_4.

1.6 Synthetic methods

Synthesis of organic polymers are usually carried out by kinetically controlled irreversible organic reactions. COFs on the other hand were synthesized by the reversible reaction which allows the formation of the covalent bonds in a reversible way. This reversibility in the reaction allows the system to make and break the bonds reversibly which will finally leads to the formation of thermodynamically most stable structure. The error checking and the proof checking characteristics of the reversible bonds formation helps to get the most ordered crystalline structure at the end with minimum number of structural defects [1.22]. COFs are usually synthesized solvothermaly in organic solvents since the building units used for the COF synthesis are organic in nature (***Figure 1.8***). For maintaining the exact condition for crystallization there should be proper control in parameters such as solvent ratios, temperature, pressure, reaction time and presence or absence of template [1.22]. Reaction was usually performed in sealed pyrex tube under high vacuum and reaction temperature vary from 80 °C to 120 °C (***Figure 1.8***). Most of the reversible

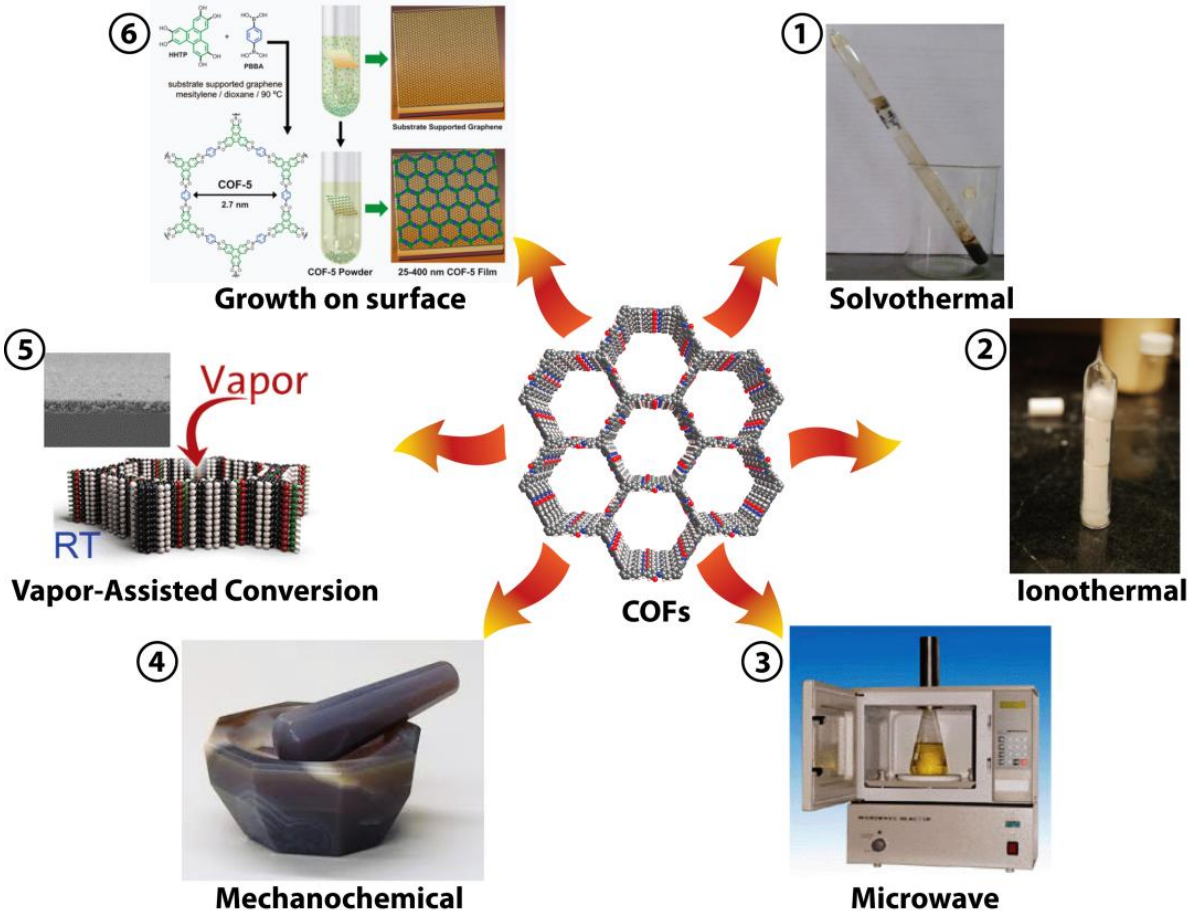

Figure 1.7*. Different synthetic methods used for the synthesis of COFs.*

COF formation reaction involves the formation of water as a byproduct during condensation reaction (***Figure 1.4***). The advantage of using a sealed tube with vacuum for the reaction is that, as the reaction progresses, the water molecule formed in the product side get diffused in to the empty space of the sealed tube due to the high vacuum. For a reversible reaction, removal of the one of the product from the system will enhances the rate of the forward reaction, which helps in the formation of the COF crystallites with a faster rate. However the water diffused out from the reaction mixture is not allowed to go completely out of the system due to the sealed condition (***Figure 1.8)***. This closed condition will help to maintain the reversibility, since the system can utilize the water during the self healing process. Apart from the solvothermal synthesis some other synthetic methods were also used for the COF synthesis which are ionothermal synthesis, microwave synthesis, mechanochemical synthesis and synthesis in presence of template.

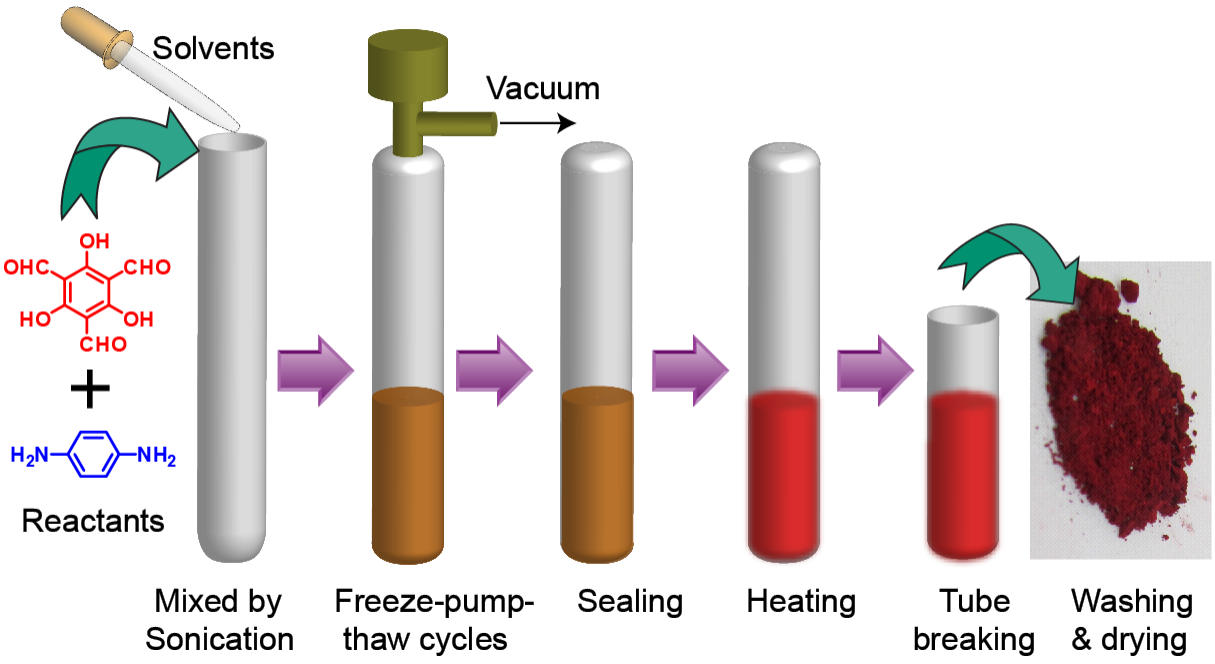

Figure 1.8: *Different steps involved in the Solvothermal COF synthesis.*

1.6.1 Solvothermal synthesis.

Solvothermal synthesis is the most widely used technique for the COF synthesis [1.22]. The Solvothermal method is usually performed for the synthesis of zeolites and MOFs in autoclaves. In the case of COFs, instead of autoclaves sealed tubes were often employed. The sealed tube techniques involve the following steps (***Figure 1.8***).

1) In the first steps reactant were transferred to an empty pyrex/ glace tube.

2) Solvents were added and the tube was sonicated for around 5 to 20 minutes (in the case of imine based COFs catalytic amount of acetic acid also added along with the solvent addition).

3) After the sonication the tube containing reactants and solvents were flash frozen in liquid nitrogen.

4) Freeze–pump–thaw cycles were applied may times to the frozen tube to create vacuum. The final pressure inside the pyrex tube is usually in the range of 50 to 150 mbar.

5) The tube was then sealed off under flame and should kept in room temperature for 10-20 minutes.

6) When the tube reaches to room temperature, it was transferred to a hot air oven and kept undisturbed for 2 to 7 days. The temperature of the oven is usually set in the range 90 °C-120 °C.

The pressure inside the pyrex tube is usually set in range 50 to 150 mbar. The low pressure and sealed condition of the tube is essential for the successful crystallization of COFs. The low pressure in the tube promotes the diffusion of by product water in to empty space of the tube during COF formation reaction. According to the Le Chatelier principle this removal of water from the reaction systems promotes the forward reaction which helps in the formation of COF product. The sealed condition of tube hinders the complete removal water from the system. Thus water vapors still remain available for maintaining the reversibility of the reaction.

Usually organic solvent combination such as Mesitylene-dioxane, tetrahydrofurane-methanol-toluene, DMAc-o-dichlorobenzene were widely used for the COF synthesis [1.22]. The choice of the solvents is mainly based on the starting materials solubility. Usually solvent ratios in which reactants are partially soluble were selected for the COF crystallization. The partial solubility slowdown the COF reaction rate by controlling the diffusion of reactants to the solvent system, which helps to improve the crystallinity of the COFs [1.12].

1.6.2 Microwave synthesis

Andrew I. Cooper and co-workers introduced a microwave based method for COF synthesis. The reaction involves heating a closed tube containing reactants in a microwave oven. As compared to the sealed tube, microwave reaction methods are faster. Andrew I. Cooper and co-workers demonstrated the synthesis of COF-5 and COF-102 in 20 minutes under microwave conditions [1.32a]. The microwave condition only produces minimum impurities during the COF formation reaction as compared to the solvothermal method. So multiple solvent washing steps are not needed for COF purification [1.32]. The microwave synthesized also shows a comparable crystallinity surface area to the solvothermaly synthesized COFs.

1.6.3 Ionothermal synthesis

Ionotheremal reactions are mainly used for the synthesis of covalent triazine

frameworks (CTFs). Synthesis of CTF is usually performed at high temperature (400 °C) [1.26]. Since pyrex and glass tube cannot be used for high temperature reaction, quartz tubes are generally employed to perform ionothernmal reaction. In a typical Ionothermal COF synthesis, solid reactants and $ZnCl_2$ catalyst were heated inside closed quartz tube at 400 °C [1.26]. At this temperature $ZnCl_2$ melts and COF reaction happens inside the molten $ZnCl_2$.

1.6.4 Synthesis of mono layers on surface

Surface synthesis of 2D COFs were reported on various metal, 2D material surface. The thin layer fabrication of COF is important for electrochemical and photo-conducting application. More over the structural details of the COFs can be explored in details from the STM images of the surface fabricated COF monolayer. Louis Porte and coworkers pioneered the research on COF surface fabrication [1.33a]. They were able to synthesize the first surface covalent organic frameworks (SCOFs) by growing COF-1 and COF-5 on the clean Ag(111) surface [1.33a]. Synthesis of SCOFs involve the vacuum sublimation of reactants on the surface of Ag(111), followed by heating at high temperature. Ditchel and co-workers developed a new method by which COFs thin films can be directly fabricated on to single layer graphene attached to SiO_2 surface (***Figure 1.9a***) [1.33b]. The COF film fabrication was done under solvothermal condition and the film thickness was controlled by adjusting the

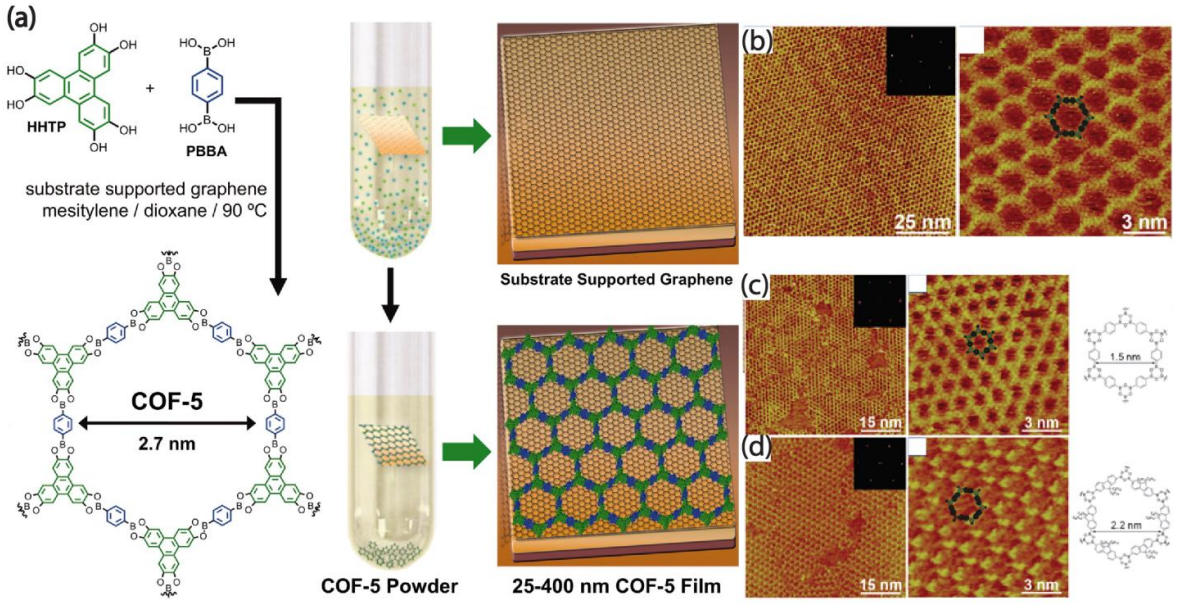

Figure 1.9.: *(a) Synthesis of COF-5 on the surface of few layer graphene. (b) & (c) STM images of COF-1 and (d) STM images of COF 10 on HOPG surface. [Reprinted with permission from Ref., Copyright Science, 2010].*

reaction time. The alignment of the COF crystallites on the SiO_2 surface was determined from the grazing incidence X-ray diffraction. Li-Jun Wan and co-workers introduced another new technique for the COF layer fabrication on the surface of 2D materials [1.33c]. The reaction involve the drop casting of boronic acid reactants on to a metal or highly oriented pyrolytic graphite (HOPG) surface, followed by heating them on a closed container in presence of copper sulphate pentahydrate ($CuSO_4.5H_2O$) (***Figure 1.9b***) [1.33c]. They have observed that the presence of $CuSO_4.5H_2O$ drastically improve the crystallinity of COFs by controlling the humidity inside the reaction chamber. The reversible release of water from $CuSO_4.5H_2O$ during the heating cooling cycles controls the reversibility of the reaction thus COF crystallinity gets drastically improved [1.33c].

1.6.5 Room temperature synthesis

It is possible to synthesis some of the COF at room temperature under certain reaction condition. Thomas Bein and coworkers were able to synthesize the thin films of COF-5 and BTD-COF via vapor assisted conversion method [1.34]. This method involve the drop casting of the boronic acid precursors on top of a glass slid, followed by a incubating them in a closed chamber. The chamber is also contains Mesitylene: dioxane solvent mixture (1:1) in a separate glass vials. As the time progresses the solvent vapors diffuses out from the glass vials and get filled inside the closed chamber. When the glass containing reactants get in contacts with solvent vapors reaction happens and COF thin film gets formed on the glass slide. It is important to note that solvent diffusion method is slow and a reaction time of 72 hours is required for the COF crystallite formation [1.34]. Crystallinity and surface area of the synthesized COF thin film is comparable to that of its solvothermal counterpart.

There is also some recent report were imine based COFs can be synthesized in room temperature. Josep Puigmartí-Luis and coworkers developed a micro-fluid based synthetic method by which imine COFs (MF-COF-1) can be synthesized at room temperature [1.34b]. The reaction process involves the injection of reactants and acetic acid in to separate nozzles (flow rate 100µL/ minutes) and mixing them inside main channel. The COF product get formed, and collected in the outlet within 11 seconds. However the concentration of the reactants and acetic acid is very crucial in micro-fluid based synthesis. If the concentration of reactants is too high then clogs used to form in the main channels, which will block the continuous flow synthesis [1.34b].

1.6.6 Mechanochemical synthesis

Mechanical method is a famous method to synthesize a wide range of materials at room temperature. The mechanochemical (MC) synthesis in COFs was first introduced by Rahul Banerjee and co-workers [1.35]. The process involve the grinding of reactants in a mortar and pestle (15 minutes) followed by heating them at high temperature (120 °C for 45 minutes). As compared to Solvothermal method MC synthesis is easy to perform, environmentally friendly, scalable and cost effective. However MC synthesized COFs posses disadvantages such as low crystallinity porosity, which was due to the delimitation of COF layer during the grinding process [1.35].

1.7 Applications of COFs

The high porosity, crystallinity and easy functionalizable nature, of the COFs made them useful for wide variety of application in the areas of storage, separation, catalysis, photo conducting materials, and sensors. The ordered and pre-designable nature of the COFs pores were utilized for storage application such as gas storage, drug and bio-molecule storage, doping of catalytic sites (***Figure 1.10***). The pi conjugated structures of 2D COF make them useful for application such as photo-conducting and charge carrier mobility. The important applications of the COFs are listed below.

1.7.1 Gas storage application

Most of the COFs are nano-porous in nature with pore size less than 2nm. Nano-porous materials are suitable candidates for gas storage application since the pores size has got a comparable match with the size of guest gas molecules. The high porosity, low density and pre-designable pores are the other attractive features for using them in gas storage application. COFs were tested for storage application of gases such as hydrogen (H_2), carbon dioxide (CO_2), methane (CH_4) and ammonia (NH_3).

1.7.2 Hydrogen storage:

Hydrogen is considered as one of the future energy source due its high energy density, and environmentally friendly nature. Cryogenic storage of hydrogen under high pressure is proved to be difficult because of its low boiling point (−252.8 °C) and explosive nature [1.35]. Microporous materials with high surface area and pore size less that 1 nm is considered to be ideal for hydrogen gas storage [1.36]. The targeted hydrogen storage value

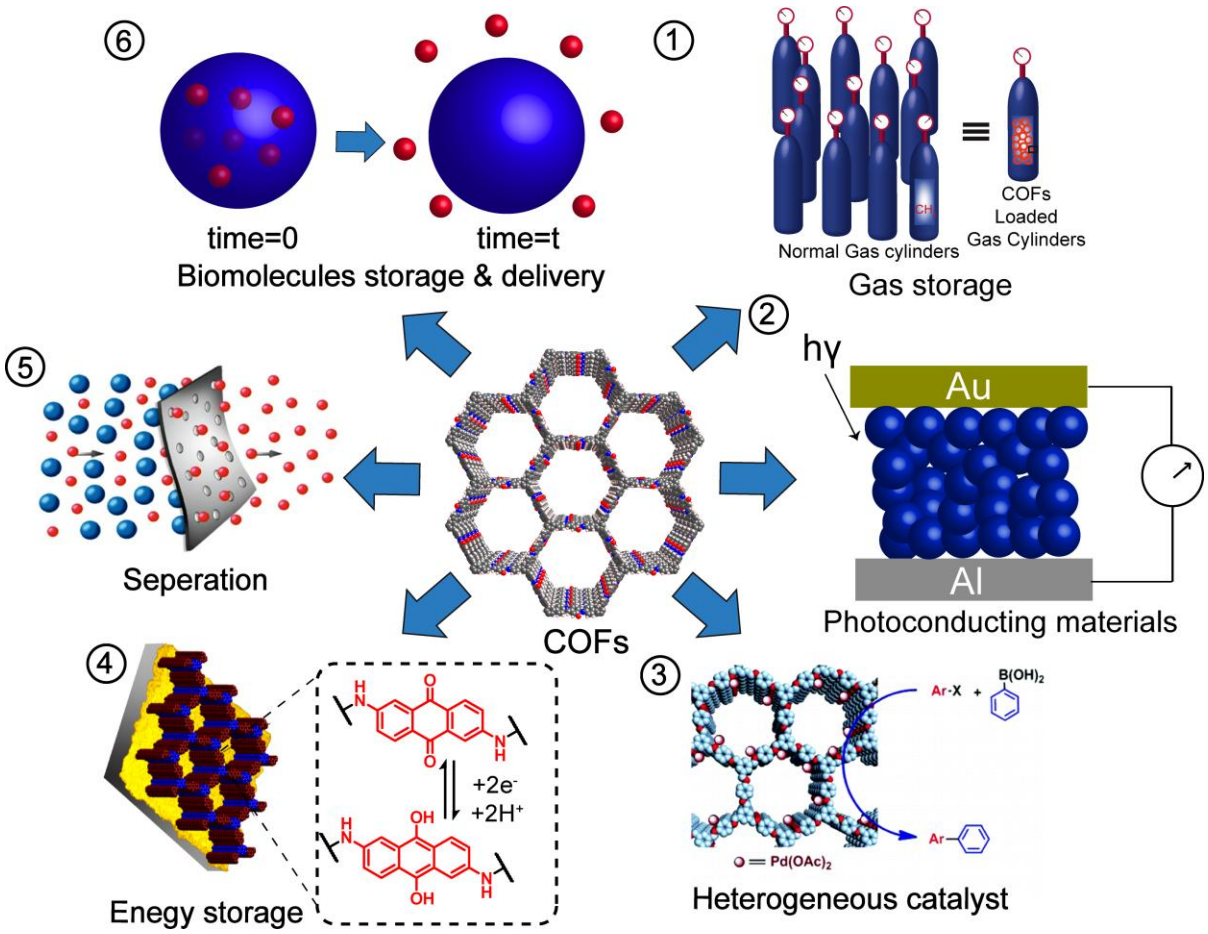

Figure 1.10: *Various applications of COFs such as gas storage, photo-conducting materials, heterogeneous catalysis, energy storage, separation and drug/bio molecules storage.*

set by US Department of Energy (DOE) till 2017 is 5.5 wt% at an operating temperature of 40 to 60 °C and a pressure of 100 atm. Several microporous COF were tested for H_2 storage application. The highest uptake of hydrogen uptake in COF was shown by 3D COF-102 (7.24 wt% at 77 K and 1 bar pressure) [1.23]. This H_2 storage value is comparable to that of MOF-5 (7.6 wt% at 77 K and 1 bar pressure) and MOF-177 (7.4 wt% at 77K and 1 bar pressure). The highly porous (S_{BET} = 3620 m^2g^{-1}) 3D framework structure and the shorter pore size (1.2 nm) enables COF-102 to have a high hydrogen storage value. The second highest hydrogen storage values is reported for another 3D COF, COF-103 (S_{BET} = 3530 m^2g^{-1}) [1.23]. Among 2D COF the highest hydrogen storage value was shown by COF-10 (S_{BET} = 1760 m^2g^{-1}) [1.37]. Although the hydrogen storage properties of the COFs at low temperature (77K) are excellent, at ambient conditions such as room temperature, hydrogen storage

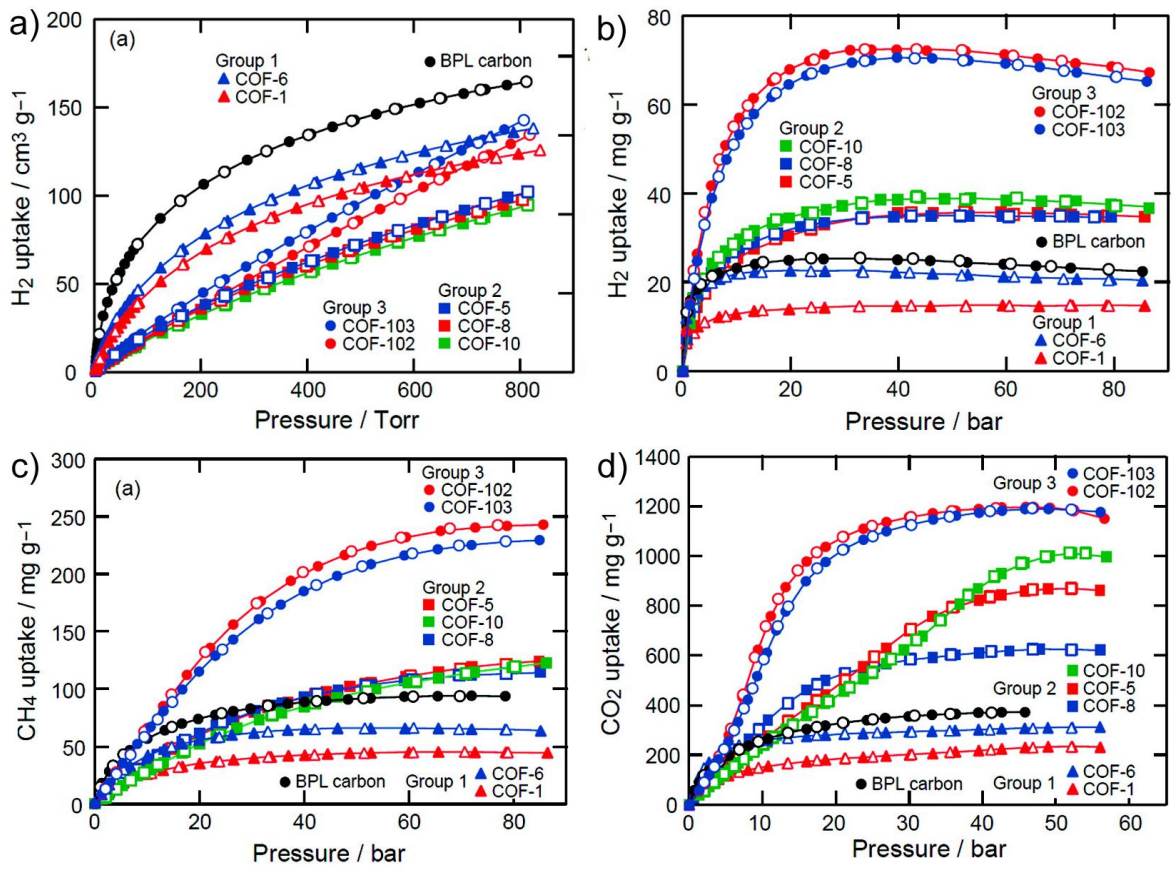

Figure 1.11. *Comparison of excess hydrogen uptake of different COFs (a) at 1 bar and (b) high pressure (open symbols represent experimental results, filled symbols simulated results). (c) Methane adsorption isotherms of COFs at high pressure. (d) Carbon dioxide adsorption isotherms of COFs at high pressure. [Reprinted with permission from Ref. J. Am. Chem. Soc., **2009**, 131, 8875[1.37], Copyright American Chemical Society, 2009].*

values are low as compared to the DOE targets. Theoreticians have predicted that hydrogen storage capacities of COF can be enhanced by increasing the binding energies of hydrogen molecules with the COF frameworks. One of the possible for achieving this target can be done by the doping of lithium ions inside COF pores. From Binding energy calculation using DFT, Møller–Plesset (MP), and Couple Cluster (CC) methods, theoreticians proposed that lithium doped COFs can be a promising candidate as hydrogen storage material [1.39].

***Table 1**: Hydrogen carbon dioxide and methane storage properties of COFs of different surface areas reported in literature.*

COF Name	BET Surface area (m^2g^{-1})	H_2 uptake (wt%)	CO_2 uptake (mg g^{-1})	CH_4 uptake (mg g^{-1})	References
COF-102	3620	7.24	1200	187	1.23
COF-103	3530	7.05	1190	175	1.23
COF-10	1760	3.92b	1010	80	1.37
CTC-COF	1710	1.12	—	—	1.38
COF-5	1670	3.58b	870	89	1.37
COF-8	1350	3.50b	630	87	1.37
COF-18A	1263	1.55 (1 bar)	—	—	1.28e
COF-14A	805	1.23 (1 bar)	—	—	1.28e
COF-16A	753	1.40 (1 bar)	—	—	1.28e
COF-6	750	2.26	310	65	1.37
COF-1	628	1.28 (1 bar)	—	—	1.37
COF-11A	105	1.22 (1 bar)	—	—	1.28e

1.7.3 Methane storage:

Methane gas is another promising candidate as an energy source for vehicular application. Currently high pressure (200 bar) is required for the effective storage of methane. The disadvantages of the high pressure storage can be surpassed by using porous materials for methane storage. It was proposed that porous materials can bring down the methane storage pressure up to 50 bar by keeping the energy density intact [1.40]. The targeted methane storage DOE target value set by US Department of Energy is 180 (v/v) at 35 bar pressure and room temperature. The high surface area, and easy functionalizable nature are the attractive features of the COFs, for testing them in methane storage applications. The highest methane storage value is reported for COF-102 (187 mg g^{-1} 35 bar and 298 K) [1.37]. The second highest methane value was reported for 3D COF COF-103

(175 mg g^{-1} 35 bar and 298 K) [1.37].

1.7.4 Carbon dioxide removal:

Carbon dioxide (CO_2) is one of the green house gas which contributes to the global warming effect. CO_2 is generated in larger amount by the combustion of fossil fuels. Flue gas emitted from various industries contains usually 10–15% of carbon dioxide. Removal of carbon dioxides from flue gas is one of the important issues for research [1.41]. Various porous materials such as zeolites, MOFs, porous carbons were tested for the CO_2 storage capacity. COFs were also tested for CO_2 storage application due to its ultra high surface area. Yaghi and coworkers reported the maximum CO_2 uptake of 27 mmol g^{-1} for COF -102 (at 298 K and 35 bar), which surpasses the performance of zeolites (8 mmol g^{-1}) and MOF-5 (22 mmol g^{-1}) [1.37]. Computational studies revealed that lithium doping in COF-102 and COF-105 can further improve the CO_2 uptake. Lithium doped COF-102 have predicted CO_2 storage capacity of 409 mg g^{-1} at 298 K and 1 bar which is around four times higher than the un doped pristine COF [1.42].

1.7.5 Ammonia storage:

Ammonia gas is an important raw materials in various industries such fertilizers, wood and paper industries. Ammonia is transported in compressed liquid form. Safe transport of the ammonia gas one of the major concerns. One of the efficient way to transport ammonia safely is to perform a reversible storage in porous materials. Boronic acid base covalent organic frameworks are one of the efficient candidates in ammonia storage. The

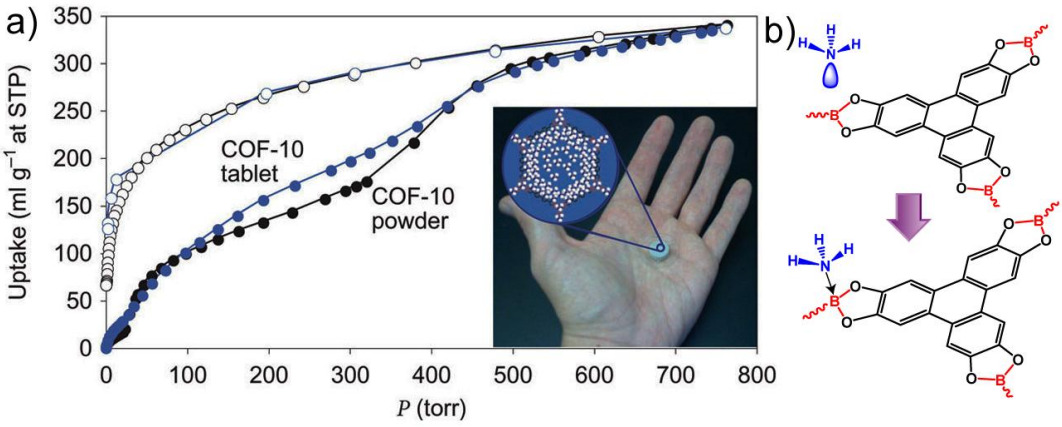

Figure 1.12: *(a) Ammonia adsorption isotherms of COF-10 powder (black) and tablet (blue). (b) Lewis adducts formation between ammonia and boronate ester. [Reprinted with permission from Ref. Nat. Chem.,* ***2010****, 2, 235[1.43], Copyright Nature Chemistry, 2010].*

Lewis acid sites in boronic acid based COFs can form strong but reversible bonding with ammonia. Yaghi and coworkers performed ammonia storage in boronic based COFs (COF-10) [1.43]. They found an ammonia storage capacity of 15 mol kg^{-1}at 1 bar and 298 K. This value is the highest ammonia uptake shown by any porous materials. COF-10 surpasses the commercially used porous materials such as zeolites 13X (9 mol kg^{-1}) and Amberlyst 15 (11 mol kg^{-1}) in terms of ammonia uptake [1.43]. Interestingly the ammonia uptake in COF-10 is completely reversible. The adsorbed ammonia in COF-10 can be released by heat.

1.7.6 Heterogeneous catalysis

The highly porous and easy functionalizable nature of the COF frameworks makes them attractive in heterogeneous catalysis application. It is easy to functionalize the COF pore walls by choosing proper building units for the framework construction. The COFs frameworks are insoluble in almost all solvent thus can be recovered easily from the reaction

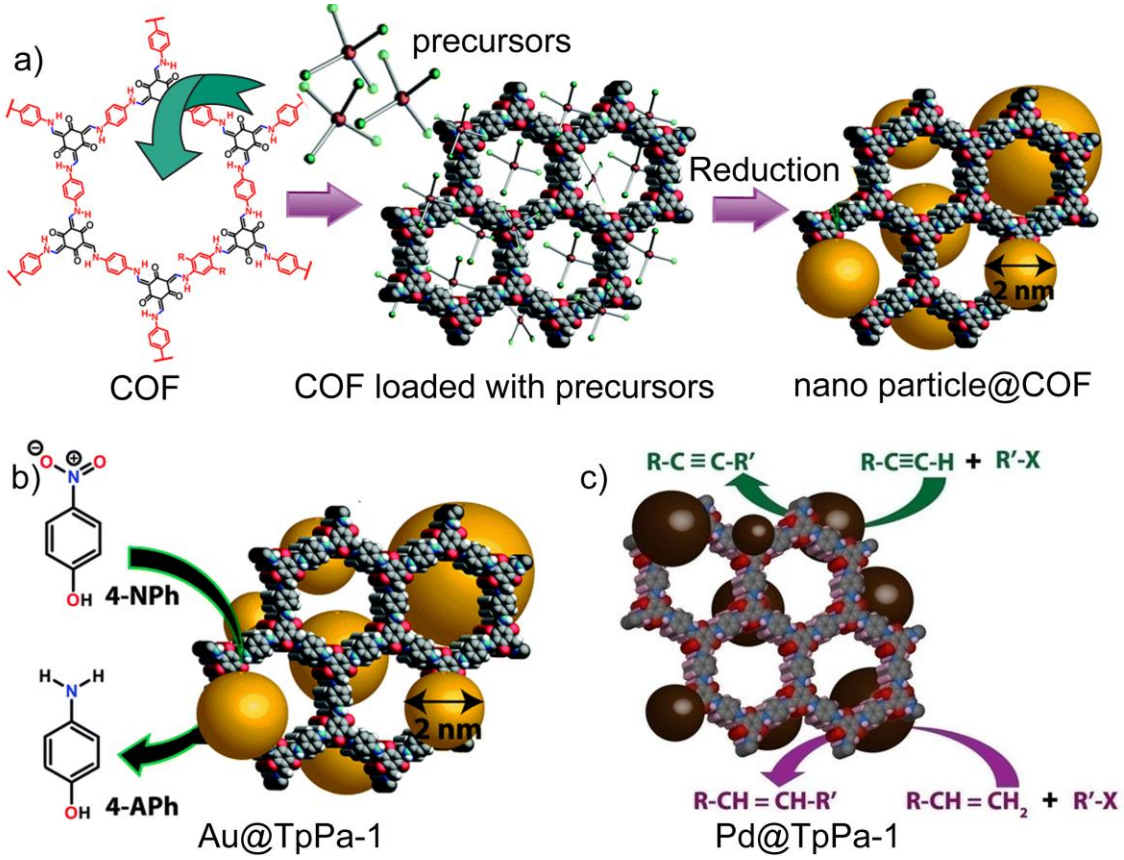

Figure 1.13*. (a) Schematic representation of synthesis of nano particle loaded COFs. (b) and (c) Catalysis performed by nano particle immobilized COF-TpPa-1. [Reprinted with permission from Ref. Chem. Commun.,* ***2015****, 51, 11717 and Chem. Commun.,* ***2014****, 50, 3169 [1.44c-d] , Copyright Royal Society of Chemistry, 2014-15].*

mixture without any significant weight loss [1.44]. The high porosity of the COFs allows easy diffusion of reactant molecules in to the catalytic sites to perform the reaction. The ordered and tunable pore channels of the COF can also help in size selective catalysis reaction. COFs can be designed in to a heterogeneous catalyst in two ways. 1) Incorporation catalytic sites in the building units [1.44a-b], 2) Doping of catalytically active nano-particles in to the COF pores [1.44c-d]. Wei Wang and Co-workers and coworkers have incorporated Pd^{2+} ions in to the imine COF (COF-LZU1) pore walls and performed Suzuki–Miyaura coupling reaction [1.44a]. They found out that the Pd^{2+} ions complexes with the imine nitrogen's of the adjacent COF layers (***Figure 1.10***). Rahul Banerjee and co- workers were able to immobilize Palladium (Pd) and Gold (Au) nano particle in β-keto-enamine based frameworks (**TpPa-1**) [1.44c-d]. The immobilization of the nano particles in COFs was performed in two steps (***Figure 1.13***). In the initial step, nano particle precursors ($AuCl_4$. $3H_2O$ and $Pd(OAc)_2$) were loaded in COF pores by simple stirring and incubation process. In the second steps the COF loaded precursors were subjected to reduction with sodium borohydride ($NaBH_4$). The Pd nano- particle loaded **TpPa-1** catalyst shows excellent activity towards C-H activation and C-C coupling reaction were as the Au nano particle loaded **TpPa-1** was used for the reduction of nitro compounds. The both catalyst are very stable and remain catalytically active even after five cycles [1.44c-d].

1.7.7 Photoelectric and semi conduction applications

Apart from the high porosity 2D-COFs also posses conjugated 2D sheet like structure analogous to graphene. The efficient long range π- π stacking interaction of the COF layers makes them suitable for semi conduction applications. When COF layers get stacks vertically on top of each other their pi- orbitals also get overlapped. The multiple overlapping between pi orbitals along c axis generates unique optical and electronic properties in COFs [1.22]. PPy-COF was the first COF tested for photoelectric application [1.45a]. Donglin Jiang and co-workers synthesized the PPy-COF by boronic trimerisation reaction between pyrene-2,7-diyldiboronic acid. Upon irradiation with visible light, Ppy-COF generates photocurrent of 5 nA (***Figure 1.14***) [1.45a]. The ordered stacked arrangement of pyrene moieties provide defined conduction paths for charge migration through the highly ordered structure (***Figure 1.14a***). In another report the same group have synthesized TP-COFs by the boronate ester formation reaction. TP-COF exhibit p-type semiconducting character, and display linear I-V

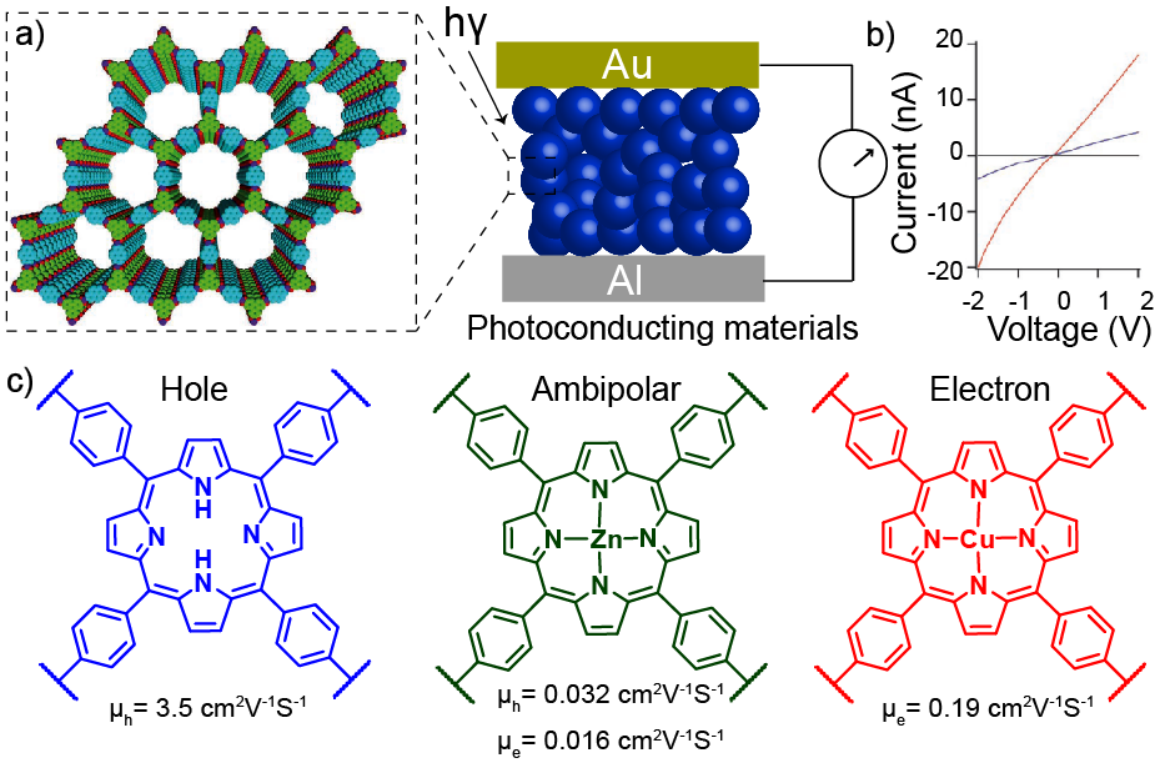

Figure 1.14 *: (a) Schematic representation of device set up used for the measurement of the photocurrent of TP-COF.(In the device COF powders (blue) were sandwiched between two electrodes). (b) I-V profiles as-synthesized TP-COF (blue) and iodine doped TP-COF (red). (c) Hole (μ_h) and electron (μ_e) carrier motilities of H_2P-COF (blue), ZnP-COF (green) and CuP-COF (red).*

curve [1.45b]. Further to extend the adsorption capacities of COFs in near infrared region, porphyrin and phthalocyanine moieties were used as building blocks. Donglin Jiang and co-workers have also synthesized three porphyrin based COFs, with different metal ions (Cu^{2+} and Zn^{2+}) at the porphyrin centers (***Figure 1.14c***) [1.45c]. The flash photolysis time resolved microwave conductivity measurement shows that different charge transport behavior in three COF. The metal ions present in the COF layers significantly affect the charge transfer properties. The metal free porphyrin COF (H_2P-COF) display hole transport capabilities, were as the Cu^{2+} doped porphyrin COF (CuP-COF) shows electron transport ability(***Figure 1.14c***). The Zn^{2+} doped porphyrin COF (ZnP-COF) surprisingly shown ambipolar characteristics [1.45c]. Omar M. Yaghi and coworkers have synthesized two porphyrin based imine COFs (COF-366 and COF-66) by reversible Schiff base reaction. Both of this COF display high hole carrier mobility (3.0 and 8.1 $cm^2V^{-1}s^{-1}$), which is highest among all the π-π

stacked layered structures [1.27d]. In another report Ni^{2+} porphyrin COF (NiPc-COF) showed light harvesting capabilities in visible and near infra red region and display a high hole carrier mobility of 1.3 $cm^2V^{-1}s^{-1}$ [1.45d]. In recent report Donglin Jiang and co-workers also attempted to synthesize new donor acceptor based 2D- COF ambipolar characteristics. 2D D-A COF display a hole mobility of 0.01 $cm^2V^{-1}s^{-1}$ and electron mobility of 0.04 $cm^2V^{-1}s^{-1}$ [1.45e].

1.7.8 *Energy storage*

The ordered porous framework structures of COFs can be utilized for energy storage application by the incorporation of redox active sites in the back born. The pioneering work in this area was reported by William Dichtel and co-workers. They have synthesized an anthraquinone based *β*-ketoenamine COF (DAAQ-TFP COF) by the Schiff base reaction between 1,3,5-triformylphloroglucinol and 2,6-diaminoanthraquinone [1.46]. Due the presence of anthraquinone moiety, DAAQ-TFP COF display reversible redox processes (***Figure 1.10***). More over due to the high chemicals stability, DAAQ-TFP COF able to maintain its capacitance property even after 5000 charge-discharge cycles[1.46a]. In another report the same group were able to fabricate DAAQ-TFP COF as oriented thin films. The capacitance measurement of thin film shows an improved value (3 $mFcm^{-2}$) in comparison to the randomly oriented COF powders (0.5 $mFcm^{-2}$) [1.46b]. Donglin Jiang and co-workers were able to impart redox-active characteristics to NiP-COF by post functionalizing them with organic radicals such as TEMPO. The TEMPO functionalize COF ($[TEMPO]_{100\%}$-NiP-COF) displayed a high capacitance value of 167 Fg^{-1} [1.46c].

1.7.9 *Separation*

The ordered channels of COFs were also utilized for the gas separation applications. Yanan Gao and coworkers have used COF-320 for H_2/CH_4 and N_2/H_2 separation application [1.47a]. The membrane fabrication was performed by the Schiff base reaction between reactants on the surface porous alumina ceramic support. The surface amine functionalities present on the surface of grafted alumina successfully hold the COF crystallites by imine bond formation. Even though authors were successful in preparing thin films membranes of COF on top of porous alumina, presence large number of inter crystalline voids reduces the overall gas selectivity of the membranes [1.47a]. Recently Rahul Banerjee and coworkers

were able to fabricate hybrid membranes of COF with PBI polymers. These hybrid membranes display moderate selectivity in CO_2/CH_4 and CO_2/N_2 separation. The covering effect on COF pores by polymer chains is one of the drawbacks of this mix matrix membrane, which prevent them in achieving high selectivity for separation [1.47b]. Theoreticians recently predicted that the self standing COF membranes are one of the options to reach high permeability and selectivity [1.47c]. But no current experimental methods area available for the fabrication of COF as freestanding membrane.

1.7.10 *Drug storage and delivery*

Since COF porosity can be extended to mesoporous region, scientist has attempted to load bigger sized drug/ bio-molecules in to the COF pores. Yushan Yan and coworkers designed a 3D polyimide based COF (PI-COF-4) for drug deliver application. PI-COF-4 displayed a high surface area of $2403 m^2 g^{-1}$ which makes them capable in storing ibuprofen (IBU) drug molecule [1.48]. From the UV-Vis studies authors were calculated drug loading capacity of PI-COF-4 as 20 wt%. The drug release profile shows a slow diffusion of drug molecules from the framework pores. The complete removal of ibuprofen (IBU) from the COF pores only happens after 6 days.

1.8 Chemical stability of COFs

Even though a diverse number of COFs are been synthesized and used in variety of applications, it suffers from a serious drawback, which is about its chemical stability. Since COFs are synthesized by reversible organic reactions, the possibility of reversible backward reactions still exists even after the COF synthesis. While coming in contact to water or humid conditions COFs in general get completely decomposed to the starting materials (***Figure 1.15***) [1.28a]. But for the real life application of the porous materials, chemical stability of the framework is one of the important aspects which should take in consideration. The gas storage application reported in COF materials till date are performed under anhydrous condition. But for practical gas storage application the adsorbents are expected to exposed to wide variety of reactive species such as water and acidic oxide (SO_2, H_2S, NO_2, etc.) [1.10d]. Even though the frameworks shows high gas storage capacity, the instability of the framework under the above mentioned condition will make them undesirable for practical gas storage application. Some general examples for the practical storage/ separation

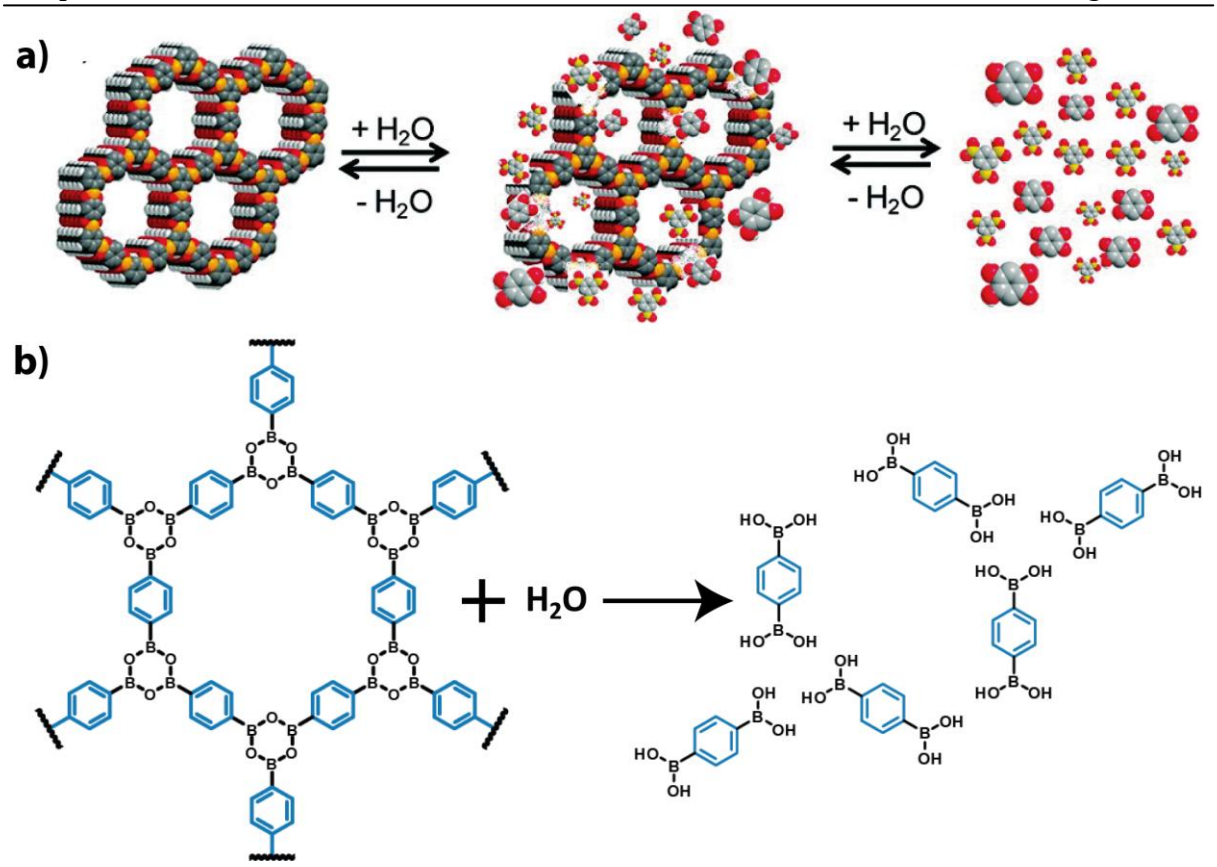

Figure 1.15. *Schematic representation of (a) as-synthesized COF (b) partial hydrolysis and release of monomers into solution upon submersion in water (c) completely hydrolyzed COF. [Reprinted with permission from Ref. 1.51a, Copyright American Chemical Society, 2011].*

condition which requires the chemical stability of the porous materials are 1) storage/ separation of natural gases, 2) removal of carbon dioxide from flue gases, 3) CO_2 capture from bio-fuel stream, 4) fuel cell hydrogen storage etc [1.10d]. Natural gas streams always contain water vapors during the excavation process. These water vapors must be removed completely before the transport and storage process of natural gas. The presence of water vapor in nature gas can creates clogs in the natural gas pipelines by the formation of clathrates. The humidity content can also decreases the heat value of the natural gas. Thus the porous materials used for natural gas storage/ separation must be stable to water. Chemical stability of the porous materials is also important in carbon dioxide sequestration process. Industrial flue gas also contain moisture and acidic oxides such as SO_2 H_2S and N_2O in addition to CO_2 and N_2 [1.10d] . The porous materials used for the CO_2 capture thus require high chemical stability in acidic and humid condition. Hydrolytic stability of the porous

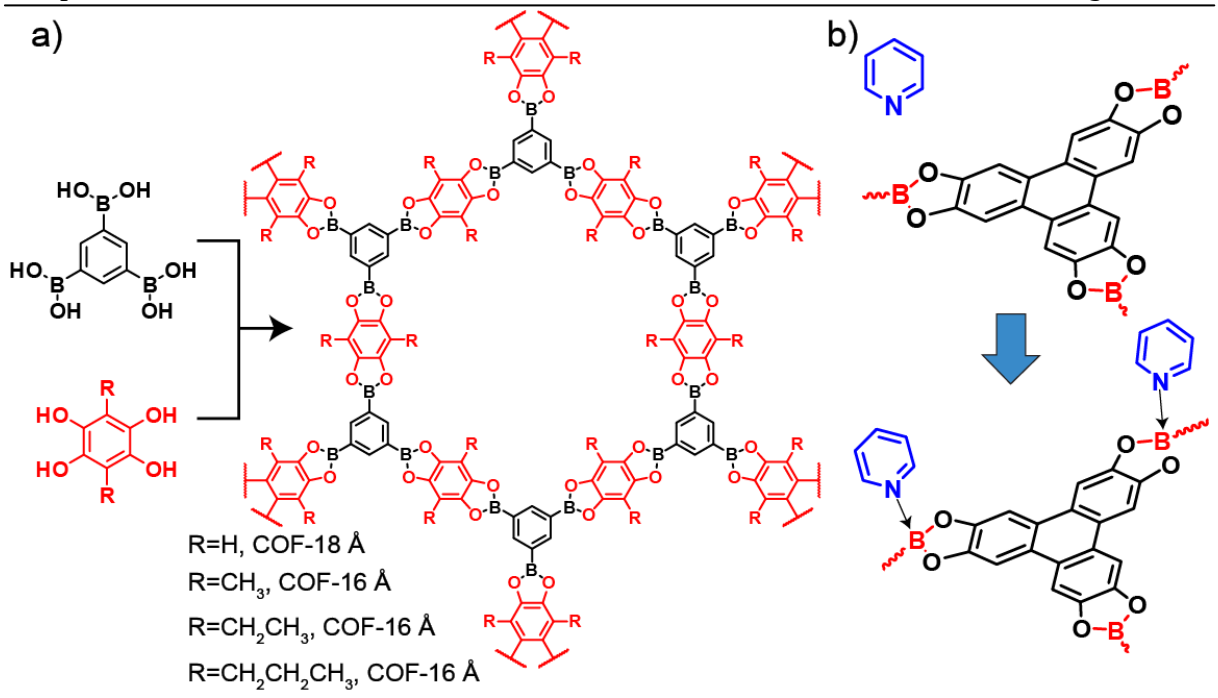

Figure 1.16. *Attempts done to improve the chemical stability in COFs (a) alkylation (b) doping of pyridine. [Redrawn with permission from Ref., Copyright American Chemical Society, 2011 and Ref. 1.51c, Copyright Royal Society of Chemistry, 2012].*

materials is an important aspect in hydrogen storage application. The H_2 storage is mainly performed for the fuel cell application. Fuel cell during the operation expels water as its end product. Thus fuel cell generally operates in humid condition. Hydrolytic stability of the porous framework material thus becomes essential for hydrogen storage application [1.10d]. Even though in dry condition COFs shows high storage capacity and placed many benchmarks in terms of total gas uptake values, in real condition they failed to perform due to their poor hydrolytic stability. The reason for the poor chemical stability COFs originates from the reversibility of the framework formation reaction. Even though the reversibility helps COFs attaining ordered crystalline structure, it becomes disadvantage when the chemical stability of the framework is considered. Thus there is an urgent need of improving the chemical stability of the COF framework materials in order make them suitable in real life applications.

Few attempts were done in literature to enhance the chemical stability of the COFs. The first attempt was reported by John J. Lavigne and coworkers in 2011[1.28a]. They have studied in detail about the hydrolytic stability of boronate ester base COFs (COF-18Å and its

derivatives) (***Figure 1.16***). COF-18Å is highly unstable to water treatment. When COF 18Å powders were submerges in water, the frameworks get decomposed to starting materials (***Figure 1.15***). Authors have proved this decomposition be various spectroscopic methods (UV absorbance and NMR). To perform the chemical stability experiment COF-18Å powders were enclosed in a filter paper and then directly submerged in water. After 20 minutes of treatment filter papers were removed and the PXRD and N_2 adsorption the recovered powders were recorded. As expected COF18Å loses it crystallinity and porosity after the water treatment process. To improve the chemical stability of COF-18Å authors have incorporated hydrophobic alkyl groups in side COF pores(***Figure 1.16a***). Based on the functionality the COFs were named as follows, COF-16Å (R=Me), COF-14Å (R=Et), COF-11Å (R=Pr). When a similar hydrolytic test was performed for these alkylated COFs, authors found improvement in hydrolytic stability as compared to the pristine COF-18Å. COF-16Å, COF-14Å, and COF-11Å do not show any significant framework decomposition after one hour of water treatment. Even though alkylation strategy was able to improve the COF framework stability up to one hour, it suffers some other disadvantages. The alkylation of the pores always decreases the surface area of the porous materials. COF -14Å have a surface area of only 496 m^2g^{-1} (which is 30% to the surface area of COF-18Å). Upon long term hydrolytic stability test (after 1 day) it was observed that the alkylated COFs (COF-16Å, COF-14Å. and COF-11Å) also starts slow decomposition. This result indicates that alkylation strategy is not a permanent solution for solving the chemical stability problem in COFs.

The second approach to improve the chemical stability of COF was reported by David Calabro and coworkers [1.28d]. They have improved the hydrolytic stability of COF-10 by pyridine vapor doping (***Figure 1.16b***). Boronate esters are prone to hydrolysis with water due to the presence of Lewis acid centers (boron). Upon hydrolytic treatment the Lewis acid centers get easily attacked by the water. This acid-base adduct formation, results in the framework decomposition. Authors, attempt was to block this Lewis acid centers with pyridine, in order to improve the hydrolytic stability of COF-10 (***Figure 1.16b***). The pyridine doping experiments was performed by submerging COF powders to 1 wt% solution of pyridine in dry acetone for 24 hours. The pyridine modified COF-10 showed superior hydrolytic stability in comparison to pristine COF-10. They remain stable and retain its

crystallinity even after 7 days of humid air treatment. But again this methodology could only improve the COF stability in humid air condition. Direct treatment of the pyridine doped COF-10 with water will cause a complete decomposition of framework. Thus there is a high demand of developing new methodology which could make COFs stable in extreme condition (water, acid etc) without altering the porosity and crystallinity.

1.9 Crystallinity and porosity of imine based 2D-COFs

Apart from chemical stability, the two important parameters which determine the quality of the COF materials are 1) crystallinity and 2) surface area. A highly crystalline and porous COF are the most desired candidates in gas storage, charge carrier mobility and catalysis application. Imine based COFs have much more improved hydrolytic stability in comparison to the boronic acid based COFs. But 2D imine based COFs suffers disadvantages

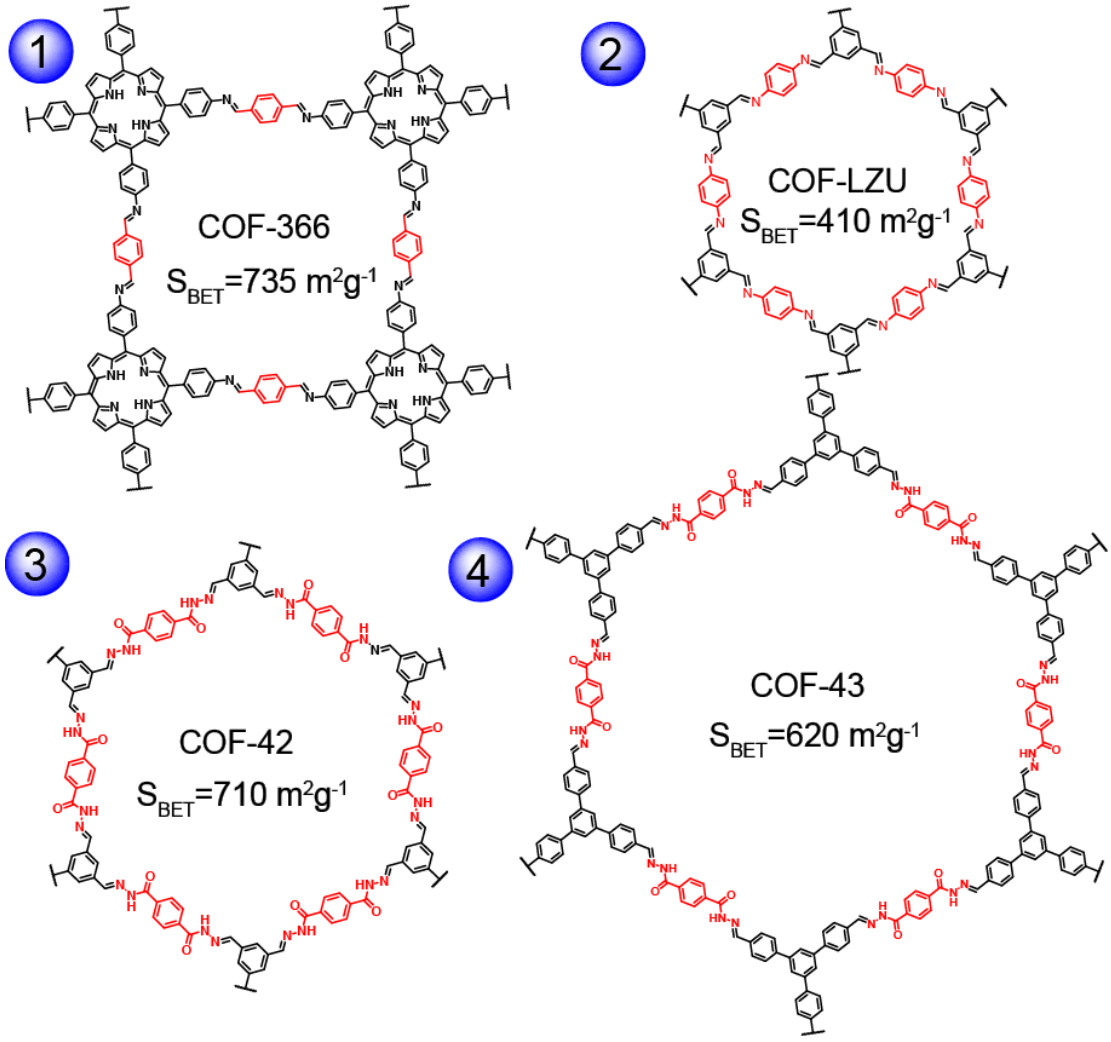

***Figure 1.17**: Structure and surface area of some of the imine 2D-COFs reported in literature.*

such as low porosity and crystallinity in comparison to the 2D-boronic acid based COFs. The surface area of the some of the 2D-imine based COFs are COF-366 (735 m^2/g) [1.27d], COF-42 (710 m^2/g^{-1}) [1.27b], COF-LZU (410 m^2/g^{-1}) [1.27c], COF-43 (620 m^2g^{-1}) [1.27b] (***Figure 1.17***). The probable reason for the low crystallinity of the imine based 2D-COFs is related to the low COF layer planarity and disorderness created by the isomeric imine bond formation during the crystallization. As compared to boronate ester ring and boroxin ring, imine bond linked units have low planarity. Moreover during the COF crystallization the possibility imine bond formation in multiple direction are more due the possibility of isomeric structures. If the crystallinity of the crystallinity of the imine COF were improved, they could be better candidates for gas storage/ separation application since it have an improved chemical stability. Donglin Jiang and co-workers introduced the concept of self complementary electronic interaction in imine COFs for improving the crystallinity and surface area of the porphyrin based imine COFs[1.49]. The COFs crystallinity and surface area was improved by managing the interlayer interaction of the COF layers (***Figure 1.18***). For this purpose authors have selected C_4 porphyrin tetra amine and fluoro and non fluoro substituted C_2 dialdehyde linkers for the COF formation. Authors have observed that when C_4 porphyrin tetraamine get reacted separately with fluoro or non fluoro substituted C_2

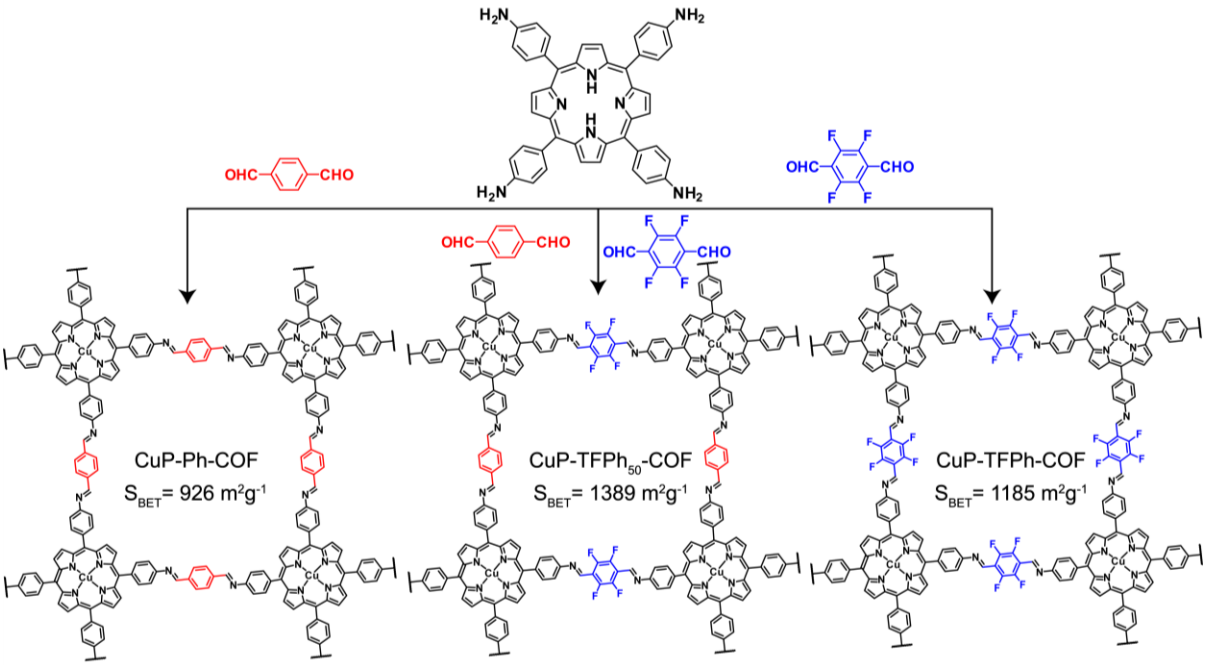

Figure 1.18*: The enhancement of crystallinity in porphyrin COFs by complementary layer stacking strategy.*

dialdehyde, crystallinity and porosity of the COF performed was moderate (***Figure 1.18***). But when a 1:1 Mixtures of fluoro and non fluoro substituted C_2 dialdehyde is allowed to react with C_4 porphyrin tetraamine a surprising improvement in crystallinity and porosity of the COF formed was seen. Authors explained this could be due to the self complementary interaction between the COF layers (***Figure 1.18***). Since tertraflouro C_2 linker is an acceptor molecule it can favorably π-π stack with the electron rich non flouro C_2 linker. This self-complementary interaction binds and stack COF layers more effectively the surface area and crystallinity of the mix link COF get improved [1.49]. Even though self complementary force enhances the crystallinity in porphyrin COFs, this method is system specific and cannot be generalized.

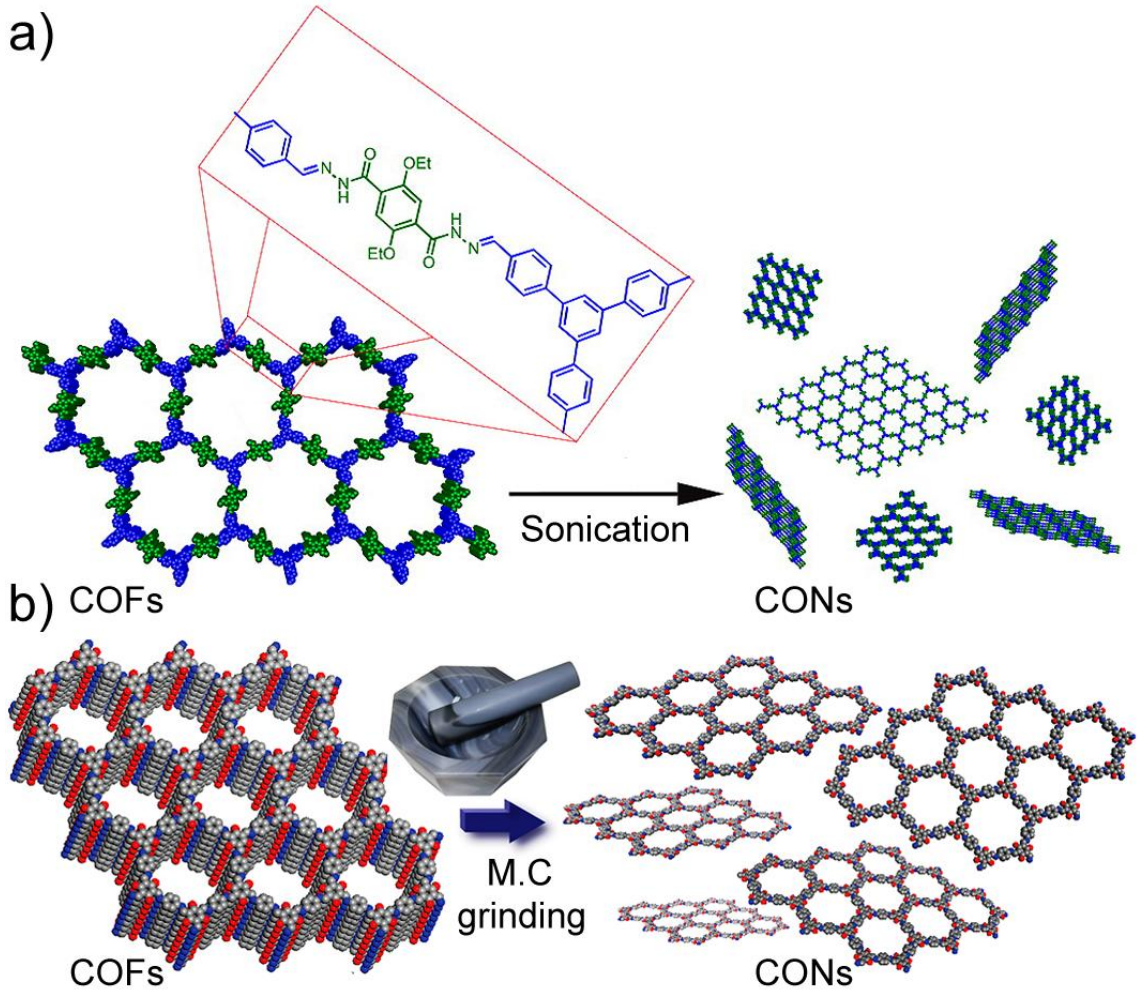

Figure 1.19. *Exfoliation of 2D-COF stacks to 2D-Covalent organic nanosheets via (a) mechanochemical approach, (b) Ultrasonication method. [Reprinted with permission from Ref, Copyright American Chemical Society, 2013].*

1.10 Covalent organic nano sheets

Sheet like structure are considered to be the basic morphologies in 2D-COFs. Other morphologies observed in COF are formed by the self assembly and selective growth COF layers in particular direction. Few attempts were performed in literature to exfoliate 2D COF layer stacks to its basic 2D- nano sheets morphologies. The pioneer works in this area was done by Rahul Banerjee and co-workers [1.50]. They have used mechnanochemical grinding to exfoliate the COF to 2D-nano sheets. Authors using this strategy were able to exfoliate a series of 2D-β-ketoenamine COFs (***Figure 1.19b***). The second attempt to exfoliate 2D-COFs was done by William Ditchel and coworkers (***Figure 1.19a***) [1.51]. They have used Ultrasonication to exfoliate COF-43. Authors have soaked initially COF-43 powders in various solvents in a 5 mL vial. The vial containing the COF powders and solvents were then subjected to sonication for 2 minutes. Dynamic light scattering measurement, scanning electron microscopy (SEM), Transmission electron microscopy (TEM) studies revealed the exfoliation of 2D-COF stacks in to ultra thin 2D-COF nano sheets. Even though the previous methods were able to prove the existence of the 2D-nanosheets morphologies of the COFs. The COF nano sheets synthesized were not subjected to any application because of the following problems. 1) The exfoliation yield is very low (less than 10%), 2) Possibility of restacking of COF layers after keeping the CONs suspension for long time, or solvent removal. Thus there is high need of developing novel methodologies which can perform the exfoliation of COF layers with high yield and high dispersional stability.

1.11 Morphology of COF crystallites

COFs are usually synthesized as microcrystalline powders, having their particle size in nanometer to micrometers ranges. The evolution internal defects during the crystal growth are responsible for the confinement of COF crystallite size in nano meter range. Li-Jun Wan and coworkers studied in detail about the COF crystallites growth at different time interval using scanning tunneling microscopy [1.33c]. For this study they have drop casted the starting materials on HOPG surface and then heated in a closed container. The STM images shows formation of COF on the surface of HOPG surface. But they have also noted that COF crystallites formation happen as island and it is very difficult to get a complete surface coverage (coating) of COFs. The presence of defects during the COF film formation restrict

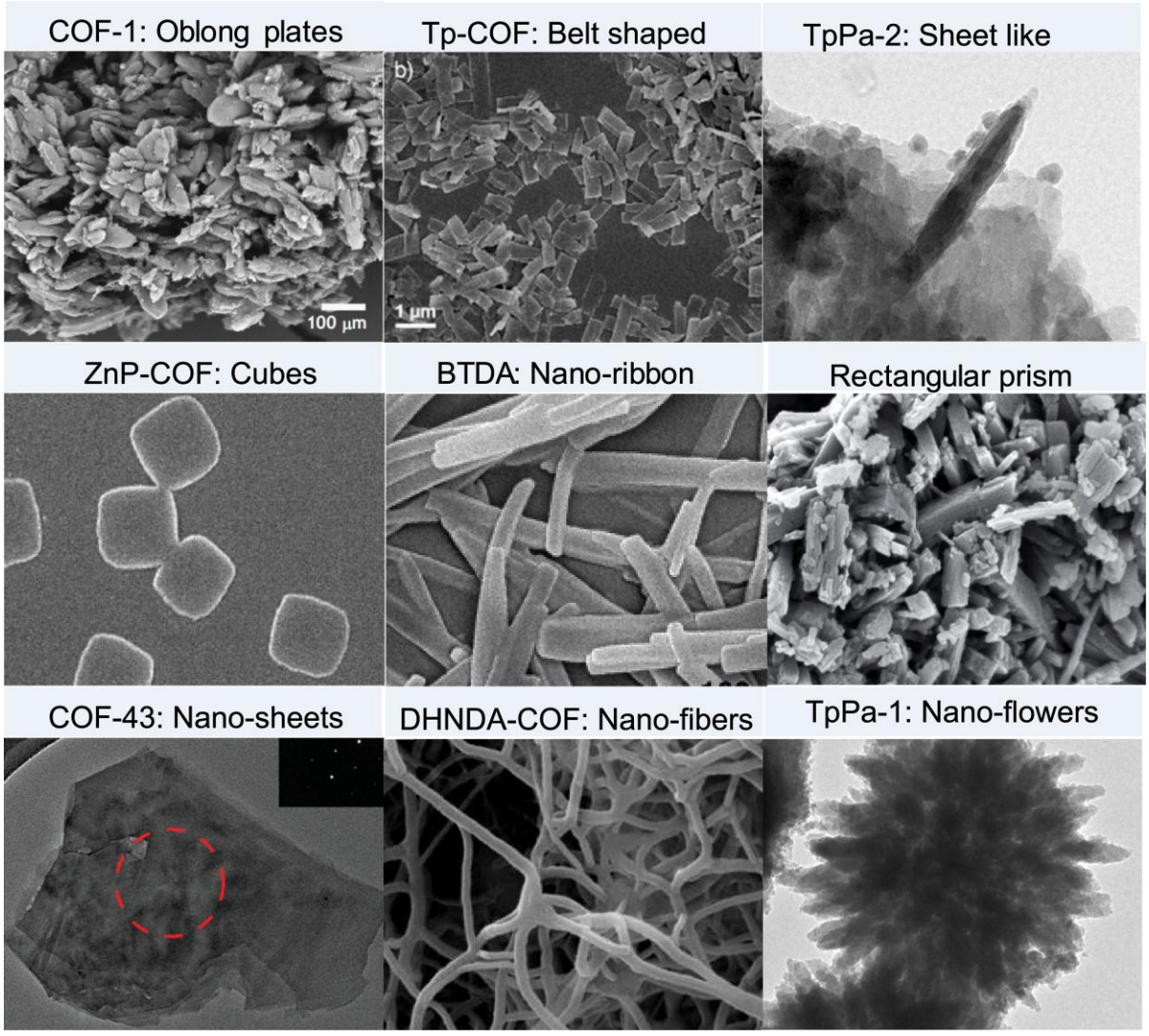

Figure 1.20: *Various Morphologies of COF crystallites reported in literature.*

them growing in larger domains. So based on the reaction condition and starting materials used COF crystallites reported to have adopted various shapes such as sheets [1.35], fibers [1.52], belts [1.45b], cubes [1.45a], rectangular prism [1.22a]etc (***Figure 1.20***). But the exact reason for the evolution such shaped in nano-domain still remains as a mystery. Shapes of the crystallites are important aspects should be considered in application such as molecular adsorption, charge carrier mobility and catalysis [1.53]. But detail investigation of the morphological evolution of COF crystallites has not been performed yet.

CHAPTER 2

Design and Synthesis of Chemically Stable 2D Covalent Organic Frameworks

Abstract: *In this chapter, we presented the novel strategy by which chemically stable Covalent Organic Framework (COF) can be synthesized. COFs in general are unstable to water and acids since they are synthesized by reversible reaction. Our strategy involve the synthesis of COFs by a combination of reversible and irreversible reaction. A reversible Schiff base reaction happens in the first step to form a crystalline framework, followed by an irreversible tautomerism to yield a keto-enamine base framework in the second step. Due the irreversible nature of the tautomerisation the synthesized COFs (TpPa-1 and -2 display high chemical stability in water and acids (9N HCl). We believe, our strategy can be further extended to synthesize a series of chemically stable COFs for real life gas storage applications.*

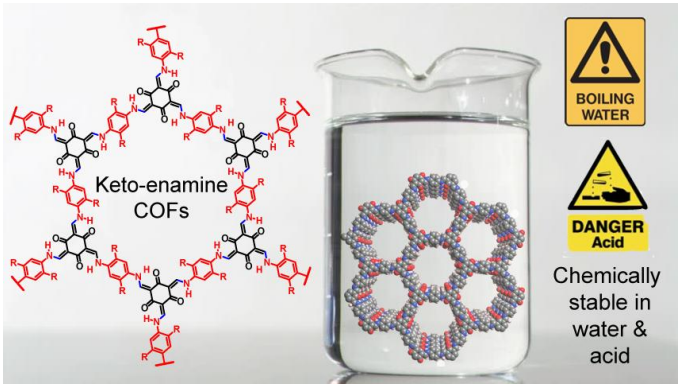

2.1 Introduction

The ultrahigh porosity and tunable pore channels makes Covalent Organic Frameworks (COFs), as an attractive candidate in wide variety of applications [2.1]. COFs were tested for applications such as gas storage [2.2], separation [2.3], catalysis [2.4], drug delivery [2.5], semiconducting application [2.6] etc. However the real life applications of COFs are yet to be realized due to the chemical stability issues [2.7]. As discussed in the previous section, Covalent Organic Frameworks (COFs) are synthesized by the reversible organic reaction (section 1.4) [2.8]. Reversibility in organic reaction highly essential to achieve successful crystallization [2.8]. Reversibility in COF formation reaction provides error checking and proof reading characteristics to the system. It allows the system to break and remake the bonds between linker units multiple times during crystal growth, and as a result, the most thermodynamically stable framework structures forms at the end [2.8]. Mainly three reversible organic dehydration reactions have been widely employed for the successful synthesis and crystallization of COFs. These are 1) boronic acid trimerisation [2.9], 2) boronate ester formation [2.10] and 3) schiff base reaction [2.11]. All these three reversible reactions involve the formation of water as a by-product. According to Le-chatelier's principle, the by-product water must be removed from the system in order to make the forward reaction (COF crystallization) feasible [2.8]. The removal of water from the reaction system was usually performed by utilizing vacuum, molecular sieves, and dry solvents [2.11]. Since the reversible back reactions can occur even after the synthesis, COFs crystallites get completely decomposed while coming in contact with water or ambient humidity [2.7]. Due to this hydrolytic stability issue, the practical implementation of COFs in real life gas storage/separation application has to be realized yet [2.7].

To improve the air and water stability of the COF materials few strategies were employed previously in the literature. Pyridine doping at Lewis acid sites [2.7b] and alkylation [2.7a] of COF pore walls were used to improve the chemical stability of boronate ester based COFs. Even though a slight improvement in chemical stability was achieved after doping; these modifications cannot be considered as an efficient strategy since the incorporation of the stabilization reagent in to the COF pores always decreases the gas

storage capacities [2.7]. Hence there is a high demand in developing new methodologies for improving the chemical stabilities of COF materials without altering its porosity and surface area.

We were able to solve this enduring chemical stability problem, by synthesizing two new chemically stable COFs (**TpPa-1** and **-2**) by a modified Schiff base reaction (***Figure***

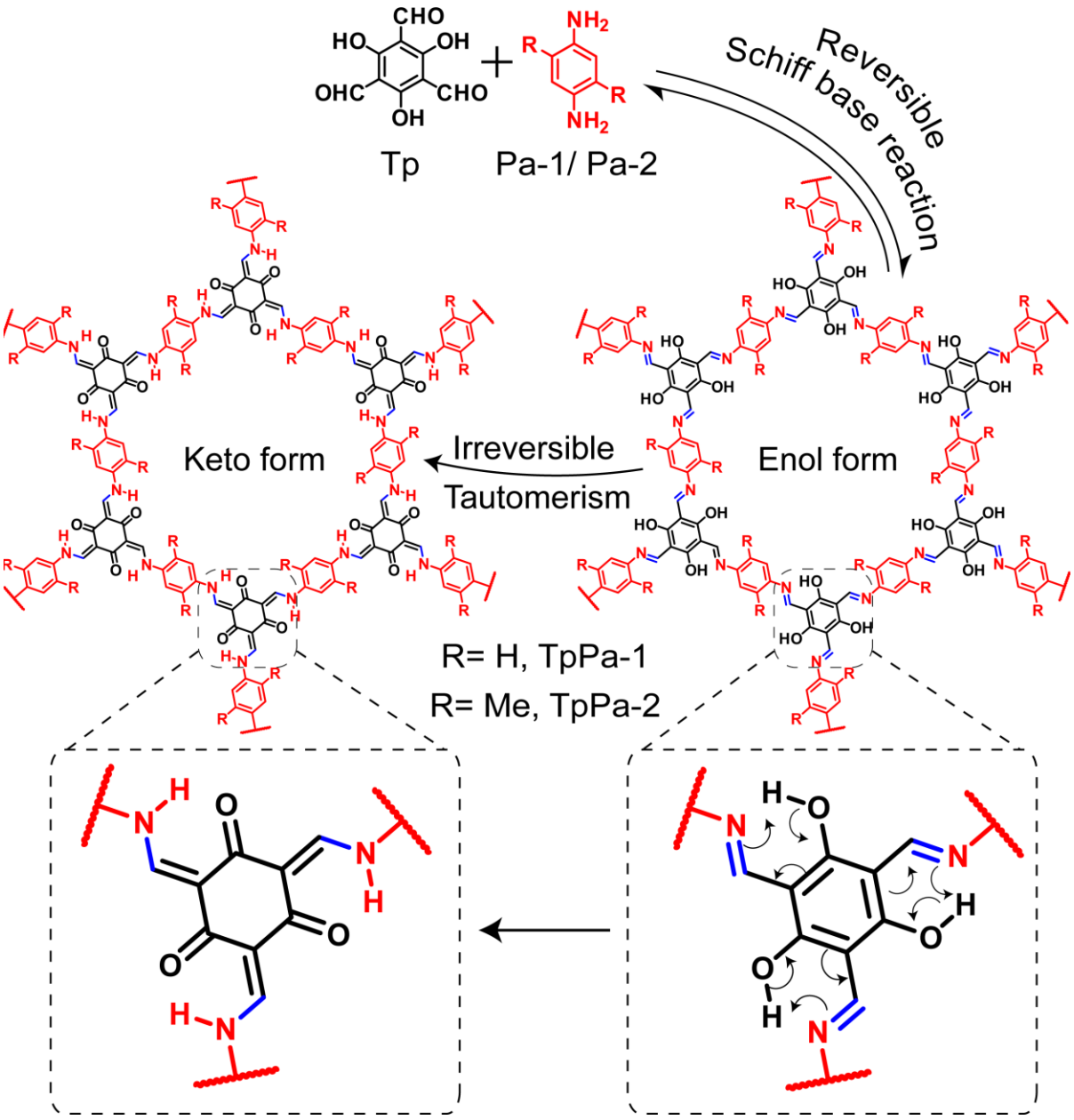

***Figure 2.1**: Schematic representation of the synthesis of highly stable β -Keto-enamine COFs by the combination of reversible and irreversible reaction.*

2.1). The overall COF formation reaction can be considered as the combination two steps. The ordered framework structure of COF was formed initially by the reversible Schiff base reaction between linker units. Followed by an irreversible tautomerism between phenol oxygen (-OH) and imine nitrogen (-C=N), which locks the framework structure in β-Keto-enamine form (***Figure 2.1***). The irreversibility in the proton tautomerization step does not perturb the crystallinity of the materials since the transformation involve only the rearrangement of few bonds while all the atomic position remains unchanged. Due to the irreversible nature of the combined COF formation reaction, the newly synthesized COFs (**TpPa-1** and **TpPa-2**) display remarkable chemical stability. These COFs (**TpPa-1** and **TpPa-2**) preserve its crystallinity, porosity and remain chemically stable in acid (9N HCl), base (9N NaOH) and water.

2.2 Result and Discussion

2.2.1 *Synthesis and characterization*

COF- TpPa-1: To a pyrex tube (i.d. × o.d. = 8 × 10 mm^2 and length 20 cm) 1, 3, 5-triformylphloroglucinol (**Tp**) (63mg, 0.3 mmol), p-phenylenediamine (**Pa-1**) (48 mg, 0.45 mmol), 1.5 mL of mesitylene, 1.5 mL of dioxane, 0.5 mL of 3 M acetic acid was added. This mixture was then sonicated for 15 minutes for obtaining a homogenous dispersion. After this, the pyrex tube was allowed flash frozen in a liquid N_2 bath (at 77K). Finally, the tube was subjected to vacuum degassing in three repeated cycles and sealed off under vacuum. The sealed tube containing the reactants is then placed undisturbed in a hot air oven at 120 °C for 3 days. After this time period, the sealed tube was broken and the insoluble COF powders formed was collected by filtration or centrifugation. The red colored COF powder collected was further purified by solvent exchanged with acetone 5-6 times and dried at 180 $^{\circ}$C under vacuum for 18 hours to give a deep red colored powder in 80% (89 mg) isolated yield. **IR (powder, cm^{-1}):** 1583 (s), 1579 (w), 1450 (s), 1254 (s), 1093 (m), 990 (s), 825 (s). **Anal. Calcld**. For $C_{80}O_{12}N_{13}H_{48}$: C, 69.4; H, 3.5; N, 13.9; found : C, 65.7; H, 3.32; N, 12.71;

COF- TpPa-2: The synthesis of **TpPa-2** was carried out by utilizing the same protocol with a mixture of 1, 3, 5- riformylphloroglucinol (**Tp**) (63mg, 0.3 mmol), 2,5-dimethyl paraphenylenediamine (**Pa-2**), (61 mg, 0.45 mmol), 1.5 mL of mesitylene, 1.5 ml of dioxane,

0.5 mL of 3 M aqueous acetic acid. The reaction mixture was heated at 120 °C for 72 h and after the reaction, the red colored solid at the bottom of the tube was isolated by centrifugation and washed with acetone. The COF powder was further purified by to solvent exchange (acetone 5-6 times) and then dried at 180 °C under vacuum for 18 hours (82% isolated yield. **IR (powder, cm^{-1}):** 2887 (w), 1587 (s), 1446 (s), 1254 (s), 1090 (w), 995 (s), 859 (m). **Anal. Calcld**. For $C_{80}O_{12}N_{13}H_{48}$: C, 73.13; H, 5.52; N, 10.9; found : C, 70.52; H, 4.87; N, 10.44.

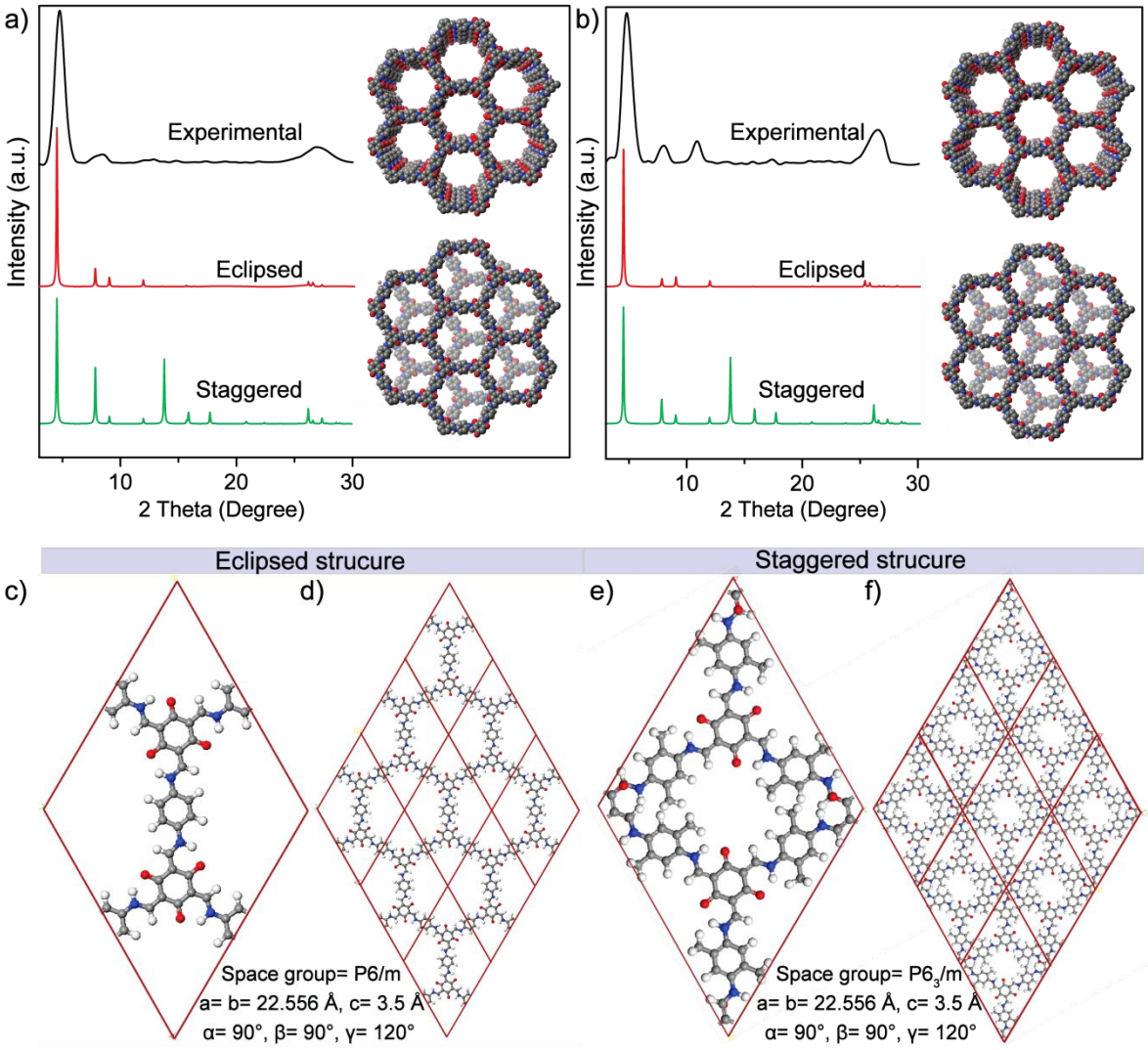

***Figure 2.2**: PXRD spectra of as-synthesized (black) compared with the eclipsed (red), staggered (green) stacking models for (a) **TpPa-1** and (b) **TpPa-2**. (c) Unit cell and (d) eclipsed crystal lattice packing of **TpPa-1**; (e) unit cell and (f) staggered crystal lattice packing of **TpPa-2**.*

2.2.2 *Structural simulation and characterization*

Since COFs are synthesized as polycrystalline powder, powder X-ray diffraction (PXRD) is used for determining the crystallinity and investigating the structural details of the material. PXRD patterns of both synthesized COFs (**TpPa-1** and **TpPa-2)** showed an intense peak at 4.7 ° followed by minor peaks at 8.3, 11.1 and 27 ° 2θ for **TpPa-1** and 7.9, 10.9, 26.5 ° 2θ for **TpPa-2** (***Figure 2.2a and 2.2b***). The peak assignment was done in the following order, the first intense peak corresponds to 100 plane followed by 210, 200 planes. The last peak appearing at 26.5° corresponds to the reflection from 001 plane. *d* spacing between 001 plane directly related to π-π stacking distance between the COF layers, which was calculated as 3.4 Å in **TpPa-1** and 3.5 Å in **TpPa-2**. In order to extract the structural details of **TpPa-1** and **TpPa-2** a possible 2-D crystal model structure was built with staggered and eclipsed stacking probabilities using the software material studio 6.1 (***Figure 2.2c and 2.2d***).

Table 2.1*: Fractional atomic coordinates for the unit cell (eclipsed) of* ***TpPa-1*** *and* ***TpPa-2****.*

COF-TpPa-1				**COF-TpPa-2**			
Hexagonal *P*6/m *a* = *b* = 22.556, *c* = 3.4 Å				Hexagonal *P*6/m *a* = *b* = 22.506, *c* = 3.4 Å			
Atom	*x*	*y*	*z*	Atom	*x*	*y*	*z*
O	0.28355	0.52709	0.5	O	0.75767	0.28474	0
N	0.41129	0.55212	0.5	N	0.55288	0.14095	0
C	0.30695	0.59146	0.5	C	0.71612	0.3075	0
C	0.38113	0.64063	0.5	C	0.64138	0.25951	0
C	0.42797	0.61784	0.5	C	0.61889	0.18979	0
C	0.45481	0.52704	0.5	C	0.52653	0.07196	0
C	0.42936	0.4559	0.5	C	0.5702	0.04388	0
C	0.52674	0.57065	0.5	C	0.45438	0.02665	0
				C	0.40464	0.05334	0

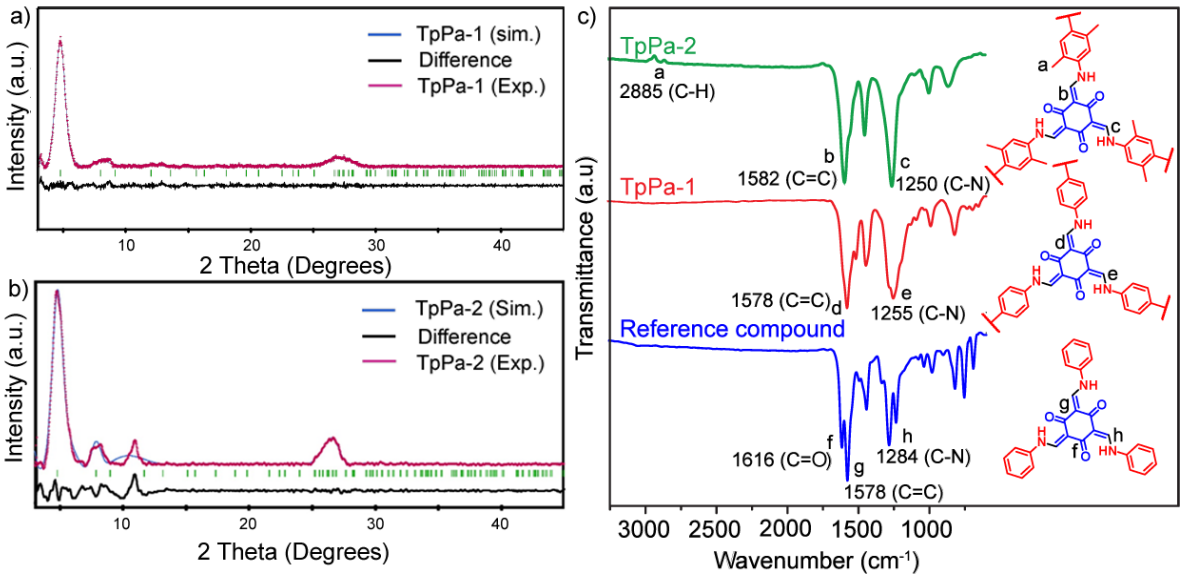

***Figure 2.3**: Experimental (Red) compared with refined (Blue) PXRD profiles of (a) COF-**TpPa-1**, (b) **TpPa-2** with an eclipsed arrangement; difference plot is given in (black). (c) FT-IR spectra of **TpPa-1** (red) **TpPa-2** compared with the reference compound, 2,4,6-tris((phenylamino)methylene)cyclohexane-1,3,5-trione (blue).*

For the eclipsed stacked structure the unit cell was built in hexagonal space group *P*6/m, and for the staggered structure, $P6_3$ space group was used for modeling. Experimental PXRD pattern was then compared with simulated PXRD patterns of both eclipsed and staggered models. It was found that experimental PXRD pattern has a greater match with the simulated pattern of the eclipsed stacking model. Pawley refinement was performed for both COFs **TpPa-1** and **TpPa-2** to elucidate the unit cell parameters (***Figure 2.3a and 2.3b***). The unit cell values of **TpPa-1** were determined as a=b= 22.556 Å, c= 3.5 Å, and for **TpPa-2** those values are a= b=22.506 Å, c= 3.4 Å, α= 90°, β=90°, γ=120°.

2.2.3 *Chemical characterization*

Fourier transmission infrared spectroscopy (FT-IR) spectra was recorded for synthesized COF **TpPa-1** and **-2**, which indicate completion of the reaction, as the characteristic stretching bands from the starting materials, such as primary amine (N-H) stretching bands (3000-3300 cm^{-1}) of **Pa** and the carbonyl stretching bands (1639 cm^{-1}) of **Tp** (***Figure 2.4a and 2.4b***) become absent in the FTIR spectra. To our surprise, the FT-IR spectrum of both COFs does not show the typical of hydroxyl (-OH) or imine (C=N) stretching bands from the expected an enol-imine form of the COFs. Instead, the spectrum

shows a new strong stretching band at 1578 cm^{-1} for **TpPa-1** and **TpPa-2** (***Figure 2.3c)***, which was assigned for the C=C stretching present in the β-Ketoenamine form, by comparing with the stretching frequencies of the reference compound reported in the literature [2.12]. The characteristic peak of carbonyl (C=O) functionality in β-Ketoenamine structure appears at 1615 cm^{-1} for **TpPa-1** and **TpPa-2**, which is very close to that of the reference compound (1616 cm^{-1}) [2.12] (***Figure 2.3c***). The shift in stretching bands of carbonyl functionality (C=O) to a lower frequency value was due to the strong intramolecular hydrogen bonding and extended conjugation in the structure. The main characteristic FT-IR peaks of the reference compound got a great match with that of **TpPa-1** and **2** (***Figure 2.3c***) indicating the existence of COF structure in β-Keto-enamine form. The extra peak at 2885 cm^{-1} appeared in the FT-IR spectrum of **TpPa-2** was assigned for the stretching from the methyl ($-CH_3$) functionality (***Figure 2.3c***). To establish the β-Keto-enamine linked framework structure of the COFs, cross-polarization magic angle spinning carbon-13 Nuclear Magnetic Resonance (^{13}C CP-MAS NMR) was recorded for both **TpPa-1** and **TpPa-2**. The absence of the signal from the aldehyde carbonyl (C=O), at δ=192 ppm in the ^{13}C CP-MAS spectra further, indicate the completion of the reaction and total consumption of the starting materials (***Figure 2.5a***). The clear signals appearing around δ=180 ppm (δ=182 ppm for

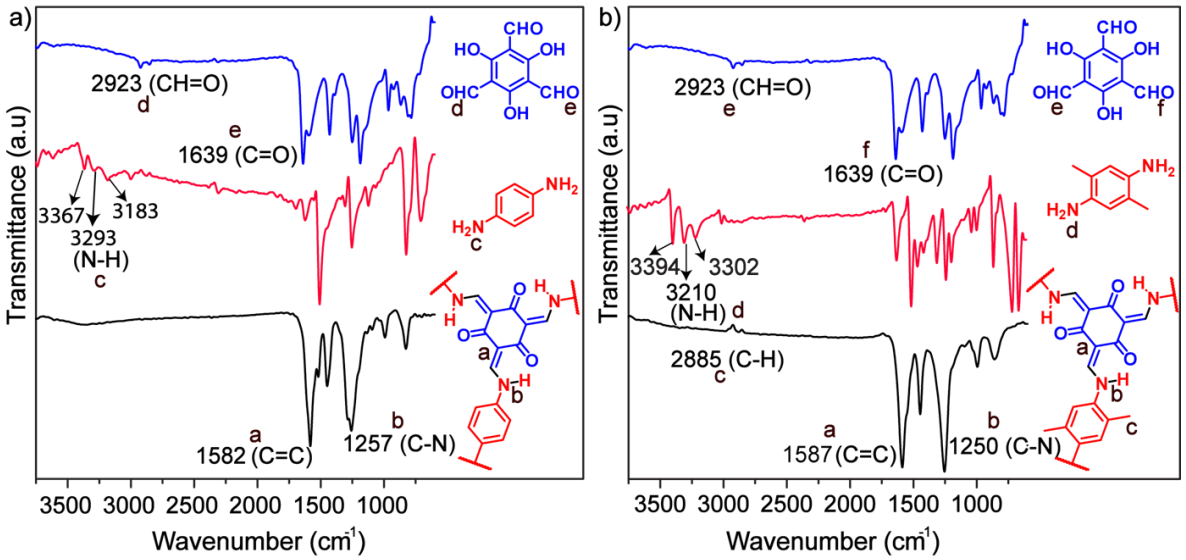

Figure 2.4*: (a) FT-IR spectra of* ***TpPa-1*** *(black) compared with starting materials p-phenylenediamine (red) and 1,3,5-triformylphloroglucinol (blue). (b) FT-IR spectra of* ***TpPa-2*** *(black) compared with 2,5-dimethylparaphenylenediamine (red) and 1,3,5-triformylphloroglucinol (blue).*

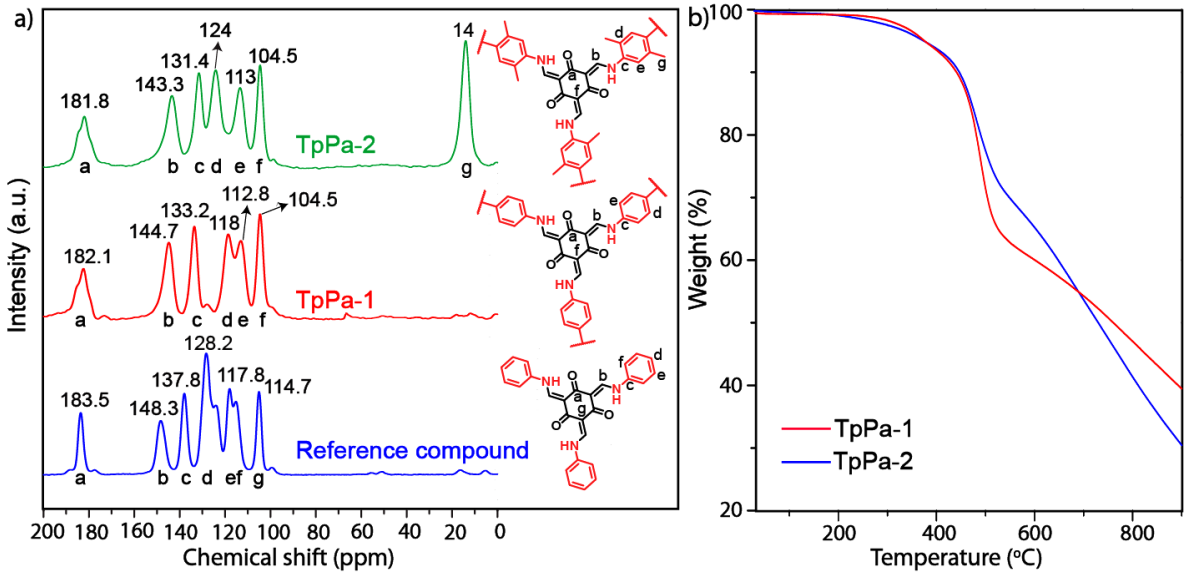

***Figure 2.5**: (a) ^{13}C CP-MAS spectrum of **TpPa-1** (Red), **TpPa-2** (green) compared with respect to the reference compound (blue).(b) TGA data of **TpPa-1** (red) and **TpPa-2** (blue).*

TpPa-1, δ=181.8 ppm for **TpPa-2** and δ=183.5 for the reference compound) corresponds to the signal from the carbonyl (C=O) carbon which undoubtedly confirms the β-Ketoenamine structure of COF **TpPa-1** and **-2** (***Figure 2.5a***). COFs are synthesized as microcrystalline powders, as their crystal growth limited to nano or micro domains due to large number of internal defects. Scanning electron microscopy (SEM) and transmission electron microscopy (TEM) are the commonly used method to identify the internal morphology of the COF crystallites. SEM images of **TpPa-1** and **-2** crystallites showed nano-flower like morphology having dimension 0.5- 5 µm (***Figure 2.6***). Upon closer inspection, it was observed that each nano-flower morphology is a result of the self assembly of a large number of nano-petals (***Figure 2.6***). For **TpPa-1**, nano-flowers, the petals are mostly of spike shaped (width 70-150 nm and thickness 30-40 nm) and for **TpPa-2** petals are much broader and appears to be plate like structure. The nano-flower type morphology was further confirmed from TEM images. Some of the TEM images of **TpPa-2** COF showed that individual nano-flower petals have a sheet like structure (***Figure 2.6c and 2.6 d***), which may be possibly arises due to π-π stacking between the COF layers. In-order to determine the thermal stability of the COF material thermo gravimetric analysis (TGA) was carried out for the activated samples (***Figure 2.5b***). The TGA profile does not show any significant weight loss before 350 °C, which indicates the high thermal stability of the materials. The gradual weight loss observed after 360 °C

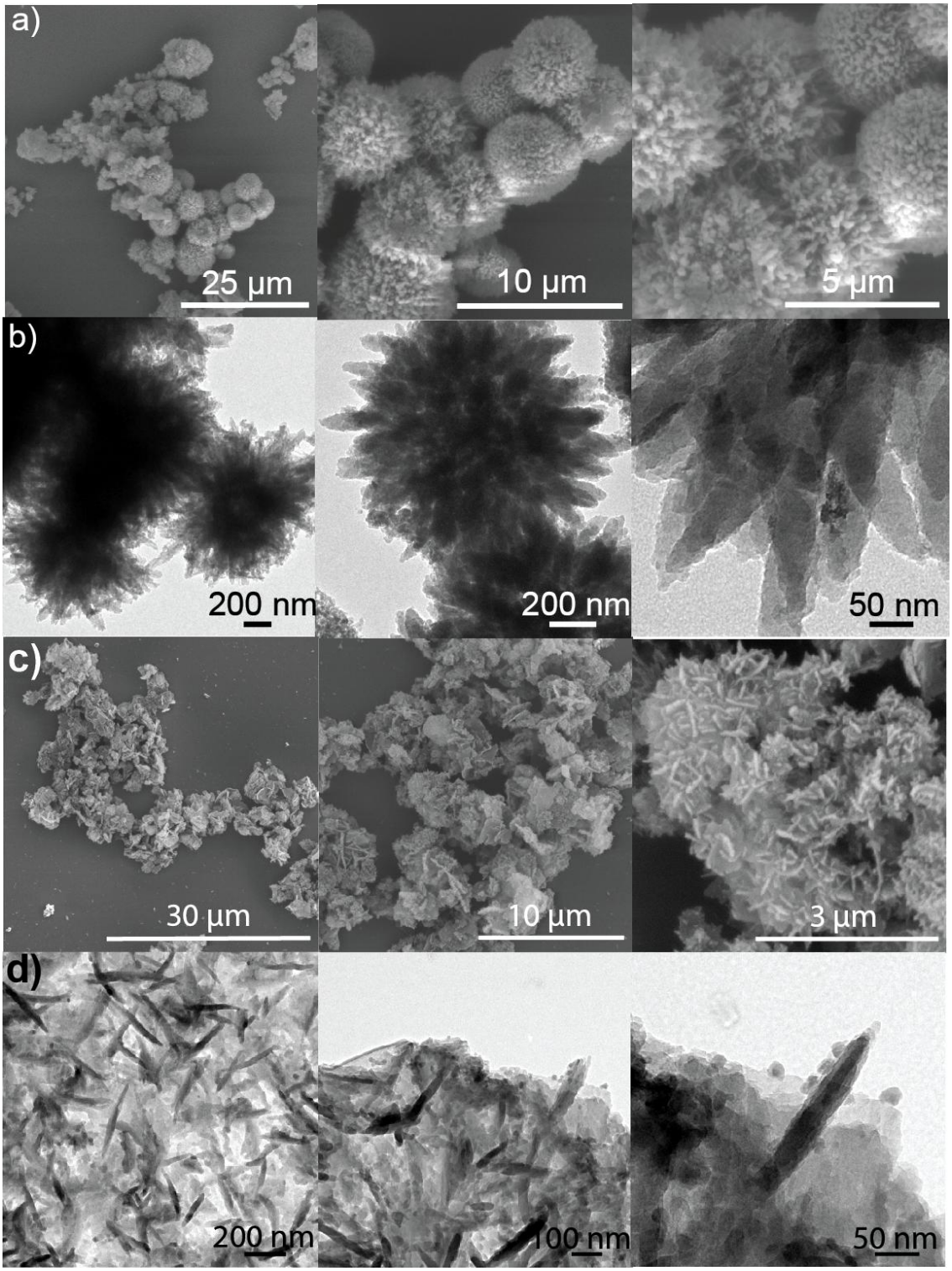

Figure 2.6: *(a) SEM and (b) TEM images of* ***TpPa-1*** *and (c) SEM and (d) TEM images of* ***TpPa-2*** *shows nano-flower like morphology.*

gradual may be probably due to the framework decomposition.

2.2.4 *Gas adsorption studies*

To evaluate the permanent porosity of the COF material (**TpPa-1** and **TpPa-1** -2) nitrogen (N_2) adsorption was performed for the pre-activated samples at 77 K. N_2 adsorption isotherm display a type-I isotherm for both COF, which is an indication of the microporous nature of the material (pore size <2 nm) (***Figure 2.7a***). Brunauer-Emmett-Teller (BET) model was used to determine the surface area of the COF samples. The BET surface area (S_{BET}) was calculated as 339 m²/g for **TpPa-2** and 534 m²/g for **TpPa-1**. The lower surface

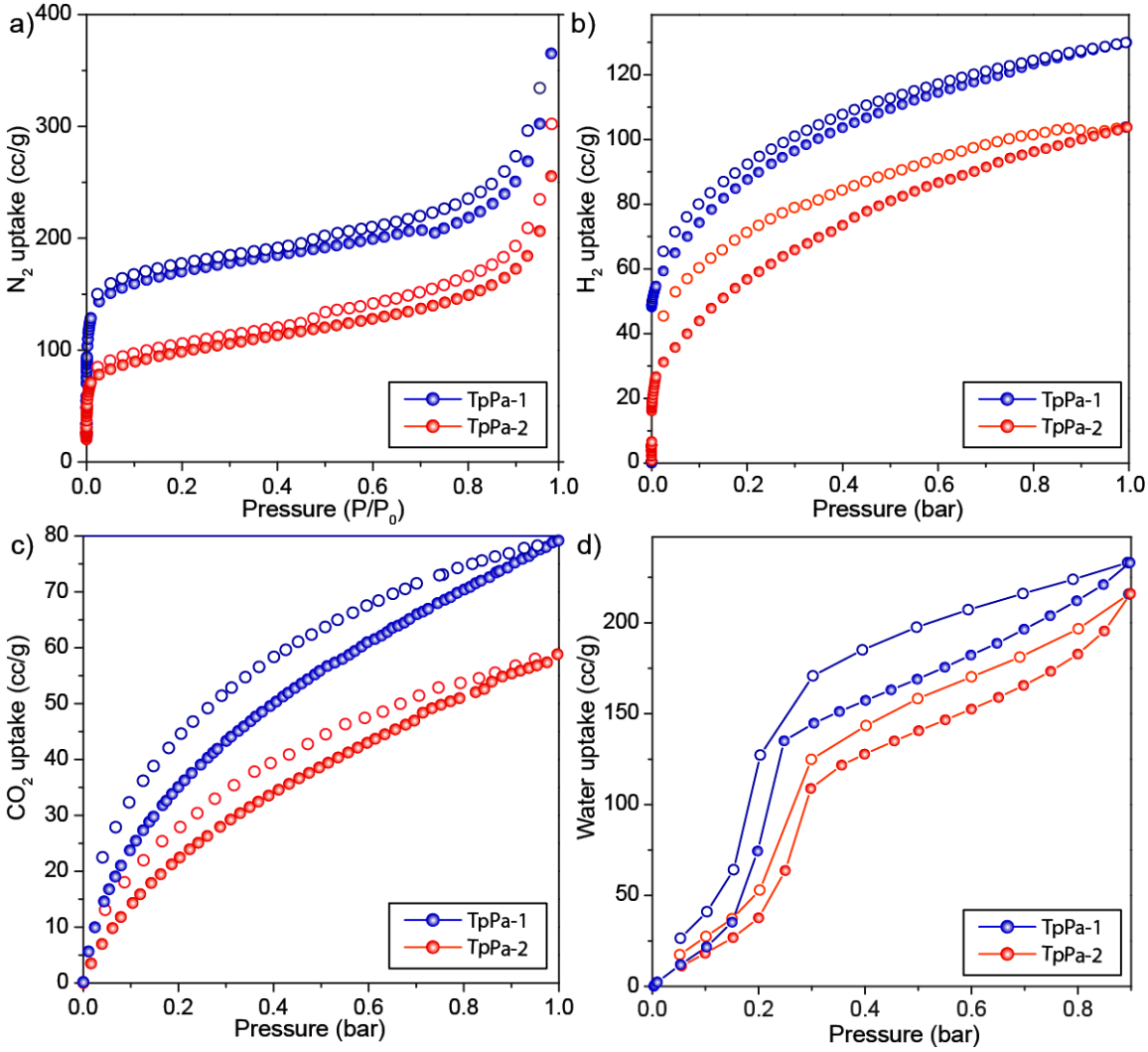

Figure 2.7: *(a) N_2 adsorption, (b) H_2 adsorption, (c) CO_2 adsorption, (d) water adsorption isotherms of* ***TpPa-1*** *(blue) and* ***TpPa-2*** *(red). The filled symbols correspond to adsorption and empty symbols represent desorption isotherms.*

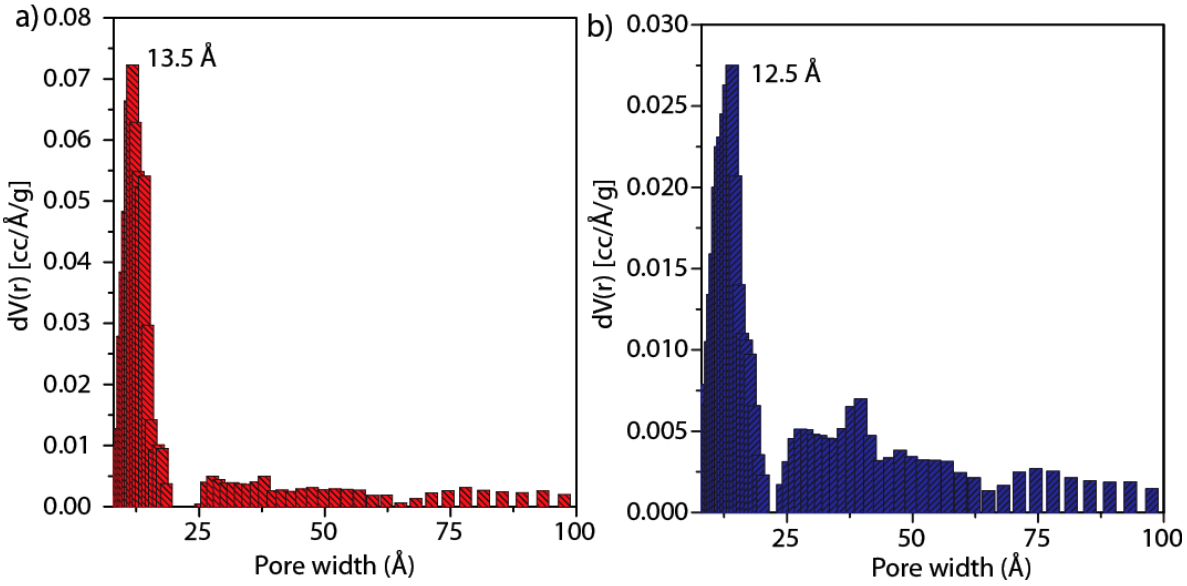

Figure 2.8: *(a) NLDFT pore size distribution of (a)* ***TpPa-1*** *and (b)* ***TpPa-2****.*

area of **TpPa-2** was due to the presence of extra methyl functionality in the pore channels. Langmuire surface area (S_L) calculation also showed a similar trend. COF **TpPa-1** got a higher S_L of 814 m²/g, whereas **TpPa-2** displayed a lower value of 506 m²/g. Non linear density functional theory (NLDFT) was used to determine the pore size distributions of COFs (**TpPa-1** and **TpPa-2**). NLDFT analysis shows that **TpPa-1** and **TpPa-2** posses a narrow uniform pore size distribution ranging between 0.8 - 1.5 nm (***Figure 2.8***). For **TpPa-1** the peak maxima were appeared at 1.35 nm and for **TpPa-2** it was coming at 1.25 nm (***Figure 2.8***). To further evaluate the gas storage properties of COFs (**TpPa-1 and TpPa-2**), hydrogen (H_2) and carbon dioxide (CO_2) adsorption isotherm was recorded. **TpPa-1 and -2** exhibit a moderate H_2 uptake of 1.1 wt% and 0.89 wt% (***Figure 2.7b***) at 77 K. These values are in close match with the performance of other COFs reported in the literature (COF-103→1.29 wt %, COF-102→1.21 wt%, COF-102→0.82 wt% and COF-52→0.84 wt%) [2.2]. CO_2 adsorption of **TpPa-1 and TpPa-2** was recorded at 273 K (***Figure 2.7c***). For **TpPa-1** CO_2 storage value was calculated as 78cc/g, while **TpPa-2** was able to store 64 cc/g of CO_2.

2.2.5 *Chemical stability investigation*

In real life gas storage and separation application, chemical stability of the host framework material is highly important. Natural gases saturated water vapors, humid

operating conditions in fuels cells, CO_2 capture from humidified bio-fuel stream are some of the practical examples were chemical stability plays a detrimental role in determining the performance of adsorbents. The porous framework adsorbent must be chemically stable to water and various acid impurities for their practical implementation in storage application. To investigate the chemical stabilities of COFs (**TpPa-1** and **TpPa-2)**, 50 mg of COFs powders were directly submerged in water (10 mL) for one week. After this time period, the COF materials were recovered by filtration and drying. PXRD and N_2 adsorption analysis were performed to analyze the retention of crystallinity and surface area of the recovered samples. To our surprise **TpPa-1** and **TpPa-2** display outstanding chemical stability in water.

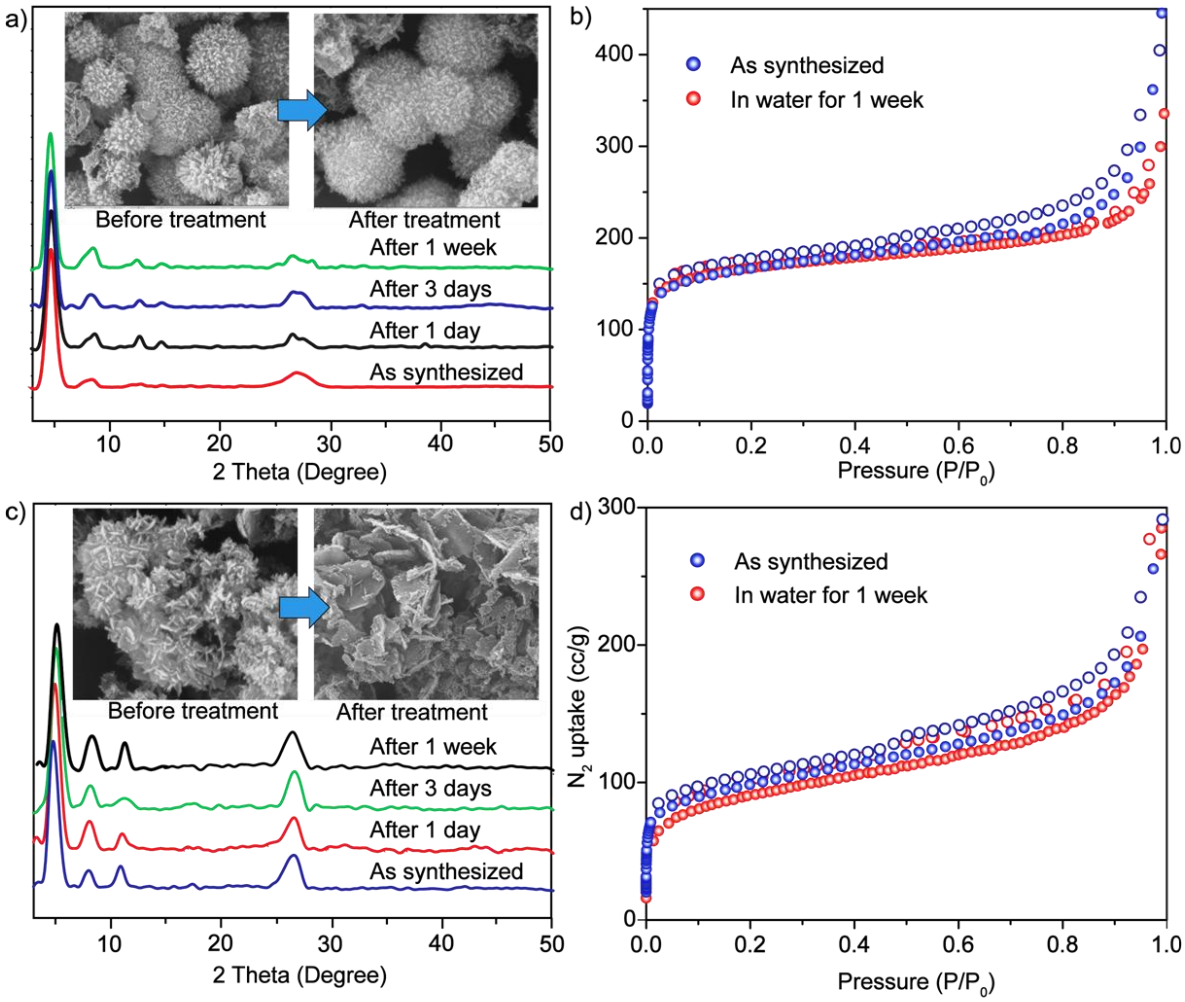

Figure 2.9: *PXRD of (a)* ***TpPa-1*** *and (c)* ***TpPa-2*** *after treatment with water for 1 week (inset: SEM images of COFs after the water treated samples shows the retention of morphology). N_2 adsorption isotherms of (b)* ***TpPa-1*** *and (d)* ***TpPa-2****, before and after the water treatment.*

The retention of peak position and relative peak intensity in the PXRD of the treated COFs indicates its high chemical stability (***Figure 2.9a and 2.9c***). To evaluate the surface area of the water treated COF samples N_2 adsorption isotherm was performed, which shows only a minor difference in surface area values (321 vs 339 m^2/g for **TpPa-2** and 520 Vs 535 m^2/g for **TpPa-1**), which confirms the high chemical stability of these COF materials (***Figure 2.9b and 2.9d***). To further evaluate the chemical stability, we have treated the COF materials (**TpPa-1** and **TpPa-2)** with hydrochloric acid (HCl) of different normality (1N, 3N, 6N and 9N) for one day. The acid treatment performed by directly submerging COF powders (50 mg) in HCl (10 ml). After filtration and drying COF powders were tested for their retention of crystallinity and porosity. COF powders do not show any color change or significant

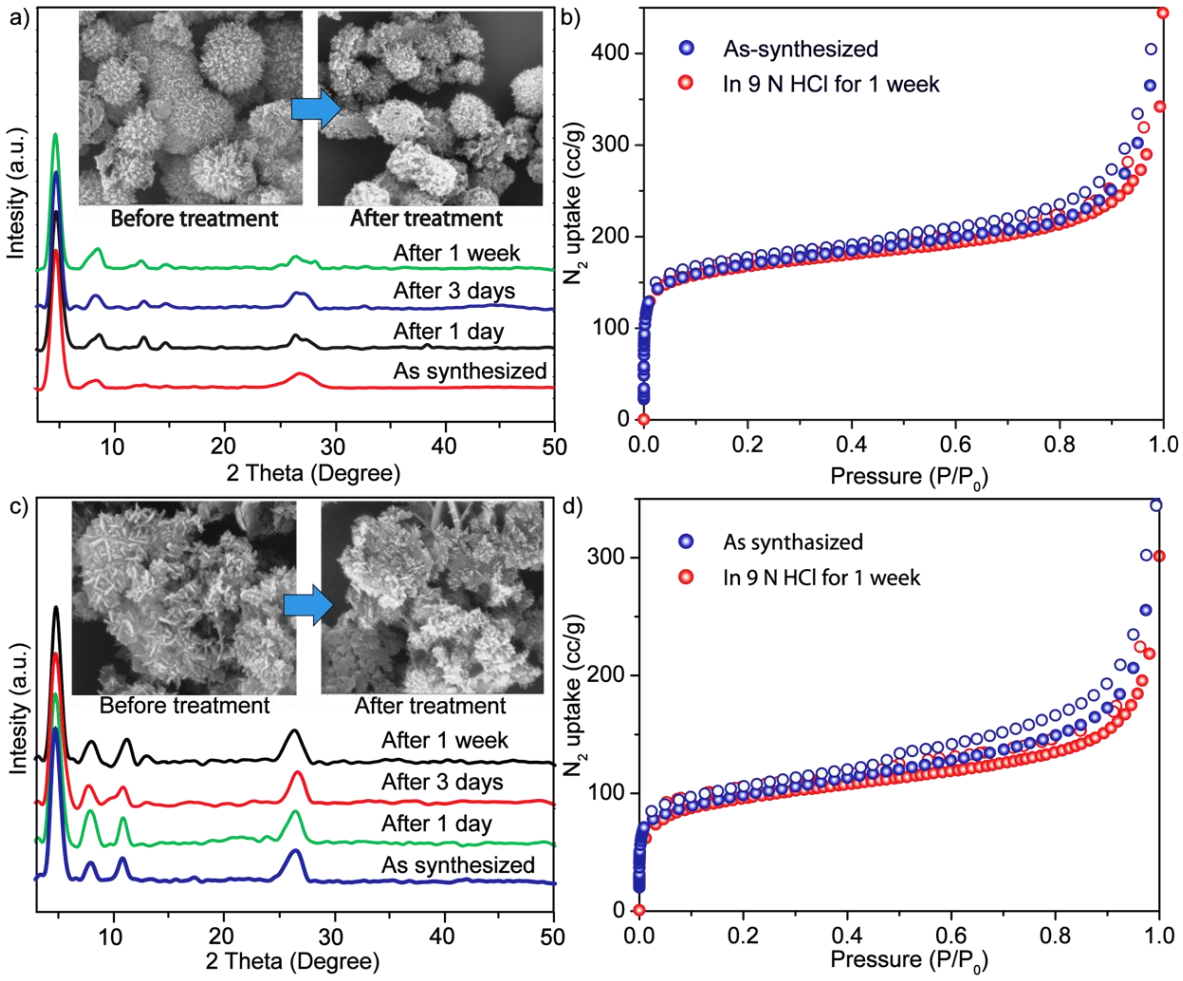

Figure 2.10: *PXRD of (a)* ***TpPa-1*** *and (c)* ***TpPa-2*** *after treatment with 9N HCl for 1 week (inset: SEM images of COFs after the acid treated samples shows the retention of morphology). N_2 adsorption isotherms of (b)* ***TpPa-1*** *and (d)* ***TpPa-2****, before and after the 9N HCl treatment.*

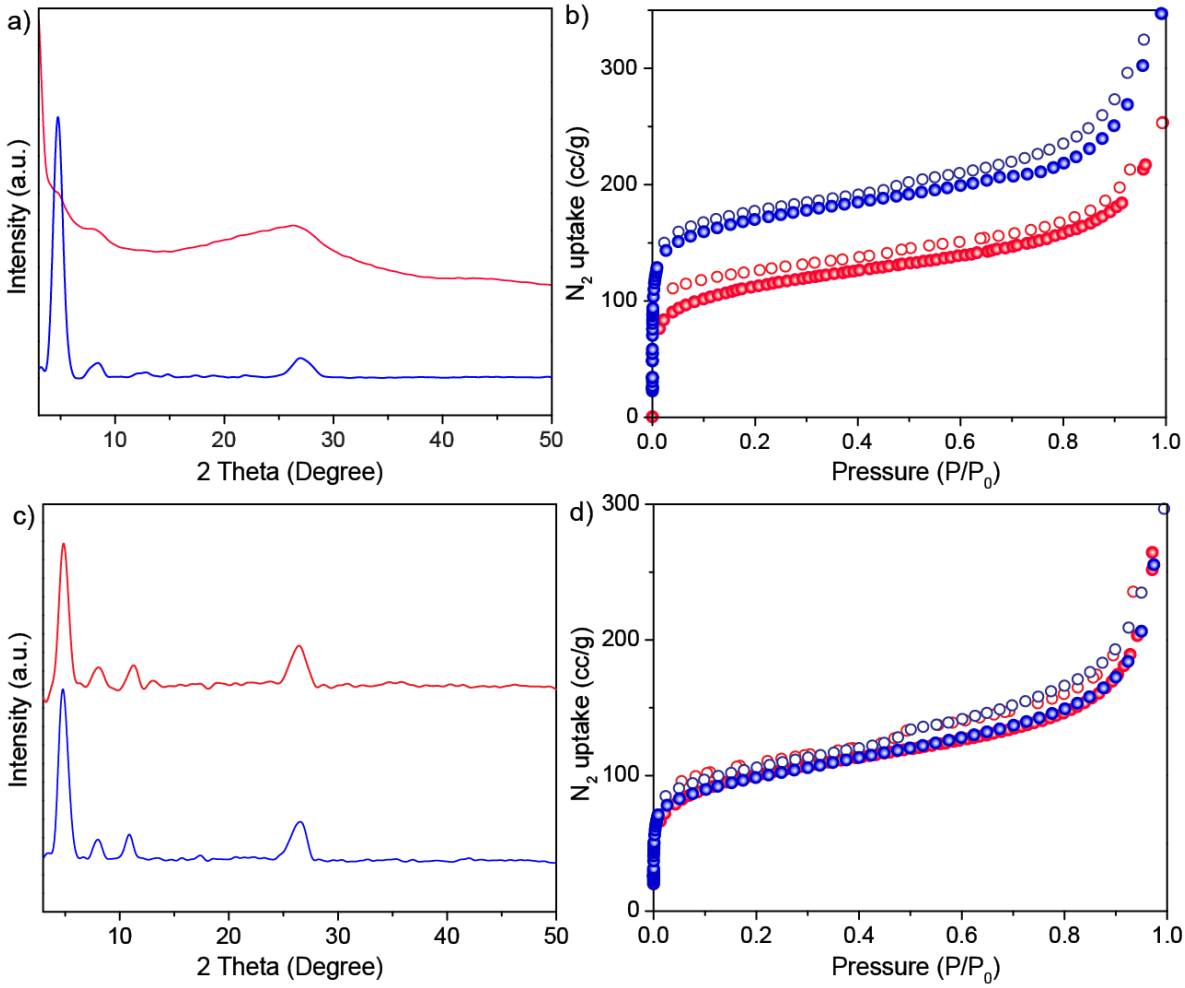

Figure 2.11: *PXRD of (a)* ***TpPa-1*** *and (c)* ***TpPa-2*** *before (blue) after (red) treatment with 9N NaOH for 1 day. N_2 adsorption isotherms of (b)* ***TpPa-1*** *and (d)* ***TpPa-2****, before (blue) and after (red) the 9N NaOH treatment.*

weight loss after the acid treatment. The PXRD and surface area values of the acid treated COFs were identical to the pristine COFs, which confirms β-Ketoenamine COF frameworks are highly resistance to acids (***Figure 2.10***). Finally, to evaluate the base stability, **TpPa-1** and **TpPa-2** were treated with 9N NaOH for 7 days. Interestingly COF **TpPa-2** retains the PXRD peak position even after seven days NaOH (9N) treatment (***Figure 2.11c***). The retention of peaks in FT-IR spectra and the unchanged surface area (324 m^2/g) further confirms the base stability of **TpPa-2** (***Figure 2.11d***). But **TpPa-1** shows a significant loss of PXRD peak intensity after one day 9N NaOH treatment (***Figure 2.11a***). After the filtration and purification, only 60% in weight of the **TpPa-1** material is recovered. Even though

characteristics peaks were retained in FT-IR spectra, surface area measurement shows a decrease by 50% (***Figure 2.11b***). This decrease in surface area of **TpPa-1** may be due to the partial loss of crystallinity upon base treatment. The unusual chemical stability of **TpPa-1** and **TpPa-2** was the result of irreversible nature in the COF formation reaction. Since the tautomerisation step locks the framework structure in β- ketoenamine form the backward framework decomposition reaction become less feasible. A similar type of enol-keto tautomerism can be possible in mono substituted N-Salicylideneanilines (***Figure 2.12a***). But in that case, only enol form is observed. There are two main factors which decide the stability of the tautomeric forms which are 1) acid-base interaction between imine nitrogen (C=N) phenolic oxygen (O-H) and 2) aromaticity [2.14]. In the case of mono substituted Schiff base compounds (N-Salicylideneanilines) the system loses the aromaticity after the tautomerisation. Since aromaticity being the most dominating factor the compound get stabilized in enol form (***Figure 2.12a***). But in the case of tri substituted Schiff base

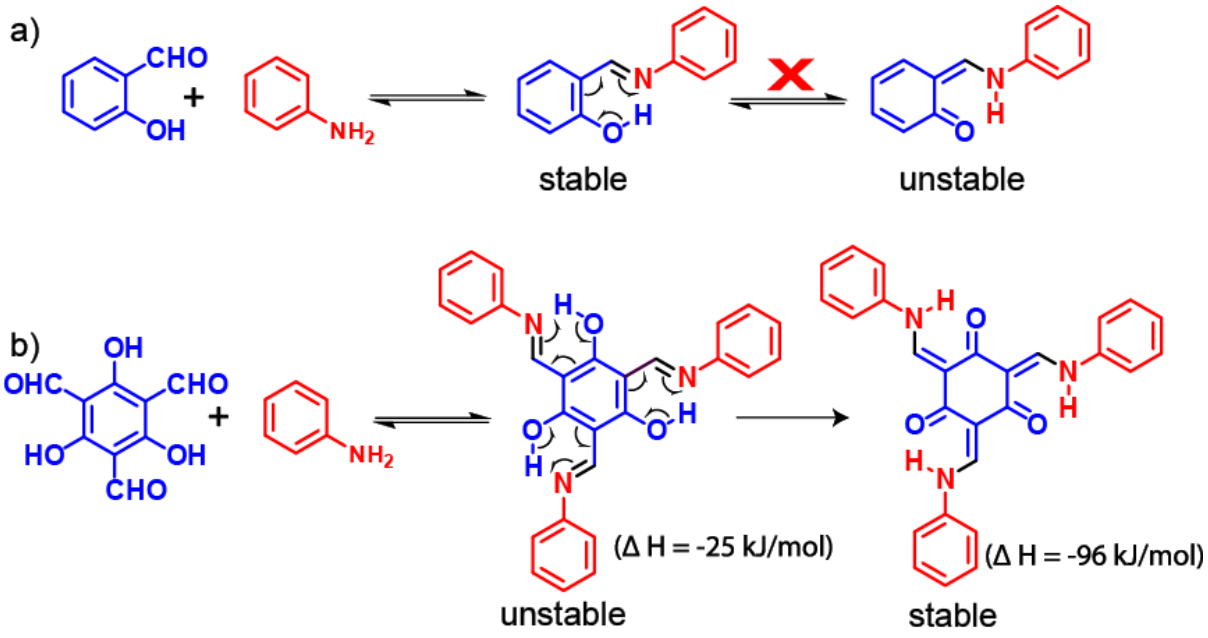

Figure 2.12: *Stability of different tautomeric forms in (a) mono substituted N-Salicylidene-anilines and (b) tri substituted N-Salicylideneanilines.*

compounds (tris (N-salicylideneaniline) the co-operative effect of basicity of imine functional group surpasses the aromaticity stabilization effect, and as a result the compound gets stabilized in *β*- ketoenamine form (***Figure 2.12b***). However, the existence of the enol-form intermediate is difficult to prove experimentally because of the rapid tautomerisation

step [2.12]. In order to find the stability of the enol intermediate, energy calculations were performed on the single unit of COF using the Turbo mole 6.0s programs. It was found that keto-form get stabilized over the enol-form with a huge energy difference of ΔE= -74.06 kcal/mol (***Figure 2.12b***).

2.3 Conclusion

In summary, we developed a novel methodology for the synthesis of highly chemically stable crystalline 2D covalent organic frameworks. The synthesized COF retains its porosity and crystallinity even after long time acid (9N HCl) and water treatment. The exceptional stability of these COF materials will allow them to be used in real life storage and separation application. We have also demonstrated the base stability of these *β*-ketoenamine based materials can be improved by incorporating a bulky alkyl group close to the secondary nitrogen centre. We believe this methodology can be further explored for the synthesis of COFs with ultra high surface area, by increasing the length of diamine ligands. The sheet like morphology of **TpPa-2** crystallites can be utilized for loading catalytically active nano-particles.

2.4 Experimental Procedures

2.4.1 *Materials*

Triformylphloroglucinol was prepared from Phloroglucinol using literature procedure [2.12]. All other reagents and solvents were commercially available and used as received.

2.4.2 *Synthesis of 2,4,6-tris((phenylamino)methylene)cyclohexane-1,3,5-trione (Reference compound)*

The reference compound was synthesized by the reaction between Triformylphloroglucinol (0.163 g, 0.8 mmol) and aniline (0.500 g, 5.4 mmol) in 70 mL ethanol under refluxing condition for one day. After this time period the heating was stopped and the solution was allowed to reach the RT. The product gets precipitated after cooling was then separated by filtration. After this the powders were thoroughly washed with ethanol, and allowed to dry under vacuum (0.210 g, 82% yield).

^{1}H NMR (300 MHz, $CDCl_3$): δ 13.0-13.4 (m, NH), 8.90 (d, HC-N), 8.77 (d, CH), 8.75 (d, CH), 7.44-7.17 (m, Ph) ppm.

IR (powder, cm^{-1}): 1616 (s), 1581, 1553, 1465, 1444, 1340, 1287, 1236, 1041.

2.4.3 *General methods for characterization*

***(a) Powder X-Ray Diffraction (PXRD)*:** The PXRD patterns were collected on a Phillips PANalytical diffractometer on a Cu Kα radiation (λ = 1.5406 Å), with a scan speed of 2° min^{-1}. The tube amperage and voltage were set at 50 mA and 40 kV respectively. The sample plate containing the COF powders was scanned between 2 and 50° 2θ (step size of 0.02°).

***(b) Thermogravimetric Analysis (TGA)*:** TGA was performed on a SDT Q 600 TG-DTA analyzer instrument. Approximately 5 mg of the sample was added to an aluminum crucible and heated from 25 to 800 °C under N_2 atmosphere (heating rate of 10 °C min^{-1}).

***(d) IR Spectroscopy*:** The Fourier transform (FT) infrared spectra of the MOFs were taken on a *PERKIN ELMER FT-IR SPECTRUM* (Nicolet) spectrometer. KBr samples (2 mg in 20 mg of KBr) were prepared and 10 scans were collected at 4 cm^{-1} resolution for each sample. The spectra were measured over the range of 4000-600 cm^{-1}

***(f) Gas Adsorption*:** The gas adsorption experiments for the activated COF powders were performed on Autosorb-1 automatic volumetric instrument (Quantachrome).

COF powder activation procedure: Approximately 50 mg of the COF powders were immersed in dry acetone at room temperature for 48 h. After this time period the solvent was removed and the COF powders were evacuated under vacuum at room temperature for 24 h. Then the temperature was raised to 150 °C and evacuation continued for 48 h. Finally, the activated samples are treated for gas adsorption (H_2, N_2 and CO_2).

***(g) Water adsorption measurements*:** Low-pressure volumetric water adsorption measurements were performed at 293K, with pressure ranging from 0 to 0.9 [relative pressure (P/P_o)] on a Quantachrome Autosorb-iQ-MP automatic volumetric instrument.

2.4.4 *Structure Modeling of COFs*

Atomic positions and cell sizes of modeled COF layers were optimized using Self-Consistent Charge Density Functional Tight-Binding (SCC-DFTB) Method. Stacking of layers is affected by the Coulomb repulsion between the partial atomic charges in adjacent layers. Hence, we performed Mulliken population analysis for the charges. The adjacent

layers were shifted with respect to each other in different directions in order to avoid Coulomb repulsion from charges alike. Several possibilities were considered, however, the best was taken from a comparison of simulated PXRD pattern with the experimental. Interlayer separation was also determined from the comparison of PXRD patterns. The fractional coordinates of **TpPa-1** and **-2** are given in Table S1 and S2, respectively.

In order to elucidate the structure of these COFs and to calculate the unit cell parameters, possible 2-D models were optimized using Density Functional Tight-Binding method. Several stacking possibilities were considered for reasons reported in the literature. The experimental PXRD patterns are agreeable with the simulated patterns of some near-eclipsed stacking models (Figure S1 and S2 in ESI). Hence we propose structures close to hexagonal space group (*P6/m*) for **TpPa-1** and **-2** by comparing the experimental and simulated PXRD patterns. Refinements of PXRD pattern were done using Reflex module of Material studio.

NOTE: The results of this chapter have already been published in *J. Am. Chem. Soc.***, 2012,** *134,* 19524. with the title: "*Construction of Crystalline 2D Covalent Organic Frameworks with Remarkable Chemical (Acid/Base) Stability via a Combined Reversible and Irreversible Route*" respectively. These publications were the results of the collaboration between the group of Dr. Rahul Banerjee and his students Sharath Kandambeth and Arijit Mallick from National Chemical Laboratory, Pune, India and the group of Dr. Thomas Heine and his students Binit Lukose from Jacobs University, Germany. Apart from computational study major works contributed by Sharath Kandambeth.

CHAPTER 3

Intra-molecular Hydrogen Bonding as a Tool for Enhancing Crystallinity, Porosity and Chemical Stability in Covalent Organic Frameworks

Abstract: *Covalent Organic Frameworks (COFs) are a new class of porous materials, which have gained immense scientific attention due to their tunable properties and diverse applicability. Porosity and crystallinity are the two main parameters which determines the quality of the COFs. Here in this chapter we introduces a new strategy of intra molecular hydrogen bonding in COFs, by which crystallinity, porosity and chemical stability frameworks can be synergically improved. The intra-molecular hydrogen bonding locks the phenyl ring rotation, improves the COF layer planarity, thus support efficient π-π stacking which helps to improve the crystallinity and porosity of COF frameworks.*

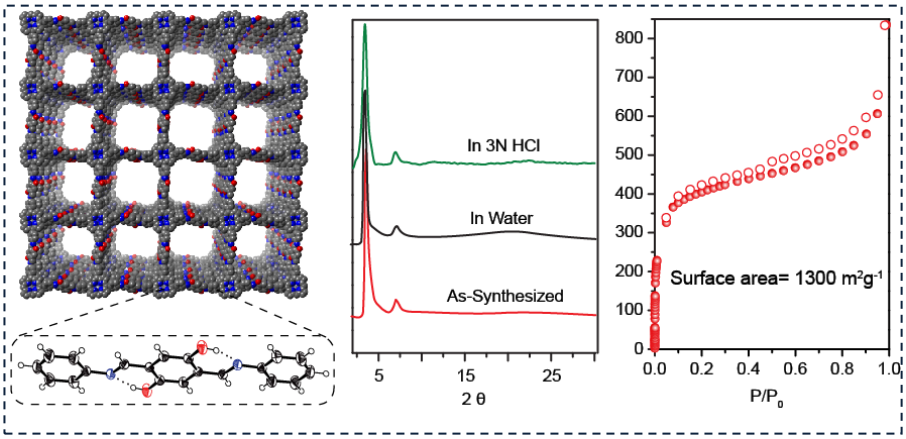

3.1 Introduction:

Crystallinity and surface area are two main important parameters for determining the quality COFs [3.1]. In ordered to synthesis a highly crystalline and porous COF, the reaction conditions must meet certain criteria's. 1) Reversibility in COF formation reaction, 2) symmetry of the COF building units are the two main criteria's which largely effect the crystallinity and porosity of the COF materials [3.2]. A highly reversible organic reaction is essential for synthesizing a highly crystalline COF material. Three reversible reactions 1) boronate ester formation, 2) boronate ester formation, 3) Schiff base reaction, have been extensively used for the synthesis of a wide variety of COFs [3.2]. Irreversible reaction, on the other hand, leads to the formation of amorphous polymers which is commonly known as POPs/PAFs/ CTFs [3.3]. The second factor which determines the COF crystallinity is the symmetry of COF building units [3.2]. The building units used for the COF synthesis should be rigid, planar and must satisfy the basic rules of symmetry combination (***section 1.5***).

The COFs formed by the reversible reactions are generally unstable to moisture, as the backward decomposition reaction gets accelerated in the presence of water [3.4]. In the previous chapter (***chapter 2***) we have discussed in detail about the synthesis of highly chemically stable *β*-ketoenamine based COFs by using a combination of reversible and irreversible reaction. Even though this *β*-ketoenamine based COFs display high chemical stability their surface area and crystallinity were moderate. The irreversible nature of the tautomerization step may be the probable reason for this characteristic [3.5]. Keeping this in mind, this chapter discusses enhancing the surface area and crystallinity of imine based COFs, with a synergic improvement in its chemical stability.

Our initial attempt was to synthesis a highly chemical stable porphyrine based COF by using the enol to keto tautomerisation strategy. The porphyrine based COFs are well known for thier high charge carrier mobility [3.6], but the chemical stability issue prevents thier further use in device applications [3.4]. However, the reaction between C_3 symmetric 1, 3, 5-triformyl phloroglucinol and C_4 symmetric porphyrin ligand (5,10,15,20-Tetrakis(4-aminophenyl)-21H,23H-porphine) failed to produce an ordered 2D COF, due the symmetric

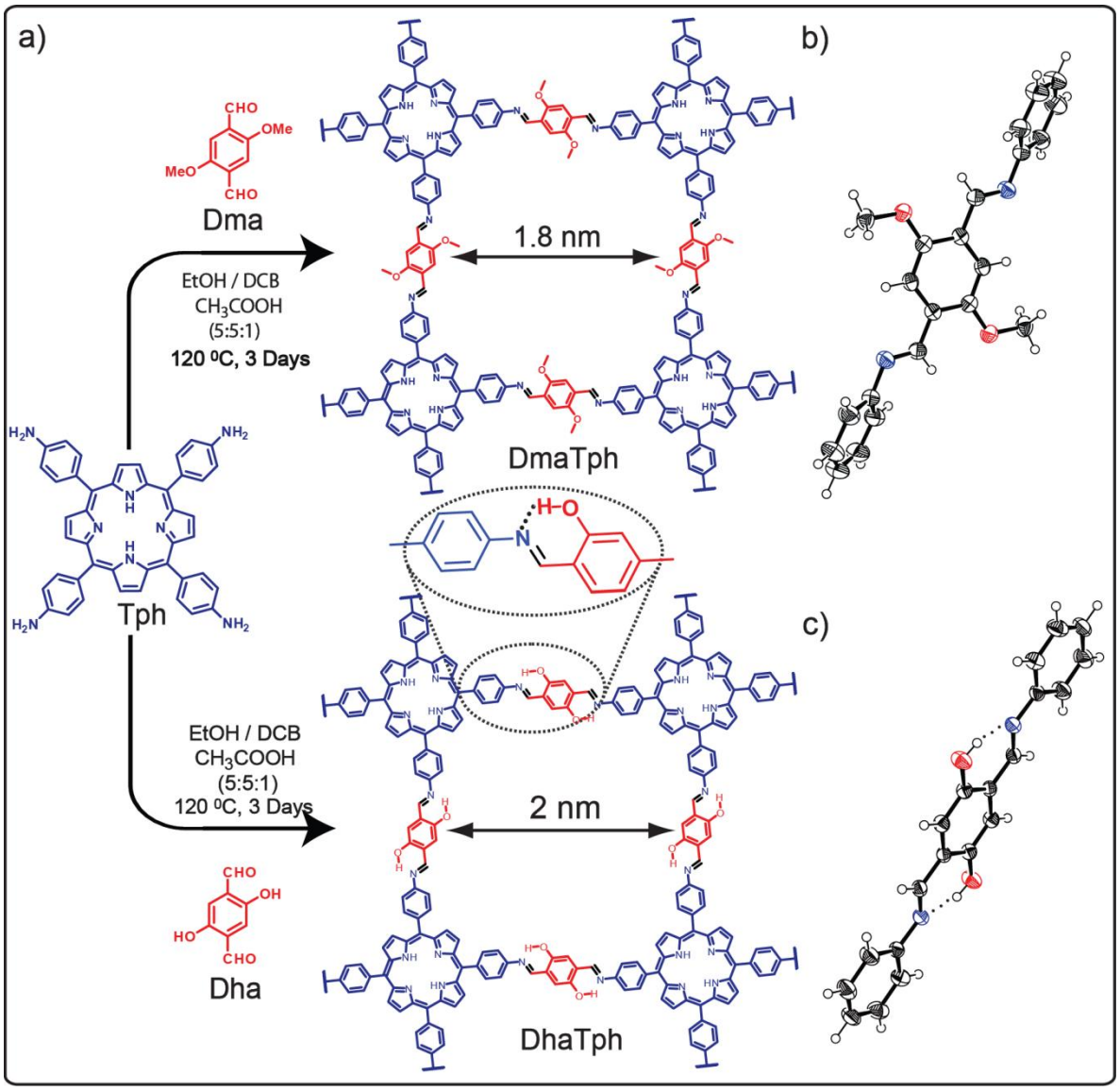

Figure 3.1*: (a) Synthesis of* ***DhaTph*** *and* ***DmaTph*** *via Schiff base condensation reaction. b) ORPTEP diagram of b)* ***DmaTph*** *and c)* ***DhaTph*** *linker units shows the influence of intramolecular hydrogen bonding in aromatic ring planarity.*

mismatch (***section 1.5***). C_3 and C_4 symmetric combination do not form closed ring structures in two dimension, instead, it might produce 3D frameworks structures. So to establish our goal we have replaced the C_3 building unit (symmetric 1, 3, 5-Triformyl phloroglucinol) by a C_2 linker (2, 5-dihydroxyterephthalaldehyde). We expect the C_2+C_4 symmetric combination will produce a tetragonal COF 2D framework structure (***Figure 3.1***). More over the presence of hydroxyl functionality can improve the chemical stability of the COF frameworks through hydrogen bonding interaction (***Figure 3.1***).

The COF (**DhaTph**) synthesis was performed by the Schiff base reaction between 2, 5-dihydroxyterephthalaldehyde (**Dha**) [3.11] and 5,10,15,20-Tetrakis(4-aminophenyl)-21H,23H-porphine (**Tph**) (***Figure 3.1a***). To our surprise, the enol to amine tautomerism was not observed for **DhaTph**. Instead, the COF get stabilized in enol-imine structure. However, we observed that the incorporation of hydroxyl functionality (-OH) close to the imine nitrogen (-C=N) creates an intramolecular hydrogen bonding interaction (O–H…N=C). This hydrogen bonding interaction locks the phenyl ring rotation and fixes them in one plane (***Figure 3.1c***). The improved planarity of the COF layer supports the efficient π-π interaction, and as a result crystallinity and surface area of **DhaTph** get drastically improved. The surface area of **DhaTph** (1300 m^2g^{-1}) is almost two times greater than that of un substituted porphyrin based COF (COF-366) reported in the literature [3.6b]. In addition to the improved surface area and crystallinity, COF-**DhaTph** displays an enhancement in chemical stability. COF-**DhaTph** retains its crystallinity even after acid (3N HCl) and water treatment. The improved chemical stability of **DhaTph** was due to the protective effect of intramolecular hydrogen bonding interaction (O–H…N=C) over imine nitrogen. We have also cross checked the importance of intramolecular hydrogen bonding interaction, by replacing the hydroxyl functionality by methoxy group (-OMe) in **DmaTph**. We observed that surface area, crystallinity and chemical stability of **DmaTph** was lower in comparison to **DhaTph**, due the lack of intramolecular hydrogen bonding interaction.

3.2 Result and Discussion

3.2.1 *Synthesis and characterization*

DhaTph and **DmaTph** were synthesized by the Schiff-base reaction between C_2 linker (2,5-dihydroxyterephthalaldehyde (**Dha**) (13.3 mg, 0.08 mmol) or 2,5-dimethoxyterephthalaldehyde (**Dma**) (15.5 mg, 0.08 mmol) with C_4 linker ((5,10,15,20-Tetrakis (4-aminophenyl)-21H,23H-porphine (**Tph**) (27.0 mg, 0.04 mmol)) in presence of catalytic amount acetic acid (0.2 mL) and using ethanol, dichlorobenzene mixture (1:1) as the solvent combination (2 mL) (***Figure 3.1a***). The reaction was performed under typical solvothermal method. The reactants and solvents were initially transferred to pyrex glass tube, followed by sealing under high vacuum. The sealed tube was then placed at 120 °C for 3 days. After this time period the tube was broken and the COF powdered were collected by filtration.

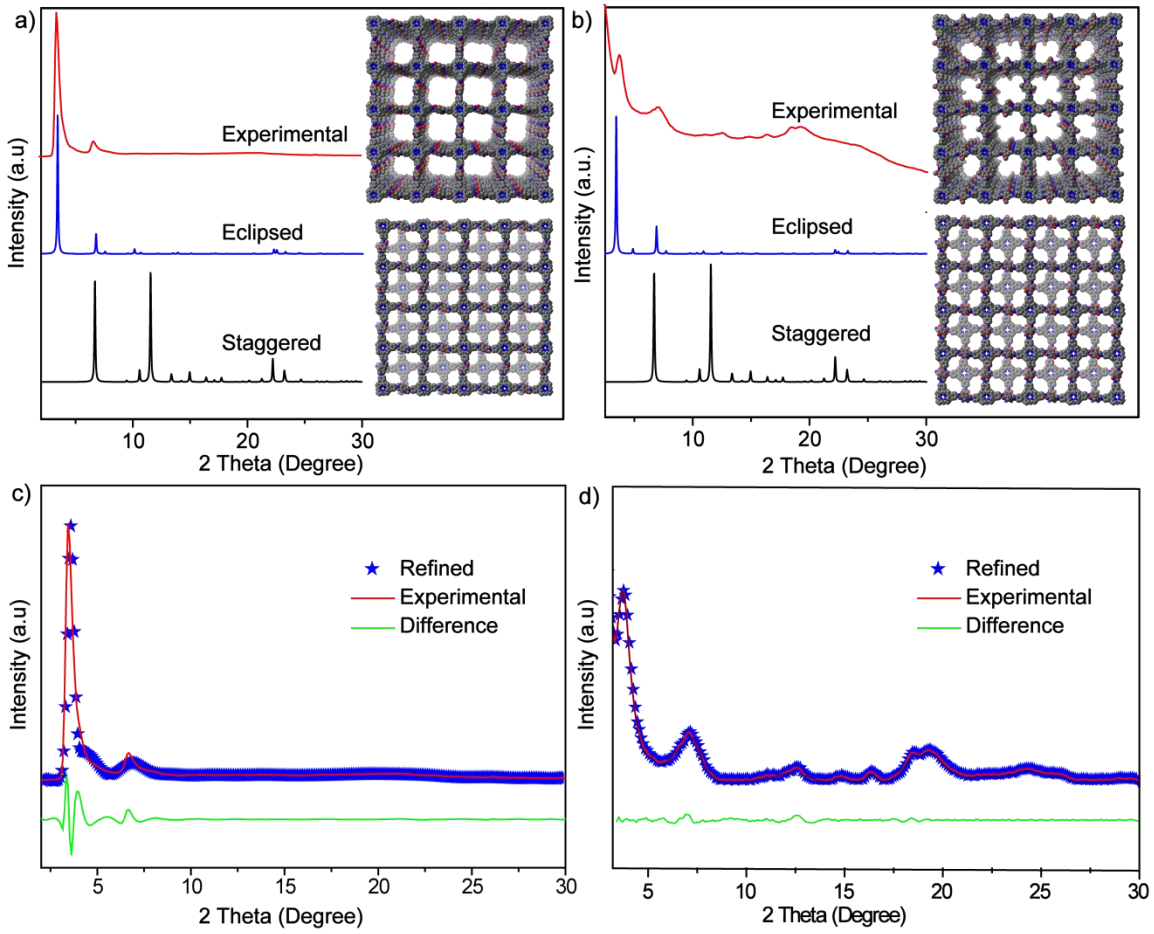

Figure 3.2*: PXRD spectra of As-synthasized (red) compared with the eclipsed (blue) and staggered (black) stacking models for (a)* ***DhaTph*** *and (b)* ***DmaTph****. Experimental (red) PXRD profiles of (c)* ***DhaTph*** *and (d)* ***DmaTph*** *compared with refined (blue) with an eclipsed arrangement; difference plot is given in (green).*

3.2.2 *Structural simulation and characterization*

The crystallinity of the **DhaTph** and **DmaTph** was investigated by PXRD analysis. The high crystalline nature of the **DhaTph** was understood from the intense first peak appearing at 3.4° (Intensity ~ 70000 cps). This first peak corresponds to the reflection from 100 plane. Additional minor peaks appearing at 6.9° and 20-23° 2θ was assigned for 200 and 001 planes by comparing the *d* spacing values (***Figure 3.2a***). From the *d* spacing value of the 001 plane the approximate COF interlayer distance was calculated as 3.8- 4.4 Å. The PXRD of **DmaTph** shows a similar trend in peak position (***Figure 3.2c***). The PXRD peaks corresponding to 100, 200, 001 facets appeared at *2θ* of 3.4°, 6.8°, 17- 25°. But as compared to **DhaTph** the peak intensity of **DmaTph** was relatively lower (***Figure3.2c***). The first peak

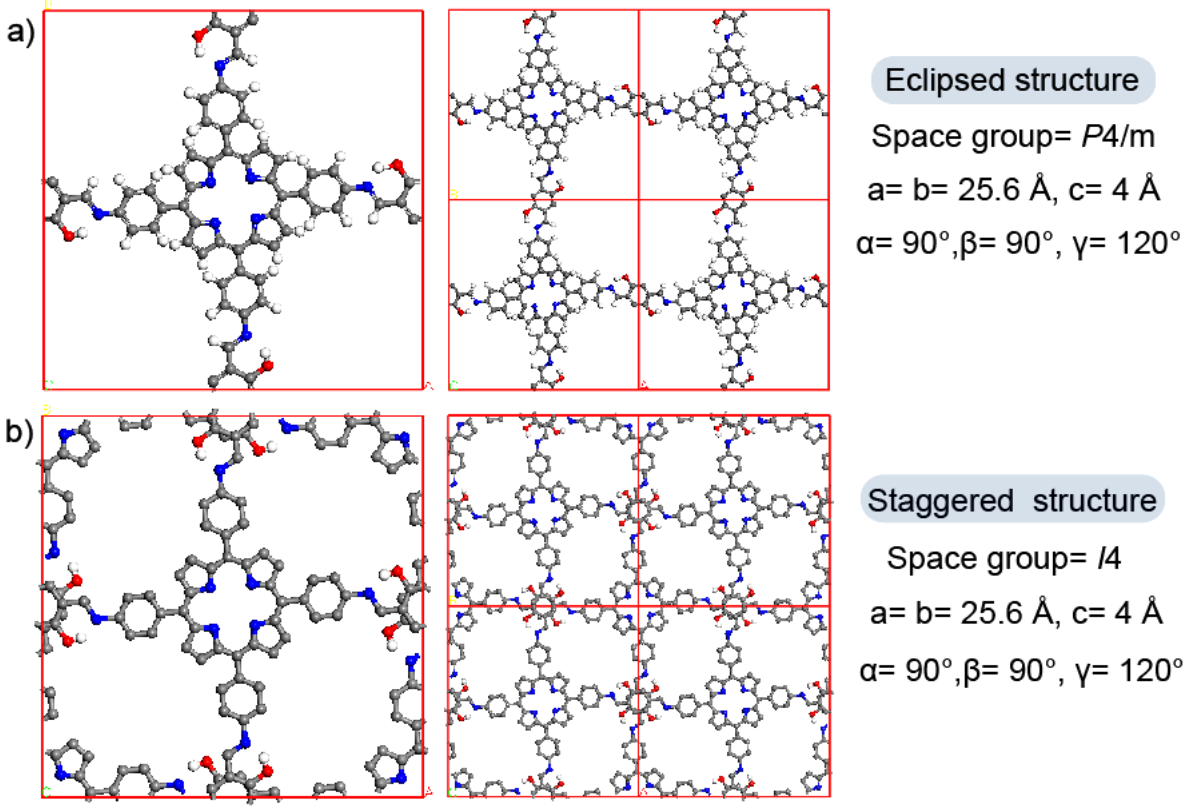

***Figure 3.3**: (a) Unit cell and eclipsed crystal lattice packing of **DhaTph**; (b) unit cell and staggered crystal lattice packing of **DhaTph**.*

which corresponds to the 100 plane posses intensity around 3000 cps (which is 23 times lower that **DhaTph**). The high crystallinity of **DhaTph** over **DmaTph** was due to the effect of strong intramolecular hydrogen bonding interaction (O–H…N=C) (***Figure 3.1b and 3.1 c***). The O–H…N=C intramolecular hydrogen bonding interaction in **DhaTph** restricts the aromatic ring rotation and forces them to remain in plane (***Figure 3.1c***). Due to this improved planarity, **DhaTph** COF layers forms more effective π-π stacking interaction, which improves the crystallinity of the material. The intramolecular hydrogen bonding interaction also enhances the possibility of imine bond formation in *trans* conformation, as a result, structural defects get minimized in **DhaTph**. In **DmaTph**, since the hydrogen bonding interaction was absent, the planarity and structural rigidity of the COF layer is not properly maintained (***Figure 3.1b***). This loss in planarity creates disorderliness in π-π stacking interaction between COF layers which reduces the crystallinity of **DmaTph** (***Figure 3.2c***). To get more insight towards the influence of intramolecular hydrogen bonding on planarity of COF layers we have crystallized the linker units of **DmaTph** and **DhaTph**. From the single

crystal data it was evident that a strong intramolecular hydrogen bonding (O–H…N=C) interaction exist in **DhaTph** linker units [D = 2.619 (2) Å, d = 1.895 (2) Å, and θ = 146.6° (3)] (***Figure 3.1c***). Due to this interaction, the three aromatic rings remain in one plane (***Figure 3.1c***). In the case of **DmaTph** linker unit due to the lack of hydrogen bonding interaction aromatic rings losses their planarity (***Figure 3.1b***).

In order to elucidate the 2D- framework structures of COF (**DhaTph** and **DmaTph)** two possible stacking models (eclipsed and staggered) were modeled in material studio 6.1 (***Figure 3.3***). The modeling of eclipsed structure was done in *P*4/m space group (***Figure 3.3a***), were the staggered structure was modeled in space group *I*4 (***Figure 3.3b***). It was observed that the experimental PXRD pattern got a better match with the simulated PXRD patterns of the eclipsed stacking model. To determine the exact unit cell values Pawley refinement was performed (***Figure 3.2c and 3.2d***). After the refinement the final unit cell values were determined as a = b = 25.6 Å, c = 4 Å (for **DhaTph**) and a = b = 25.7 Å, c = 4 Å (for **DmaTph**).

3.2.3 *Chemical characterization*

The successful formation of imine bonds in COFs (**DhaTph** and **DmaTph)** was investigated by FT-IR and ^{13}C CP-MAS solid state NMR. FTIR of the COFs shows the completion of the reaction, as the starting material peaks were absent (*i.e.* C=O stretching bands of **Dma** (1670 cm^{-1}) and **Dha** (1660 cm^{-1}) and –N-H stretching bands from tetramine (3100-3400 cm^{-1} of **Tph**) (***Figure 3.4a and 3.4b***) . The appearance the new peaks at 1613 cm^{-1} (for **DhaTph**) and 1612 cm^{-1} (for **DhaTph**) was assigned for the characteristic imine (–C=N) stretching bands (***Figure 3.4a***). These values are in close match with the –C=N stretching values observed in linker units (1613 cm^{-1}). To confirm the imine bonded framework structure of **DhaTph** and **DmaTph**, ^{13}C CP-MAS solid state NMR was performed. The appearance of signal at δ=160.9 ppm (for **DmaTph)** and δ= 160.8 ppm (for **DhaTph)** corresponds to the characteristic imine (–<u>C</u>=N) signal (***Figure 3.4c***). Most of the ^{13}C CP-MAS solid state NMR signals of **DmaTph** appear close to that of **DhaTph**. The appearance of the extra peak at δ 53.2 for **DmaTph** corresponds to the methoxy carbon (-OCH_3) (***Figure 3.4c***). The further evidence about the existence of COF structure as enol-imine form was obtained from the single crystal data of the linker units (***Figure 3.1b and 3.1c***). To reveal the internal morphologies of the COFs transmission electron microscope (TEM)

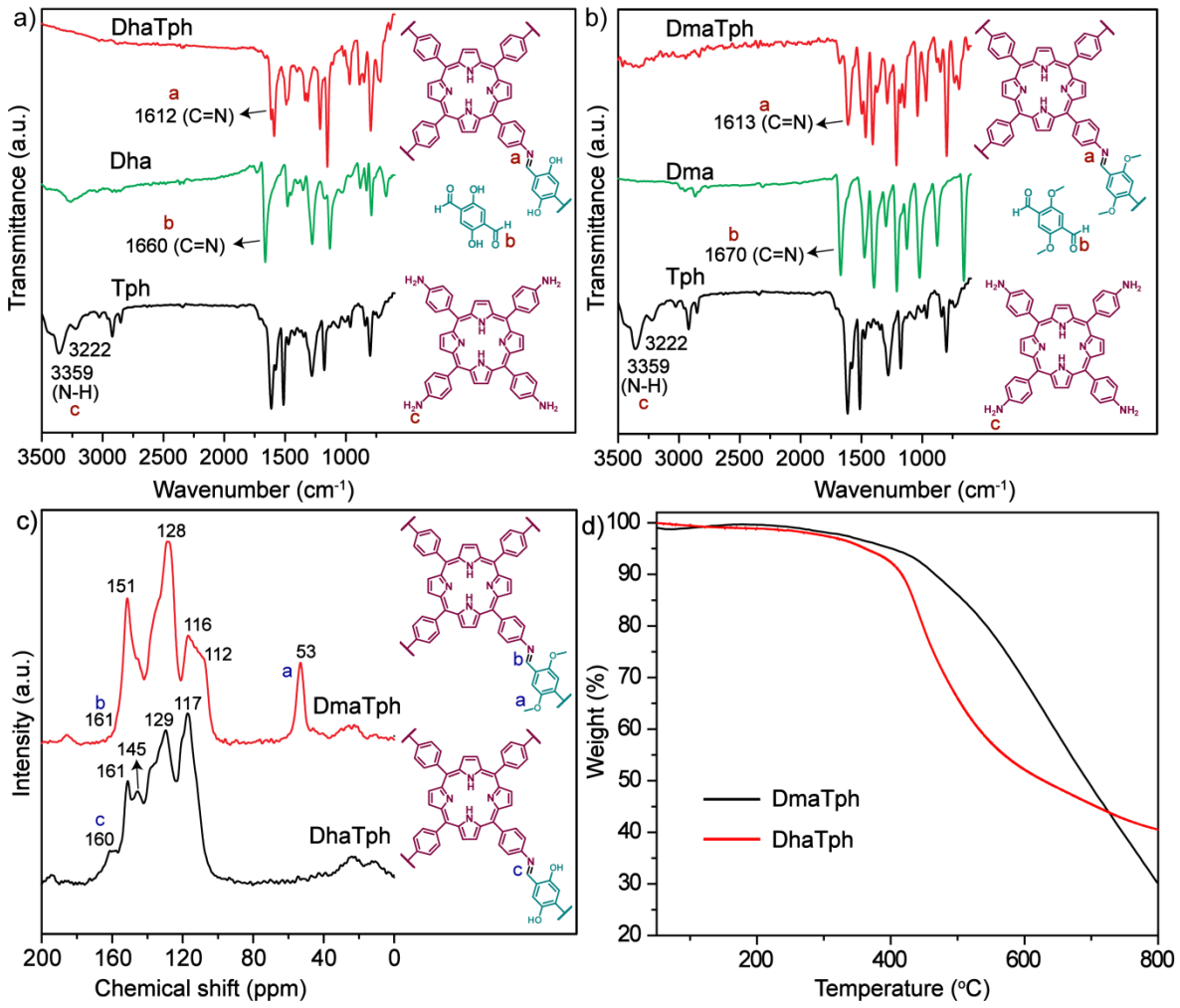

***Figure 3.4**: (a) FT-IR spectra of **DhaTph** (red) compared with starting materials 2,5-dihydroxyterephthalaldehyde (Dha) (green) and and 5,10,15,20-Tetrakis-(4-aminophenyl)-21H,23H-porphine (Tph) (black). (b) FT-IR spectra of **DmaTph** (red) compared with 2,5-dimethoxyterephthalaldehyde (Dma) (green) and 5,10,15,20-Tetrakis-(4-aminophenyl)-21H,23H-porphine (Tph) (black). (c) Comparison of ^{13}C CP-MAS spectrum of **DmaTph** (red) and **DhaTph** (black). (d) TGA data of activated COF **DhaTph** (red) and **DmaTph** (black) under N_2 atmosphere.*

images was used. TEM images of **DhaTph** shows squire shaped nano crystallites having dimension around 50 nm (***Figure 3.5a-c***). While the length of the **DmaTph** crystallites is much more elongated, forming belt or rectangular shapes (***Figure 3.5d-f***). The width of the **DmaTph** crystallites was around 200 nm while the length is more than 200 nm. To determine the framework thermal stability, thermo gravimetric analysis (TGA) was performed on activated COF samples (**DhaTph** and **DmaTph)**. The TGA profiles show that the both COFs are thermally stable up to 300 °C (***Figure 3.4d***). After this temperature, a gradual weight loss was observed which may be related to the framework decomposition.

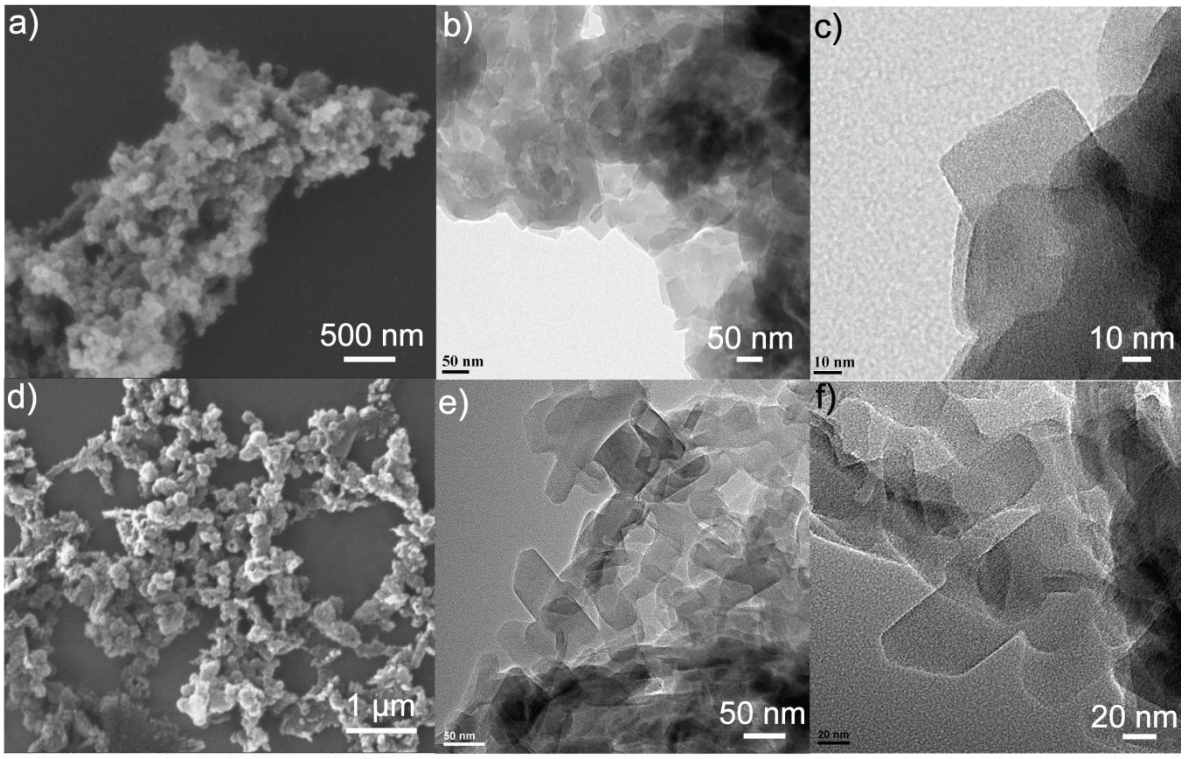

Figure 3.5: *(a) SEM and (b, c) TEM images of COF* ***DhaTph****, (d) SEM and (e, f) TEM images of COF* ***DmaTph****.*

3.2.4 *Gas adsorption Properties*

N_2 adsorption was recorded for the activated COF samples to evaluate the porosity and surface area. A type IV adsorption isotherm was observed both **DhaTph** and **DmaTph** which is due to COFs mesoporous nature (***Figure 3.6a***). The steep rice in the N_2 uptake observed after 0.8 bar (P/P_0) was due to the condensation of nitrogen within the inter particle voids (***Figure 3.6a***). To calculate the surface area of COFs Brunauer-Emmett-Teller (BET) model was used. **DhaTph** showed a high surface area of 1305 m^2g^{-1} as compared to the methoxy substituted **DmaTph** (431 m^2g^{-1}). The lower surface area of **DmaTph** was a result of its low crystallinity. The surface area value of the **DhaTph** is significantly (two times) higher than that the non hydroxy analogue COF-366 (S_{BET} = 735 m^2g^{-1}) reported in the literature [3.6b]. This improvement in surface area was due to the extra intramolecular hydrogen bonding (O–H…N=C) interaction present in the system. This hydrogen bonding interaction makes the COF layers more planar and makes the π-π interaction between the COF layers more feasible. As a result ordered pore channels get formed in the COF, which

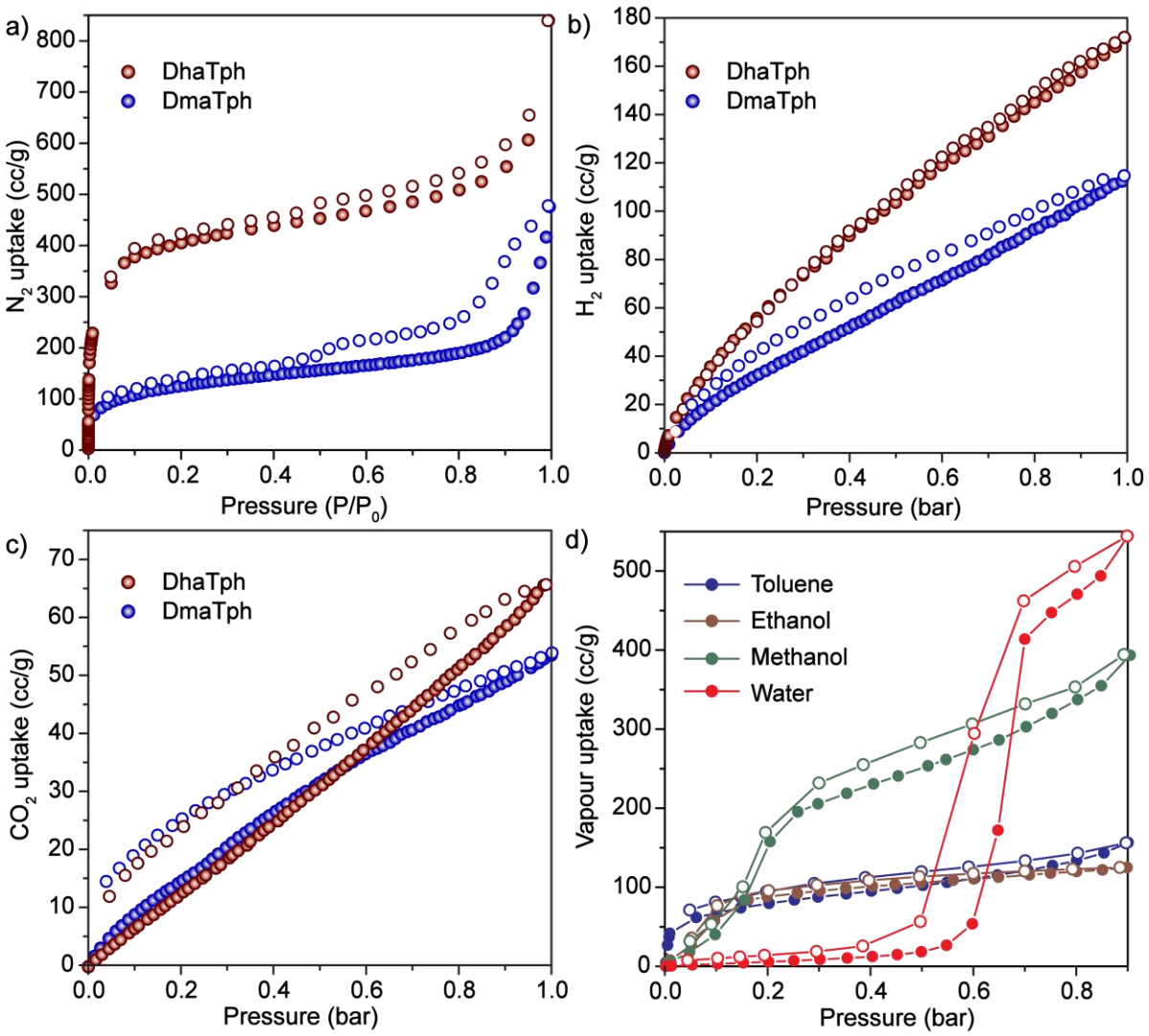

***Figure 3.6**: (a) N_2 adsorption, (b) H_2 adsorption, (c) CO_2 adsorption, (d) water adsorption isotherms of **DhaTph** (wine) and **DmaTph** (blue). The filled symbols corresponds to adsorption and empty symbols represents desorption isotherms.(d) Vapor adsorption isotherm of DhTph, water(red),methanol (green), ethanol (wine), toluene (blue).*

improves the surface area of **DhaTph**. Langmuire surface area calculation also showed a similar trend, **DhaTph** shows a higher surface area (1900 m^2 g^{-1}) as compared to **DmaTph** (677 m^2g^{-1}). Non linear density functional theory (NLDFT) model was used to evaluate the pore sizes of COFs. The peak maxima of **DhaTph** appear at 2 nm were as **DmaTph** shows a lower value of 1.5 nm (***Figure 3.7***). Both these values have a close match with the theoretically predicted pores size. To evaluate the gas storage properties of the COF, H_2 and CO_2 isotherm was reordered at 1 bar pressure. H_2 storage values are are found to be 171 cm^3 g^{-1} (for **DhaTph**) and 78 cm^3g^{-1} (for **DmaTph**) at 77 K (***Figure 3.6b***). The CO_2 uptake values

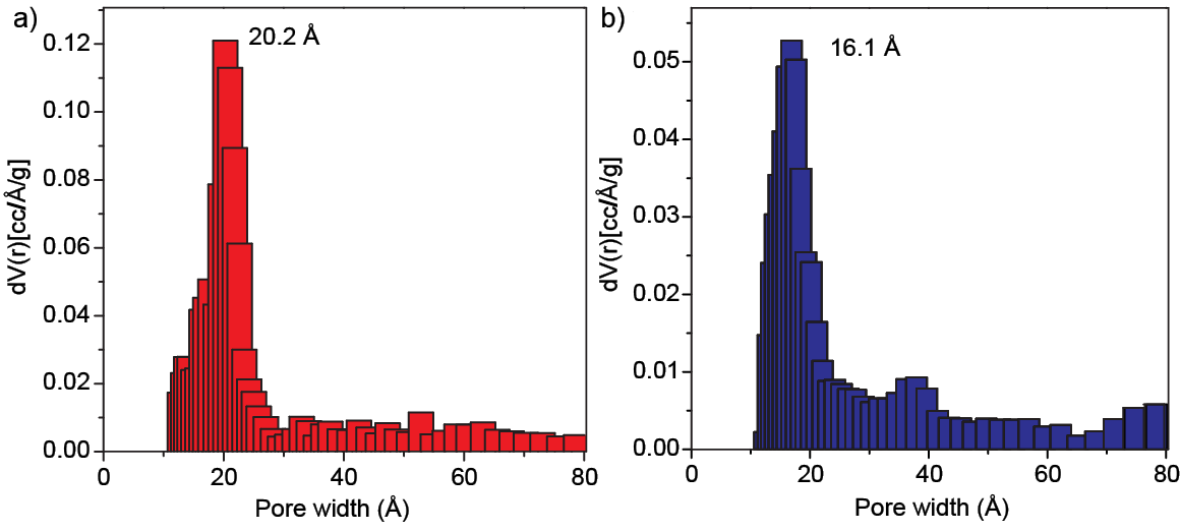

Figure 3.7: *NLDFT Pore size distribution of (a)* ***DhaTph*** *and (b)* ***DmaTph****.*

were calculated as 65 cm^3g^{-1}(for **DhaTph**) and 53 cm^3g^{-1} (for **DmaTph**) at 273 K (***Figure 3.6c***). This high porosity of **DhaTph** encouraged to us collect water adsorption isotherms at 298 K and 0 to 0.9 bar (***Figure 3.6d***). It was found that both **DhaTph** show a reversible water vapor uptake similar to **TpPa-1** which is an indication of frameworks chemical stability. **DhaTph** shows almost zero uptake of water vapor below 0.5 bar, due to the strong hydrophobicity inside the pores of these materials. However above 0.6 bar abrupt increase of water adsorption was recorded due to the water vapor condensation in the pores. The presence of the conjugated porphyrin and phenyl ring present in these COFs can be considered as the origin of this hydrophobicity [3.7]. In order to investigate this hydrophobicity aspect we had further collected the methanol, isopropanol and toluene vapor adsorption at 298 K and 0 to 0.9 bar (***Figure 3.6d***). As expected, **DhaTph** show very high methanol, isopropanol and toluene vapor uptake (Figure 4e and f). As we have shifted from polar to non-polar solvent (from water to toluene) vapor adsorption starts at low pressure region (even below 0.1 bar) which is another evidence of this hydrophobicity (***Figure 3.6d***). The decrease in total volume uptake on going from methanol to toluene may be related to the increase in Van der Waal radii of the vapor molecules (***Figure 3.6d***).

3.2.5 *Chemical stability investigation*

To check the chemical stability of the COF materials, they were submerged in water (30 mL) for one week. After this time period COF powders were separated by filtration and then dried under vacuum at 150°C. PXRD of the water treated COF-**DhaTph** shows a retention of crystallinity (***Figure 3.8a***), which indicates the chemical stability of this material in water. To investigated further N_2 adsorpton isotherm was recorded for the water treated COF samples (***Figure 3.8b***). The surface area of **DhaTph** only showed a slight decrease (1252 m^2 g^{-1}) which confirms the high chemical stability the COF in water. On the other hand nonhydroxy, analogue COF-366 reported in literature loses its crystallinity upon water

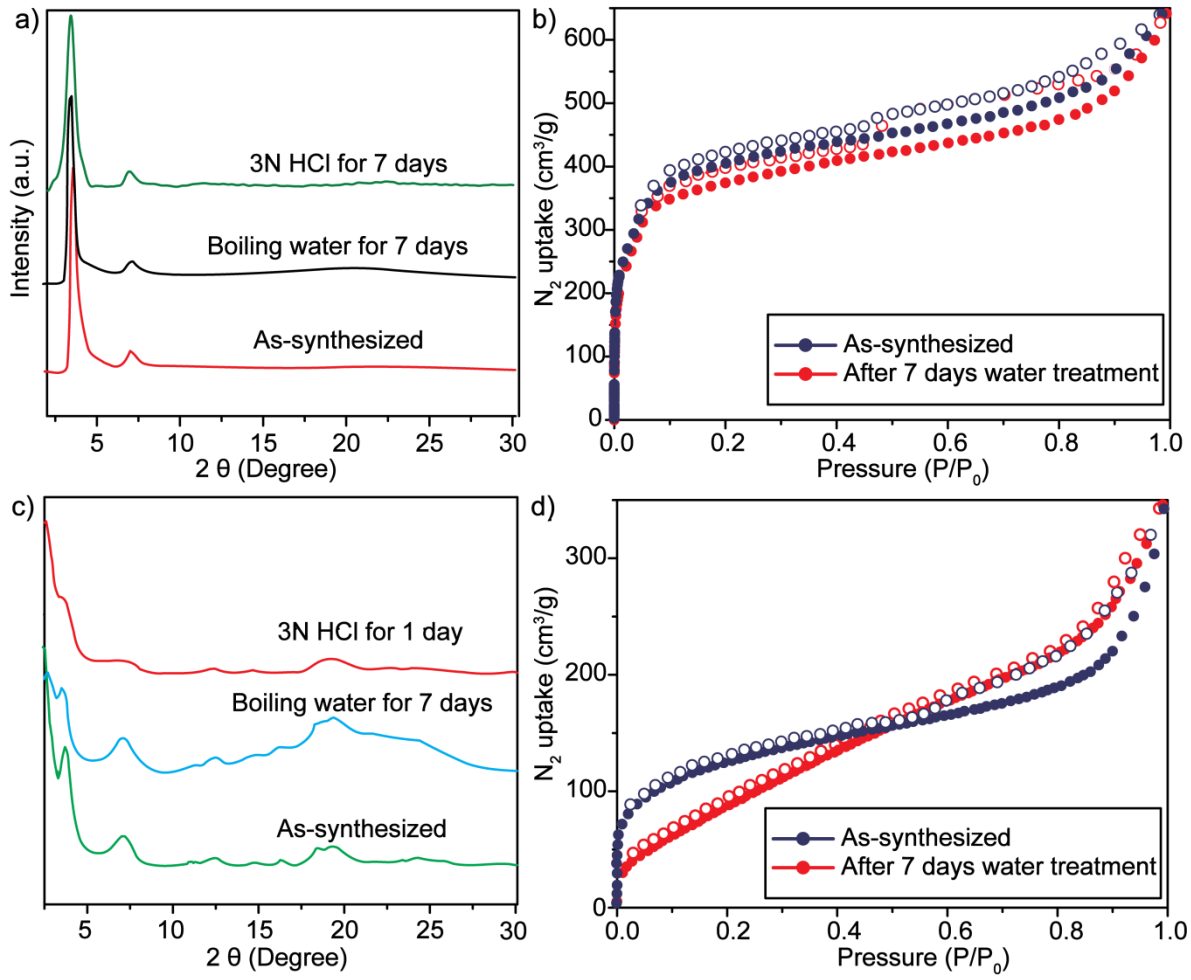

Figure 3.8: *(a) PXRD comparison of as synthesized, water and acid treated* ***DhaTph*** *samples. (b) Comparison of N_2 adsorption isotherms of as synthesized and water treated* ***DhaTph*** *samples. (c) PXRD comparison of as synthesized, water and acid treated* ***DmaTph*** *samples. (d) Comparison of N_2 adsorption isotherms of as synthesized and water treated* ***DmaTph*** *samples.*

treatment. This shows the importance of intramolecular hydrogen bonding interaction in improving the chemical stability of **DhaTph**. A similar water stability test was also performed for **DmaTph**, but the PXRD peak intensity gradually decreased after the long time water treatment (***Figure 3.8c***). To find out the acid stability of the material **DhaTph** and **DmaTph** were directly treated with 3N hydrochloric acid. Both COF displayed a green colouration to the treated solution. After filtration and purification, PXRD was recorded for both **DhaTph** and **DmaTph** (***Figure 3.8a and3.8c***). Surprisingly **DhaTph** shows retention of main PXRD peaks, which indicate the high chemical resistance of the materials (***Figure 3.8a***). **DmaTph** lost most of the PXRD peak intensity after long time acid treatment (1 week) which may be related to the framework decomposition (***Figure 3.8c***). It is important to note that the surface area of the acid treated **DhaTph** samples shows a large decrease in the surface area value (570 m^2g^{-1}) (***Figure 3.8d***). Although the exact reason is not known, we speculate the surface decomposition of the frameworks, and the presence of chloride ions in COF pores due to the acid doping are the possible reason for the decrease in surface area values. **DhaTph** and **DmaTph** were further treated with 3N NaOH in order to evaluate their base stability. Both the COFs suffers a significant weight loss (< 70%) after the base treatment. The PXRD of the base treated COF shows loss of main PXRD peaks which indicate the framework decomposition in 3N NaOH. The chemical stability of the **DhaTph** was the result of the (O–H…N=C) intramolecular hydrogen bonding present in the system. This hydrogen bonding interaction locks the phenyl ring movement and keeps the framework structure rigid under solvent and acid treatments. It also protects the imine nitrogen's from fast hydrolysis. Phenolic –OH forms the most stable hydrogen bonds with the imine nitrogen's (-C=N) among all the hydrogen bond acceptors. The hydrogen bonding strength of different acceptors with phenolic –OH increases in the following order $–CF_3$< –F<–P=O < –C=O <$–NO_2$<–C=N [3.8].

3.3 Conclusion

In this chapter, we have discussed the importance of intramolecular hydrogen bonding in improving crystallinity, porosity and chemical stability of the Covalent Organic Framework materials. The intramolecular hydrogen bonding locks the phenyl ring in one planes thus improve the π- π stacking interaction between COF layers which is the principal reason behind the high crystallinity of **DhaTph**. The ordered pore channels formed as a

result of better π- π stacking interaction increases the surface area of COF. The protective effect of hydrogen bonding interaction on imine nitrogen increases the chemical stability. We have crosschecked the importance of intramolecular hydrogen bonding interaction by synthesizing the methoxy analogue **DmaTph**. We believe this methodology can be further extended to synthesis a series of highly crystalline and porous COFs for gas storage and charge carrier mobility application.

3.4 Experimental Procedures

3.4.1 *Materials*

Synthesis of 2,5- dihydroxyterephthalaldehyde [3.9] and 5,10,15,20-Tetra(nitro)phenyl-21H,23H-porphyrin [3.10] were performed as according to the literature procedure. Pyrrole, 4-nitrobenzaldehyde, 1,4-dimethoxybenzene, propionic acid, $SnCl_2.2H_2O$ were purchased from Sigma Aldrich. All other reagents and solvents were commercially available and used as received.

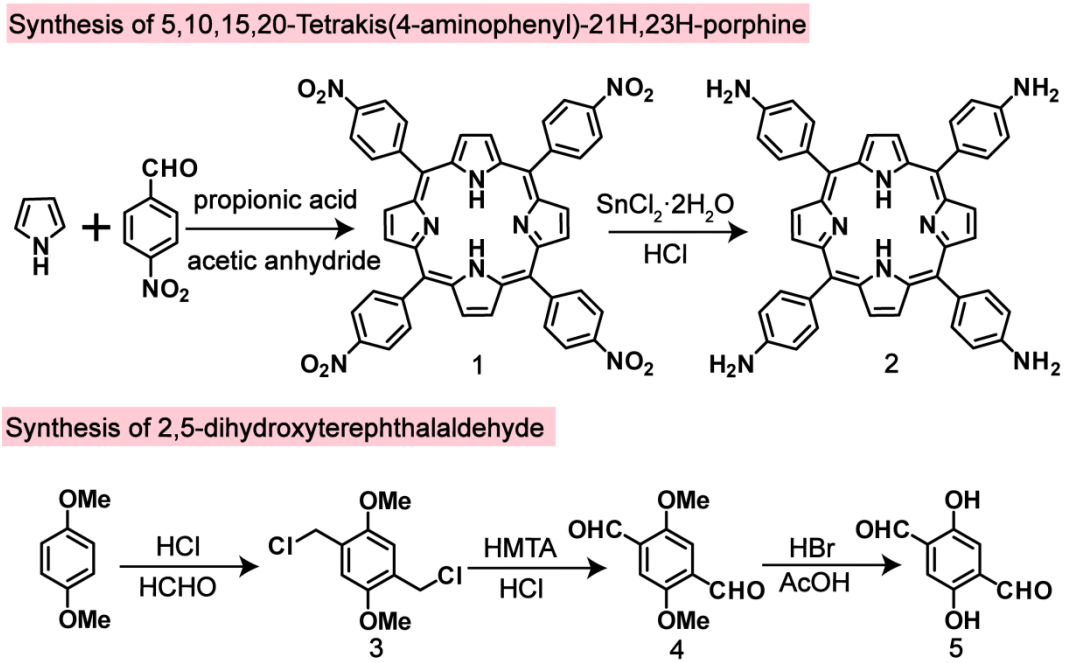

Figure 3.9: *(a) Scheme of synthesis of C_4 ligand 5,10,15,20-Tetra(nitro)phenyl-21H,23H-porphyrin. (b) Scheme of synthesis of C_2 ligand 2,5-dihydroxyterephthalaldehyde (HMTA- Hexamethylene tetramine).*

3.4.2 *Synthesis of (1E,1'E)-1,1'-(2,5-dimethoxy-1,4-phenylene) bis(N-phenylmethanimine) (Reference compound for DmaTph)*:

The reference compound was synthesized by the reaction between 2,5-dimethoxyterephthalaldehyde (**Dma**) (0.100 g, 0.515 mmol) and aniline (0.225 g, 2.060 mmol) in 30 mL ethanol under refluxing condition for 24 h. After this time the solution was cooled to room temperature and the precipitate was collected by filtration, washed with ethanol, and dried under vacuum to give 0.163 g, 82% of a yellow solid. **FT-IR (powder): υmax** 1615, 1584, 1480, 1458, 1404, 1368, 1200, 1136, 970, 875, 829, 756, 688 cm^{-1}; **^{1}H NMR** ($CDCl_3$, 200 MHz): δ 8.92 (s, 2H), 7.81 (s, 2H), 7.46-7.44 (m, 4H), 7.30-7.28 (m, 6H), 3.99 (s, 6H); **^{13}C NMR** ($CDCl_3$, 50 MHz): δ 155.9, 153.9, 152.4, 129.2, 128.5, 126.1, 121.2, 109.6 and 56.2.

3.4.3 *Synthesis of 2,5-bis((E)-(phenylimino)methyl)benzene-1,4-diol (Reference compound for DhaTph)*:

The reference compound was synthesized by the reaction between 2,5-dihydroxyterephthalaldehyde (**Dha**) (0.100 g, 0.602 mmol) and aniline (0.225 g, 2.408 mmol) in 30 mL ethanol under refluxing condition for 24 h. After this time the solution was cooled to room temperature and the precipitate was collected by filtration, washed with ethanol, and dried under vacuum to give 0.158 g, 84% of a yellow solid. FT-IR (powder): υmax 1611, 1582, 1486, 1455, 1394, 1344, 1207, 1158, 970, 878, 857, 798, 778, 761, 686 cm^{-1}; ^{1}H NMR ($CDCl_3$, 200 MHz): δ 12.60 (s, 2H), 8.62 (s, 2H), 7.43-7.27 (m, 10H), 7.10 (s, 2H); ^{13}C NMR ($CDCl_3$, 50 MHz): δ 161.8, 153.0, 132.9, 129.5, 127.5, 123.4, 121.3 and 119.3.

3.4.4 *Synthesis of COF DmaTph*:

The synthesis of **DmaTph** was carried out by utilizing the same protocol with a mixture of 2,5-dimethoxyterephthalaldehyde (**Dma**) (15.5 mg, 0.08 mmol) and tetra(*p*-amino-phenyl)porphyrin (**Tph**) (27.0 mg, 0.04 mmol) in presence of 6 M acetic acid (0.2 mL) using dichlorobenzene, ethanol (1:1) as solvent combination (2 mL). This mixture was sonicated for 10-15 minutes in order to get a homogenous dispersion. The tube was then flash frozen at 77 K (liquid N_2 bath) and degassed by three freeze-pump-thaw cycles. The tube was sealed off and then heated at 120 °C for 3 days. After the reaction the COF powders are filtered out, washed with ethanol and dried under vacuum at 150 °C for 12 hours to give purple colored powder in 79 % (28 mg) isolated yield based on **Tph**. IR (powder): υmax 1612,1585, 1498, 1466, 1409, 1370, 1289, 1212, 1148, 970, 883, 851, 798, 736 cm^{-1}.

3.4.5 *Synthesis of COF DhaTph*:

The synthesis of **DhaTph** was carried out by utilizing the same protocol with a mixture of 2,5-dihydroxyterephthalaldehyde (**Dha**) (13.3 mg, 0.08 mmol) and tetra(*p*-amino-phenyl)porphyrin (**Tph**) (27.0 mg, 0.04 mmol) in presence of 6 M acetic acid (0.2 mL) using dichlorobenzene, ethanol (1:1) as solvent combination (2 mL). This mixture was sonicated for 10-15 minutes in order to get a homogenous dispersion. The tube was then flash frozen at 77 K (liquid N_2 bath) and degassed by three freeze-pump-thaw cycles. The tube was sealed off and then heated at 120 °C for 3 days. After the reaction the COF powders are filtered out, washed with ethanol and dried under vacuum at 150 °C for 12 hours to give purple colored powder in 79 % (28 mg) isolated yield based on **Tph**. IR (powder): υmax 1613, 1590, 1491, 1399, 1338, 1313, 1213, 1149, 968, 888, 849, 797, 718 cm^{-1}.

3.4.6 *General methods for characterization*

All reagents were commercially available and used as received. Microscopy images of these hollow fibers were taken in Zeiss SteREO Discovery V20.

a) ***Wide-angle X-Ray Diffraction (WAXD)*:** The wide-angle X-Ray Diffraction (WAXD) analysis of MOFs and the composite membranes were carried on a Rigaku SmartLab X-ray diffractometer in reflection mode using CuKα radiation (λ = 1.54 Å). The 2θ range from 5° to 40° was scanned with a scan rate of 3° min^{-1}. The instrument was previously calibrated using a silicon standard.

b) ***FT-IR spectroscopy*:** The Fourier transform infrared spectra (FT-IR) were taken on a Bruker Optics ALPHA-E spectrometer with a universal Zn-Se ATR (attenuated total reflection) accessory in the 600-4000 cm^{-1} region or using a Diamond ATR (Golden Gate). The spectra were measured over the range of 4000-400 cm^{-1}.

c) ***Scanning Electron Microscopy*:** Scanning Electron Microscopy (SEM) was performed on a FEI Quanta 200 3D ESEM (dual beam) instrument with a field emitter as an electron source and in FEI Nova Nano SEM 650 Scanning Electron Microscope. SEM images of membrane cross section were taken after freeze cut off membranes in LN_2. Samples for SEM were gold sputtered before analyses.

NOTE: The results of this chapter have already been published in *Angew. Chem. Int. Ed.*, 2013, *52*, 13052–13056. with the title: "*Enhancement of chemical stability and crystallinity in porphyrin containing covalent organic frameworks using intra-molecular hydrogen bonding.*" These publications were the results of the collaboration between the group of Dr. Rahul Banerjee and his students Sharath Kanadambeth, Digambar Balaji Shinde and Manas K. Panda from National Chemical Laboratory, Pune, India and the group of Dr. Thomas Heine and his students Binit Lukose from Jacobs University, Germany. Apart from computational study major works contributed by Sharath Kandambeth.

CHAPTER 4

Self-Exfoliated Chemically Stable Guanidine Based Ionic Covalent Organic Nanosheets (iCONs) for Antimicrobial Application

Abstract: *2D-Covalent Organic Frameworks (COFs) posses a stacked layered structures, with intrinsic micro-porosity. The strong π-π stacking interaction binds the individual COF layers. Attempts such as mechanical grinding and sonication were employed previously to exfoliate the stacked layered COF structures to ultrathin 2D covalent organic nano sheets (CONs). But these methods bear's disadvantages such as low yield, and plausible layer restacking after the exfoliation. Here we introduced a new methodology of incorporating positively charged linker unit (guanidine moiety) in the COF back born, by which COFs can be easily exfoliated to CONs under mild sonication. The repulsion between the positively charged guanidine moieties in the layer reduces the inter layer interaction between COF layers. The ionic CONs can be synthesized in good yield and display high dispersional stability. Due to the presence of guanidine moieties, CONs display antimicrobial activity towards both gram positive and gram negative bacteria.*

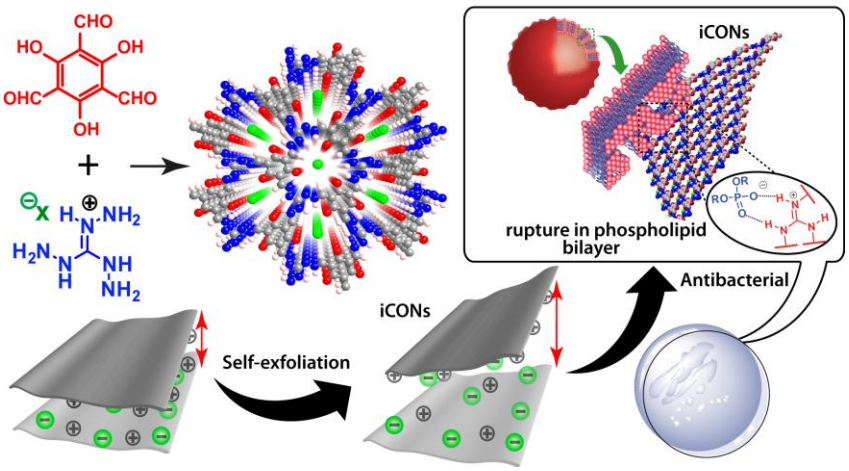

4.1 Introduction

Exploring two dimensional (2D) materials in a few atom thicknesses with unique properties has been a long standing challenge by the researchers [4.1a]. Pioneering discovery of graphene and its gradual development on to thin layered materials opened up the opportunity for other 2D materials [4.1]. Covalent organic nano-sheets (CONs) belongs to such 2D materials which posses tunable porosity and diverse functionality constructed by symmetrically arranged organic linkers *via* strong covalent bonds [4.2]. 2D COFs are usually synthesized in stacked layer stucture, with strong π-π stacking interaction between the layers [4.2c]. Bringing down COF thickness to the atomic level and exploring their diverse properties are yet to be achieved because of the synthtic difficulties [4.3] and chemical stability issues [4.4]. On this line, researchers have synthesized few layered CONs by conventional exfoliation of covalent organic frameworks (COFs) using ultrasonication [4.3a] and mechanical delamination [4.3b]. However, poor dispersion stability, low yield, lack of control on exfoliation, difficult synthetic challenges hinders their practical application [4.3] especially in biomedical perspectives, which are in high demand [4.1c]. In contrast, stable, biocompatible, good dispersions are the prerequisites to design thin layered functional CONs that could enhance their lifetime, stability and bioavailability for energy and health care materials [4.1c]. The major road blocks to obtain monolayer or few layered CONs includes strong π-π stacking between the growing layers, hydrolytic stability for most of the COFs [4.4], possible restacking onto COF layers [4.5] and difficult synthetic procedures [4.6]. Notably, these downfalls could be surpassed by the rational designing of stable CONs with inbuilt ionic character and decreasing the Van der Waal interaction between the layers. Nevertheless, the direct synthesis of ultrathin 2D CONs have rarely been explored in their monolayer or few layer thicknesses and thus remain a daunting task. Recently, ionic liquid mediated exfoliations of 2D materials have attracted attention to produce thin nano sheets from their bulk counterparts presumably by intercalation of charged species in between the layers [4.7]. Therefore, we anticipated judicious introduction of intrinsic ionic linker into the framework might result lower π-π stacking to produce directly exfoliated CONs during synthesis in the absence of any external stimuli. Although designed synthesis of thin layered CONs together with ionic character within a single domain is in demand, but such materials are unprecedented. In the same pursuit we, for the first time have introduced the concept of

rational designing for self exfoliated guanidinium halide based porous ionic CONs (iCONs) for antimicrobial applications.

Considerable attentions have been paid on antimicrobial application of few typical 2D materials due to its encasement property. However, tedious synthetic procedure, use of highly oxidizing agents, narrow functionalization opportunity and often multistep fabrications limits their practical applications [4.8]. Alternatively, suitably designed very thin or few layered CONs could pave the way with tunable porosity and functionality for biomedical perspectives especially in antimicrobial applications. In this regard, some of the guanidine based materials are known to demonstrate antimicrobial property [4.9], which is believed to occur through electrostatic interaction with the cell membrane of the microorganism [4.9]. High water solubility of these materials sometimes limit their application for heterogeneous water resistant antimicrobial coatings, but introduction of such an ionic guanidine linker to construct porous COFs or CONs is yet to observe till date. Strategically designed guanidine based porous iCONs could evolve with both the properties within a single domain. Acknowledging such archetypal features we have chosen guanidinium halide that contains two free -NH_2 groups, and was further amine functionalized to yield C_3 symmetric triamine. This triaminoguanidinium halide was allowed to react with 1,3,5-triformylphloroglucinol (**Tp**) to construct the iCONs. Positively charged guanidinium unit could result interlayer repulsion to self exfoliate into few layered iCONs; meanwhile it is expected to induce the antimicrobial property within the framework.

Herein, we demonstrate synthesis and characterizations of three intrinsically exfoliated iCONs ($TpTG_{Cl}$, $TpTG_{Br}$ and $TpTG_{I}$) with three different counter anions (Cl^-, Br^-, I^-) (***Figure 4.1***). The iCONs display porosity, high chemical stability and importantly antimicrobial property against *Escherichia coli* (gram negative) bacteria and *Staphylococcus aureus* (gram positive) bacteria. On evaluation of its mode of action, we found the rupture in cell membranes of bacteria in course of interaction with iCONs plays the pivotal role for its antibacterial property, which was well supported by microscopic and molecular dynamics study. We further anticipated that these thin layered nano sheets could be easily processed to design membranes. Keeping this in mind, we further fabricated iCONs@ polyacrylonitrile based membrane with potent antimicrobial property, which could be useful for antimicrobial coatings and biomedical applications. To best of our knowledge, this is the first report for

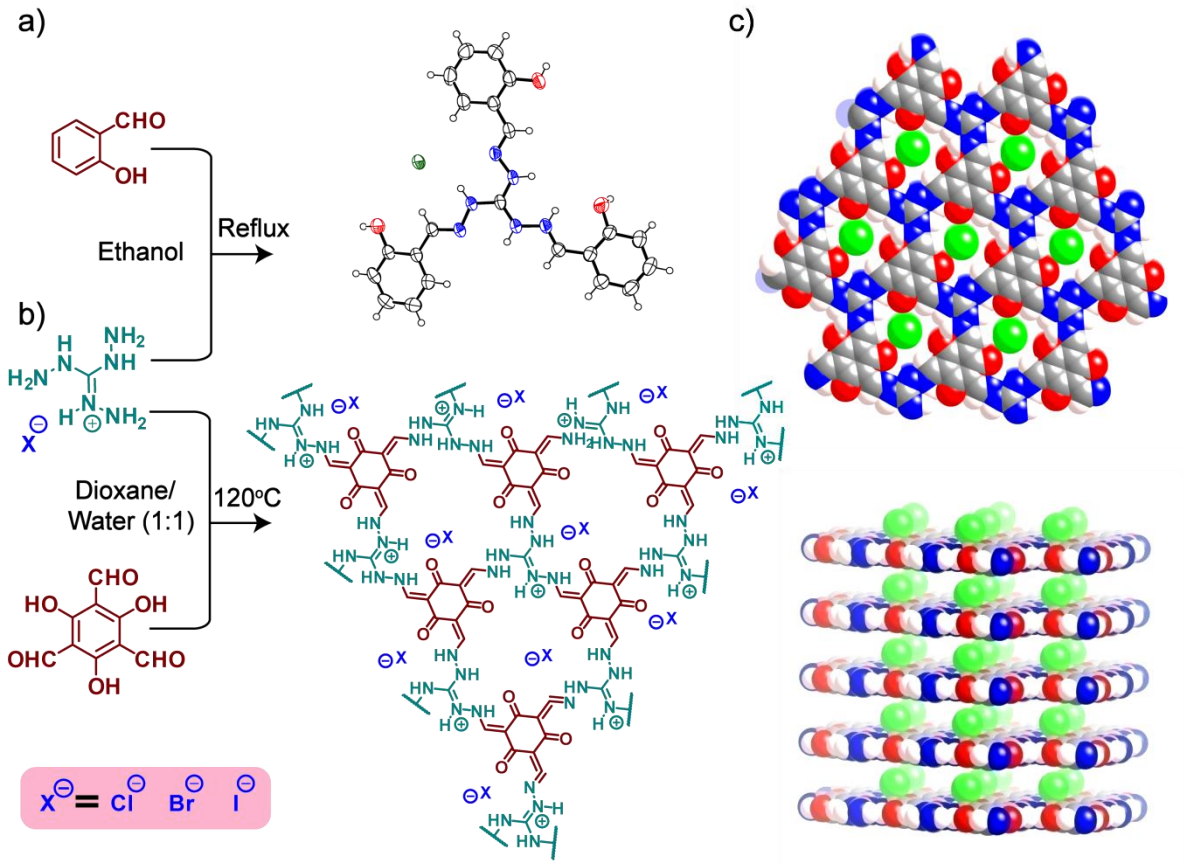

Figure 4.1. *(a) Schematic representation of the synthesis of (a)* ***TpTG$_{Cl}$*** *monomer (top) and (b) iCONs (****TpTGx*** *were x=Cl^{-1}, Br^{-1}, I^{-1} .(c) Space fill models of eclipsed stacked structures of* ***TpTG$_{Cl}$****.*

rational designing of porous antimicrobial iCONs by judicious selection of ionic linker for biomedical perspectives.

4.2 Result and discussion

4.2.1 *Synthesis of iCONs*

iCONs were synthesized by the Schiff base reaction between 0.2 mM 1,3,5-triformylphloroglucinol (Tp) (42 mg) and 0.2 mM triaminoguanidinium halide [4.10] (TG_{Cl}: 28 mg, TG_{Br}: 37 mg and TG_{I}: 47.4 mg) in as sealed pyrex tube. At first, both reactants were mixed together inside a pyrex tube, in presence of dioxane: water solvent combination (2: 0.6 mL). In the second step, the mixtures were sonicated for about 20 minutes and the tube was sealed off after applying three freeze-pump-thaw cycles. The sealed tube containing reactants and solvents was kept in an oven at 120 ˚C for 3 days. $TpTG_{Cl}$, $TpTG_{Br}$ and $TpTG_{I}$ were

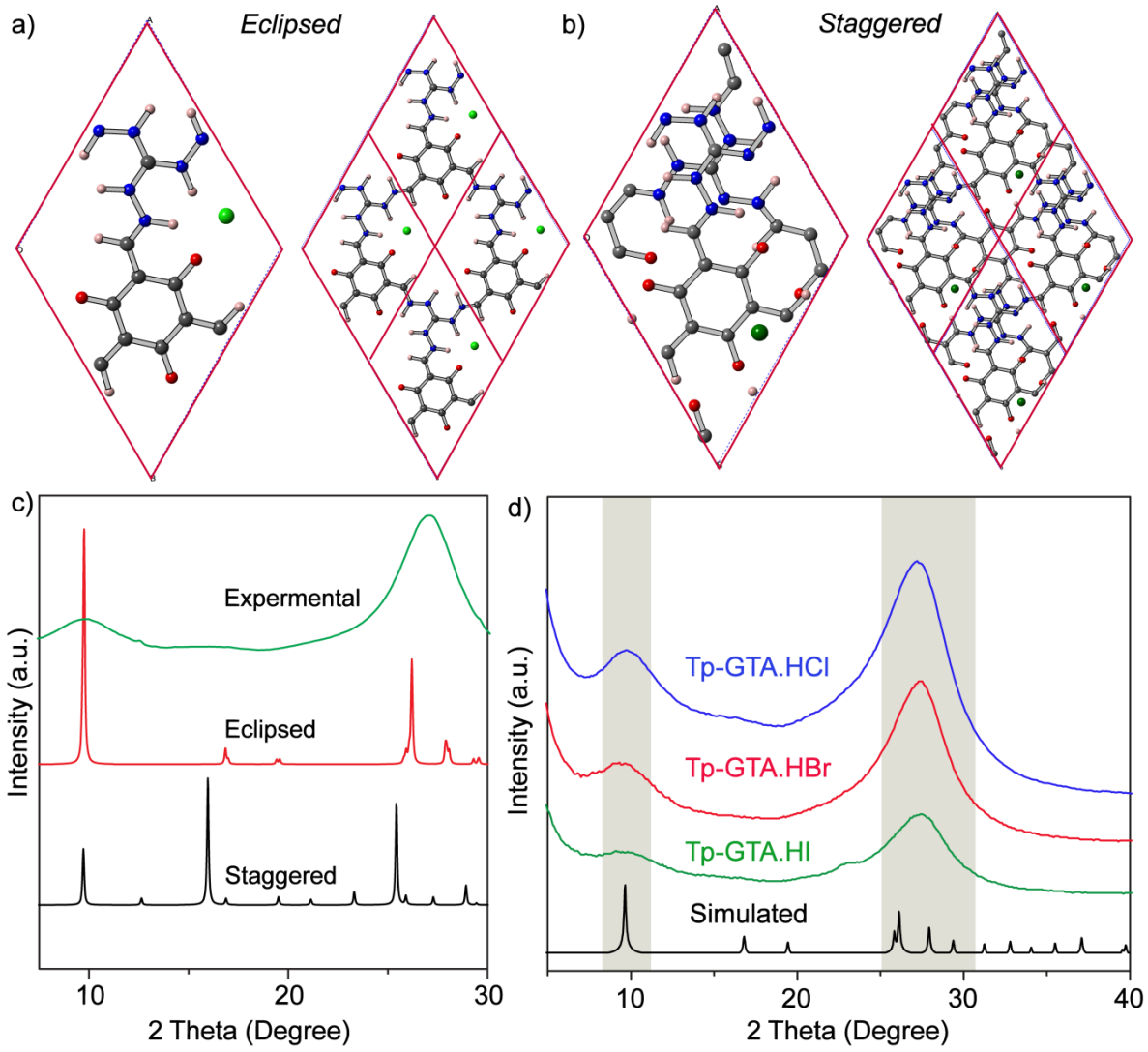

***Figure 4.2**: (a) Unit cell and eclipsed crystal lattice packing of **TpTG$_{Cl}$**. (b) Unit cell and staggered crystal lattice packing of **TpTG$_{Cl}$**. (c) PXRD spectra of As-synthesized (green) iCONs **TpTG$_{Cl}$** compared with the eclipsed (red), staggered (black) stacking models.(d) Comparison of the PXRD patterns of **TpTG$_{Cl}$**, **TpTG$_{Br}$**, **TpTG$_{I}$** with the eclipsed simulated PXRD pattern.*

obtained as brown colored precipitate and washed thoroughly with DMAc, water and acetone respectively. Finally the product was dried at 90 ˚C for overnight and collected in ~80 % isolated yield. C, H, N micro-elemental analysis of TpTG$_{Cl}$, TpTG$_{Br}$ and TpTG$_{I}$ closely matched with the theoretical formula indicating their purity.

4.2.2 *Structural simulation and characterization*

Crystallinity of these iCONs was measured *via* PXRD analysis, which indicated that they were moderately crystalline in nature as expected. PXRD pattern revealed the first peak

of the three iCONs appear almost in the similar position with 2θ = 9.78°, 9.78°, 9.77° for $TpTG_{Cl}$, $TpTG_{Br}$ and $TpTG_I$ respectively, which corresponds to the 100 plane (***Figure 4.2c and 4.2d***). The major broad peak appeared at 2θ = 27.2°, 27.3°, 27.4° for $TpTG_{Cl}$, $TpTG_{Br}$ and $TpTG_I$ signified the π-π stacking between the vertically stacked sheets (***Figure 4.2c and 4.2d***). It is worth to mention that the π-π stacking peak predominates the first peak due to intrinsic ionic TG_x moiety (produces interlayer repulsion and posses sandwiched halide ions). In order to understand this (broad nature of 001 peaks) phenomenon, monomeric unit of our desired iCONs were synthesized by the reaction between salicylaldehyde and TG_{Cl} and crystallized accordingly (***Figure 4.1a***) [4.10]. Synthetic scheme of *N*', *N*",-2-tris((E)-2-hydroxybenzylidene)hydrazine-1-carbohydrazonhydrazide hydrochloride ($TpTG_{Cl}$ monomer) is shown in ***Figure 4.1.a***. ORTEP diagram of the corresponding monomer is represented at 50% probability level ellipsoid (***Figure 4.1a***). Interestingly, the stacking diagram of monomer showed the presence of chloride anion sandwiched between the monomer molecules, which remain hydrogen bonded with the guanidinium hydrogen and hydroxyl group of salicylaldehyde (***Figure 4.1c***). This results in an interlayer distance of 3.4 Å between the aromatic rings (***Figure 4.1c***). The presence of this loosely bound chloride ions between the COF layer disturbs the pi-pi stacking interaction between the COF layer which we believe is the reason for the broad nature of 001 peaks (***Figure 4.2c and 4.2d***).

Based on the monomer structure, three of the iCONs structures ($TpTG_{Cl}$, $TpTG_{Br}$ and $TpTG_I$) were modelled in possible 2D eclipsed and staggered mode using Materials Studio (version 6.1). Conventional modelling of $TpTG_{Cl}$ in fully eclipsed AA stacking mode was carried out using *P*1 space group with the unit cell parameters *a*=10.52 *b*= 10.5. Å, *c*= 3.4 Å, and α= 89.2 β= 90.8°, γ= 119.0 ° (***Figure 4.2a***). Similarly, modelling of other two iCONs *viz.*. It is worth to mention that in all the cases experimental PXRD pattern matches well with the eclipsed AA stacking mode of simulated one (Figure 4.2c). The π-π stacking distance was found to be ~3.35 Å, ~3.3 Å, ~3.4 Å for $TpTG_{Cl}$, $TpTG_{Br}$ and $TpTG_I$ respectively, where sandwiched halide ions were present between the layers (***Figure 4.1c***). Although the monomeric unit was planner, but the ionic layers with sandwiched ions in between them prevented stronger stacking between the layers (***Figure 4.1c***), which resulted in lower crystallinity of the samples. This brightened our hunch that as obtained iCONs could lead to the formation of few layered thick nano sheets.

4.2.3 *Chemical characterization.*

FTIR spectra revealed the formation of iCONs from corresponding amines (TG_x) and aldehyde (Tp). Characteristic carbonyl (–C=O) stretching frequency at 1636 cm^{-1}, C–H stretching frequency (2923 cm^{-1}) of the aldehyde in Tp and N–H stretching frequency (3314 cm^{-1}) of primary amine (TG_x) was disappeared in the corresponding product (***Figure 4.3a***). This suggested complete utilization of the starting materials to form the product. Meanwhile in $TpTG_x$ instead of imine signals characteristic exocyclic C=C stretching frequency was noted (***Figure 4.3a***). For example in $TpTG_{Cl}$, a characteristic C=C stretching frequency was observed at 1597 cm^{-1} and the characteristic stretching at 1291 cm^{-1} was pertained to C–N stretching frequency. $TpTG_{Br}$ and $TpTG_I$ also demonstrated similarity in their peak patterning (***Figure 4.3a***). Formation of C=C was attributed to the irreversible enol to keto tautomerism in course of reaction and is consistent with our previous reports. Although a keto (C=O)

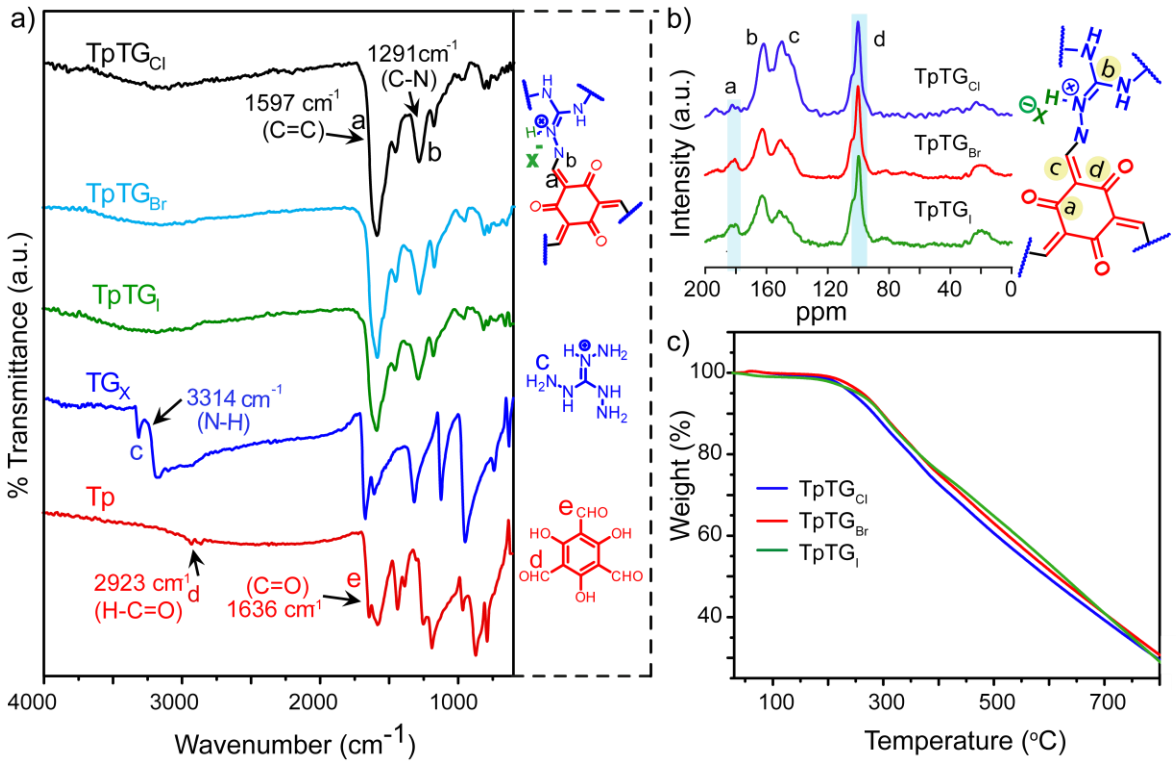

***Figure 4.3**: (a) Comparison of the FT-IR spectra of **TpTG$_{Cl}$** (Black), **TpTG$_{Br}$** (cyan), **TpTG$_I$** (Green) with the starting materials Tp (red) and TG_{Cl} (blue). (b) Comparison of the , ^{13}C CP-MAS solid state NMR of **TpTG$_{Cl}$** (Black), **TpTG$_{Br}$** (cyan), **TpTG$_I$** (Green). (c) TGA profile of **TpTG$_{Cl}$** (blue), **TpTG$_{Br}$** (red), **TpTG$_I$** (green) under N_2 atmosphere.*

signal was inevitable in this process, but peak broadening in the extended structure resulted overlapping of –C=O signal with C=C stretching bands (***Figure 4.3a***). For further structural insights of iCONs, ^{13}C CP-MAS solid state NMR spectroscopy was carried out. $TpTG_{Cl}$ displayed an intense peak at 101 ppm which corresponds to the exocyclic carbon adjacent to the keto carbon; in contrast the C=C attached to the N was obtained at 149 ppm (***Figure 4.3b***). Deshielded carbon center attached to charged imine of guanidinium unit appeared at 162 ppm and a small signal obtained at 182 ppm belonged to the keto (–C=O) carbon of $TpTG_{Cl}$ (***Figure 4.3b***). Meanwhile $TpTG_{Br}$ and $TpTG_{I}$ showed almost identical NMR signal owing to the structural similarity of the iCONs framework. Exocylclic C=C signal and the keto carbon signal appeared at 100.2 ppm and 101.5 ppm for $TpTG_{Br}$ and $TpTG_{I}$ respectively (***Figure 4.3b***). Therefore NMR evidences confirmed the tautomerization into more stable keto form than to its less stable enol form. Thermal stability of these iCONs were verified by thermo-gravimetric analysis (TGA) carried out under N_2 atmosphere. The iCONs were almost stable up to ~250 °C and then started to decompose slowly. Nearly 60% weight loss was observed at higher temperature of 700 °C resulted in from the decomposition of the framework; meanwhile the initial weight loss (~2%) was attributed to the escaping of guest molecules from the framework (***Figure 4.3c***).

4.2.4 *Gas and water vapour adsorption studies*

Permanent porosity of these iCONs were measured by N_2 adsorption isotherms, at 77K (***Figure 4.4a***). All the three iCONs showed regular Type-II adsorption isotherm which was consistent with our proposed modelling; where the small pores of iCONs were blocked by subsequent anions. The Brunauer–Emmett–Teller (BET) surface area of $TpTG_{Cl}$, $TpTG_{Br}$ and $TpTG_{I}$ were found to be 267 m^2g^{-1}, 305 m^2g^{-1} and 298 m^2g^{-1} respectively. The lower surface area of iCONs may be related to the poor layer stacking, small pore diameter and pore blocking effect by the counter anion present in the pores. Non linear density function theory (NLDFT) was used for the pore size calculation of the three iCONs. Pore size distribution does not display any sharp peaks (***Figure 4.4c and 4.4d***) because of the disordered stacked structure and pore blocking effect by subsequent counter anions.

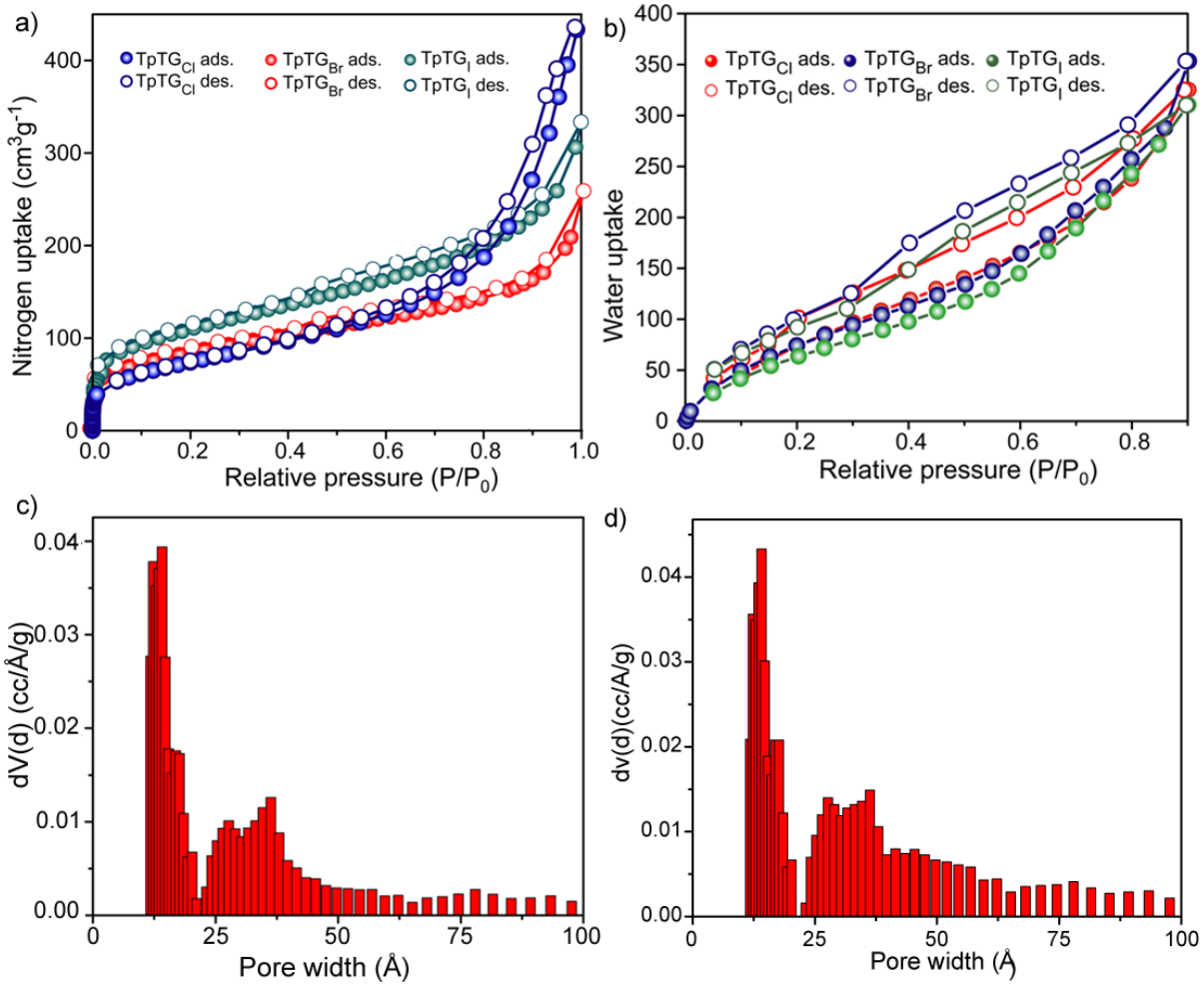

Figure 4.4: *(a) N_2 adsorption (at 77 K) and (b) water vapor adsorption of* ***TpTG$_{Cl}$*** *(blue),* ***TpTG$_{Br}$*** *(red),* ***TpTG$_{I}$*** *(cyan), (c) pore size distribution of TpTG$_{Cl}$. (d) pore size distribution of TpTG$_{Br}$.*

4.2.5 *Morphology analysis*

We measured the morphological attributes of all three iCONs by means of SEM, TEM and AFM. SEM imaging of TpTG$_{Cl}$, TpTG$_{Br}$ and TpTG$_{I}$ of all three showed nano sheet like morphology (***Figure 4.5***). TEM imaging of TpTG$_{Cl}$, TpTG$_{Br}$ and TpTG$_{I}$ showed thin Nano sheet like morphology and they were marginally puckered (***Figure 4.6***). Interestingly transparency in the TEM imaging of iCONs signified very thin layers of subsequent iCONs (***Figure 4.6***). TEM analysis was well supported by corresponding AFM measurements of iCONs drop casted on mica surfaces (***Figure 4.7***). Sheet like iCONs with high aspect ratio showed that their average height profile of around 2-4 nm, 3-4 nm and 3-4 nm for TpTG$_{Cl}$,

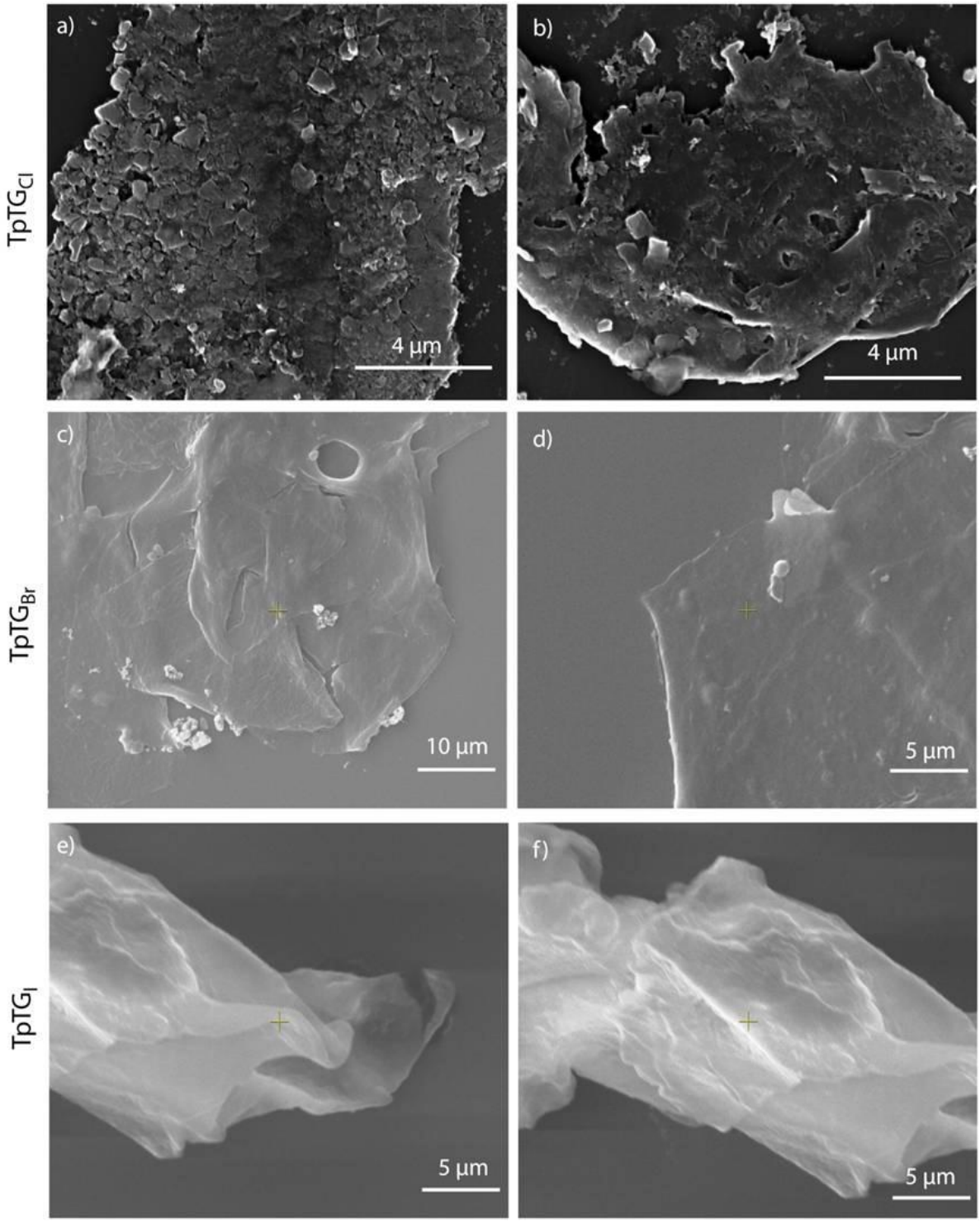

Figure 4.5: *SEM and images of iCONs (a) & (b)* ***TpTG$_{Cl}$****, (c) & (d)* ***TpTG$_{Br}$****, (e) & (f)* ***TpTG$_{I}$****.*

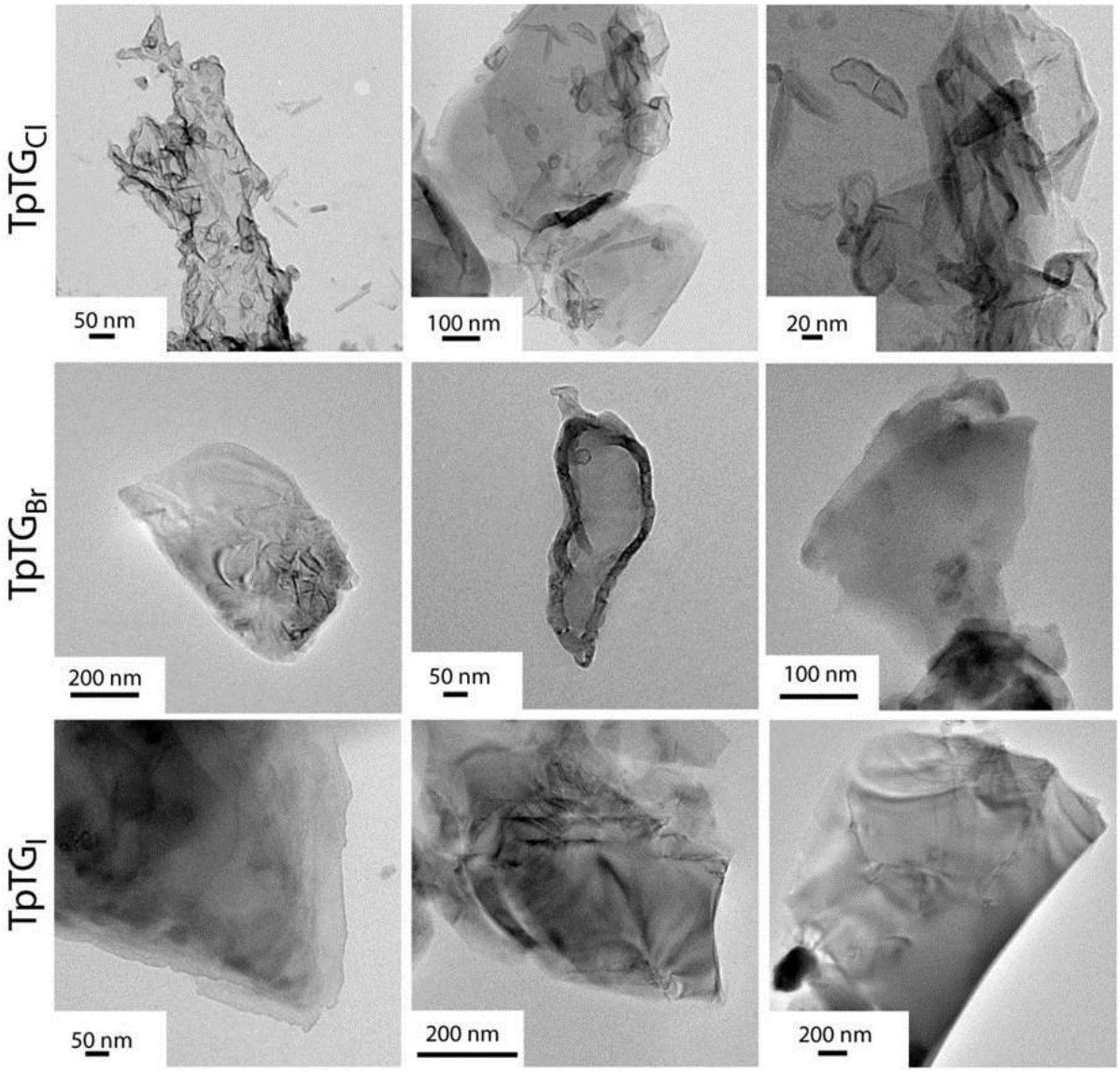

Figure 4.6: *(a) TEM and images of iCONs (* ***TpTG$_{Cl}$, TpTG$_{Br}$, TpTG$_{I}$****) under different magnifications.*

$TpTG_{Br}$ and $TpTG_{I}$ respectively. Hence, considering the π-π stacking distance of 3.35 Å, these iCONs were exfoliated into few thin layers accordingly or even comprised of 3-5 layers in some cases (***Figure 4.7***). Thin layered 2D materials are of prime importance in terms of applications, although difficult procedures or external stimuli are required for their exfoliation. Here, deliberate designing of TG_x based ionic backbone and sandwiched anions (Cl^-, Br^- and I^-) in between them resulted in interlayer repulsion hence rapid exfoliation into a few layered structures in absence of external stimuli or harsh conditions. Interestingly, pore

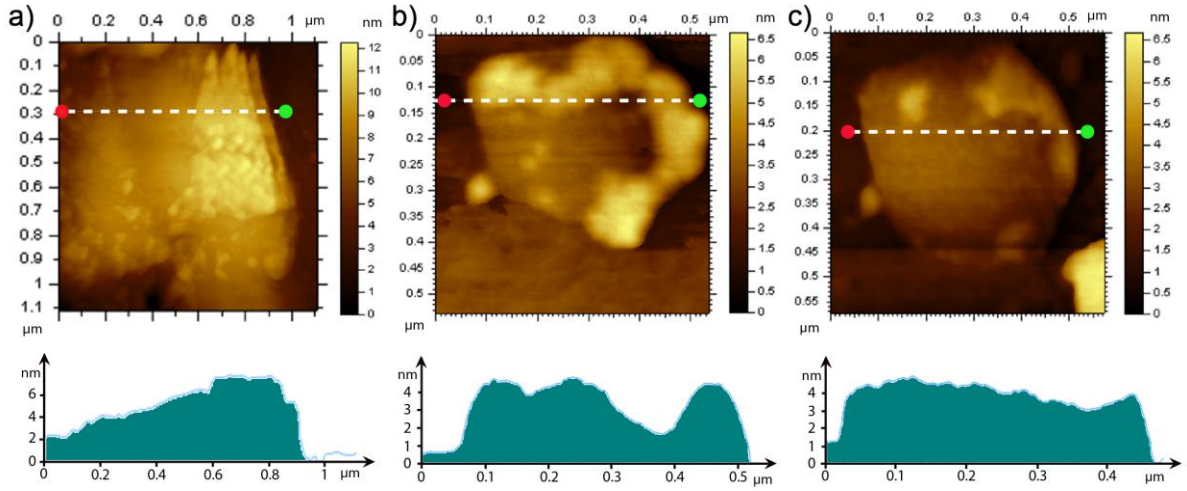

Figure 4.7: *3D height profile diagram of $TpTG_{Cl}$, $TpTG_{Br}$ and $TpTG_{I}$ respectively as obtained from AFM images.*

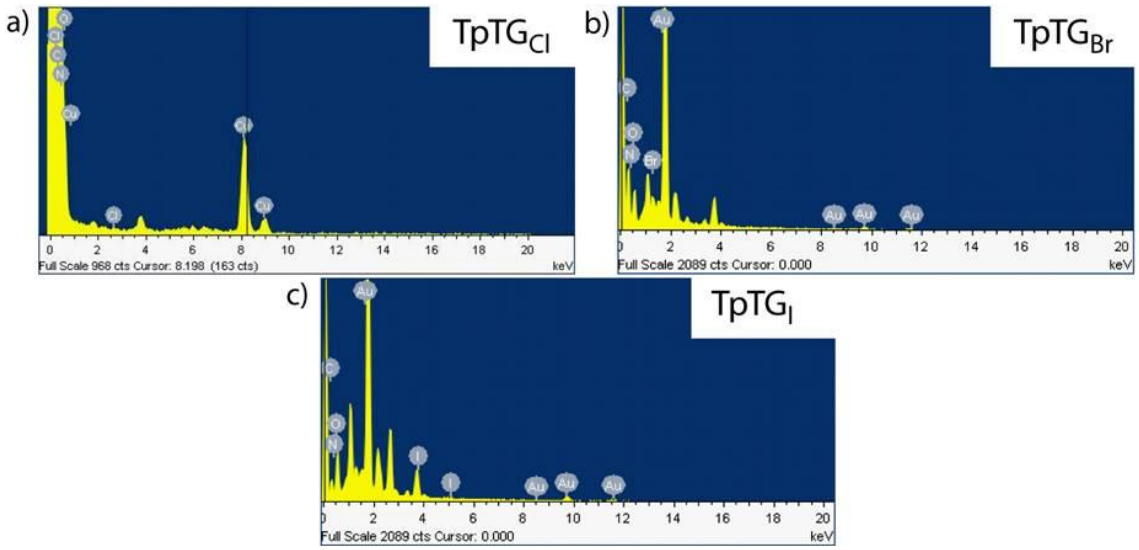

Figure 4.8. *EDX analysis of $TpTG_{Cl}$, $TpTG_{Br}$ and $TpTG_{I}$ associated with SEM, which showed C, H, O, N and corresponding halogens as the major chemical constituents respectively.*

blocking by counter anions together with very small pore size distribution could contribute to exfoliation mechanism as well (***Figure 4.9a***). All the three iCONs were dispersed in aqueous medium quite easily owing to their ionic backbone, and the dispersions were stable up to 20 days (***Figure 4.9***). When a red laser light was passed through the dispersions of $TpTG_{Cl}$ in isopropanol, it showed Tyndall effect signifying its stable colloidal suspension (***Figure 4.9d***). Notably Tyndall effect was observed for other two iCONs ($TpTG_{Br}$ and TpTGI) as well (***Figure 4.9e***).

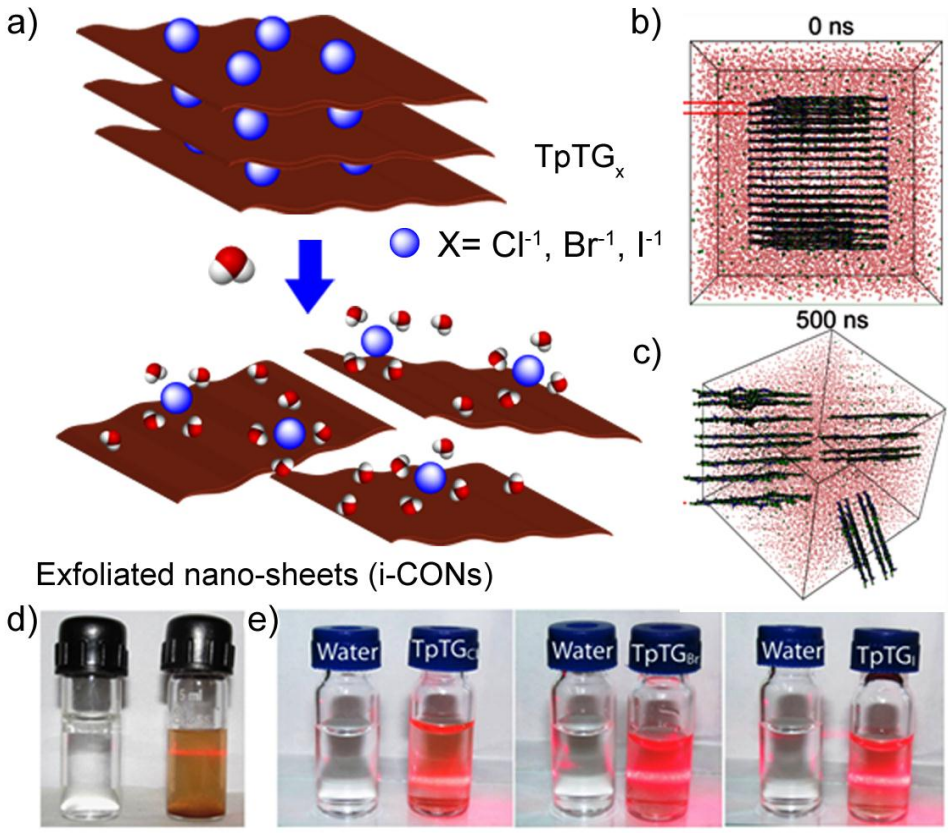

***Figure 4.9**: (a) Schematic representation of the self exfoliation of i-CONs in presence of water. (b) Snapshots from the MD simulation of i-CONs when treated with water (b) at 0s and (c) at 500 ns shows the formation of hydration sphere around chloride ions and self exfoliation of CONs. (d) & (e) Pictorial demonstration of 'Tyndall Effect' exhibited by TpTG$_X$ CONs in aqueous medium after 20 days. (d) When a red laser light was passed through the aqueous dispersions of TpTG$_{Cl}$ (right) 'Tyndall Effect' was noted, while pure water (left) did not exhibit any kind of such effect. This signified stable colloidal dispersion of TpTG$_{Cl}$.*

4.2.6 *Chemical stability*

The chemical stability of these iCONs were further verified by immersing about 10 mg of iCONs in 5 mL of different solvents such as methanol, acetone, THF and water for about 7 days. The iCONs were isolated and then subjected to PXRD and FTIR measurements. No significant changes were noted in the PXRD patterns with respect to the as synthesized one (***Figure 4.10***). It is noteworthy to mention that solvent mediated exfoliation could result increase in the (001) peak (for π-π stacking) and decrease in (100) peak (first intense one). Since, these iCONs were intrinsically exfoliated therefore additional

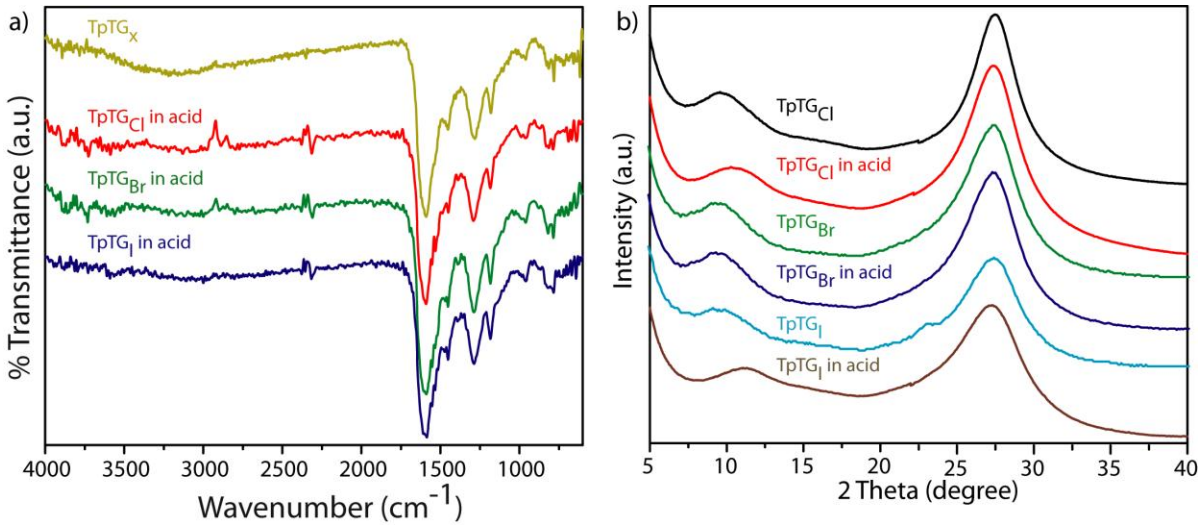

Figure 4.10: *(a) FTIR spectra and (b) PXRD pattern of TpTGCl, TpTGBr and TpTGI respectively in presence of 3N HCl for 7 days. No significant alterations were noted in the spectral pattern signifying its stability.*

changes in PXRD patterns were not observed in presence of different solvents. Similarly no significant alterations in FTIR spectra were noted in presence of aforementioned solvents in contrast to the as synthesized one (***Figure 4.10a***). Therefore the frameworks retained their structural integrity and the compositions were not leached out subsequently. Hydrophilic environment within the framework backbone of the iCONs was reflected in corresponding water adsorption isotherms (***Figure 4.4b***). 320 ccg^{-1}, 325 $ccg^{-1}$and 350 ccg^{-1} water uptakes was noted at 0.9 bar atmospheric pressure for $TpTG_{Cl}$, $TpTG_{Br}$ and $TpTG_I$ respectively (***Figure 4.4b***). It is noteworthy to mention that hydrophilic nature of these iCONs could enable their potential application in biomedical sectors.

4.2.7 *Antimicrobial activity*

Guanidine based compounds and polymeric materials are known to exhibit good antimicrobial activity [4.9]. Therefore we judiciously incorporated this TGx ($X=Cl^{-1}$, Br^{-1}, I^{-1}) moiety within iCONs such that it could have antimicrobial property together with exfoliated thin layered morphology owing to the positively charged guanidinium core. Since, basic framework of these three iCONs remained same, only difference was the counter anions sandwiched between the layers. Therefore, we have selected $TpTG_{Cl}$ as the model iCONs for detailed biological studies. Antibacterial analysis of $TpTG_{Cl}$ was carried out on both gram positive (*Staphylococcus aureus*) and gram negative (*Escherichia coli*) bacteria by

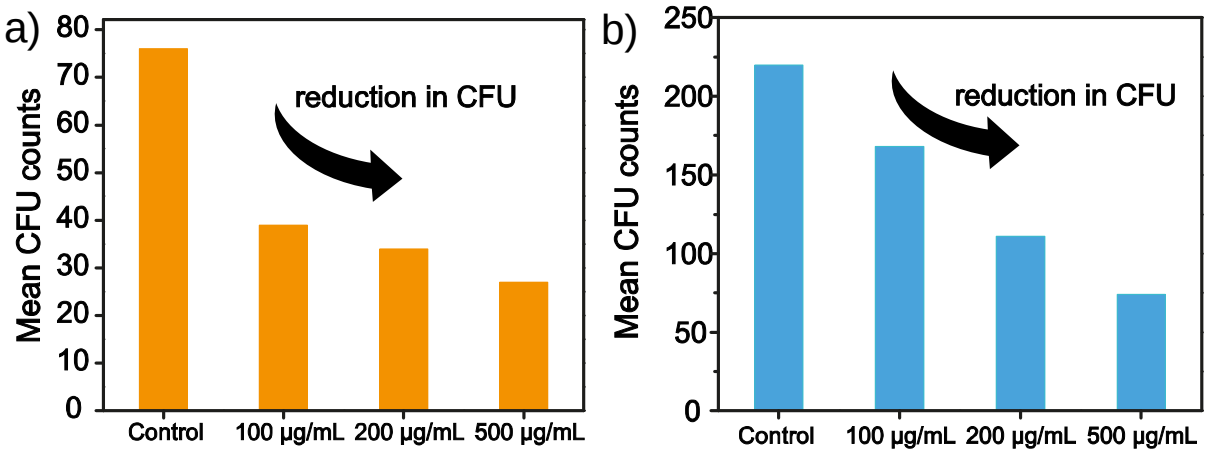

Figure 4.11. *Measurements of CFU against E. coli and S. aureus using three different concentration of* $TpTG_{Cl}$

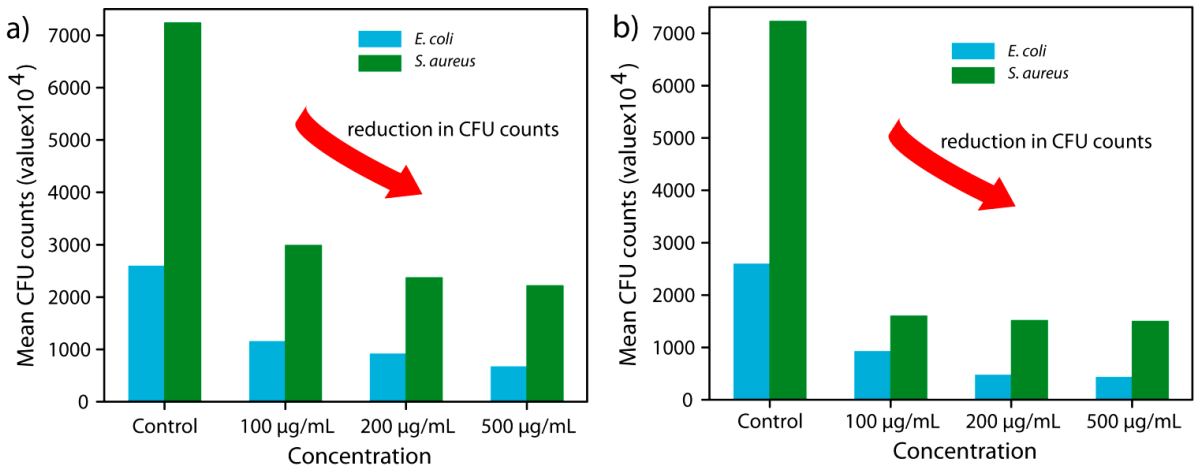

Figure 4.12. *Measurements of CFU against E. coli and S. aureus using three different concentration of* $TpTG_{Br}$ *and* $TpTG_{I}$.

measuring the colony forming units (CFU) according to standard protocols (***Figure 4.11 and 4.12***). $TpTG_{Cl}$ of three desired concentrations (100 µg mL^{-1}, 200 µg$mL^{-1}$and 500 µg mL^{-1}) were tested against both the strains of bacteria and after 24 h of incubation we found that the CFU counts in $TpTG_{Cl}$ treated sets were drastically reduced in contrast to the control ones in a concentration dependant manner (***Figure 4.11 and 4.12***). In order to determine the minimum inhibitory concentration (MIC) value, corresponding absorbance of treated bacterial suspensions were measured at 600 nm. MIC value of $TpTG_{Cl}$ was found to be 500 µg/mL and 500 µg/mL against *S. aureus* and *E. coli* respectively. Therefore, $TpTG_{Cl}$ could be used as potent antibacterial agent against a broad spectrum of microbial system. Time

Table 4.1. *Tabular summary of mean CFU counts per mL using three iCONs at 500 µgmL^{-1} .*

	Control (*E. coli*)	**Treated (*E. coli*)**	**Control (*S. aureus*)**	**Treated (*S. aureus*)**	**Activity on gram - ve**	**Activity on gram + ve**
TpTG$_{Cl}$	1100×10^4	370×10^4	380×10^4	135×10^4	+	+
TpTG$_{Br}$	2600×10^4	440×10^4	7230×10^4	1500×10^4	+	+
TpTG$_{I}$	2600×10^4	675×10^4	7240×10^4	2220×10^4	+	+

(+) denotes antibacterial property is present.

dependant CFU counts were also measured against *S. aureus* where TpTG$_{Cl}$ showed time dependency at a particular TpTG$_{Cl}$ concentration. Antibacterial activities of other two iCONs (TpTG$_{Br}$ and TpTG$_{I}$) were also measured against both the strains of bacteria where we found that both the iCONs showed antibacterial property against both the strains (***Figure 4.11 and 4.12***). The guanidinium Moieties present in the iCONs is mainly responsible for the antimicrobial activity [4.13]. In order to gain better insights into the mode of action we carried out microscopic studies (SEM and TEM) of control and TpTG$_{Cl}$ treated bacterial samples (***Figure 4.13***). SEM image of control *S. aureus* displayed spherical morphology

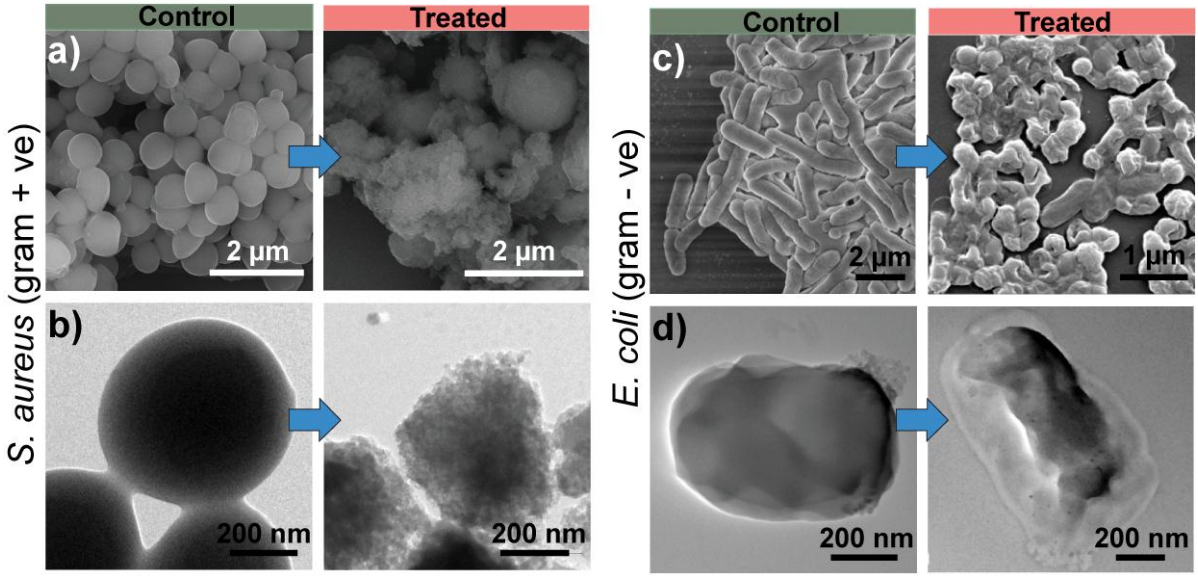

Figure 4.13. *(a) SEM images and (b) TEM images of control and TpTG$_{Cl}$ treated S. aureus, (c) SEM images and (d) TEM images of control and TpTG$_{Cl}$ treated E. coli.*

while the treated one showed ruptured spherical structure (***Figure 4.13a and 4.13b***). The same result was noted when we observed TEM images of control and treated *S. aureus*. Control samples showed smooth, spherical, continuous and unbroken cell membranes with spherical morphology; while the treated ones demonstrated shrunken, broken membrane with a ruptured spherical morphology (***Figure 4.13a and 4.13b***). The same observation was noted for *E. coli* treated with iCONs. The SEM and TEM image of the control *E. coli* sample displayed uniform rod like morphology, while the iCONs treated ones showed a significant alternation in shape, to shrunken, twisted rod like morphology (***Figure 4.13c and 4.13d***). We speculate that the guanidinium ion bearing iCONs were positively charged which could bind

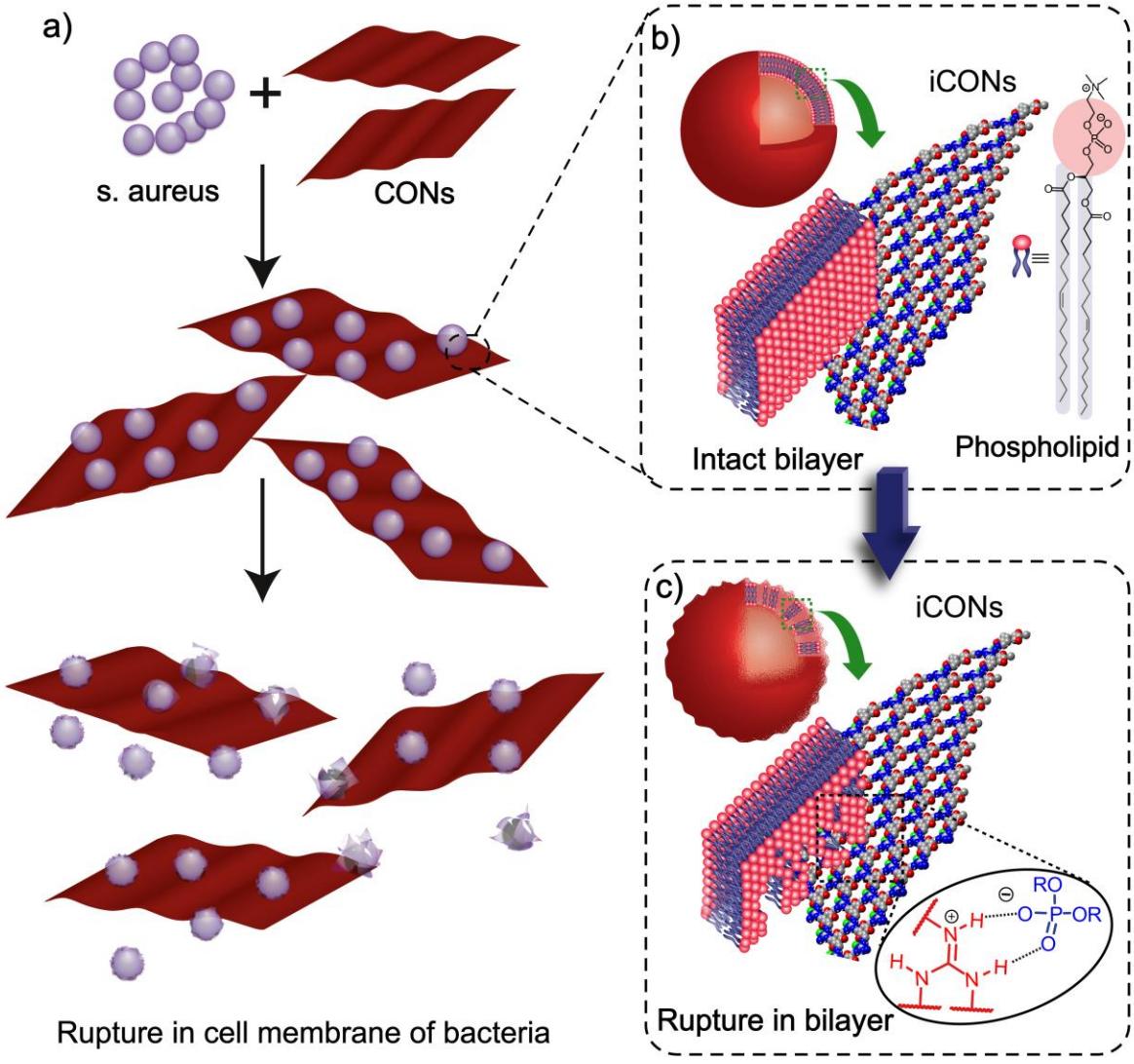

Figure 4.14. *Schematic representation for its mode of action between bacteria and iCONs.*

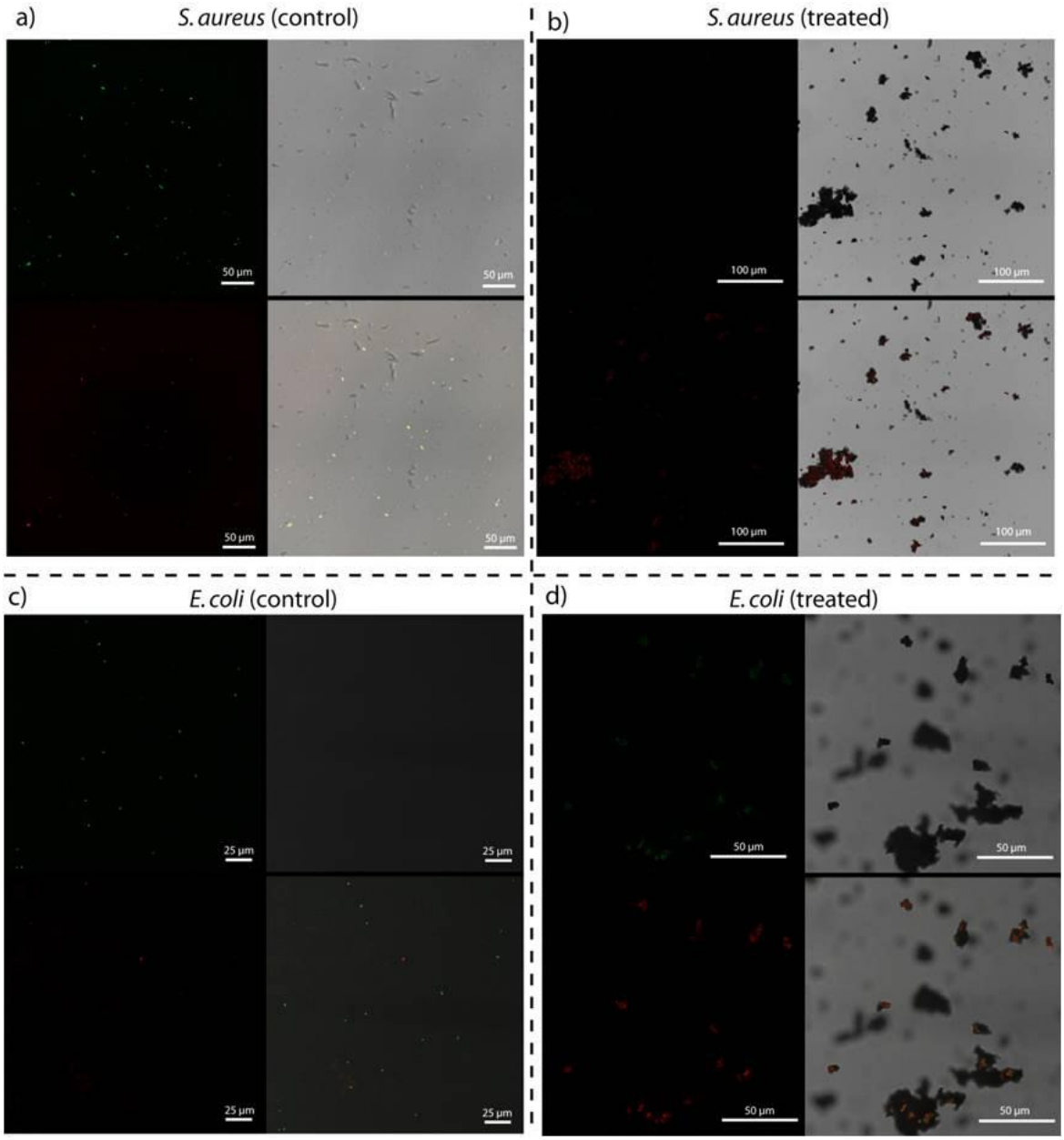

Figure 4.15*. Live/dead cell imaging using dye mixture of PI and FITC of control and TpTGCl treated bacterial cell. FITC is a non specific dye which can stain both the live and dead cell and is permeable through the bacterial cell membrane. On the other hand PI could only stain the dead cell to exhibit red fluorescence. In both the control bacterial cell (S. aureus and E. coli) we found abundance of green coloration than the red one signifying that greater amount of live cells were present. In both the TpTGCl treated sets (both S. aureus and E. coli) abundancy of red coloration was noted (i.e. dead cells). Even, sometimes red and green coloration was merged with some twisted, puckered morphology. We conclude that, control cells were intact; hence FITC could only penetrate to give green fluorescence signal. In contrary, treated cells showed rupture in the membrane; hence PI could show red coloration and FITC could simultaneously enter into the cell nonspecifically to give a merged signal.*

with the negatively charged phospholipid bilayer of the bacterial systems [4.14]. More importantly iCONs were obtained in nano-sheet like morphology which might have similar encasement/ wrapping property like graphene sheet or other 2D materials. Therefore iCONs could play a pivotal role by wrapping the bacteria cell followed by extraction of phospholipid bilayer *via* 'phospholipid sponge' type of mechanism which is much familiar with charged cationic polymeric unit and negatively charged bacterial surface reported in literature [4.9] (***Figure 4.14***). This could trigger rupture in cell membrane of the bacteria; finally lead to the leaching of cellular content and hence death of bacteria. The entire mode of action has been illustrated in schematically in ***Figure 4.14***. This proposed mode of action was well supported by live/dead cell imaging study (***Figure 4.15***). Both control and treated bacterial system was stained with a dye mixture of propydium iodide (PI) and fluorescein-B-isothiocyante (FITC). FITC is a non specific dye which can stain both the live and dead cell and is permeable through the bacterial cell membrane. On the other hand PI could only stain the dead cell to exhibit red fluorescence. In both the control bacterial cell (*S. aureus* and *E. coli*) we found abundance of green coloration than the red one signifying that greater amount of live cells were present. But in both the $TpTG_{Cl}$ treated sets (both *S. aureus* and *E. coli*) red and green coloration was merged with some twisted, puckered morphology (***Figure 4.15***). We conclude that, control cells were intact; hence FITC could only penetrate to give green fluorescence signal. In contrary, treated cells showed rupture in the membrane which was already evident from the TEM imaging (***Figure 4.15***). Hence PI could intercalate with DNA of the bacterial cell to give red coloration and FITC could simultaneously enter into the cell nonspecifically to give a merged signal. Entire imaging study corroborated with cell cycle analysis where treated one showed 19.4% specific binding in PI co-ordinate with respect to the control one. The structural aspects of the iCONs were intrinsically related with iCONs-bacteria interaction and antibacterial property.

4.2.8 *iCONs membrane fabrication*

Considering the health issues against bacterial infections, antibacterial agents are in high demand which could withstand the stability issues. Polymeric antibacterial material has been used to device textile, plastic and for purification to some extent. Also graphene based materials have been used to fabricate antibacterial paper. Inspired by such applications we

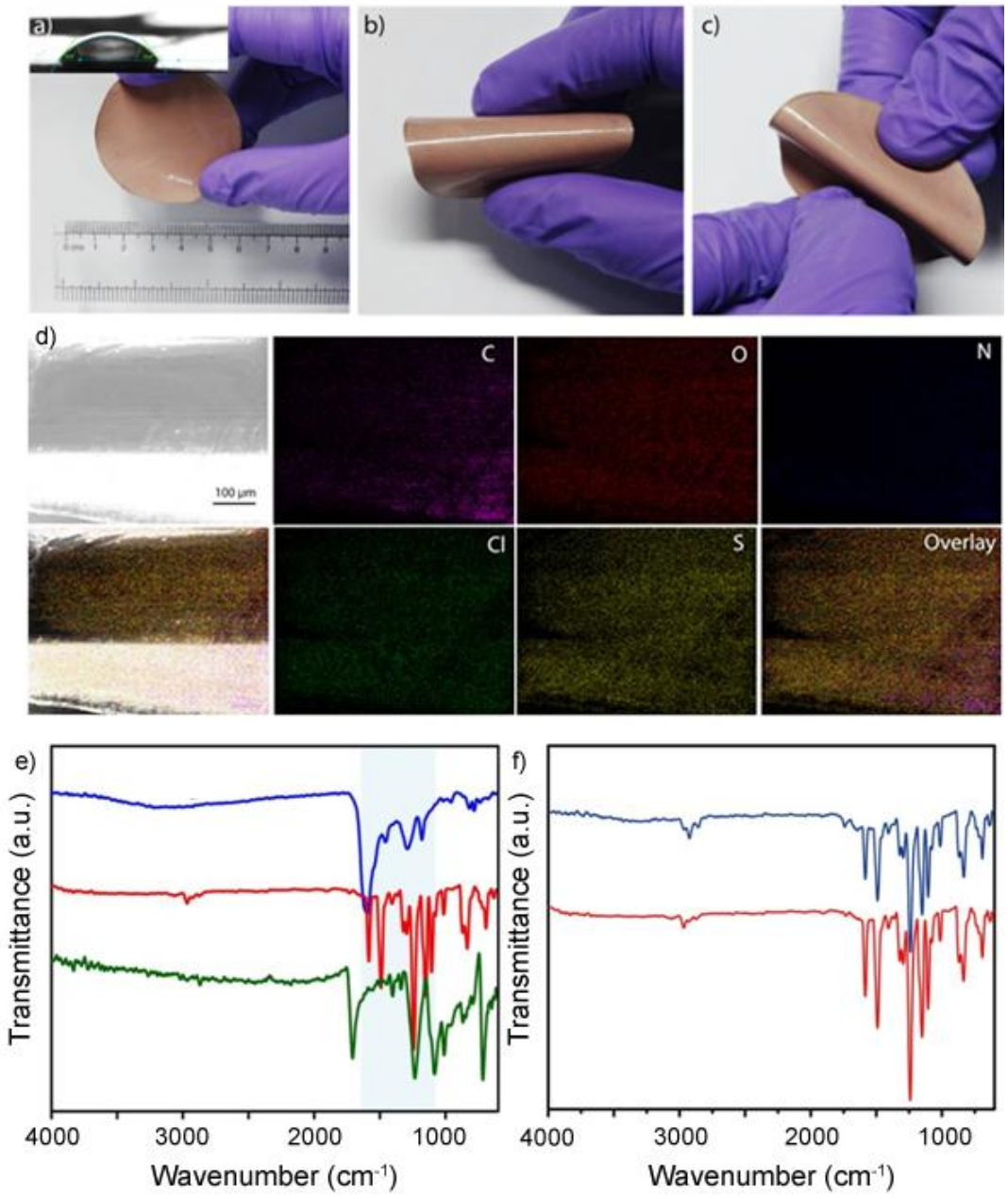

Figure 4.16. *(a-c) Digital image of $TpTG_{Cl}$@PSF mixed matrix membrane showing its good flexibility. Figure (a) inset shows the contact angle (~53˚) measurement of water at the water-air interface.(d) Elemental mapping of $TpTG_{Cl}$@PSF mixed matrix membrane. It indicates C, O, N, Cl and S as the major chemical constituents. Among them S is coming from PSF counterpart and Cl is coming from $TpTG_{Cl}$ counterpart. Elemental mapping suggested that they were homogeneously mixed and distributed over the membrane.(e)* Comparison of FTIR spectra between $TpTG_{Cl}$ (blue), PSF (green) and fabricated *$TpTG_{Cl}$@PSF membrane (red). (f) FTIR of $TpTG_{Cl}$@PSF membrane (red) showing their stability in water(blue).*

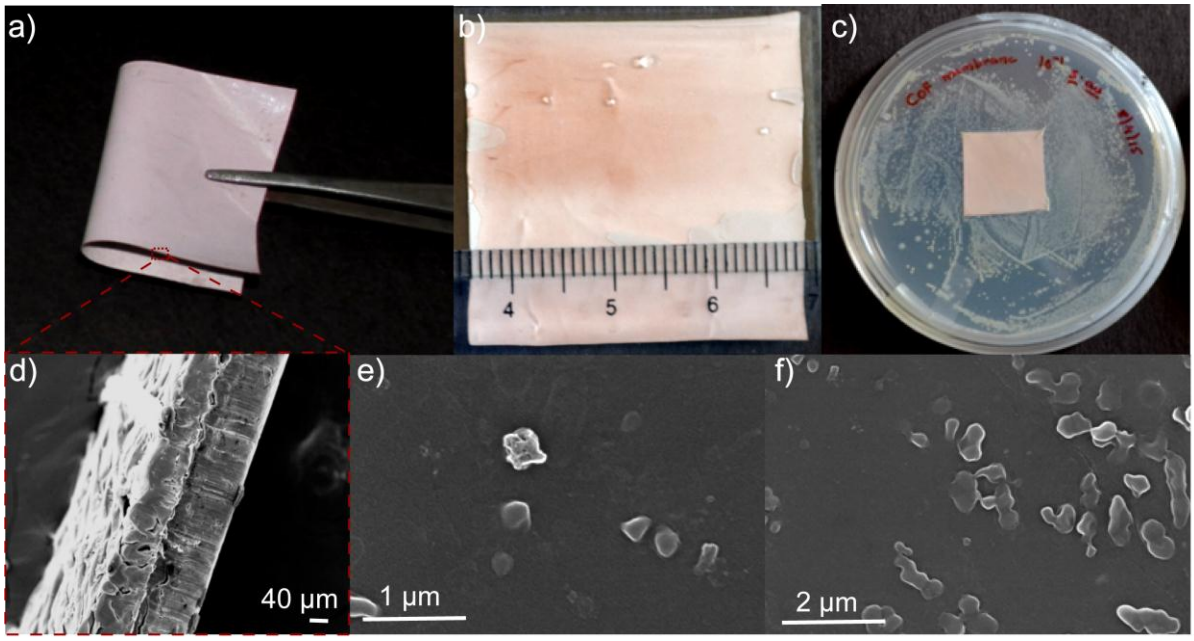

Figure 4.17*: (a) and (b) Digital image of $TpTG_{Cl}$@PSF mixed matrix membrane,(c)Antibacterial property of $TpTG_{Cl}$@PSF mixed matrix membrane by growth of (e) S. aureus and (e) E. coli on to it. (d) SEM image of the $TpTG_{Cl}$@PSF mixed matrix membrane.*

have attempted to device an antimicrobial membrane which could have potential application in medical sectors, since these iCONs emerged as antibacterial agents against a broad spectrum of bacteria. Antimicrobial mixed matrix membrane was devised with the help of polyacrylonitrile (PAN) and $TpTG_{Cl}$ on a support (***Figure 4.16***). The membrane was robust, free standing, stable and flexible as well (***Figure 4.16 a, b***). Stability of the membrane was retained for a long time in aqueous medium, iCONs ($TpTG_{Cl}$) were not leached out from the membrane materials. FTIR spectra of membrane showed distinguished peak of $TpTG_{Cl}$ even after membrane formation. It is noteworthy to mention that pristine TG_x or commonly used water soluble guanidine based polymeric materials could also exhibit antibacterial property, but their solubility issues in aqueous medium limits their mixed membrane formulations for further applications. ***Figure 4.17d*** illustrates SEM image of the membrane where presence of $TpTG_{Cl}$ and PAN on backing support was clearly observed. Antibacterial activity of this $TpTG_{Cl}$ membrane was evaluated by growth of the bacteria on to it; in contrast we took a normal filter paper as a control *S. aureus* and *E. coli* was allowed to grow on agar plate following standard protocols. To it square shaped filter paper and $TpTG_{Cl}$ membrane was placed and incubated for 24 h at 37 ˚C. Filter paper and $TpTG_{Cl}$ membrane was washed, fixed

and then subjected to SEM imaging. Interestingly in filter paper both the *S. aureus* and *E. coli* retained morphological integrity. While in $TpTG_{Cl}$ membrane both showed shrunken and rupturing of the morphology (***Figure 4.17 e, f***). This could be attributed to the antibacterial activity of iCONs mentioned earlier which is retained in the membrane as well and corroborated with our previous experiments. Taking into accounts such observations we propose iCONs mix matrix membrane, could be utilized as antibacterial coatings. It prevents bacterial infections which are often observed during wound healing. Herein, we devised 'band-aid' where the polymeric strip is replaced by our antibacterial $TpTG_{Cl}$ (iCONs) membrane which could prevent bacterial infection during wound healing. We believe strategic development of antibacterial iCONs together with antibacterial coatings could have significant impact in biomedical sectors.

4.3 Conclusion

In summary, we were able introduce a novel strategy by which 2D- covalent organic nanosheets can be synthesized and exfoliated in single step by imparting ionic character to the individual COF layer. The synthesized iCONs display high dispersional stability in water. iCONs display antibacterial activity against both gram negative (*E. coli*) and gram positive bacteria (*S. aureus*), due to the presence of guanidine moieties. Hyrogen bonding interaction between guanidine moieties of iCONs and phosphate anions of phospholipids is responsible for the rupture of cell membrane and hence the death of bacteria. We proposed that iCONs could act as 'phospholipid sponge' that dragged the negatively charged phospholipid out the bilayer through electrostatic interaction resulting in rupture of the membrane that finally led to death of bacteria in due course. This phenomenon was well established by detailed microscopic analysis and well supported by DFT, MD study as well. Taking into account these observations along with exposed surface of 2D iCONs we fabricated antibacterial membrane which could have potential medical benefits. iCONs could emerge as unique materials in water purification process which are underway and could have significant industrial impact. However, designing of functional 2D material with unique properties are still in a nascent stage and requires further attention. Nevertheless this work highlighted the first rational designing of thin layered iCONs with a distinct biomedical application, promising aspects of such materials for versatile applications are envisioned.

4.4 Experimental procedures

4.4.1 *Materials*

Guanidine hydrochloride and phloroglucinol was obtained from Sigma Aldrich; guanidine hydrobromide and guanidine hydroiodide was purchased from TCI chemicals. All other reagents were of analytical grade and used without further purification.

4.4.2 ***Synthesis of Triaminoguanidinium halide:*** Triaminoguanidinium chloride (TG_{Cl}) was synthesized using hydrazine hydrate in 1,4-dioxane under refluxing condition.[1] Briefly, 1.91 g of guanidine hydrochloride was added to 10 mL of 1,4-dioxane under stirring condition. To it, 3.41 g of hydrazine hydrate was added; the mixture was refluxed for 2 h. Then cooled to room temperature, filtered and washed with 1,4-dioxane to remove excess hydrazine hydrate and finally dried to yield TG_{Cl} (Yield: 98%). Similar methodology was used for synthesis of triaminoguanidinium bromide (TG_{Br}) [350 mg of guanidine hydrobromide and 500 µL of hydrazine hydrate] and triaminoguanidinium iodide (TG_I) [467 mg of guanidine hydroiodide and 500 µL of hydrazine hydrate].

4.4.3 ***Synthesis of iCONs:*** Three of the iCONs ($TpTG_{Cl}$, $TpTG_{Br}$ and $TpTG_I$) were synthesized *via* Schiff base condensation between 0.2 mmol 1,3,5-triformylphloroglucinol (Tp) (42 mg) and 0.2 mmol amines (TG_{Cl}: 28 mg or TG_{Br}: 37 mg or TG_I: 47.4 mg) in a sealed Pyrex tube. We used dioxane: water in the ratio (2: 0.6 mL) for subsequent synthesis of iCONs, the reaction mixtures were charged into Pyrex tube and sonicated for 20 min. The mixtures were degassed under liquid N_2 (77K) by freeze-pump-thaw cycles for three times. The Pyrex tube was then vacuum sealed and kept at room temperature until the reaction mixtures attended the room temperature. The sealed Pyrex tube containing the reaction mixture was kept at 120 ˚C for 3 days. $TpTG_{Cl}$, $TpTG_{Br}$ and $TpTG_I$ were obtained as brown colored precipitate. The product was washed thoroughly with DMAc, water and acetone respectively and dried at 90 ˚C for overnight to obtain ~70 % isolated yield. FTIR (ATR, cm^{-1}): 1597 (s), 1457 (w), 1291 (s), 1180 (m), 965 (w), 820 (w), 782 (w).

4.4.4 ***Synthesis of $TpTG_{Cl}$ monomer ($SaTG_{Cl}$) [N', N'',-2-tris((E)-2-hydroxybenzylidene)hydrazine-1-carbohydrazonhydrazide hydrochloride]:*** Triaminoguanidinium chloride (2.34 g, 0.017 mol) was dissolved in a hot mixture of ethanol (54 mL) and water (27 mL). A solution of 2-hydroxybenzaldehyde (0.05 mol) in ethanol was slowly added to it.[4] The resulting mixture was refluxed and the precipitate of $TpTG_{Cl}$ monomer [N', N'',-2-tris((E)-2-hydroxybenzylidene)hydrazine-1-carbohydrazonhydrazide hydrochloride] was collected accordingly. The precipitate of monomer was washed with acetone and dried under reduced pressure. Finally the monomer was crystallized by dissolving in hot ethanol.

4.4.5 ***Antibacterial assay:*** Antibacterial activity of iCONs were evaluated against both gram positive (*Staphylococcus aureus*) and gram negative (*Escherichia coli*) bacterial strains by measuring the colony forming units (CFU). Two of the bacterial strains were grown separately in potato dextrose agar (PDA) media and routinely cultured. Three different concentrations (100 μgmL^{-1}, 200 $\mu gmL^{-1}$and 500 μgmL^{-1}) of $TpTG_{Cl}$ iCONs were dispersed in autoclaved deionized water and allowed to incubate with bacterial strains for about 4h. The resulting mixture was plated in Petri plates containing solidified potato dextrose agar media. Meanwhile control samples contained deionized water instead of iCONs dispersions. The Petri plates were incubated at 37 ˚C for 24h and the resulting CFU counts were measured visually. All the experiments were carried out in triplicate and mean values were represented accordingly. Same experimental procedure was followed for $TpTG_{Br}$ and $TpTG_{I}$ respectively.

4.4.6 ***Morphological study of control and treated bacterial samples:*** Morphology of the control and treated bacterial samples were observed under SEM and TEM. For morphological studies the bacterial samples were cultured in potato dextrose broth (PDB) media. To it 500 μgmL^{-1} of $TpTG_{Cl}$ was added and incubated for 4h. Control and treated bacterial samples were isolated by centrifugation and washed with deionized water for three times. The samples were fixed with 2.5% glutaraldehyde solution and incubated at 4 ˚C for 30 min. The samples were further washed, dehydrated with graded ethanol (30%, 50%, 60%, 80% and 100%) and observed for morphological analysis.

4.4.7 ***Live/dead cell imaging study:*** Live/dead cell imaging analysis was performed under confocal microscope containing two staining dye mixture of propydium iodide (PI) and fluorescein-B-isothiocyante (FITC). Control and treated bacterial samples were cultured in potato dextrose broth (PDB) media as mentioned above and collected by centrifugation. To it dilute fluorescent dye mixture was added in an eppendorf tube. The samples were gently tapped and incubated for 30 mins at 4 ˚C. Then the samples were washed 2-3 times to remove excess dye molecules. Finally the samples were drop casted in a glass slide and observed under confocal microscope. For PI excitation wavelength was 540 nm and for FITC excitation wavelength was 488 nm.

4.4.8 ***Fabrication of membrane*****:** The dope solutions of PSF was prepared (20% w/w) using DMF as the solvent at room temperature and stirring under dry atmosphere for 6 h, after that $TpTG_{Cl}$ (5% by wt. of PSF) was added to the solution, stirred well for another 6 h, degassed for 3 min. to remove the trapped gases. $TpTG_{Cl}$PSF@PS-3329 membranes were prepared using Sheen Automatic Film Applicator-1132 on porous non-woven support fabrics (3329) at 25 ºC and exposed in air for 15 seconds prior to dipping in nonsolvent (water) bath. The knife movement was set to 10 $cm.sec^{-1}$ transverse speed with a gap of 250 μm. The total thickness (along with support) of the supported membrane was ~100 μm. These membranes were washed with distilled water and stored in aqueous formalin (0.5%) solution. The flux analysis of $TpTG_{Cl}$@PSF composite membrane was done in dead end cell with active area 14.5 cm^2 and the water flux was found to be ~ 27 $l.m.^{-2}h.^{-1}$ at 1.5 bar.

4.4.9 ***Antibacterial activity of membrane*****:** For antibacterial activity of membrane we studied the growth of two bacteria on to it. Routinely cultured bacterial strains were plated on Petri plate containing solidified potato dextrose agar and to it. A piece of sterilized membrane was placed over it and incubated for 24 h at 37 ˚C. In contrast sterilized filter paper was kept as a control. After 24 h of incubation filter paper and the membrane was separated and washed with deionized water for three times.[20] The samples were then fixed with 2.5% glutaraldehyde solution and incubated at 4 ˚C for 30 min. The samples were further washed, dehydrated with graded ethanol (30%, 50%, 60%, 80% and 100%) and observed under SEM for morphological analysis.

NOTE: The results of this chapter have already been published in *J. Am. Chem. Soc.*, **2016**, *138*, 2823. with the title: "*Self-Exfoliated Guanidine Based Ionic Covalent Organic Nanosheets (iCONs)*". These publications were the results from the group of Dr. Rahul Banerjee and his students Mr. Shouvik Mitra, Sharath Kandambeth, Bishnu P. Biswal and Abdul Khayum M., from CSIR-National Chemical Laboratory, Pune, India. Dr. Sandeep Verma and his student Gagandeep Kaur from Indian Institute of Technology, Kanpur have performed the AFM analysis of the COF samples. Major work was contributed by Mr. Shouvik Mitra and Mr. Sharath Kandambeth with the help of the instrumental facilities of CSIR-National Chemical Laboratory.

CHAPTER 5

Self Templated Synthesis of Chemically Stable Hollow Spherical Covalent Organic Framework

Abstract: *Covalent Organic Frameworks (COFs) are new class of organic porous nano-materials, which got wide attention due to their tunable structure and diverse applicability. COFs are usually synthesized as micro/ nano crystalline powders. COF nano-crystallite forms various morphology/ shape in nano domain. The shape of the nano-porous crystallites is an important factor for application such as molecular adsorption, charge carrier mobility etc. But systematic understanding about the mechanism of COF crystallization and driving force behind the formation of COF crystallites were poorly understood. Here in this chapter we discuss in detail about the synthesis and mechanism of formation of hollow sphere COF (DhaTab). The detailed time depended microscopic studies revealed that an inside out Ostwald ripening is responsible for COF hollow sphere formation. We have further utilized the COF hollow spheres for enzyme immobilization application.*

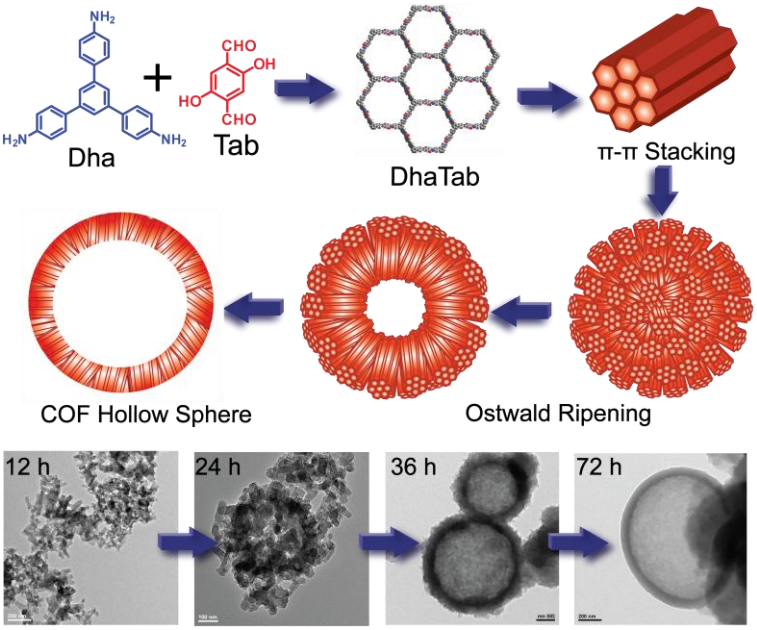

5.1 Introduction

The previous chapters discussed about synthesising highly crystalline and porous covalent organic frameworks (COFs) with excellent chemical stability. Apart from the chemical stability issue the one more prevailing problem in COF field is about understanding mechanism behind the COF crystallization [5.1]. COFs were generally synthesized as insoluble micro-crystalline powders [5.1]. The COFs crystallite growth has been limited in nano domains due to the inevitable internal defects during crystallization [5.1b]. As a result COFs crystallites adopt different shapes (such as sheets [5.2], belt [5.3], cubes [5.4], rectangular prism [5.5], fibres [5.6] and nano-flowers [5.7]) in nano domain. The shape of the nano crystallites is an important factor in application such as charge carrier mobility [5.8], drug delivery, energy storage and molecular adsorption[5.9]. But no detail study has ever done to explore the mechanism of COF nano-crystallites formation. Moreover there is no method is currently available to predict the final morphology of COF crystallites. Among various morphologies, hollow spheres are considered to be important in nano porous materials, due to its potential application in drug delivery [5.10], energy storage [5.11], molecular sensors and catalysis [5.12]. Hollow spherical morphology is scarcely reported in COF [5.13]. Xin Zhao and co-workers reported boronate estre based 2D polymer hollow spheres [5.13]. But this boronate ester based hollow sphere is very difficult to isolate, since it is synthesized as a mixture along with nano-sheets. Moreover due to its poor chemical stability, performing any practical application found to be challenging [5.13].

This chapter describe the synthesis of chemically stable hollow spherical COFs (**DhaTab**) without using any templates or surfactants. A detailed time depended mechanism studies showed that an inside out Ostwald ripening is responsible for the formation of this COF hollow spheres. The synthesized COF hollow spheres are highly crystalline and porous (surface area =1500 m^2g^{-1}) due to the presence of intramolecular hydrogen bonding present in the system. The self template strategy used for the COF hollow sphere synthesis is considered to be cost effective since it avoids the use of templates and unnecessary steps to remove the contaminants from the pores [5.9]. Even though the self template strategy was been widely utilized in the synthesis of inorganic metal oxide based hollow structures [5.9], in organic materials such as polymers and COFs this method is scarcely explored. The

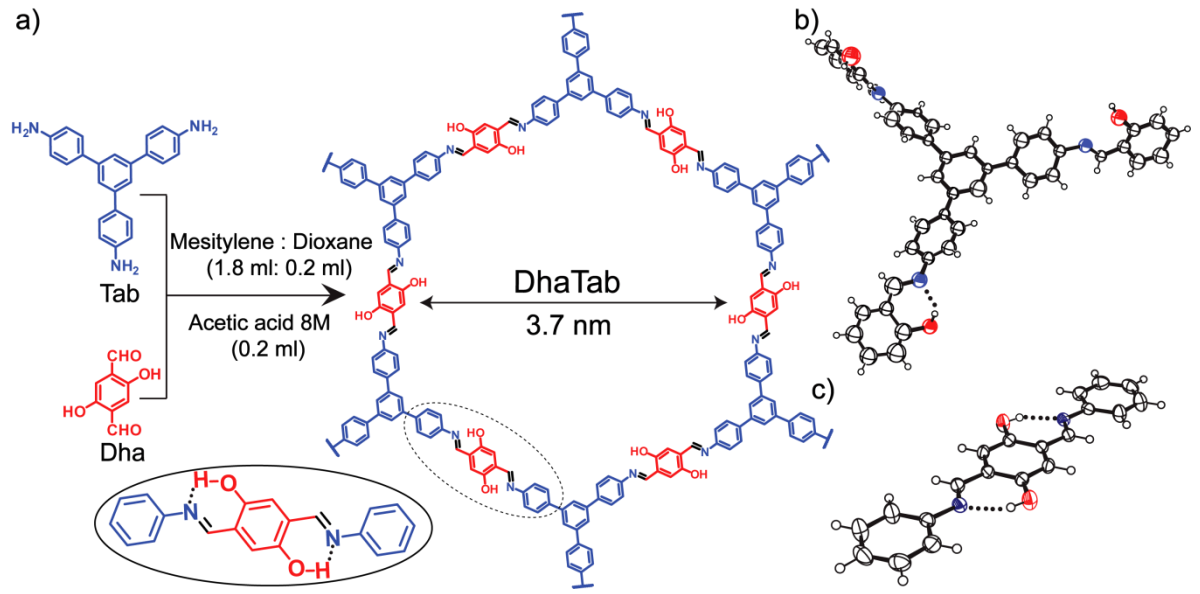

Figure 5.1. *(a) Schematic representation of the synthesis of mesoporous* ***DhaTab*** *COF. (b) and (c) ORTEP diagrams of C_3 and C_2 linker units.*

mechanism behind the COF hollow sphere formation was explored by the time depended microscopic studied (SEM, TEM and AFM). The studies revealed that an inside out Ostwald ripening is responsible for the COF hollow sphere formation.

The synthesised COF hollow spheres have got a mesoporous walls (3.7 nm) (***Figure 5.1***). Mesoporous materials are generally not considered to suitable for gas storage due to the large size difference between guest molecules and framework pores [5.10]. The interaction between small gas molecules with the pore walls of the mesoporous materials is not strong enough to have a favourable gas uptake. Apart from gas storage, COFs materials were scarcely used for the storage of bigger sized molecules (such as drugs, bio-molecules etc.). The bigger pores (3.7 nm) enable COF **DhaTab** to be capable for the adsorption of large bio-molecule such as enzymes. So we have done the adsorption study of enzyme trypsin in to the COF-**DhaTab** pores. The maximum loading of trypsin in to the **DhaTab** pores was calculated as 15.5 µmol/g. Immobilization of trypsin in to the COF pores improves its stability, life time and recyclability.

5.2 Result and discussion

5.2.1 *Synthesis of DhaTab hollow sphere*

Synthesis of COF-**DhaTab** hollows sphere was performed by the conventional sealed tube based technique (***Figure 4.1***). The powdered reactants 2,5-dihydroxyterephthalaldehyde (**Dha**) (21.6 mg) and 1,3,5-tris(4-aminophenyl)benzene (**Tab**) (30.2 mg) was initially transferred to a pyrex tube followed by the addition of solvents mesitylene (1.7 mL), dioxane (0.3 mL) and 8M acetic acid (0.2 mL). The sealed pyrex tube after the freeze pump thaw cycles was then placed in a hot air oven at 120 °C for 3 days. After this reaction time the tube was opened and the yellow coloured **DhaTab** powders were separated by filtration. After solvent exchange by DMAc and ethanol and drying under vacuum, the **DhaTab** hollow spheres were isolated in 82% yield. For the time depended study to explore the mechanism of formation, the reaction tubes were taken out from the oven at different time intervals (12 h, 24 h, 36 h, 48 h and 72 h). After the isolation of **DhaTab** powders by filtration a similar purification, and activation steps were employed.

5.2.2 *Structural simulation and characterization*

Crystallinity of the synthesized COF- **DhaTab** powders was checked by the PXRD analysis. COF-**DhaTab** display high crystallinity, due to the presence of intramolecular hydrogen bonding present in the system ((***Figure 5.1 and 5.2c***). The first intense peak appeared at 2.8° 2θ, corresponds to the 100 planes. The high intensity of the first peak (around 150000 cps) indicates the high crystallinity of the COF material (***Figure 5.2c***). The other peaks in the PXRD pattern appearing at a 4.9, 5.6, 7.4, 9.8, 26.3° 2θ corresponds to 110, 200, 120, 220, 001 planes. From the direct relation between d spacing of 001 planes and π-π stacking distance, the COF interlayer distance was calculated as 3.4 Å. The presence of the strong intra-molecular hydrogen bonding (O−H···N=C) between the linker unit was the main reason for the high crystallinity of **DhaTab** (***Figure 5.1***). The intramolecular hydrogen bonds improve the COF layer planarity by restricting the phenyl rings rotation and maintaining the imine bond in *trans* conformation. The improved planarity of the COF layers further support effective π- π stacking interaction between them as a result crystallinity of the COF-**DhaTab** get significantly improved. In order to understand this intramolecular H-bonding interaction in molecular level, we have crystallized the C_3 and C_2 linker units (***Figure 5.1b and 5.1c***). The crystal structure of the C_3, C_2 linker units revealed the presence of a six membered hydrogen bonding interaction between phenolic and imine functionalities (O−H···N=C) [D= 2.619(2) Å, d= 1.895(2) Å, θ= 146.68° (3)]. This interaction forces the

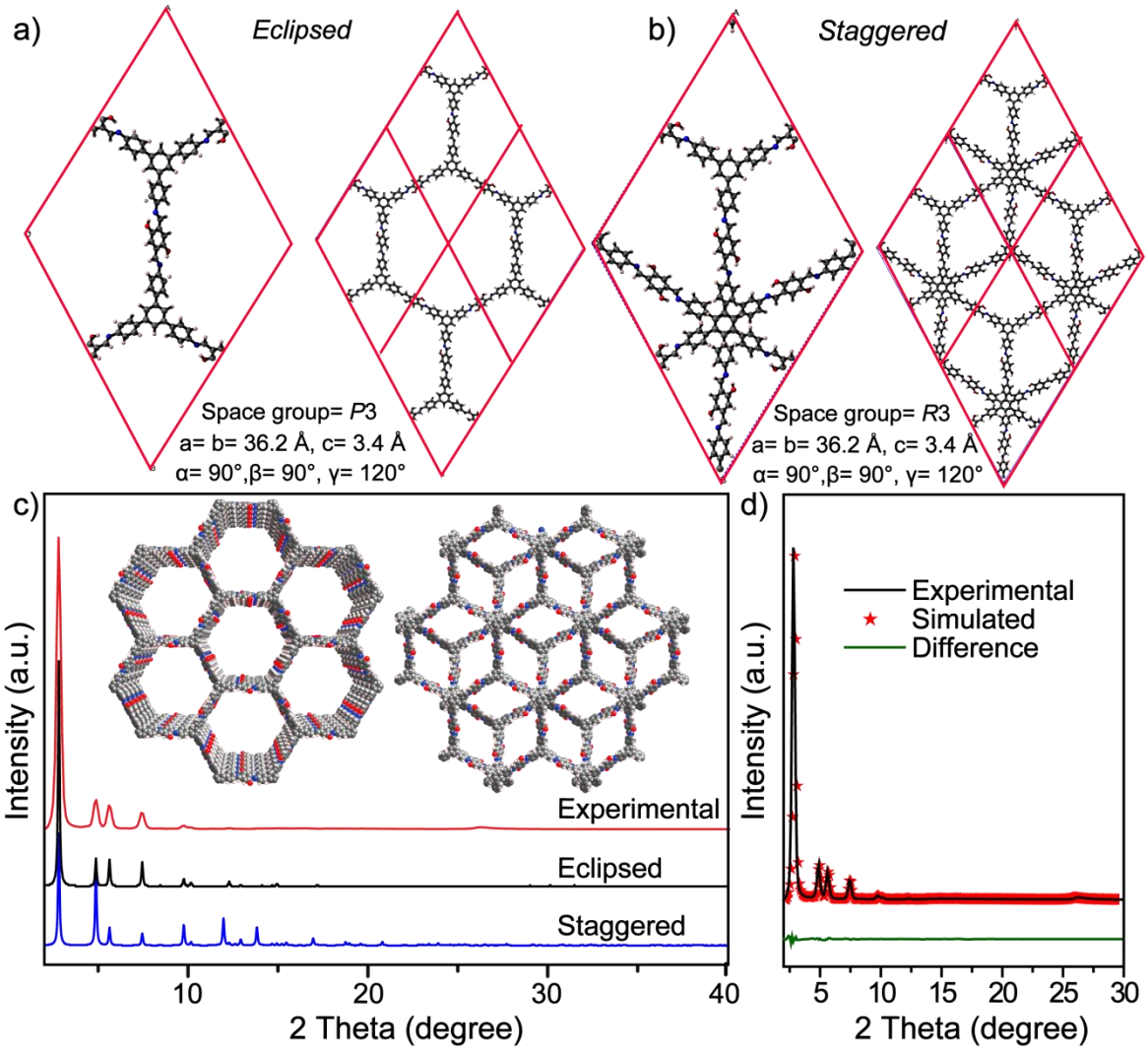

Figure 5.2*: (a) Unit cell and eclipsed crystal lattice packing of* ***DhaTab****; (b) unit cell and staggered crystal lattice packing of* ***DhaTab****.(c) PXRD spectra of As-synthesized (Red) COF* ***DhaTab*** *compared with the eclipsed (black), staggered (blue) stacking models.(d) Experimental (black) compared with refined (Red) PXRD profiles of* ***DhaTab*** *with an eclipsed arrangement; difference plot is given in (green).*

phenyl rings to remain in one plane, in the case of C_2 linker. Since the imine nitrogen forms (-C=N-) forms hydrogen bonding with phenolic group (-OH) the conformation of imine bonds (-C=N-) get fixed in trans form in both C_2 and C_3 linker units. By PXRD peak indexing and calculating the *d* spacing of the atomic planes, we have found that the COF-**DhaTab** crystallizes in hexagonal unit cell. Two possible stacking models were constructed (eclipsed and staggered) in *P*3 and *R*3 space groups using Materials Studio 6.1 software (***Figure 5.2a and 5.2b***). Up on comparison of the experimental PXRD pattern of **DhaTab** with the

simulated PXRD patterns, it was found that **DhaTab** follows eclipsed stacking model. To get the exact unit cell parameters Pawley refinement was performed between simulated PXRD pattern of the eclipsed model and the experimental PXRD pattern of **DhaTab**. The *Rp* and *Rwp* values indicate an excellent agreement between simulated pattern of the eclipsed model and the experimental data (*Rp*=2.5%, *Rwp*=4.5%) (***Figure 5.2d***). The final unit cell parameters were determined as, $a=b$=36.2 Å, c= 3.4 Å, and $\alpha=\beta$= 90°, γ=120°. On the other hand the Pawley refinement between PXRD pattern for the staggered stacking model and experimental showed a large deviation [*Rp*=70.5%, *Rwp*=78%].

5.2.3 *Chemical characterization*

The imine bond formation in COF-**DhaTab** was determined from FT-IR and ^{13}C CP-MAS solid state NMR spectroscopy (***Figure 5.3***). The absence of the characteristic peaks of the starting materials (–C=O (1662 cm^{-1})) stretching band of **Dha** and –N-H (~3300 cm^{-1})

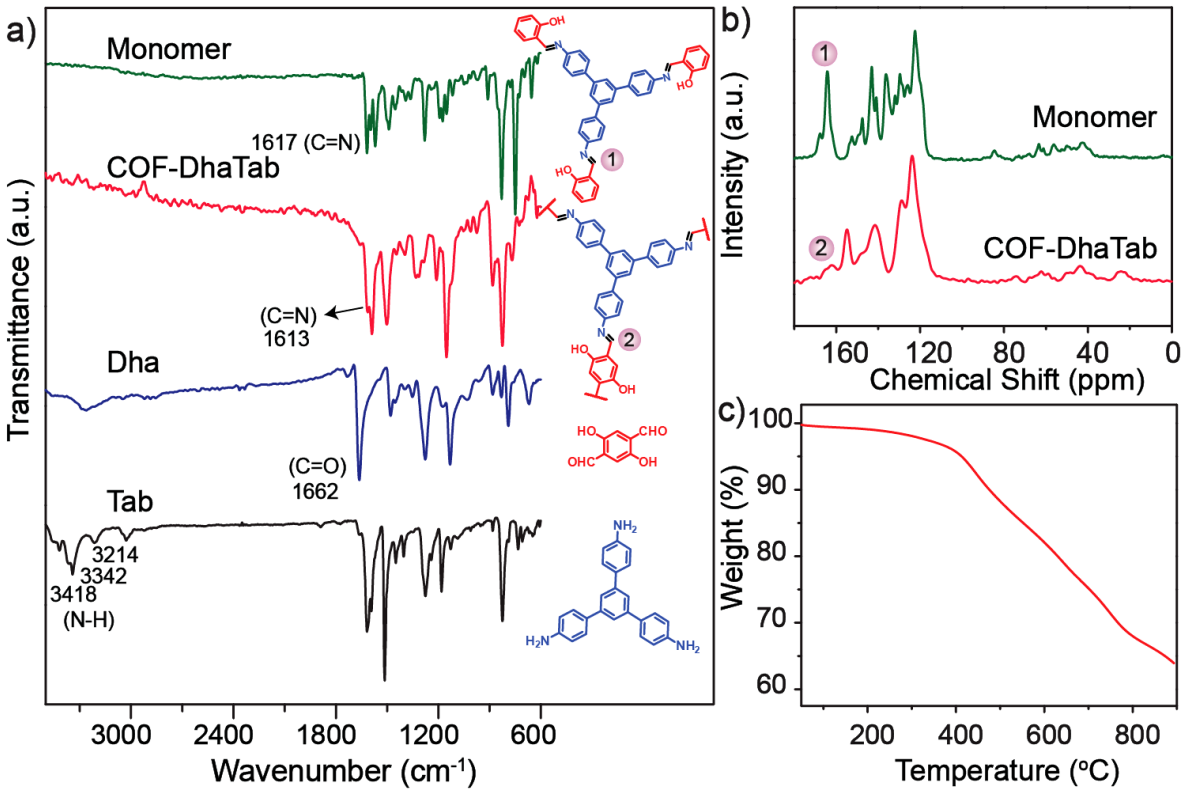

***Figure 5.3**: (a) FT-IR spectra of **DhaTab** (Red) compared with starting materials 2,5-dihydroxyterephthalaldehyde (**Dha**) (blue), 1, 3, 5-tris (4-aminophenyl)benzene (**Tab**) (black) and C_3 linker unit (green). (b) ^{13}C CP-MAS spectrum of **DhaTab** (red) compared with C_3 linker unit (green). (c) TGA profile of **DhaTab** under N_2 atmosphere.*

stretching band of **Tab)** in the FT-IR spectra of COF-**DhaTab** indicates the completeness of the Schiff base reaction. The appearance of FT-IR peak at 1613 cm^{-1} indicates the formation of imine bonds in COF (***Figure 5.3a***). This peak value also have close match with the FT-IR

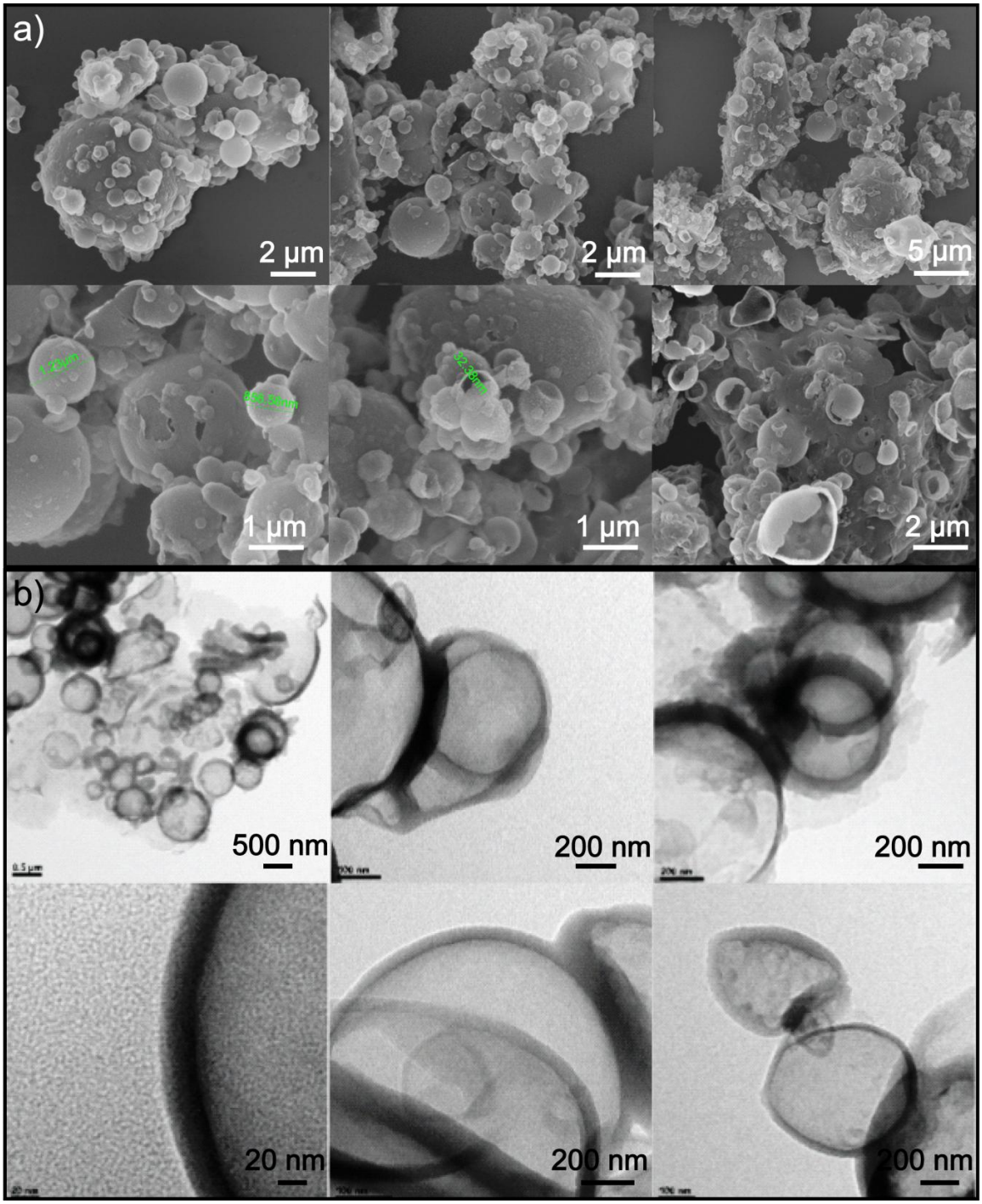

Figure 5.4: *(a) SEM and (b) TEM images of COF* ***DhaTab*** *hollow spheres at different magnifications.*

imine stretching value (1617 cm^{-1}) of the linker units (***Figure 5.3a***). To confirm the imine bond formation ^{13}C CP-MAS solid state NMR was recorded for the COF-**DhaTab** powders (***Figure 5.3b***). The appearance of peak at 155 ppm (δ) corresponds to the signal from imine carbon (-C=N). This value has a comparable match with the imine carbon signal from the linker unit (152 ppm) (***Figure 5.3b***).

To explore the internal morphologies of the COF-**DhaTab** crystallites Scanning electron microscopy (SEM), transmission electron microscopy (TEM) and atomic force microscopy (AFM) was recorded. The SEM images of the **DhaTab** showed spherical morphology have an average diameter of 0.4-5 µm (***Figure 5.4a***). The hollow spherical morphology of the **DhaTab** can be understood as some of the spheres with broken walls showed a hollow interior (***Figure 5.4a***). The breakage of the hollow sphere walls may be caused by the sonication, during the sample preparation process. TEM was recorded for the **DhaTab** hollow spheres to get more information about the hollow interior (***Figure 5.4b***). TEM images of hollow spheres showed two regions, a darker contrast seen at the sphere walls and at sphere centre relatively brighter contrast was observed. This characteristic was also seen in TEM images of silica, metal oxide and supra-molecular polymers hollow spheres. From the TEM images the thickness of the hollow spheres was calculated to be in

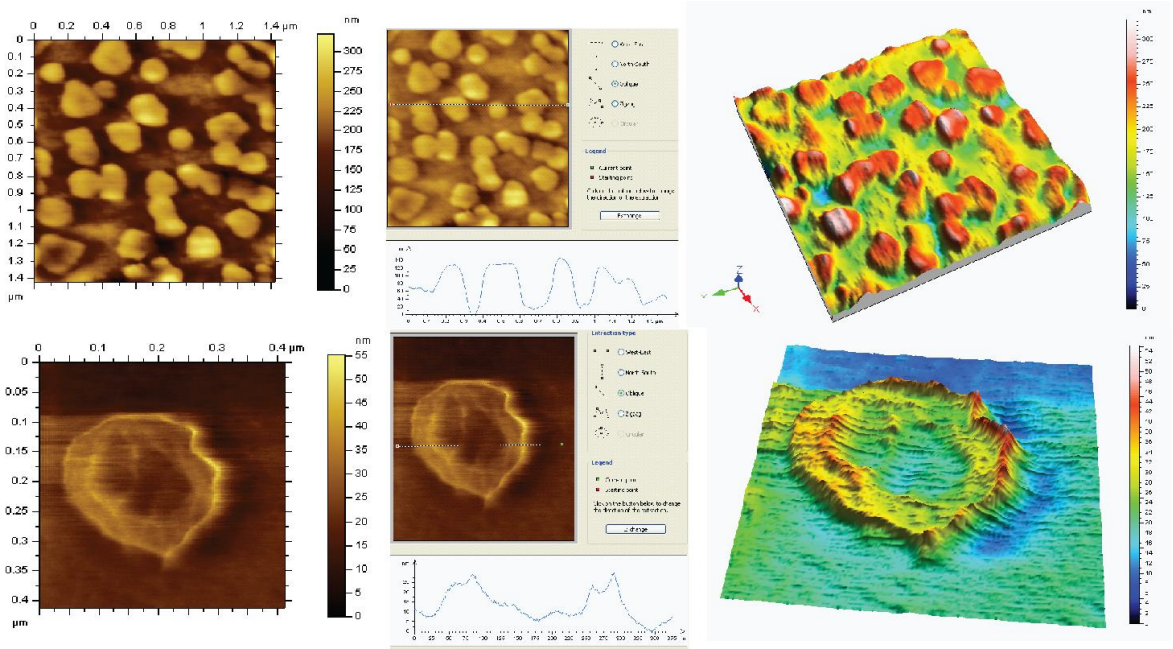

Figure 5.5: *AFM images of* ***DhaTab*** *hollow spheres.*

the range of 40-80 nm (***Figure 5.4b***). To further explore the morphology details of **DhaTab**, AFM was recorded. The AFM height profile analysis revealed the height of the hollow spheres was in the range of 100-140 nm, and the lateral dimensions were measured in range of 0.4 to 3 µm (***Figure 5.5***). But for a spherical object a comparable height/ width ratio is expected in AFM height profile analysis. The large difference in height and diameter values seen for the hollow spheres was due to the deformation of COF hollow sphere, by AFM tips during the scanning process. The thermal stability of **DhaTab** hollow spheres was determined from the TGA analysis (***Figure 5.3c***). The TGA profiles shows the **DhaTab** frameworks are stable up to 350 °C, since no significant weight loss was observed before this point. The weight loss (40%) seen after 400 °C, was related to the framework decomposition.

5.2.4 *Gas adsorption studies*

The porosity and surface area of the **DhaTab** hollow spheres was determined from N_2 adsorption isotherm. N_2 adsorption isotherm of **DhaTab** display type reversible *type IV*

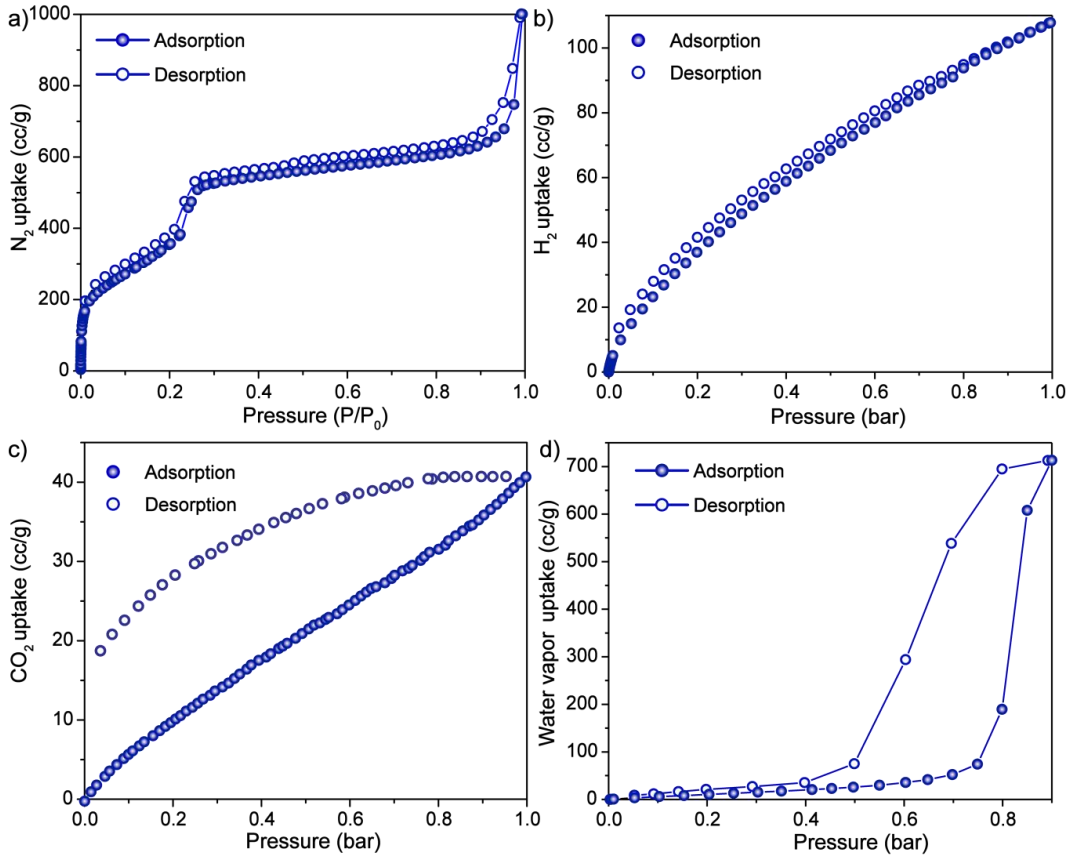

Figure 5.6: *(a) N_2 adsorption (at 77 K), (b) H_2 adsorption (at 77 K), (c) CO_2 adsorption (at 298 K), (d) water vapor adsorption (at 298 K) isotherms of* ***DhaTab*** *hollow sphere.*

charecteristics, which is commonly observed in mesoporous materials (***Figure 5.6a***). **DhaTab** hollow spheres show a surface area (Brunauer–Emmett–Teller (BET) model) value of 1480 m^2g^{-1}. This value is almost three times greater than the surface area value of the non-hydroxy analogue COF MOP (A-B1) reported previously in literature. The high surface area of COF **DhaTab** was due to the presence of intramolecular hydrogen bonding present in the system. The intramolecular hydrogen bonding improves the COF layer planarity and favors effective π-π stacking interaction between COF layers. Due to this improved interactions ordered COF pore channels forms which promotes the crystallinity and gas storage properties of COF-**DhaTab**. To get more insight about the pore channels of **DhaTab**, pore size distribution calculation was performed by using Barrett–Joyner–Halenda **(BJH)** model. The pore size calculation shows the existence of only single pore in COF **DhaTab**, with a peak maxima centered around 3.7 nm (***Figure 5.7a***). To check the gas storage properties of **DhaTab** H_2 adsorption (at 77 K) and CO_2 adsorption isotherm (at 273 K) were recorded (***Figure 5.6b and 5.6c***). The H_2 and CO_2 storage value were calculated as 120 cm^3g^{-1} (77 K) and 78 cm^3g^{-1} at 1 bar pressure.

5.2.5 *Chemical stability*

The COFs chemical stability (in water and buffer of different pH) is important for performing applications such as bio-molecule loading or immobilization. To check the chemical stability of **DhaTab** hollow spheres, the COF powders were immersed in water for one week. After this time period, the COF powders filtered, vacuum dried. The **DhaTab** powders do not shown any color change or weight loss after the long time water treatment. To check the retention of crystallinity and surface area of the COF sample PXRD and N_2 adsorption isotherm were performed (***Figure 5.7b and 5.7c***). PXRD of water treated **DhaTab** sample retain all the PXRD peaks with comparable peak intensity (***Figure 5.7d***), which indicates the high chemical stability of the **DhaTab** hollow spheres. N_2 adsorption isotherm shows that the water treated COF material still remain highly porous, with a BET surface area of 1220 m^2g^{-1} (***Figure 5.7c***). After the water stability test, **DhaTab** COF's acid stability was carried out (3N HCl for 7 days). Even though a slight weight loss (20%) was observed for **DhaTab** COF after the acid treatment, the main PXRD peaks remain intact after the acid treatment (***Figure 5.7d***). This result indicates that **DhaTab** COF framework can retain its crystallinity under acidic conditions. The O-H···N=C intramolecular hydrogen

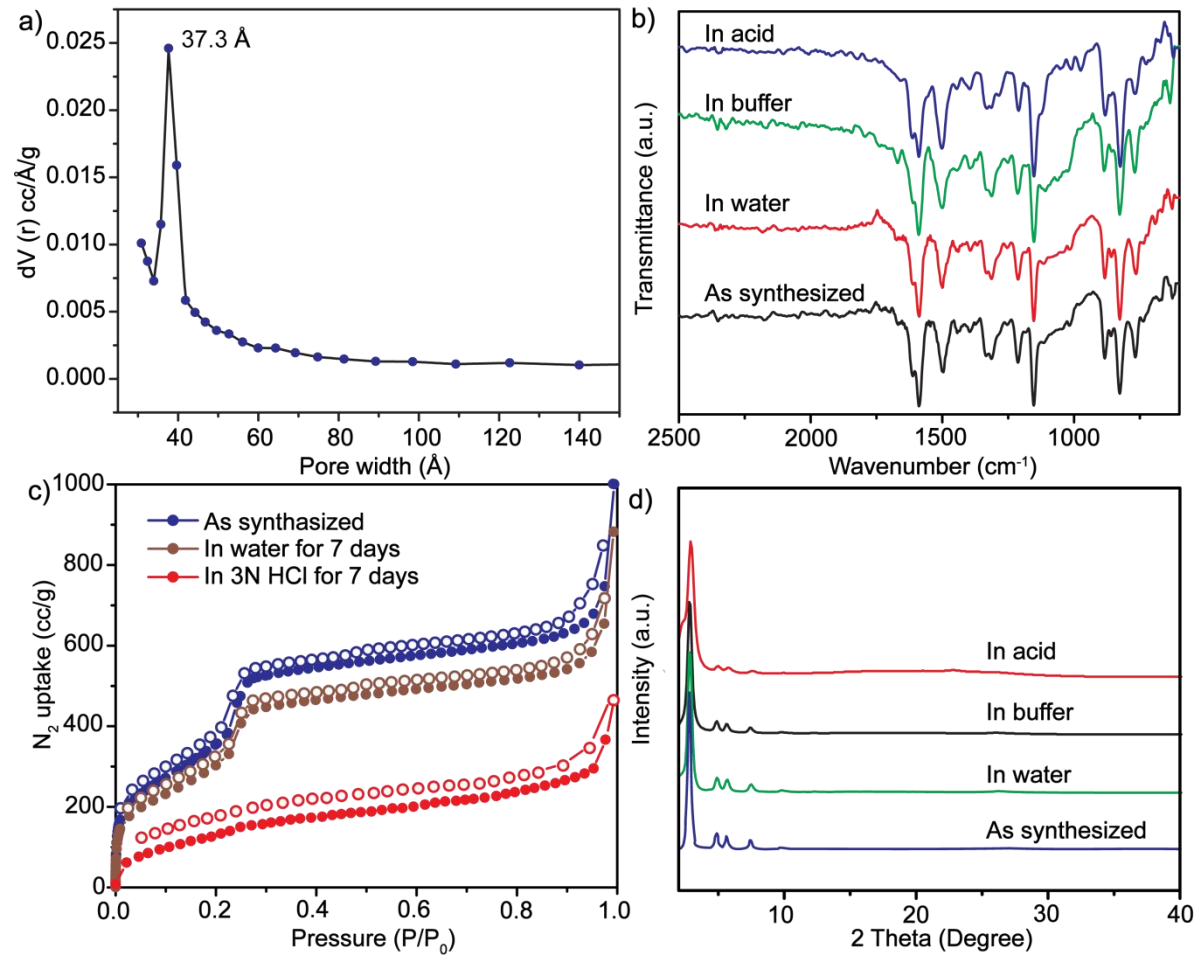

Figure 5.7: *(a) BJH pore size distribution of* ***DhaTab*** *hollow sphere. (b) FTIR, (c) N_2 adsorption isotherm, (d) PXRD of COF* ***DhaTab*** *treated with water, acid (3N HCl) and buffer compared with pristine COF samples.*

bonding have a protective effect on imine nitrogen, which makes the COF **DhaTab** chemically stable. Finally **DhaTab** hollow spheres were tested for their base stability (3N NaOH for 1 day). Unfortunately most of the COF powders get leached out after the base treatment (60%). PXRD analysis shows that the COF **DhaTab** losses its characteristic peaks after the base treatment, which indicate the instability of COF framework in basic condition.

5.2.6 *Mechanism of hollow sphere formation*

As discussed in the introduction part COFs are generally synthesized as microcrystalline powders and their growth were restricted in nanometer range, due to the presence of internal defects during the crystal growth. Being a 2D material COFs generally forms in sheet, ribbon, flake or platelet like morphologies. The hollow spherical morphology

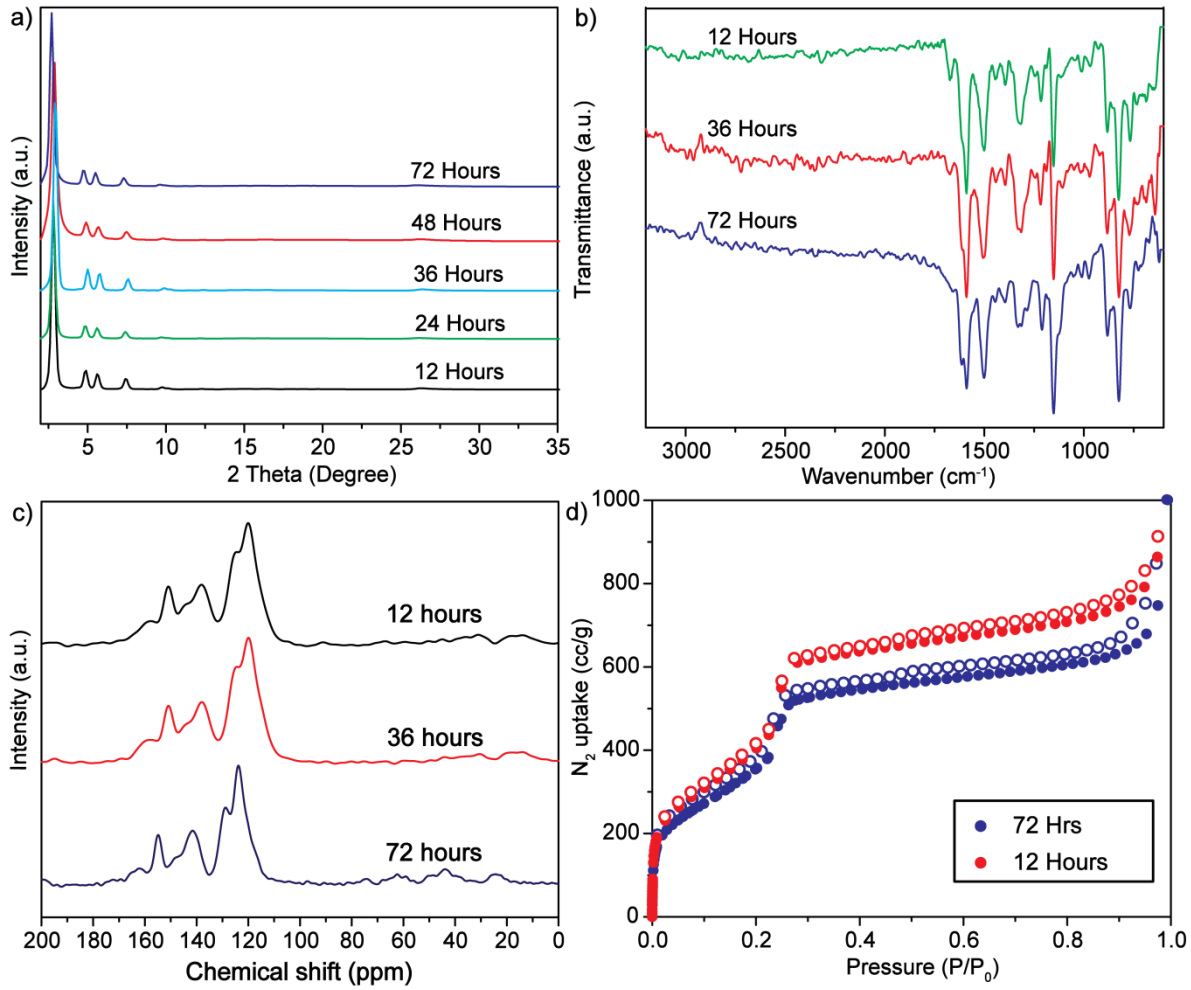

Figure 5.8: *(a) PXRD, (b) FTIR, (c) ^{13}C CP-MAS spectrum of* ***DhaTab*** *synthesized at different time intervals. (d) Comparison of N_2 adsorption isotherm of* ***DhaTab*** *synthesized at 12 hours (red) and 72 hours (blue) of reaction time.*

seen in the case of COF **DhaTab** is totally unexpected and we investigate the mechanism behind the hollow sphere formation in detail by using various microscopic techniques (SEM, TEM and AFM).

To investigate the mechanism of hollow sphere formation, COF reactions were quenched at different time intervals (72, 48, 36, 24 and 12 h). After the isolation and purification steps, COF powders crystallinity, porosity and internal morphology were analyzed. Interestingly the PXRD of 12 hours COF reaction samples displayed all the characteristic peaks, which indicate COF framework formation is even possible at a short reaction time of 12 hours (***Figure 5.8a***). Further the PXRD pattern of the other COF samples synthesized at the intermediate steps (48, 36, 24 hours) also displayed similar crystallinity

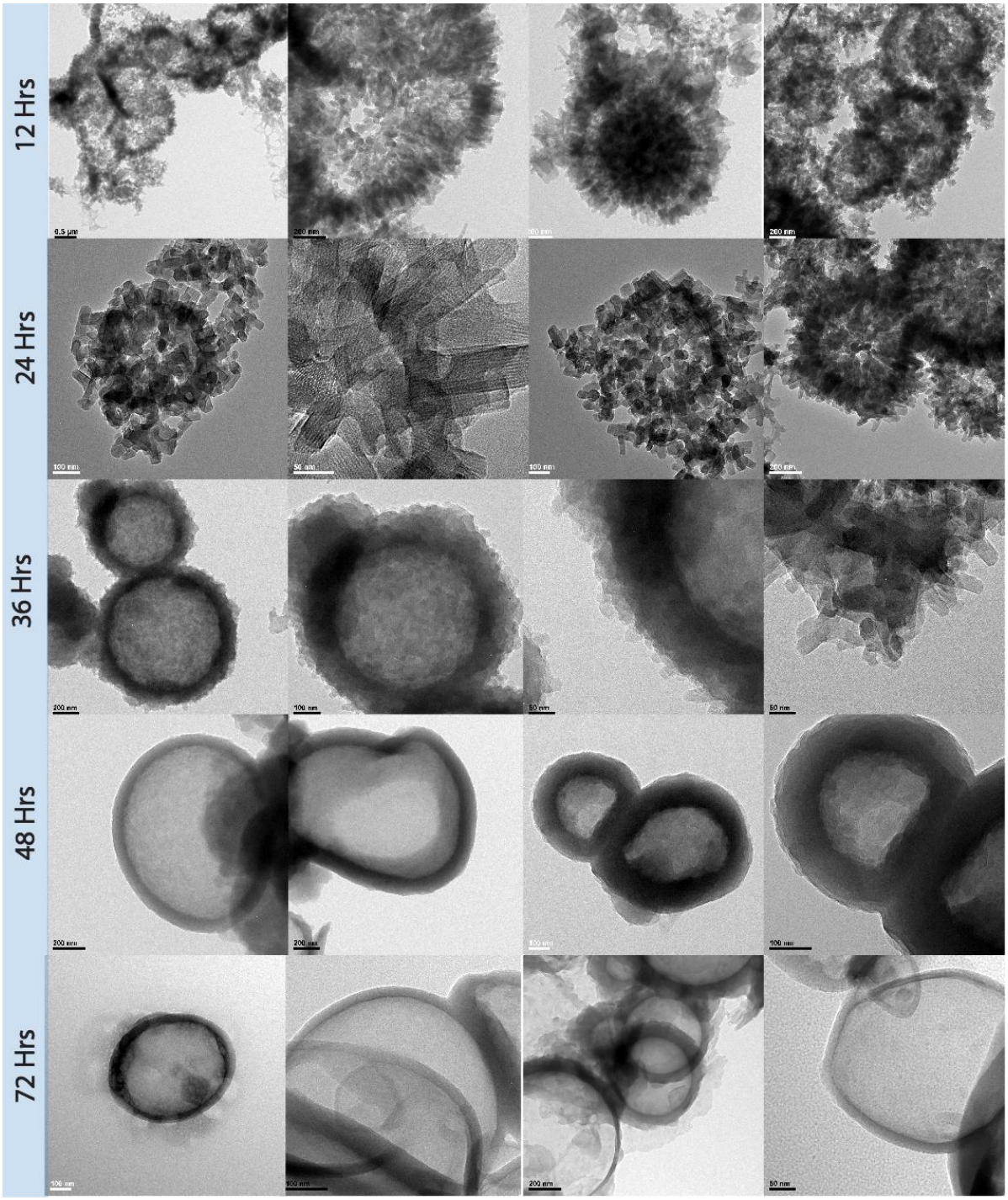

Figure 5.9: *TEM images of* ***DhaTab*** *synthesized at different intervals of time.*

(***Figure 5.8a***). The characteristic FT-IR and ^{13}C CP-MAS of the 48, 36, 24 and 12 hours samples match completely with the final 72 hours **DhaTab** COF hollow sphere sample (***Figure 5.8b and 5.8c***). This result also confirms the COF framework formation at different

time intervals. We have also checked the porosity of the COF **DhaTab** sample isolated at the shortest reaction time (12 hours). As expected the 12 hours COF sample also showed a similar surface area to the final 72 hours COF samples (***Figure 5.8d***). For the detail exploration of the mechanism of formation of **DhaTab** hollow sphere, we have characterized the internal morphology of the intermediate samples using various microscopic techniques (TEM, SEM and AFM imaging). At first we have used the TEM images of the COF sample for the mechanism investigation (***Figure 5.9***). **DhaTab** sample synthesized at 12 hours

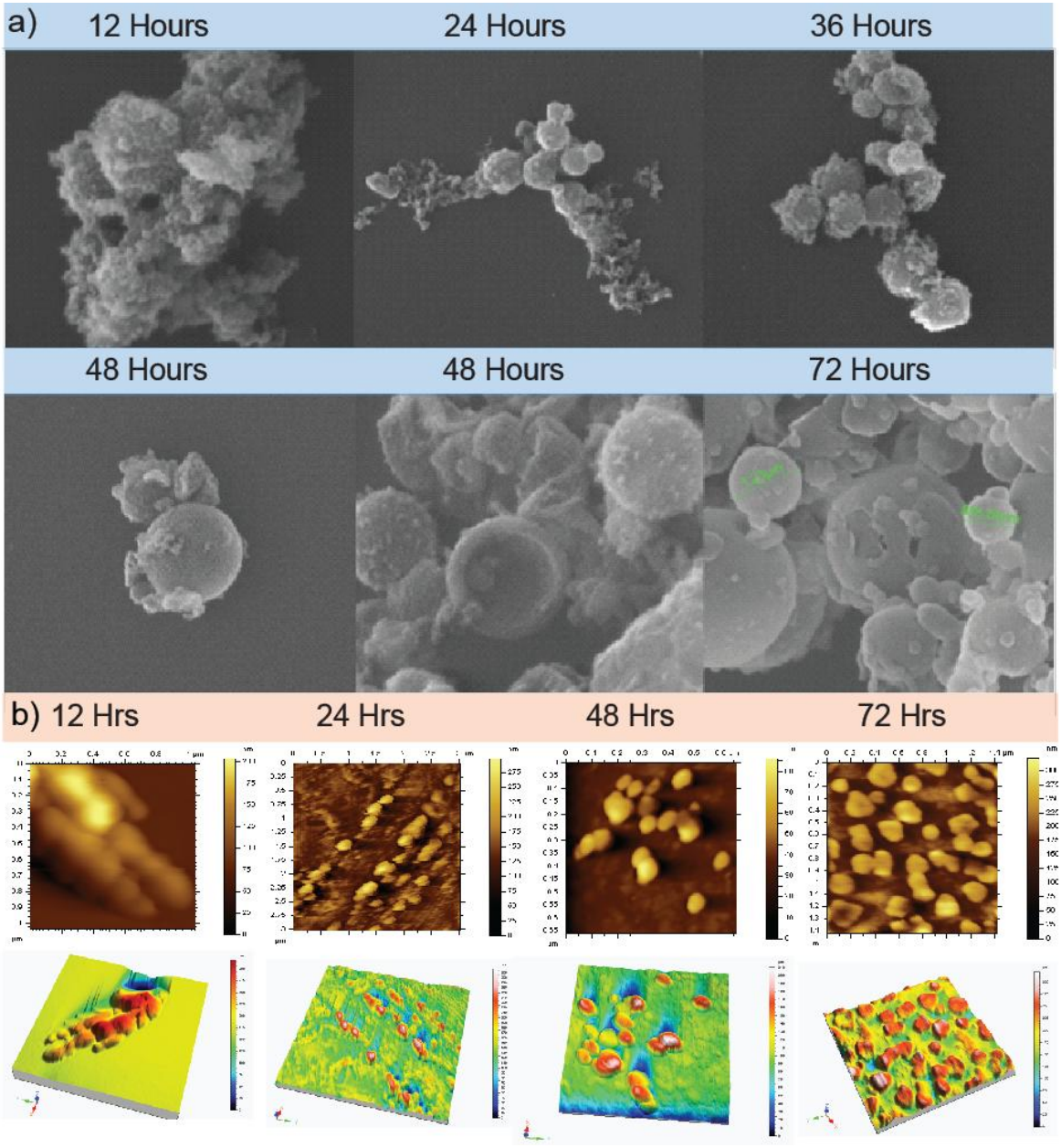

Figure 5.10: *(a) SEM (b) AFM images of* ***DhaTab*** *synthesized at different intervals of time.*

showed rod like morphology (length 100-150 nm) (***Figure 5.9***). The rod morphology of the COF crystallites were formed due to the self-assembly (π-π stacking) of COF layers along the c axis. The COF crystallites are randomly aggregated in different shapes at 12 hours reaction time (***Figure 5.9 and Figure 5.11***). The morphology of the crystallite aggregation includes dense spheres, coiled structure and aggregated sheet like structure. As the time progress at 24 hours **DhaTab** samples TEM image mainly shows dense spheres, which was formed by the aggregation of COF crystallites (***Figure 5.9 and Figure 5.11***). Upon closer inspection along c axis, COFs hexagonal pore window can be directly seen at higher magnification (***Figure 5.9***). View along *a* or *b* axis shows the pore channel of the COF crystallites. When the 36 hours **DhaTab** samples were analyzed in TEM, an important transformation had been seen. A hollow interior was developed in **DhaTab** sphere at 36 hours reaction time and dense sphere morphology now no longer able to see in the TEM grids (***Figure 5.9***). But the basic COF rod crystallites are still visible at the hollow sphere walls in higher magnification TEM images (***Figure 5.9***). The transformation of **DhaTab** dense sphere to **DhaTab** hollow spheres were happened due to a phenomenon called inside out Ostwald ripening (***Figure 5.9 and Figure 5.11***) [5.9]. This phenomenon happens due to the difference in free energy of the crystallites. The crystallites in the inner part of the COF

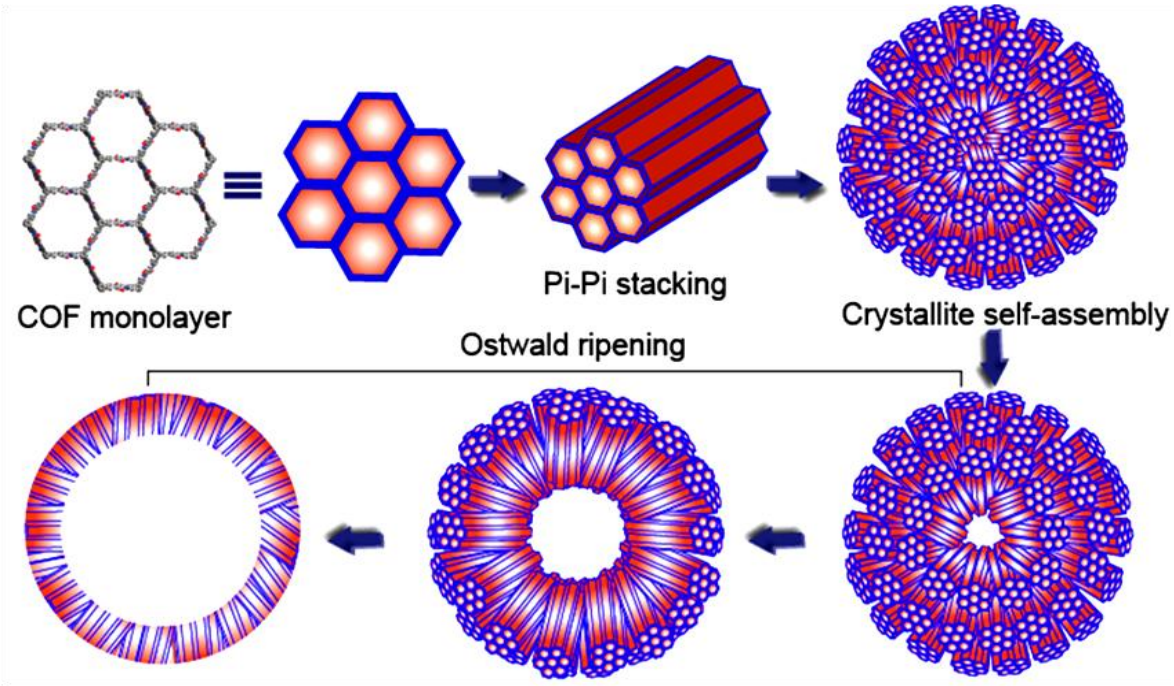

Figure 5.11*: Schematic representation of the mechanism of* ***DhaTab*** *hollow sphere formation.*

dense sphere have got a higher free energy as compared to those in the outer walls. To minimize this anomaly, system promotes the diffusion of crystallites from the centre part of the sphere to the sphere walls, which results in the formation of hollow structure [5.9]. The diffusion of COF crystallites can either happened by migration or dissolution (since reversible condition for COF reaction still exists in sealed tube). The inside out Ostwald ripening, is a well reported phenomena responsible for the formation of inorganic hollow structures (metal oxide, silica, metal sulfide etc). But this phenomena is scarcely observed in organic materials such as polymers, COFs, graphene. TEM images of the 48 hours and 72 hours **DhaTab** sample does not show any significant transformation in morphology (***Figure 5.9***). Hollow spherical morphology continues to form at this higher reaction time. But at the

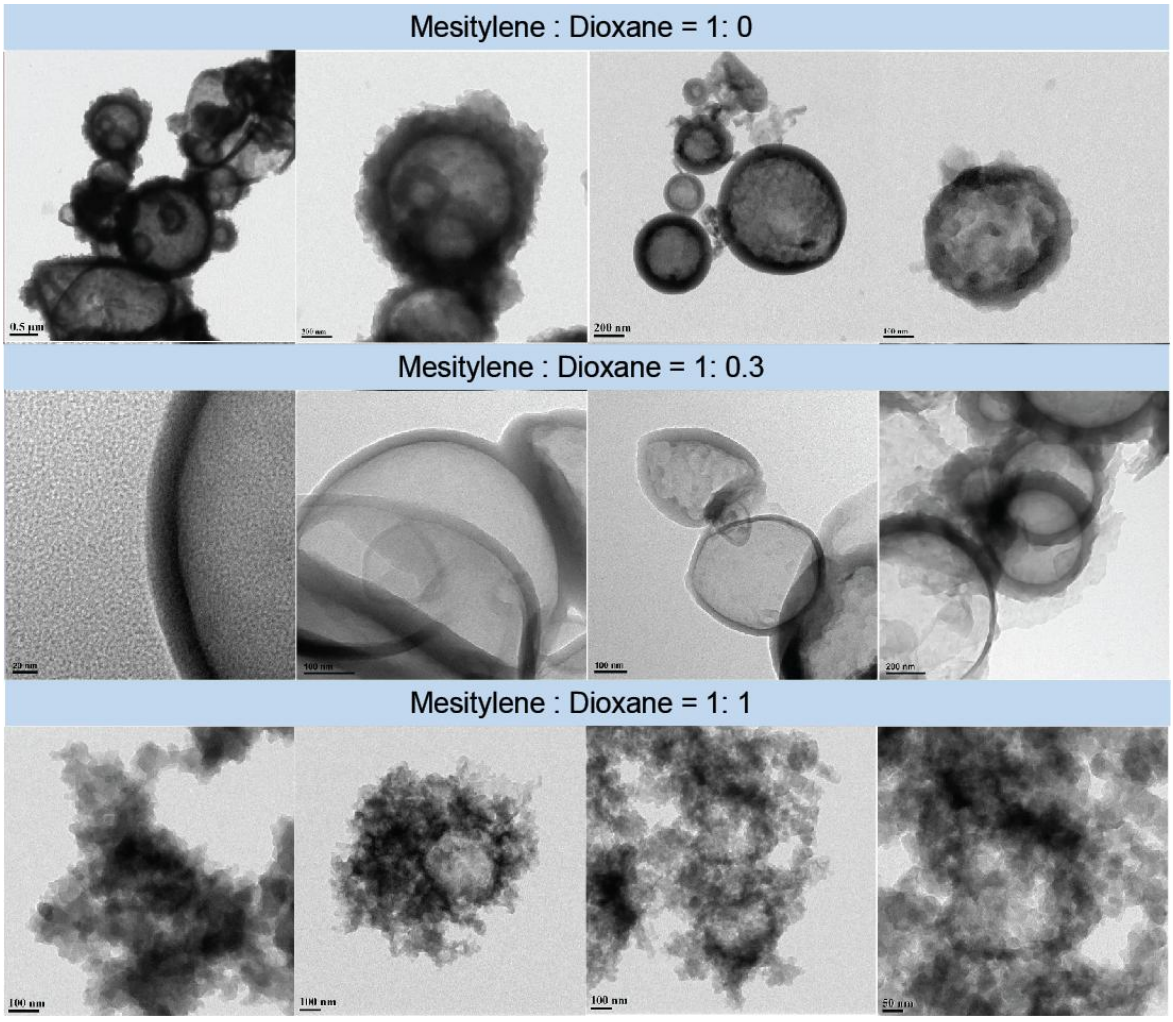

Figure 5.12*: TEM images of COF* ***DhaTab*** *synthesized at different solvent combinations.*

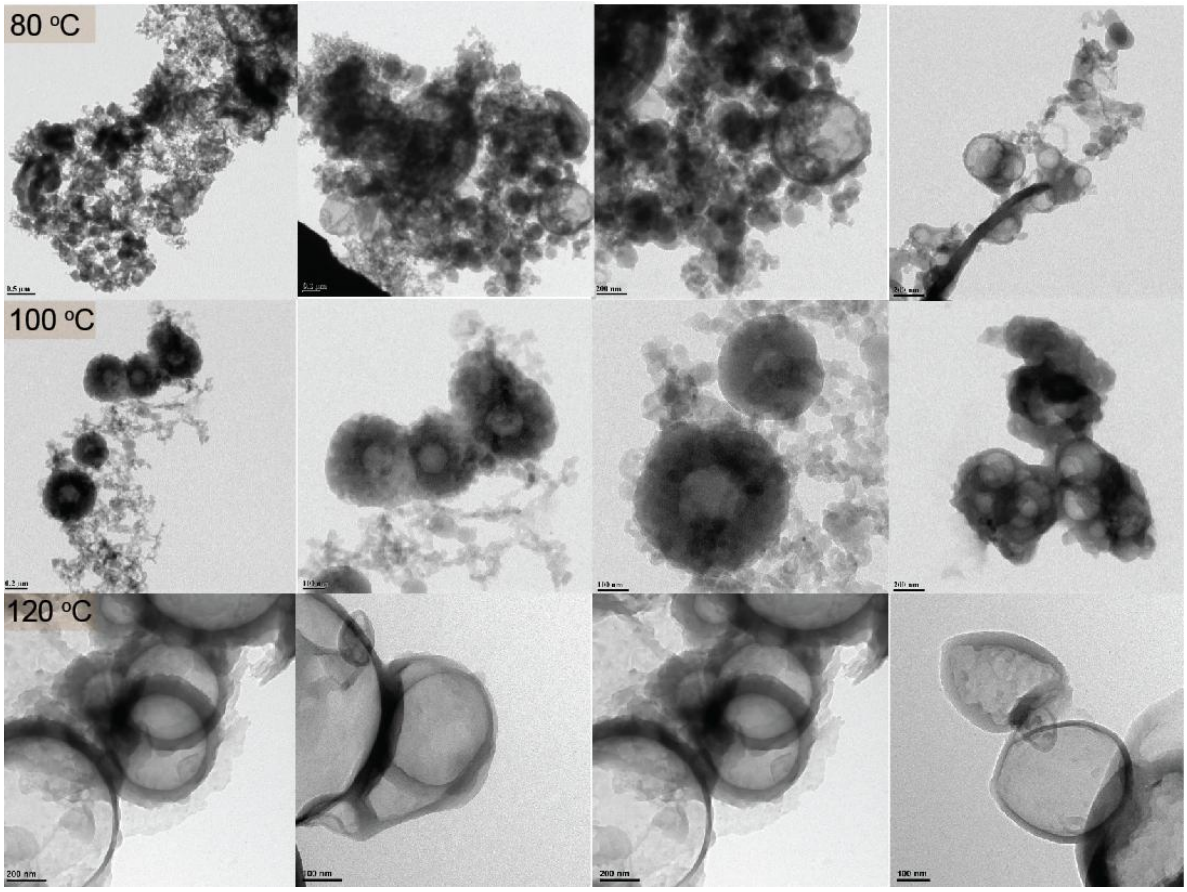

Figure 5.13*: TEM images of COF* ***DhaTab*** *synthesized at different temperature.*

hollow sphere walls turned to very smooth and continuous at 48 and 72 hours reaction time. No individual COF crystallites can be observed even at higher magnification (***Figure 5.9***). This may be happened due to the COF crystallites after prolonged heating (***Figure 5.11***). Since COF crystallites still contains end functionality (amine and aldehyde), crystallites may have bind together by reversible Schiff base reaction. Further we have recorded the SEM and AFM images of the intermediate COF samples (***Figure 5.10a***). SEM and AFM images also supported the TEM data (***Figure 5.10***). It is important to note that the COF hollow sphere formation is largely effected by solvent combination. COF **DhaTab** was synthesized in four different solvent combination ((a) mesitylene: dioxane-2: 0, b) mesitylene: dioxane-1.7: 0.3, c) mesitylene: dioxane-1.3: 0.7, d) mesitylene: dioxane-1: 1) (***Figure 5.12***). TEM images of the synthesized samples showed that hollow sphere formation is feasible only in a) mesitylene: dioxane-2: 0, b) mesitylene: dioxane-1.7: 0.3 solvent combination. As the dioxane content is increased in (in mesitylene: dioxane-1.3: 0.7, and mesitylene: dioxane-1:

1) a distorted hollow sphere morphology was seen (***Figure 5.12***). The reason for this results may be related to water in oil character of mesitylene: dioxane-1: 1, and mesitylene: dioxane-1.3: 0.7 solvent combination (***Figure 5.12***). Ostwald ripening in reported to be more feasible in water in oil emulsion [5.9]. The effect of temperature on **DhaTab** morphology was checked by synthesizing COFs at different temperatures (120°C, 100°C and 80°C) (***Figure 5.13***). TEM images show that hollow sphere formation is feasible in all three temperatures.

5.2.7 *Enzyme adsorption*

The COF **DhaTab** shows only moderate gas storage properties, since the pore size (3.7) nm is too big as compared to the smaller sized gas molecules (***Figure 5.1***). The

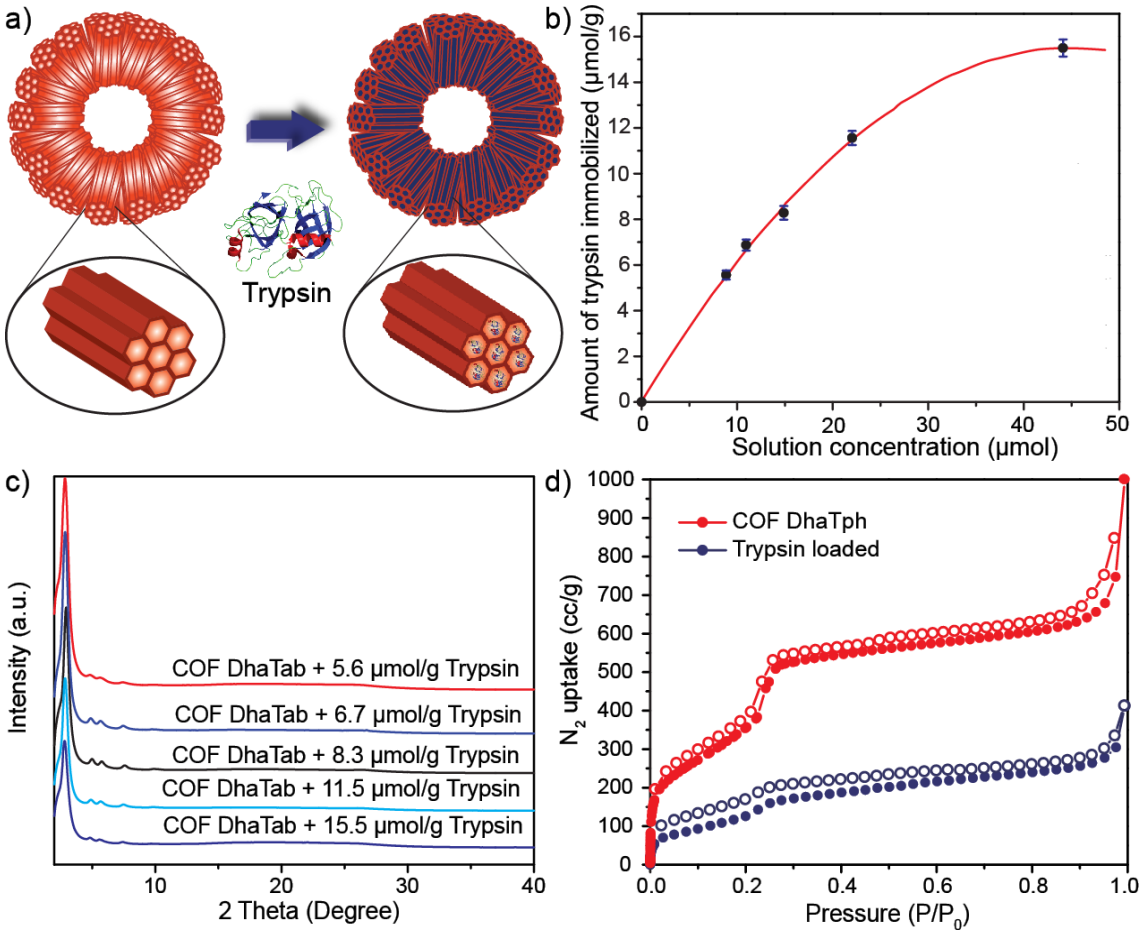

Figure 5.14*: (a) Pictorial representation of enzyme loading in* ***DhaTab*** *hollow spheres.(b) Trypsin loading in COF-****DhaTab*** *hollow sphere at different concentration of the stock solution. (c) Change in PXRD peak intensity of* ***DhaTab*** *COF after trypsin loading. (d) Comparison of N_2 adsorption isotherm before (red) and after (blue) trypsin loading.*

mesopores of **DhaTab** can be utilized for the storage of bio-molecules such as enzyme and proteins. Among porous materials, mesoporous silica has been extensively used for enzyme adsorption and immobilization [5.14]. Mesoporous silica and zeolites lacks diversity in building units and functionality. To improve the immobilization of enzymes, pore walls of silica or zeolites often require fictionalizations [5.14]. Mesoporous COF **DhaTab** can be a good choice for the enzyme immobilization studies, since it possesses bigger meso-pores (3.7 nm) and hydrogen bonding sites on the pore wall (this can effectively interact with enzymes). Immobilization of enzyme in to porous solid support is highly important in biopharmaceutical industries [5.14]. The immobilization process improves the stability, recyclability of costly enzymes [5.14a]. We have selected enzyme bovin trypsin for the immobilization studies. Trypsin is a protein hydrolyzing enzymes, and posse's storage stability problem. Trypsin can undergo autolysis at lower pH. Trypsin got hydrodynamic size of 3.8 nm, which matches with the **DhaTab** pore size. Immobilization of trypsin in **DhaTab** pores was performed in phosphate buffer (100 mM). After an incubation period of 24 hours, **DhaTab** hollow spheres containing the trypsin were separated by centrifugation from the phosphate buffer (***Figure 5.14***). Centrifugate absorbance at 280 nm was analyzed by UV-visible spectroscopy. The maximum trypsin loading in **DhaTab** were calculated as 15.5 µmol (***Figure 5.14***). The enzyme loaded **DhaTab** COF were then characterized by various spectroscopic techniques.

PXRD of the trypsin loaded COF shows a significant decrease in intensity (***Figure 5.14***), which could be probably due to the disordered arrangement of the trypsin molecule inside COF pores (***Figure 5.14c***). N_2 adsorption of the trypsin loaded COF shows a lower surface area (400 m^2g^{-1}) as compared to the pristine COF hollow sphere samples (1480 m^2g^{-1}). This is an indication of trypsin loading inside COF pores. SEM images of the trypsin loaded **DhaTab** shows the hollow sphere morphology is retained after the adsorption. This shows that **DhaTab** is stable under the enzyme loading conditions. Further to locate the exact position of trypsin immobilization confocal laser scanning microscopy (CLSM) was recorded for the fluorescein labeled trypsin loaded **DhaTab** (***Figure 5.15***). CLSM images revealed that the trypsin is not located in the macroporous interior of the hollow sphere, instead it get loaded at hollow sphere walls (***Figure 5.15***). The location of the trypsin loading was mapped

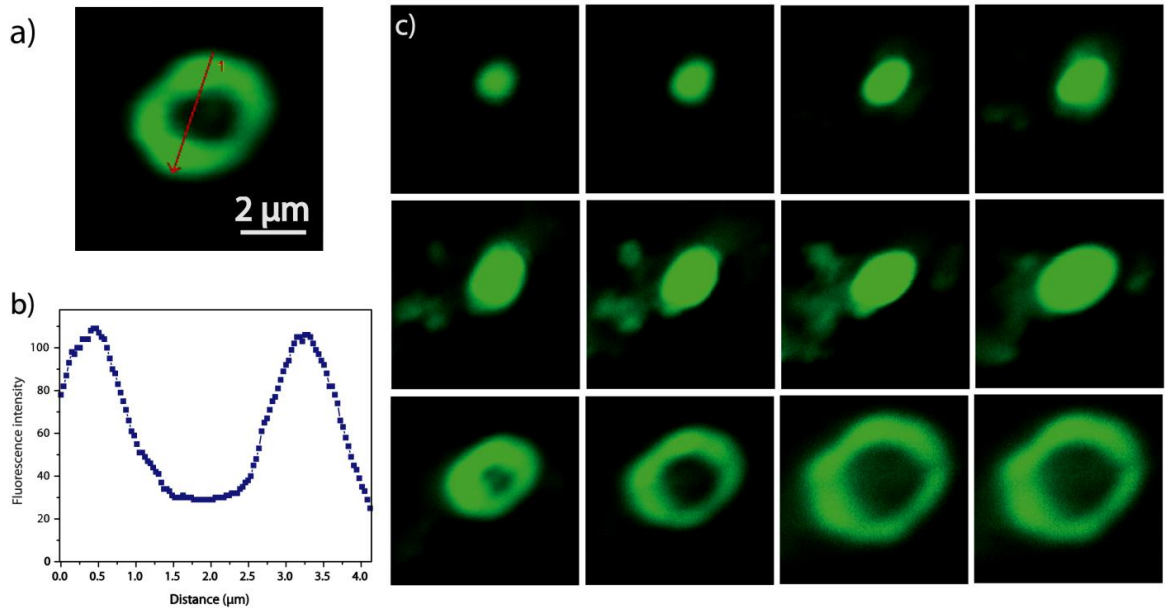

Figure 5.15*: Confocal z-stack sectioning of single COF* ***DhaTab*** *hollow sphere pores.*

on the basis of relative fluorescence intensity. At the hollow sphere centre no florescence was observed but up on moving to the sphere walls a maximum florescence intensity was seen (***Figure 5.15***). Further to check the trypsin catalytic activity after the immobilization process we have performed a model reaction using the substrate N-Benzoyl-L-arginine 4-nitroanilide (BAPNA). BAPNA is an amide bond containing molecule which shows an absorbance of 314 nm. Upon treating with trypsin the amide bond of BAPNA get hydrolyzed and p-nitroaniline get generated in solution (***Figure5.16***). Since p-nitroaniline shows an absorbance of 405 nm, solution color changes from colorless to yellow during trypsin catalysis. As expected the trypsin loaded **DhaTab** displayed catalytic activity toward BAPNA. The catalytic activity is estimated to be 56.5 mmol $g^{-1}min^{-1}$, which almost the 60% of the activity of free trypsin enzyme. The decrease in catalytic activity of trypsin after the immobilization process may be related to the blockage of some of the catalytic sites of enzyme in the adsorbed state.

We have also checked the storage capacity of **DhaTab** towards doxorubicin (anticancer drug). **DhaTab** hollow spheres shows a good doxorubicin loading capacity of 0.35 mg/g. More over the drug release studies shows that doxorubicin is slowly get released (42%) after one week in phosphate buffer (pH=5). This result indicates that **DhaTab** hollow

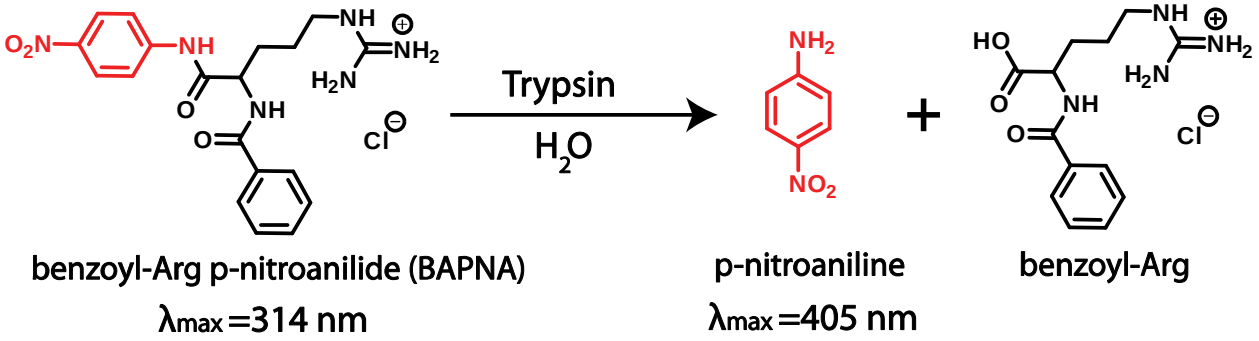

Figure 5.16*: Mechanism of BAPNA hydrolysis by enzyme trypsin.*

spheres can also be used as carrier in drug delivery application.

5.3 Conclusion

In summary, for the first time we were able to synthesize a chemically stable COF with hollow sphere morphology. The hollow sphere COF synthesis does not require any template or surfactant. The detailed time depended studies revealed that an inside out Ostwald ripening process is the main cause for the COF hollow sphere evolution. The COF **DhaTab** display high crystallinity and surface area (1500 m^2g^{-1}) due to the presence intramolecular hydrogen bonding present in the system. The chemical stability studies shows that the COF hollow spheres stable in water and buffer. Due the mesoporous nature we have utilized **DhaTab** COFs for enzyme immobilization studies. **DhaTab** showed trpsin uptake of 15.5 $\mu molg^{-1}$. CLSM images revealed that trypsin loading happens mainly at the sphere walls. Interestingly the COF loaded enzyme still shows catalytic activity.

5.4 Experimental procedures

5.4.1 *Materials*

Synthesis of 2,5- dihydroxyterephthalaldehyde was performed as according to the previous literature report [5.15]. All other materials were purchased from Sigma Aldrich and used without any further purification.

5.4.2 *Reference compound of DhaTab: 2,2''-[[5''-[4-[[(2-hydroxy-phenyl)methylene] amino]phenyl] [1,1':3',1''-terphen-yl]-4,4''-diyl]bis (nitrilomethylidyne)]*

The reference compound was synthesized by the reaction between 1,3,5-Tris(4-aminophenyl)benzene (**Tab**) (0.175 g, 0.5 mmol) and salicylaldehyde (0.366 g, 3.0 mmol) in 20 mL ethanol under refluxing condition for 24 h. After this time the solution was allowed to reach room temperature. The precipitate formed was then collected by filtration. After washing with ethanol and drying under vacuum the final product was isolated as yellow solid 0.265 g (80%). The single crystals of the reference compound were grown in DMF, chloroform solvent combination. **IR (powder, ATR)**: 1617, 1595, 1568, 1448, 1391, 1363, 1280, 1193, 1152, 910, 829, 749, 654; **^{1}H NMR (300 MHz, $CDCl_3$)**: δ 13.28 (s, 3H), 8.71 (s, 3H), 7.83 (s, 3H), 7.78 (d, *J* = 8.24 Hz, 6H), 7.48-7.39 (m, 12H), 7.07 (d, *J* = 8.24 Hz, 3H) and 6.98 (t, *J* = 7.32 Hz, 3H); **^{13}C NMR (75 MHz, $CDCl_3$):** δ 166.55, 169.19, 147.19, 141.68, 139.53, 133.28, 133.23, 128.30, 124.88, 121.75, 119.22, 119.13 and 117.29.

5.4.3 *Reference compound of DhaBad : 2,2',2''-((1E,1'E,1''E)-((nitrilotris(benzene-4,1-diyl))tris(azanylylidene))tris(methanylylidene))triphenol*

The reference compound was synthesized by the reaction between N^1,N^1-bis(4-aminophenyl)benzene-1,4-diamine (**Bad**) (0.145 g, 0.5 mmol) and salicylaldehyde (0.244 g, 2.0 mmol) in 20 mL ethanol under refluxing condition for 24 h. After this time the solution was allowed to reach room temperature. The precipitate formed was then collected by filtration. After washing with ethanol and drying under vacuum the final product was isolated as yellow solid 0.126 g (80%). The single crystals of the reference compound were grown in DMF, chloroform solvent combination. **IR (powder, ATR)**: 1611, 1490, 1315, 1274, 1181, 1148, 1109, 1193, 1028, 970, 903, 833, 751, 657.

5.4.4 *Hollow sphere formation under different reaction conditions*

1) With respect to solvent combination

We have synthesized the COFs in different solvent combination such as a) Mesitylene: Dioxane-1:1, b) Mesitylene: Dioxane-1.3:0.7, c) Mesitylene: Dioxane-1.7:0.3, d) Mesitylene: Dioxane-2:0. TEM images clearly indicate that the hollow sphere formation is highly favorable in very low concentration of the dioxane (Mesitylene: Dioxane-2:0 and 1.7 : 0.3). At higher concentration of dioxane (Dioxane : Mesitylene- 0.7: 1.3) the number of COF

hollow spheres observed in the TEM grid get decreased and the morphology the COF **DhaTab** observed is like randomly aggregated particles, with distorted spheres. At 1:1 concentration of Mesitylene and dioxane no more hollow spheres are observed and the morphology is now like aggregation of small crystallite particles. The possible reason for this phenomena may be due to the water in oil type behavior of Mesitylene-dioxane 2: 0 or 1.7 : 0.3 system. Since dioxane and water is mixable, dioxane- 6M AcOH will act as one system. In presence of larger amount of hydrophobic mesitylene solvent dioxane – AcOH system will act as an water oil type emulsion which can facilitate the formation of the hollow spheres.

2) With respect to substrate concentrations

We have done the COF synthesis at two different concentrations. One at a concentration of Tab (0.09 mmol) and Dha (0.13 mmol) (As reported in the paper), and another at half dilution of **Tab** (0.045mmol), **Dha** (.065 mmol). In both cases hollow sphere formation was observed. The only difference observed was that the sphere wall thickness of the COF synthesized at half dilution was little less as compared with higher concentrated one.

3) With respect to Different temperature.

We have synthesized the COF-**DhaTab** at three different temperatures (80 °C, 100 °C and 120 °C). At all the three temperatures hollow sphere formation was seen. But the number density of the hollow spheres observed at 80°C is low as compared with 100 °C and 120 °C. Along with hollow spheres some dense spherical structure are also seen at 80 °C. At 100 °C hollow spheres were found along with scattered crystallites.

5.4.5 *Trypsin loading in COF-DhaTab*

1 mg of COF- **DhaTab** in 1.1 mL, 100 mM phosphate buffer was sonicated for 5 minutes and the freeze pump thawed thrice. To this 1 mg of trypsin was added under inert atmosphere and stirred at 4 °C for 24 h to adsorb trypsin in the pores of AZP-SBA. After this time interval solution was centrifuged and washed once with 1 mL, 100 mM phosphate buffer. Centrifugate and washing were collected together and absorbance at 280 nm noted to determine amount to trypsin present in solution.

5.4.6 *Synthesis of fluorescein labeled trypsin*

10 mg of trypsin was added to 10 mL of phosphate buffer (50 mM, pH 7.4) containing 0.4 mg of 5 (6)-carboxy fluorescein-*N*-hydroxy succinimidyle ester and stirred at 4 °C for 12 h. After 12 h the solution was dialyzed using cellulose membrane (cut off molecular weight 12kD) in 10 mM ammonium bicarbonate buffer (4 x 500 mL). Finally the solution was lypholized to obtain fluorescein labeled trypsin in solid form.

Trypsin adsorption happens mainly at the mesoporous walls of the hollow sphere since the pore size of the sphere wall closely matches with the hydrodynamic size of the enzyme (3.7 nm and 3.8 nm). The inner cavity of the COF hollow spheres are macro-porous (0.5 µm- 3µm). Even though the enzymes are capable to enter in the macro-porous cavities of the hollow sphere, these hollow spherical cavities can't hold the enzymes due to the large difference in the relative size. From the confocal images of the of fluorescein labeled trypsin loaded COF **DhaTab**, we were able to understand that the spherical morphology of the COF **DhaTab** was retained after the enzyme loading process and the green fluorescence observed indicates that the enzyme loading happens at the sphere wall. For more detailed information about the special distribution of the immobilized_enzymes we have recorded the CLSM imaging of the *single* fluorescein labeled hollow sphere at different height along z axis. At the top cross sections, hollow nature of the COF-**DhaTab** can't be understood as it reaches only at the top of sphere wall. Upon moving to more depth, the cross section shows the hollow nature of the COF-**DhaTab** and also showcase the inner cavity is not fluorescent labeled.

5.4.6 *Determination of activity of trypsin*

Preparation of 2 mM BAPNA solution: 22 mg of BAPNA (Benzoyl-Arg *p*-nitroanilide) dissolved in 0.4 mL of DMSO and diluted to 25 mL by tris buffer (50 mM, pH 8).

Activity Determination: 1.5 mL of BAPNA solution (2 mM) was added to the residue containing encapsulated enzyme in a 2 mL eppendorf tube and rotated on a rotator at 30 rpm for 20 minutes. After minute solution was centrifuged and quickly washed with tris buffer (50 mM, pH 8) three times (1 x 1.5 mL and then 2 x 1 mL). Centrifugate and washings were collected together (total volume ~5 mL) and absorbance was noted at 405 nm. Trypsin encapsulated solid was used for the next cycle. The activity of the trypsin was calculated as micromoles of *p*-nitroaniline (PNA) formed per gram of trypsin per minute.

5.4.6 *Comparison of the relative activity of the immobilized enzymes with native trypsin enzyme.*

In two separate 2 mL eppendorf tube COF containing encapsulated enzyme and 15.5 µmol/g of trypsin was taken. 1.5 mL of BAPNA solution (2 mM) was added to each of the eppendorf tube and rotated on a rotator at 30 rpm for 30 minutes. After 30 minute solution was centrifuged and quickly from the eppendorf tube containing COF with encapsulated enzyme and washed with tris buffer (50 mM, pH 8) three times (1 x 1.5 mL and then 2 x 1 mL). Centrifugate and washings were collected together (total volume ~5 mL) and absorbance was noted at 405 nm. Eppendorf tube with 15.5 µmol/g of trypsin was diluted with 3.5 mL tris buffer and absorbance was noted at 405 nm. The activity of the trypsin was calculated as micromoles of para-nitroaniline (PNA) formed per gram of trypsin per minute.

The activity of the encapsulated trypsin = 56.5 mmol g^{-1} min^{-1}

The activity of the free trypsin = 93.82 mmol $g^{-1}min^{-1}$

Relative activity of the immobilized enzymes = 56.5 X 100/93.82= **60.62 %**

5.4.7 *Michaelis-Menten analysis*

Kinetic parameters of free trypsin enzyme and encapsulated enzyme were evaluated at 25 °C by varying BAPNA substrate concentration between 2 mM to 0.1 mM. For the free enzyme, initial reaction rate were determined by continuous mode, were as for the enzyme loaded COF, reaction rates were determined by using a discontinuous assay (Due to the scattering of the COF powder, base line in uv visible spectra shifts, as a result kinetics of the enzyme loaded COF can't be done in continuous assay). K_m and V_{max} were evaluated by plotting reaction velocity against substrate concentration. For the free enzyme (trypsin) kinetic parameters were calculated as V_{max}=2.237× 10^{-7}, K_m = 1.2 mM and K_{cat}= 1.15 s^{-1}. Kinetic parameters for trypsin loaded COF-**DhaTab** were calculated as V_{max}=9.7 ×10^{-7}, K_m = 0.43 mM and K_{cat}= 0.57 s^{-1}. It was found that the turn over number (K_{cat}) almost decreases to half value when trypsin got immobilized in to COF **DhaTab**.

NOTE: The results of this chapter have already been published in *Nat. Commun.* **2015,** *6,* 6786, with the title: "*Self-templated chemically stable hollow spherical covalent organic*

framework". These publications were the results from the group of Dr. Rahul Banerjee and his students Mr. Sharath Kandambeth, Digambar B. Shinde, Arjun Halder, from CSIR-National Chemical Laboratory, Pune, India. Dr. Sandeep Verma and his student V. Venkatesh (from Indian Institute of Technology, Kanpur) have performed the AFM analysis of the COF samples. Major work was contributed by Mr. Sharath Kandambeth with the help of the instrumental facilities of CSIR-National Chemical Laboratory. The manuscript was primarily written by Mr. Sharath Kandambeth under the guidance of Dr. Rahul Banerjee.

CHAPTER 6

Conclusions of all Chapters and Future Directive

6.1 Conclusions

The first chapter of the thesis includes the introduction of advanced porous crystalline frameworks specifically covalent organic framework (COFs), their synthetic development and important applications with a special emphasis on the chemistability issues of COF. COFs are generally synthesized by reversible reaction and the possibility of the reversible back reaction after the COF formation is responsible for the chemical instability of COFs. The reported methods to enhance the chemical stability of COF are thoroughly discussed in the initial introduction section. We have outlined the importance of intramolecular hydrogen bonding in COFs for enhancing the crystallinity, porosity and chemical stability of COFs. In the later part we have discussed about morphological diversity in COF. Literature reports about COF 2D- nano layer synthesis are also discussed.

In chapter 2, we have discussed about the solution for the chemical stability problem in COFs. For the first time, we could introduce a new protocol for the synthesis of highly acid and base stable crystalline covalent-organic frameworks. Chemically stable COFs were synthesized by a combination of reversible and irreversible reaction. A reversible Schiff base reaction happens initially to for an ordered crystalline COF, followed by an irreversible tautomerism which locks the framework structure in β-ketoenamine form. The irreversible nature of the tautomerism is responsible for the high chemical stability of the synthesized COFs. Both COFs (TpPa-1 and -2) display exceptional chemical resistance towards boiling water and acid treatment. The crystallinity and porosity of the treated COFs remain intact after prolonged water and acid treatments. The high chemical resistance of the β-ketoenamine COF makes them suitable for real life practical applications.

In the third chapter, we were able to introduce a new strategy of intramolecular hydrogen bonding as an extra tool to improve the crystallinity, porosity, and chemical stability in COFs. The intramolecular hydrogen bonding locks the phenyl ring rotation and

improves the COF layer planarity thus support efficient pi-pi stacking interaction between COF layers. Due to the improved pi-pi stacking interaction, intramolecular hydrogen bonded DhaTph COF display high crystallinity and porosity (S_{BET} = 1300m^2g^{-1}). We have also observed that the intramolecular hydrogen bonding also helps in enhancing the chemical stability of DhaTab. We have validated our results by removing this hydrogen bond using the methoxy analog DmaTph. Due to the lack of intramolecular hydrogen bonding interaction DmaTph display lower crystallinity, surface area and chemical stability. The H_2 uptake of DhaTph and DmaTph was found to be 171 cm^3g^{-1} and 78 cm^3g^{-1}, respectively, at 77 K and a pressure of 1 atm.

In the fourth chapter, we have designed and synthesized ionic guanidine based iCONs by Schiff base reaction. Judiciously designed iCONs were comprised of few thin layers, thanks to the intrinsic charge within the framework back bone and sandwiched anions in between the layers. Due to the intrinsic ionic character iCONs readily get exfoliated to 2D-nano sheets in presence of water. The synthesized iCONs displayed chemical stability and good antibacterial activity against both gram positive (S. aureus) and gram negative bacteria (E. coli). The electrostatic interactions between positively charged guanidine moieties iCONs and negatively charged phospholipid bilayer of bacterial membrane resulted in such antibacterial response. We were also able to incorporate iCONs to PSF membrane. This hybrid membrane also displayed good antimicrobial activity, indicating its potential as an antimicrobial coating.

In the fifth chapter, we for the first time report the hollow sphere morphology in COFs. We have used cost effective self template method for the synthesis of COF hollow spheres. The COF hollow sphere synthesis was performed by the Schiff base reaction between 1,3,5-tris (4-aminophenyl)benzene and 2,5-dihydroxyterephthalaldehyde. Up on detailed investigation it was understood that, an inside out Ostwald ripening is responsible for the hollow spherical morphology evolution in COF. The synthesized COF hollow spheres display high porosity (S_{BET}= 1500m^2g^{-1}) crystallinity and chemical stability which was a result of strong intramolecular hydrogen bonding interaction present in the system. The meso-porous walls of the hollow sphere COF was then further utilize for enzyme (trypsin) immobilization application. Trypsin loading in DhaTab hollow sphere was estimated to be 15.5 µmol g^{-1}.

6.2 Future directive

Developing covalent organic frameworks as self standing membranes.

Covalent organic frameworks (COFs) are new class organic porous framework materials, which possesses ordered pore channels in nano domain [6.1]. Even though COFs were widely applied in storage application such as gas, bio-molecules and drugs, the utilization of the ordered channels of COFs in separation application are scarcely achieved. The main reason behind this problem is the difficulty in fabricating COFs as self standing form. Complex problems such as insolubility of COF crystallites, chemical stability and synthetic huddles, prevent the fabrication of COF as self-standing membranes. Although, it had been predicted that the standalone COF membranes can solve world's most prominent challenges such as desalination of seawater [6.2], but, in reality, this has not yet been achieved. The attempts to fabricate COF crystallite to membranes using polymer binders often results in poor performance due to the covering effect of polymer chains. Thus in order to utilize the full potential of COFs ordered pore channels, designing a self-standing and flexible membrane which is exclusively derived from COF crystallites is essential. If the self standing form of the COF membrane is realized, it could show promises for various molecular separation applications.

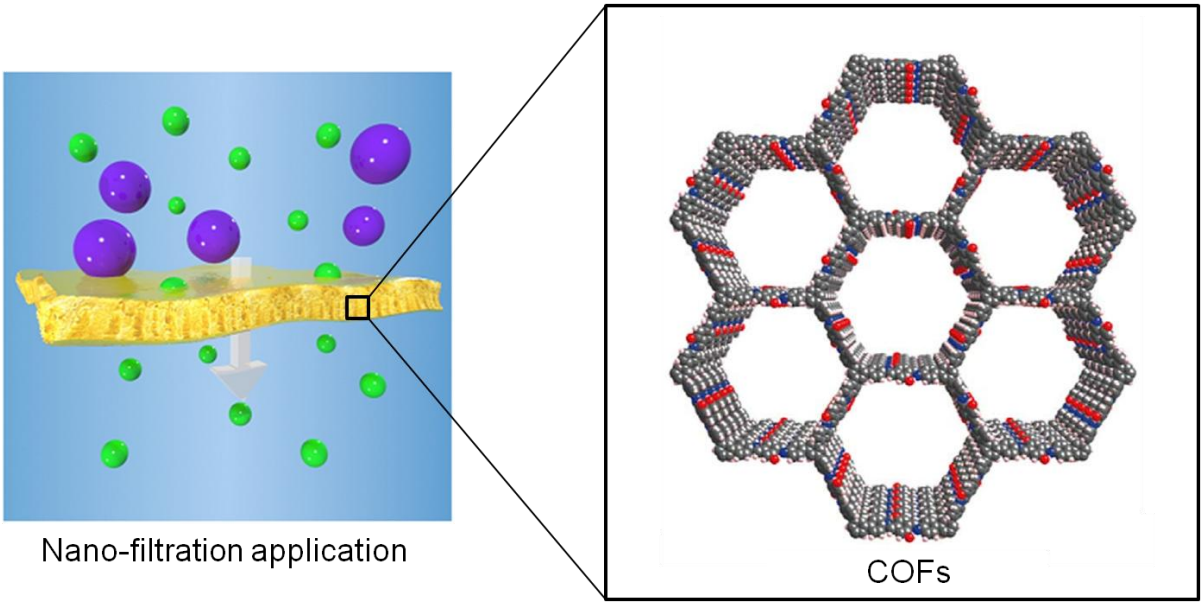

Figure 6.1. *Covalent organic framework membranes for nano-filtration applications.*[6.3]

REFERENCES

CHAPTER 1

[1.1] (a) D. Wu, F. Xu, B. Sun, R. Fu, H. He, K. Matyjaszewski, *Chem. Rev.*, **2012**, *112*, 3959. (b) G. M. Whitesides, E. E. Simanek, J. P. Mathias, C. T. Seto, D. Chin, M. Mammen, D. M. Gordon, *Acc. Chem. Res.*, **1995**, *28*, 37. (c) J. D. Wuest, *Chem. Commun.*, **2005**, *47*, 5830. (d) J. M. Zayed, N. Nouvel, U. Rauwald, O. A. Scherman, *Chem. Soc. Rev*., **2010**, *39*, 2806. (e) S. J. Rowan, S. J. Cantrill, G. R. L. Cousins, J. K. M. Sanders, J. F. Stoddart, *Angew. Chem., Int. Ed.*, **2002**, *41*, 898.

[1.2] K. Ishizaki, S. Komarneni, M. Nanko, *Porous Materials: Process, technology and applications.* Kluwer Academic, **1998**.

[1.3] (a) M. Eddaoudi, D. B. Moler, H. Li, B. Chen, T. M. Reinekee, M. O'Keeffe, O. M. Yaghi, *Acc. Chem. Res.*, **2001**, *34*, 319. (b) C. Janiak, *Angew. Chem., Int. Ed.*, **1997**, *36*, 1431. (c) A. J. Blake, N. R. Champness, P. Hubberstey, W.-S. Li, M. A. Withersby, M. Schroder, *Coord. Chem. Rev.*, **1999**, *183*, 117. (d) B. Kesanli, Y. Cui, M. Smith, E. Bittner, B. Bockrath, W. Lin, *Angew. Chem., Int. Ed.*, **2005**, *44*, 72. (e) S. Kitagawa, R. Kitaura, S. -I. Noro, *Angew. Chem., Int. Ed.*, **2004**, *43*, 2334. (f) G. Ferey, *Chem. Soc. Rev.* **2008**, *37*, 191. (g) B. Chen, S. Xiang, G. Qian, *Acc. Chem. Res.*, **2010**, *43*, 1115.

[1.4] (a) Y. Ma, W. Tong, H. Zhou, S. L Suib, *Microporous Mesoporous Mater.*, **2000**, *37*, 243. (b) S. Cavenati, C. A. Grande, A. E. Rodrigues, *J. Chem. Eng. Data*, **2004**, *49*, 1095. (c) J. Rouquerol, D. Avnir, C. W. Fairbridge, D. H. Everett, J. H. Haynes, N. Pernicone, J. D. F. Ramsay, K. S. W. Sing, K. K. Unger, *Pure and Applied Chemistry*, **1994**, *66*, 1739. (d) T. Sawaki, T. Dewa, Y. Aoyama, *J. Am. Chem. Soc*., **1998**, *120*, 8539. (e) R. E. Morris, P. S. Wheatley, *Angew. Chem., Int. Ed*., **2008**, *47*, 4966.

[1.5] (a) H. Huang, W. Zhang, X. Gan, C. Wang, L. Zhang, *Mater. Lett*., **2007**, *61*, 296. (b) A. B. K Ernst, R. Konenkamp, *Semicond. Sci. Technol*., **2003**, *18*, 475. (c) E. Grun, Z. Sternovsky, M. Horanyi, V. Hoxie, S. Robertson, J. Xi, S. Auer, M. Landgraf, F. Postberg, M. Price, R. Srama, N. Starkey, J. Hillier, I. Franchi, P. Tsou, A. Westphal, Z. Gainsforth, *Planetary and Space Science*, **2012**, *60*, 261.

[1.6] (a) J. Lee, J. Kim, T. Hyeon, *Adv. Mater.*, **2006**, *18*, 2073. (b) M. C. Orilall, U. Wiesner, *Chem. Soc. Rev.*, **2011**, *40*, 520. (c) Y. Zhou, Y. Kim, C. Jo, J. Lee, C. W. Lee, S. Yoon, *Chem. Commun.*, **2011**, *47*, 4944. (d) Y. Ishii, Y. Kanamori, T. Kawashita, I. Mukhopadhyay, S. Kawasaki, *J. Phys. Chem. Solids*, **2010**, *71*, 511. (e) L. Fu, H. Liu, H. Zhang, C. Li, T. Zhang, Y. Wu, H. Wu, *J. Power Sources*, **2006**, *159*, 219. (f) D.-H. Lee, J. -G. Park, K. Jin Choi, H. -J. Choi, D.-W. Kim, *Eur. J. Inorg. Chem.*, **2008**, *2008*, 878.

[1.7] (a) D. W. Breck, *Zeolite molecular sieves: structure, chemistry, and use*. Wiley: New York, **1974**. (b) C. S. Cundy, P. A. Cox, *Chem. Rev.*, **2003**, *103* , 663. (c) Z. Wang, J. Yu, R. Xu, *Chem. Soc. Rev*., **2012**, *41*, 1729. (d) J. Yu, R. Xu, *Acc. Chem. Res*., **2010**, *43*, 1195. (e) J. J. Pluth, J. V. Smith, *Am. Mineral*., **1990**, *75*, 501. (f) R. M. Barrer, P. J. Denny, *J. Chem. Soc.*, **1961**, *0*, 971. (g) A. F. Cronsted, *Akad. Handl*., **1756**, *17*, 20.

[1.8] F. Schuth, K. S. W. Sing, J. Weitkamp, editors. *Handbook of Porous Solids*. Wiley-VCH Verlag GmbH, **2002**.

[1.9] (a) M. Eddaoudi, D. B. Moler, H. Li, B. Chen, T. M. Reinekee, M. O'Keeffe, O. M. Yaghi, *Acc. Chem. Res.*, **2001**, *34*, 319. (b) C. Janiak, *Angew. Chem., Int. Ed.*, **1997**, *36*, 1431. (c) A. J. Blake, N. R. Champness, P. Hubberstey, W.-S. Li, M. A. Withersby, M. Schroder, *Coord. Chem. Rev.*, **1999**, *183*, 117. (d) O. M. Yaghi, G. Li, H. Li, *Nature*, **1995**, *378*, 703. (e) S. Kitagawa, R. Kitaura, S. -I. Noro, *Angew. Chem., Int. Ed.*, **2004**, *43*, 2334. (f) G. Ferey, *Chem. Soc. Rev.*, **2008**, *37*, 191. (g) B. Chen, S. Xiang, G. Qian, *Acc. Chem. Res.*, **2010**, *43*, 1115. (h) L. Ma, C. Abney, W. Lin, *Chem. Soc. Rev.*, **2009**, *38***,** 124. (i) Z. G. Gu, Y. P. Cai, H. C. Fang, Z. Y. Zhou, P. K. Thallapally, J. A. Tian, J. Liu, G. J. Exarhos, *Chem. Commun.*, **2010**, *46*, 5373. (j) B. Chen, M. Eddaoudi, S. T. Hyde, M. O'Keeffe, O. M. Yaghi, *Science*, **2001**, *291*, 1021. (k) P. Pachfule, Y. Chen, J. Jiang, R. Banerjee *J. Mater. Chem.*, **2011**, *21*, 17737. (l) J. W. Yoon, S. H. Jhung, Y. K. Hwang, S. M. Humphrey, P. T. Wood, J. -S. Chang, *Adv. Mater.*, **2007**, *19*, 1830. (m) K. L. Mulfort, O. K. Farha, C. D. Malliakas, M. G. Kanatzidis, J. T. Hupp, *Chem. Eur. J.*, **2010**, *16*, 276. (n) H. -S. Choi, M. P. Suh, *Angew. Chem*., **2009**, *121*, 6997. (o) X. Gu, Z.-H. Lu, Q. Xu, *Chem. Commun.*, **2010**, *46*, 7400. (p) S**.** -T. Zheng, J. T. Bu, Y. Li, T. Wu, F. Zuo, P. Feng, X. Bu. *J. Am. Chem. Soc.*, **2010**, *132*, 17062. (q) J. An, N. L. Rosi, *J. Am. Chem. Soc.*, **2010**,

132. 5578. (r) A. G. Wong-Foy, O. Lebel, A. J. Matzger, *J. Am. Chem. Soc.*, **2007**, *129*, 15740. (s) H. Chun, D. N. Dybtsev, H. Kim, K. Kim, *Chem. Eur. J.*, **2005**, *11*, 3521. (t) J. Rowsell, A. Millward, K. Park, O. Yaghi, *J. Am. Chem. Soc.*, **2004**, *126*, 5666.

[1.10] (a) Y. Li, R. T. Yang, *AIChE J.*, **2008**, *54*, 269. (b) Z. Liang, M. Marshall, A. L. Chaffee, *Energy Fuels*, **2009**, *23*, 2785. (c) F. Gul-E-Noor, B. Jee, A. Poppl, M. Hartmann, D. Himsl, M. Bertmer, *Phys. Chem. Chem. Phys*., **2011**, *13*, 7783. (d) N. C. Burtch, H. Jasuja, K. S. Walton, *Chem. Rev*., **2014**, *114*, 10575.

[1.11] (a) Y. Luo, B. Li, W. Wang, K. Wu, B. Tan, *Advanced Materials*, **2012**, *24*, 5703. (b) D. C. Wu, F. Xu, B. Sun, R. W. Fu, H. K. He, K. Matyjaszewski, *Chem. Rev.*, **2012**, *112*, 3959. (c) P. kaur, J. T. Hupp, S. T. Nguyen, *ACS Catal*., **2011**, *1*, 819. (d) Z. H. Xiang, D. P. Cao, *J. Mater. Chem. A*, **2013**, *1*, 2691.

[1.12] A. P. Cote, A. I. Benin, N. W. Ockwig, M. O'Keeffe, A. J. Matzger, O. M. Yaghi, *Science*, **2005**, *310*, 1166.

[1.13] P. A. Wright, *Microporous Framework Solids*, RSC Publishing, Cambridge, **2008**.

[1.14] S. T. Wilson, B. M. Lok, C. A. Messina, T. R. Cannan, E. M. Flanigen, *J. Am. Chem. Soc.*, **1982**, *104*, 1146.

[1.15] (a) Q. Huang, M. Ulutagay, P. A. Michener, S.-J. Hwu, *J. Am. Chem. Soc*., **1999**, *121*, 10323. (b) J. B. Parise, *Inorg. Chem*., **1985**, *24* , 4312. (c) T. E. Gier, G. D. Stucky, *Nature*, **1991**, *349*, 508.

[1.16] (a) U. Wingenfelder, C. Hansen, G. Furrer, R. Schulin, *Environ. Sci. Technol.*, **2005**, *39*, 4606. (b) N. Moreno, X. Querol, C. Ayora, C. F. Pereira, M. Janssen-Jurkovicová, *Environ. Sci. Technol*., **2001**, *35*, 3526. (c) A. Clearfield, *Chem. Rev.*, **1988**, *88* , 125.

[1.17] (a) Y. Cui, H. Xu, Y. Yue, Z. Guo, J. Yu, Z. Chen, J. Gao, Y. Yang, G. Qian, B. Chen, *J. Am. Chem. Soc*., **2012**, *134*, 3979. (b) A. M. Shultz, O. K. Farha, J. T. Hupp, S. T. Nguyen, *J. Am. Chem. Soc*., **2009**, *131*, 4204. (c) V. Stavila, R. K. Bhakta, T. M. Alam, E. H. Majzoub, M. D. Allendorf, *ACS Nano*, **2012**, *6*, 9807.

[1.18] (a) Y. Lee, J. Kim, W. Ahn, *Korean J. Chem. Eng*., **2013**, *30*, 1667. (b) A. Schneemann, V. Bon, I. Schwedler, I. Senkovska, S. Kaskel, R. A. Fischer, *Chem. Soc. Rev*., **2014**, *43*, 6062. (c) F. X. Coudert, *Chem. Mater*., **2015**, *27*, 1905.

[1.19] (a) H. Furukawa, K. E. Cordova, M. O'Keeffe, O. M. Yaghi, *Science*, **2013**, *341*, 6149. (b) R. J. Kupplera, D. J. Timmonsb, Q. –R. Fanga, J. –R. Lia, T. A. Makala, M. D. Younga, D. Yuana, D. Zhaoa, W. Zhuanga, H .-C. Zhou, *Coord. Chem. Rev.*, **2009**, *253*, 3042. (c) A. Morozan, F. Jaouen, *Energy Environ. Sci.*, **2012**, *5*, 9269, (d) A. U. Czaja, N. Trukhan, U. Müller, *Chem. Soc. Rev.*, **2009**, *38*, 1284. (e) U. Mueller, M. Schubert, F. Teich, H. Puetter, K. Schierle-Arndt, J. Pastré, *J. Mater. Chem.*, **2006**, *16*, 626.

[1.20] (a) Y. Luo, B. Li, W. Wang, K. Wu, B. Tan, *Advanced Materials*, **2012**, *24*, 5703. (b) T. Ben, S. L. Qiu, *Cryst Eng Comm*, **2013**, *15*, 17. (c) T. Ben, H. Ren, S. Q. Ma, D. P. Cao, J. H. Lan, X. F. Jing, W. C. Wang, J. Xu, F. Deng, J. M. Simmons, S. L. Qiu, G. S. Zhu, *Angew. Chem., Int. Ed*., **2009**, *48*, 9457. (d) S. Y. Ding, W. Wang, *Chem. Soc. Rev*., **2013**, *42*, 548. (e) P. M. Budd, B. S. Ghanem, S. Makhseed, N. B. McKeown, K. J. Msayib, C. E. Tattershall, *Chem. Commun*., **2004**, 230. (f) X. Feng, X. Ding, D. Jiang, *Chem. Soc. Rev*., **2012**, *41*, 6010.

[1.21] (a) G. Cheng, T. Hasell, A. Trewin, D. J. Adams, A. I. Cooper, *Angew. Chem., Int. Ed.*, **2012**, *51*, 12727. (b) L. Chen, Y. Honsho, S. Seki, D. Jiang, *J. Am. Chem. Soc*., **2010**, *132*, 6742. (c) J. X. Jiang, F. B. Su, A. Trewin, C. D. Wood, N. L. Campbell, H. J. Niu, C. Dickinson, A. Y. Ganin, M. J. Rosseinsky, Y. Z. Khimyak, A. I. Cooper, *Angew. Chem., Int. Ed*., **2007**, *46*, 8574. (d) J. X. Jiang, A. Trewin, D. J. Adams, A. I. Cooper, *Chem. Sci.*, **2011**, *2*, 1777. (e) Y. H. Xu, L. Chen, Z. Q. Guo, A. Nagai, D. Jiang, *J. Am. Chem. Soc*., **2011**, *133*, 17622. (f) S. W. Yuan, B. Dorney, D. White, S. Kirklin, P. Zapol, L. P. Yu, D. J. Liu, *Chem. Commun*., **2010**, *46*, 4547. (g) A. Li, R. F. Lu, Y. Wang, X. Wang, K. L. Han, W. Q. Deng, *Angew. Chem., Int. Ed.*, **2010**, *49*, 3330. (h) A. Li, H. X. Sun, D. Z. Tan, W. J. Fan, S. H. Wen, X. J. Qing, G. X. Li, S. Y. Li, W. Q. Deng, *Energy Environ. Sci*., **2011**, *4*, 2062. (i) Q. Chen, J. X. Wang, F. Yang, D. Zhou, N. Bian, X. J. Zhang, C. G. Yan, B. H. Han, *J. Mater. Chem*., **2011**, *21*, 13554. (j) Y. Kou, Y. Xu, Z. Guo, D. Jiang, *Angew. Chem., Int. Ed.*, **2011**, *50*, 8753. (k) A. I. Cooper, *Advanced Materials*, **2009**, *21*, 1291. (l) J.-X. Jiang, F. Su, A. Trewin, C. D. Wood, H. Niu, J. T. Jones, Y. Z. Khimyak, A. I. Cooper, *J. Am. Chem. Soc*., **2008**, *130*, 7710.

[1.22] (a) E. L. Spitler, W. R. Dichtel, *Nat. Chem*., **2010**, *2*, 672. (b) J. X. Jiang, A. I. Cooper, *Top. Curr. Chem*., **2010**, *293*, 1. (c) P. J. Waller, F. Gandara, O. M. Yaghi, *Acc. Chem. Res*., **2015**, *48*, 3053.

[1.23] H. M. El-Kaderi, J. R. Hunt, J. L. Mendoza-Cortes, A. P. Cote, R. E. Taylor, M. O'Keeffe, O. M. Yaghi, *Science*, **2007**, *316*, 268.

[1.24] E. L. Spitler, B. T. Koo, J. L. Novotney, J. W. Colson, F. J. Uribe-Romo, G. D. Gutierrez, P. Clancy, W. R. Dichtel, *J. Am. Chem. Soc*., **2011**, *133*, 19416.

[1.25] (a) A. P. Côté, H. M. El- Kaderi, , H. Furukawa, J. R. Hunt, O. M. Yaghi, *J. Am. Chem. Soc*., **2007**, *129*, 12914. (b) A. Nagai, Z. Guo, X. Feng, S. Jin, X. Chen, X. Ding, D. Jiang, *Nat. Commun*., **2011**, *2*, 536.

[1.26] (a) P. Kuhn, M. Antonietti, A. Thomas, *Angew. Chem., Int. Ed*., **2008**, *47*, 3450. (b) M. J. Bojdys, J. Jeromenok, A. Thomas, M. Antonietti, *Adv. Mater.*, **2010**, *22*, 2202. (c) R. Palkovits, M. Antonietti, P. Kuhn, A. Thomas, F. Schuth, *Angew. Chem., Int. Ed*., **2009**, *48*, 6909. (d) C. E. Chan-Thaw, A. Villa, L. Prati, A. Thomas, *Chem.–Eur. J.*, **2011**, *17*, 1052.

[1.27] (a) F. J. Uribe-Romo, J. R. Hunt, H. Furukawa, C. Klock, M. O'Keeffe, O. M. Yaghi, *J. Am. Chem. Soc.*, **2009**, *131*, 4570. (b) F. J. Uribe-Romo, C. J. Doonan, H. Furukawa, K. Oisaki, O. M. Yaghi, *J. Am. Chem. Soc*., **2011**, *133*, 11478. (c) S.-Y. Ding, J. Gao, Q. Wang, Y. Zhang, W.-G. Song, C.-Y. Su, W. Wang, *J. Am. Chem. Soc*., **2011**, *133*, 19816. (d) S. Wan, F. Gandara, A. Asano, H. Furukawa, A. Saeki, S. K. Dey, L. Liao, M. W. Ambrogio, Y. Y. Botros, X. Duan, S. Seki, J. F. Stoddart, O. M. Yaghi, *Chem. Mater*., **2011**, *23*, 4094.

[1.28] (a) L. M. Lanni, R. W. Tilford, M. Bharathy, J. J. Lavigne, *J. Am. Chem. Soc*., **2011**, *133*, 13975. (b) R. W. Tilford, W. R. Gemmill, H.-C. Z. Loye, J. J. Lavigne, *Chem. Mater*., **2006**, *18*, 5296. (c) B. M. Rambo, J. J. Lavigne, *Chem. Mater*., **2007**, *19*, 3732. (d) Y. Du, K. Mao, P. Kamakoti, P. Ravikovitch, C. Paur, S. Cundy, Q. Li, D. Calabro, *Chem. Commun*., **2012**, *48*, 4606. (e) R. W. Tilford, S. J. Mugavero III, P. J. Pellechia, J. J. Lavigne, *Adv. Mater*., **2008**, *20*, 2741.

[1.29] L. Chen, K. Furukawa, J. Gao, A. Nagai, T. Nakamura, Y. Dong, D. Jiang, *J. Am. Chem. Soc*., **2014**, *136*, 9806.

[1.30] S. Dalapati, M. Addicoat, S. Jin, T. Sakurai, J. Gao, H. Xu, S. Irle, S. Seki, D. Jiang, *Nat. Commun*., **2015**, *6*, 7786.

[1.31] T. Y. Zhou, S. Q. Xu, Q. Wen, Z. F. Pang, X. Zhao, *J. Am. Chem. Soc*., **2014**, *136*, 15885.

[1.32] (a) N. L. Campbell, R. Clowes, L. K. Ritchie, A. I. Cooper, *Chem. Mater*., **2009**, *21*, 204. (b) M. Dogru, A. Sonnauer, A. Gavryushin, P. Knochel, T. Bein, *Chem. Commun.*, **2011**, *47*, 1707.

[1.33] (a) N. A. A. Zwaneveld, R. Pawlak, M. Abel, D. Catalin, D. Gigmes, D. Bertin, L. Porte, *J. Am. Chem. Soc.*, **2008**, *130*, 6678. (b) J. W. Colson, A. R. Woll, A. Mukherjee, M. P. Levendorf, E. L. Spitler, V. B. Shields, M. G. Spencer, J. Park, W. R. Dichtel, *Science*, **2011**, *332*, 228.(c) X. H. Liu, C. Z. Guan, S. Y. Ding, W. Wang, H. J. Yan, D. Wang, L. J. Wan, *J. Am. Chem. Soc*., **2013**, *135*, 10470.

[1.34] (a) D. D. Medina, J. M. Rotter, Y. H. Hu, M. Dogru, V. Werner, F. Auras, J. T. Markiewicz, P. Knochel, T. Bein, *J. Am. Chem. Soc*., **2015**, *137*, 1016. (b) D. R. S. Miguel, A. Abrishamkar, J. A. R. Navarro, R. R. Trujillo, D. B. Amabilino, R M. Ballesté, F. Zamora, J. P. Luis, *Chem. Commun*., **2016**, *52*, 9212.

[1.35] B. P. Biswal, S. Chandra, S. Kandambeth, B. Lukose, T. Heine, R. Banerjee, *J. Am. Chem. Soc*., **2013**, *135*, 5328.

[1.35] (a) L. Schlapbach, A. Zuttel, *Nature*, **2001**, *414*, 353. (b) J. Graetz, *Chem. Soc. Rev*., **2009**, *38*, 73.

[1.36] M. P. Suh, H. J. Park, T. K. Prasad, D.-W. Lim, *Chem. Rev*., **2012**, *112*, 782.

[1.37] H. Furukawa, O. M. Yaghi, *J. Am. Chem. Soc*., **2009**, *131*, 8875.

[1.38] J.-T. Yu, Z. Chen, J. Sun, Z.-T. Huang, Q.-Y. Zheng, *J. Mater. Chem.*, **2012**, *22*, 5369.

[1.39] (a) E. Klontzas, E. Tylianakis, G. E. Froudakis, *J. Phys. Chem. C*, **2009**, *113*, 21253. (b) F. Li, J. Zhao, B. Johansson, L. Sun, *Int. J. Hydrogen Energy*, **2010**, *35*, 266.

[1.40] H. Furukawa, N. Ko, Y. B. Go, N. Aratani, S. B. Choi, E. Choi, A. O. Yazaydin, R. Q. Snurr, M. O'Keeffe, J. Kim, O. M. Yaghi, *Science*, **2010**, *329*, 424.

[1.41] K. Sumida, D. L. Rogow, J. A. Mason, T. M. McDonald, E. D. Bloch, Z. R. Herm, T.-H. Bae, J. R. Long, *Chem. Rev*., **2012**, *112*, 724.

[1.42] Y. J. Choi, J. H. Choi, K. M. Choi, J. K. Kang, *J. Mater. Chem*., **2011**, *21*, 1073.

[1.43] C. J. Doonan, D. J. Tranchemontagne, T. G. Glover, J. R. Hunt, O. M. Yaghi, *Nat. Chem*., **2010**, *2*, 235.

[1.44] (a) S. Y. Ding, J. Gao, Q. Wang, Y. Zhang, W. G. Song, C. Y. Su, W. Wang, *J. Am. Chem. Soc*., **2011**, *133*, 19816. (b) D. B. Shinde, S. Kandambeth, P. Pachfule, R. R. Kumar R. Banerjee, *Chem. Commun*., **2015**, *51*, 310. (c) P. Pachfule, S. Kandmabeth, A. Mallick, R. Banerjee, *Chem. Commun*., **2015**, *51*, 11717. (d) P. Pachfule, S. Kandambeth, D. Diaz Diaz, R. Banerjee, *Chem. Commun*., **2014**, *50*, 3169.

[1.45] (a) S. Wan, J. Guo, J. Kim, H. Ihee, D. Jiang, *Angew. Chem.,Int. Ed*., **2009**, *48*, 5439. (b) S. Wan, J. Guo, J. Kim, H. Ihee, D. Jiang, *Angew. Chem.,Int. Ed*., **2008**, *47*, 8826. (c) X. Feng, L. Liu, Y. Honsho, A. Saeki, S. Seki, S. Irle, Y. Dong, A. Nagai, D. Jiang, *Angew. Chem., Int. Ed*., **2012**, *51*, 2618. (d) X. S. Ding, J. Guo, X. Feng, Y. Honsho, J. D. Guo, S. Seki, P. Maitarad, A. Saeki, S. Nagase, D. Jiang, *Angew. Chem., Int. Ed*., **2011**, *50*, 1289. (e) X. Feng, L. Chen, Y. Honsho, O. Saengsawang, L. Liu, L. Wang, A. Saeki, S. Irle, S. Seki, Y. Dong, D. Jiang, *Adv.Mater*., **2012**, *24*, 3026.

[1.46] (a) C. R. DeBlase, K. E. Silberstein, T. T. Truong, H. D. Abruna,W. R. Dichtel, *J. Am. Chem. Soc*., **2013**, *135*, 16821. (b) C. R. DeBlase, K. Hernandez-Burgos, K. E. Silberstein, G. G. Rodriguez-Calero, R. P. Bisbey, H. D. Abruna, W. R. Dichtel, *ACS Nano*, **2015**, *9*, 3178. (c) F. Xu, H. Xu, D. Wu, Y. Wu, H. Liu, C. Gu, R. Fu, D. Jiang Chen, *Angew. Chem Int. Ed*., **2015**, *54*, 6814.

[1.47] (a) H. Lu, C. Wang, J. Chen, R. Ge, W. Leng, B. Dong, J. Huang, Y. Gao, *Chem. Commun*., **2015**, *51*, 15562. (b) B. P. Biswal, H. D. Chaudhari, R. Banerjee, U. K. Kharul, *Chem. Eur. J*., **2016**, *22*, 4695. (c) L. C. Lin, J. Choi, J. C. Grossman, *Chem. Commun*., **2015**, *51*,14921.

[1.48] Q. Fang, J. Wang, S. Gu, R. B. Kaspar, Z. Zhuang, J. Zheng, H. Guo, S. Qiu, Y. Yan, *J. Am. Chem. Soc*., **2015**, *137*, 8352.

[1.49] X. Chen, M. Addicoat, S. Irle, A. Nagai, D. Jiang, *J. Am.Chem. Soc*., **2013**, *135*, 546.

[1.50] S. Chandra, S. Kandambeth, B. P. Biswal, B. Lukose, S. M. Kunjir, M. Chaudhary, R. Babarao, T. Heine, R. Banerjee, *J. Am. Chem. Soc*., **2013**, *135*, 17853.

[1.51] D. N. Bunck, W. R. Dichtel, *J. Am. Chem. Soc*., **2013**, *135*, 14952.

[1.52] W. Huang, Y. Jiang, X. Li, X. Li, J. Wang, Q. Wu, X. Liu, *ACS Appl. Mater*. Interfaces, **2013**, *5*, 8845.

[1.53] X. W. Lou, L. A. Archer, Z. C. Yang, *Adv. Mater*., **2008**, *20*, 3987.

CHAPTER 2

[2.1] (a) X. Feng, X. S. Ding, D. L. Jiang, *Chem. Soc. Rev.*, **2012**, *41*, 6010. (b) S. Y. Ding, W. Wang, *Chem. Soc. Rev*., **2013**, *42*, 548.

[2.2] H. Furukawa, O. M. Yaghi, *J. Am. Chem. Soc*., **2009**, *131*, 8875.

[2.3] (a) H. Lu, C. Wang, J. Chen, R. Ge, W. Leng, B. Dong, J. Huang, Y. Gao, *Chem. Commun*., **2015**, *51*, 15562. (b) B. P. Biswal, H. D. Chaudhari, R. Banerjee, U. K. Kharul, *Chem. Eur. J*., **2016**, *22*, 4695. (c) L. C. Lin, J. Choi, J. C. Grossman, *Chem. Commun*., **2015**, *51*,14921.

[2.4] (a) S. Y. Ding, J. Gao, Q. Wang, Y. Zhang, W. G. Song, C. Y. Su, W. Wang, *J. Am. Chem. Soc*., **2011**, *133*, 19816. (b) D. B. Shinde, S. Kandambeth, P. Pachfule, R. R. Kumar, R. Banerjee, *Chem. Commun*., **2015**, *51*, 310. (c) P. Pachfule, S. Kandmabeth, A. Mallick, R. Banerjee, *Chem. Commun*., **2015**, *51*, 11717. (d) P. Pachfule, S. Kandambeth, D. Diaz Diaz, R. Banerjee, *Chem. Commun*., **2014**, *50*, 3169.

[2.5] Q. Fang, J. Wang, S. Gu, R. B. Kaspar, Z. Zhuang, J. Zheng, H. Guo, S. Qiu, Y. Yan, *J. Am. Chem. Soc*., **2015**, *137*, 8352.

[2.6] (a) S. Wan, J. Guo, J. Kim, H. Ihee, D. Jiang, *Angew. Chem.,Int. Ed*., **2009**, *48*, 5439. (b) S. Wan, J. Guo, J. Kim, H. Ihee, D. Jiang, *Angew. Chem., Int. Ed*., **2008**, *47*, 8826. (c) X. Feng, L. Liu, Y. Honsho, A. Saeki, S. Seki, S. Irle, Y. Dong, A. Nagai, D. Jiang, *Angew. Chem., Int. Ed*., **2012**, *51*, 2618. (d) X. S. Ding, J. Guo, X. Feng, Y. Honsho, J. D. Guo, S. Seki, P. Maitarad, A. Saeki, S. Nagase, D. Jiang, *Angew. Chem., Int. Ed*., **2011**, *50*, 1289.

[2.7] (a) L. M. Lanni, R. W. Tilford, M. Bharathy, J. J. Lavigne, *J. Am. Chem. Soc*., **2011**, *133*, 13975. (b) B. M. Rambo, J. J. Lavigne, *Chem. Mater*., **2007**, *19*, 3732. (d) Y. Du, K. Mao, P. Kamakoti, P. Ravikovitch, C. Paur, S. Cundy, Q. Li, D. Calabro, *Chem. Commun*., **2012**, *48*, 4606.

[2.8] E. L. Spitler, W. R. Dichtel, *Nat. Chem*., **2010**, *2*, 672.

[2.9] H. M. El-Kaderi, J. R. Hunt, J. L. Mendoza-Cortes, A. P. Cote, R. E. Taylor, M. O'Keeffe, O. M. Yaghi, *Science*, **2007**, *316*, 268.

[2.10] (a) Côté, A. P., El- Kaderi, H. M., Furukawa, H., Hunt, J. R. & Yaghi, O. M. *J. Am. Chem. Soc*., **2007**, *129*, 12914. (b) A. Nagai, Z. Guo, X. Feng, S. Jin, X. Chen, X. Ding, D. Jiang, *Nat. Commun*., **2011**, *2*, 536.

[2.11] M. E. Belowicha, J. F. Stoddart, *Chem. Soc. Rev*., **2012**, *41*, 2003.

[2.12] J. H. Chong, M. Sauer, B. O. Patrick, M. MacLachlan, *Org. Lett*., **2003**, *5*, 3823.

CHAPTER 3

[3.1] E. L. Spitler, W. R. Dichtel, *Nat. Chem*., **2010**, *2*, 672.

[3.2] (a) X. Feng, X. S. Ding, D. L. Jiang, *Chem. Soc. Rev.*, **2012**, *41*, 6010, (b) S. Y. Ding, W. Wang, *Chem. Soc. Rev*., **2013**, *42*, 548.

[3.3] (a) G. Cheng, T. Hasell, A. Trewin, D. J. Adams, A. I. Cooper, *Angew. Chem., Int. Ed.*, **2012**, *51*, 12727. (b) L. Chen, Y. Honsho, S. Seki, D. Jiang, *J. Am. Chem. Soc*., **2010**, *132*, 6742. (c) J. X. Jiang, F. B. Su, A. Trewin, C. D. Wood, N. L. Campbell, H. J. Niu, C. Dickinson, A. Y. Ganin, M. J. Rosseinsky, Y. Z. Khimyak, A. I. Cooper, *Angew.Chem., Int. Ed*., **2007**, *46*, 8574. (d) J. X. Jiang, A. Trewin, D. J. Adams, A. I. Cooper, *Chem. Sci.*, **2011**, *2*, 1777. (e) Y. H. Xu, L. Chen, Z. Q. Guo, A. Nagai, D. Jiang, *J. Am. Chem. Soc*., **2011**, *133*, 17622.

[3.4] (a) L. M. Lanni, R. W. Tilford, M. Bharathy, J. J. Lavigne, *J. Am. Chem. Soc*., **2011**, *133*, 13975. (b) B. M. Rambo, J. J. Lavigne, *Chem. Mater*., **2007**, *19*, 3732. (c) Y. Du, K. Mao, P. Kamakoti, P. Ravikovitch, C. Paur, S. Cundy, Q. Li, D. Calabro, C*hem. Commun*., **2012**, *48*, 4606.

[3.5] S. Kandambeth, A. Mallick, B. Lukose, M. V. Mane, T. Heine, R. Banerjee, *J. Am. Chem. Soc.*, **2012**, *134*, 19524.

[3.6] (a) L. Chen, K. Furukawa, J. Gao, A. Nagai, T. Nakamura, Y. Dong, D. Jiang, *J. Am. Chem. Soc*., **2014**, *136*, 9806. (b) S. Wan, F. Gandara, A. Asano, H. Furukawa, A. Saeki, S. K. Dey, L. Liao, M. W. Ambrogio, Y. Y. Botros, X. Duan, S. Seki, J. F. Stoddart, O. M. Yaghi, *Chem. Mater*., **2011**, *23*, 4094.

[3.7] X.-S. Wang, J. Liu, J. M. Bonefont, D. -Q. Yuan, P. K. Thallapally, S. Ma, *Chem. Commun*., **2013**, *49*, 1533.

[3.8] (a) G. R. Desiraju, T. Steiner, *The Weak Hydrogen Bond in Structural Chemistry and Biology*, Oxford University Press, Oxford, **1999**. (b) A. Kovcs, A. Szab, I. Hargittai, *Acc. Chem. Res.*, **2002**, *35*, 887.

[3.9] T. Kretz, J. W. Bats, H. W. Lerner, M. Z. Wagner, *Naturforsch*., **2007**, *62b*, 66.

[3.10] C. E. Anderson, S. I. Vagin, W. Xia, H. Jin, B. Rieger, *Macromolecules*, **2012**, *45*, 6840.

CHAPTER 4

[4.1] (a) A. K. Geim, K. S. Novoselov, *Nature Mater*., **2007**, *6*, 183. (b) G. R. Whittell, I. Manners, *Angew. Chem.*, **2011**, *123*, 10470. (c) Y. Liu , X. Dong, P. Chen, *Chem. Soc. Rev*., **2012**, *41*, 2283.

[4.2] (a) X. Feng, X. S. Ding, D. L. Jiang, *Chem. Soc. Rev.*, **2012**, *41*, 6010, (b) S. Y. Ding, W. Wang, *Chem. Soc. Rev*., **2013**, *42*, 548. (c) E. L. Spitler, W. R. Dichtel, *Nature. Chem*., **2010**, *2*, 672.

[4.3] (a) D. N. Bunck, W. R. Dichtel, *J. Am. Chem. Soc*., **2013**, *135*, 14952. (b) S. Chandra, S. Kandambeth, B. P. Biswal, B. Lukose, S. M. Kunjir, M. Chaudhary, R. Babarao, T. Heine, R. Banerjee, *J. Am. Chem. Soc*., **2013**, *135*, 17853. (c) I. Berlanga, M. L. Ruiz-Gonzalez, J. M. Gonzalez-Calbet, J. L. G. Fierro, R. Mas-Balleste, F. Zamora, *Small*, **2011**, *7*, 1207. (d) I. Berlanga, R. M. Balleste, F. Zamora, *Chem. Commun*., **2012**, *48*, 7976. (e) T.-Y. Zhou, F. Lin, Z. T. Li, X. Zhao, *Macromolecules*, **2013**, *46*, 7745. (f) X. H. Liu, Y. P. Mo, J. Y. Yue, Q. N. Zheng, H. J. Yan, D. Wang, L. –J. Wan, *Small*, **2014**, *10*, 4934. (g) G. Das, B. P. Biswal, S. Kandambeth, V. Venkatesh, G. Kaur, M. Addicoat, T. Heine, S. Verma, R. Banerjee, *Chem. Sci.*, **2015**, *6*, 3931.

[4.4] (a) L. M. Lanni, R. W. Tilford, M. Bharathy, J. J. Lavigne, *J. Am. Chem. Soc*., **2011**, *133*, 13975. (b) B. M. Rambo, J. J. Lavigne, *Chem. Mater*., **2007**, *19*, 3732. (c) Y. Du, K. Mao, P. Kamakoti, P. Ravikovitch, C. Paur, S. Cundy, Q. Li, D. Calabro, *Chem. Commun*., **2012**, *48*, 4606.

[4.5] L. Stegbauer, K. Schwinghammer, B. V. Lotsch, *Chem. Sci*., **2014**, *5*, 2789.

[4.6] (a) K. Baek, G. Yun, Y. Kim, D. Kim, R. Hota, I. Hwang, D. Xu, Y. H. Ko, G. H. Gu, J. H. Suh, C. G. Park, B. J. Sung, K. Kim, *J. Am. Chem. Soc.*, **2013**, *135*, 6523. (b) P. Payamyar, K. Kaja, C. Ruiz-Vergas, A. Stemmer, D. J. Murray, C. J. Johnson, B. T. King, F. Schiffmann, J. V. Vondele, A. Renn, S. Götzinger, P. Ceroni, A. Schütz, L.-T. Lee, Z. Zheng, J. Sakamoto, A. D. Schülter, *Adv. Mater.*, **2014**, *26*, 2052.

[4.7] S. Ravula, S. N. Baker, G. Kamath, G. A. Baker, *Nanoscale*, **2015**, ***7***, 4338.

[4.8] X. Zou, L. Zhang, Z. Wang, Y. Luo, *J. Am. Chem. Soc*., **2016**, *138*, 2064.

[4.9] (a) J. Budhathoki- Uprety, L. L. Peng, C. Melander, B. M. Novak, *ACS Macro Lett.*, **2012**, *1*, 370. (b) L. Qian, H. Xiao, G. Zhao, B. He, *ACS Appl. Mater. Interfaces*, **2011**, *3*, 1895. (c) J. H. Yim, M. S. Fleischman, V. Rodriguez-Santiago, L. T. Piehlar, A. A. Williams, J. L. Leadore, D. D. Pappas, *ACS Appl. Mater. Interfaces*, **2013**, *5*, 11836.

[4.10] (a) Y. –H. Gong, F. Miomandre, R. Méallet-Renault, S. Badré, L. Galmiche, J. Tang, P. Audebert, G. Clavier, *Eur. J. Org. Chem.*, **2009**, *234*, 6121. (b) I. M. Müller, R Robson, *Angew. Chem. Int. Ed.*, **2000**, *39*, 4357. (b) I. M. Müller, D. Möller, K. Föcker, *Chem. Eur. J.*, **2005**, *11*, 3318.

CHAPTER 5

[5.1] (a) E. L. Spitler, W. R. Dichtel, *Nat. Chem*., **2010**, *2*, 672. (b) X. H. Liu, C. Z. Guan, S. Y. Ding, W. Wang, H. J. Yan, D. Wang, L. J. Wan, *J. Am. Chem. Soc*., **2013**, *135*, 10470.

[5.2] (a) B. P. Biswal, S. Chandra, S. Kandambeth, B. Lukose, T. Heine, R. Banerjee, *J. Am. Chem. Soc.*, **2013**, *135*, 5328.

[5.3] S. Wan, J. Guo, J. Kim, H. Ihee, D. Jiang, *Angew. Chem.,Int. Ed*., **2008**, *47*, 8826.

[5.4] S. Wan, J. Guo, J. Kim, H. Ihee, D. Jiang, *Angew. Chem.,Int. Ed*., **2009**, *48*, 5439.

[5.5] E. L. Spitler, W. R. Dichtel, *Nat. Chem*., **2010**, 2, 672.

[5.6] W. Huang, Y. Jiang, X. Li, X. Li, J. Wang, Q. Wu, X. Liu, *ACS Appl. Mater*. Interfaces, **2013**, *5*, 8845.

[5.7] S. Kandambeth, A. Mallick, B. Lukose, M. V. Mane, T. Heine, R. Banerjee, *J. Am. Chem. Soc*., **2012**, *134*, 19524.

[5.8] (a) S. Wan, J. Guo, J. Kim, H. Ihee, D. Jiang, *Angew. Chem.,Int. Ed*., **2009**, *48*, 5439. (b) S. Wan, J. Guo, J. Kim, H. Ihee, D. Jiang, *Angew. Chem.,Int. Ed*., **2008**, *47*, 8826. (c) X. Feng, L. Liu, Y. Honsho, A. Saeki, S. Seki, S. Irle, Y. Dong, A. Nagai, D. Jiang, *Angew. Chem., Int. Ed*., **2012**, *51*, 2618. (d) X. S. Ding, J. Guo, X. Feng, Y. Honsho, J. D. Guo, S. Seki, P. Maitarad, A. Saeki, S. Nagase, D. Jiang, *Angew. Chem., Int. Ed*., **2011**, *50*, 1289. (e) X. Feng, L. Chen, Y. Honsho, O. Saengsawang, L. Liu, L. Wang, A. Saeki, S. Irle, S. Seki, Y. Dong, D. Jiang, *Adv. Mater*., **2012**, *24*, 3026.

[5.9] X. W. Lou, L. A. Archer, Z. C. Yang, *Adv. Mater*., **2008**, *20*, 3987.

[5.10] Q. Fang, J. Wang, S. Gu, R. B. Kaspar, Z. Zhuang, J. Zheng, H. Guo, S. Qiu, Y. Yan, *J. Am. Chem. Soc*., **2015**, *137*, 8352.

[5.11] (a) C. R. DeBlase, K. E. Silberstein, T. T. Truong, H. D. Abruna,W. R. Dichtel, *J. Am. Chem. Soc*., **2013**, *135*, 16821. (b) C. R. DeBlase, K. Hernandez-Burgos, K. E. Silberstein, G. G. Rodriguez-Calero, R. P. Bisbey, H. D. Abruna, W. R. Dichtel, *ACS Nano*, **2015**, *9*, 3178.

[5.12] (a) S. Y. Ding, J. Gao, Q. Wang, Y. Zhang,W. G. Song, C. Y. Su, W. Wang, *J. Am. Chem. Soc*., **2011**, *133*, 19816. (b) D. B. Shinde, S. Kandambeth, P. Pachfule, R. R. Kumar, R. Banerjee, *Chem. Commun*., **2015**, *51*, 310.

[5.13] T. Y. Zhou, F. Lin, Z.-T. Li, X. Zhao, *Macromolecules*, **2013**, *46*, 7745.

[5.14] (a) B. Malvi, S. Sen Gupta, *Chem. Commun*., **2012**, *48*, 7853. (b) C. H. Lei, Y. S. Shin, J. Liu, E. J. Ackerman, *J. Am. Chem. Soc*., **2002**, *124*, 11242. (c) A. Vinu, Murugesan, V. O. Tangermann, M. Hartmann, *Chem. Mater*., **2004**, *16*, 3056.

[5.15] T. Kretz, J. W. Bats, H. W. Lerner, M. Z. Wagner, *Naturforsch*., **2007**, *62b*, 66.

[6.1] (a) X. Feng, X. S. Ding, D. L. Jiang, *Chem. Soc. Rev*., **2012**, *41*, 6010. (b) S. Y. Ding, W. Wang, *Chem. Soc. Rev*., **2013**, *42*, 548.

[6.2] L. C. Lin, J. Choi, J. C. Grossman, *Chem. Commun*., **2015**, *51*,14921.

[6.3] P. Marchetti, M. F. Jimenez-Solomon, G. Szekely, A. G. Livingston, *Chem. Rev*., **2014**, *114*, 10735.

ABOUT THE AUTHOR

Mr. Sharath Kandambeth, son of Ganeshan Arayambeth Mangool and Rasija Kandambeth, was born in Chirakkal village of Kannur district, Kerala, India, in 1989. He did his schooling from Pallikunnu higher secondary school, Kannur (2004) and higher secondary education from Pappinisseri panchayath higher secondary school (2006). He has completed his B.Sc. (Chemistry) from Sree narayana guru college, Kannur (2009). Then he moved to Department of Applied Chemistry, Cochin University, Kochi, Kerala to pursue his M.Sc. (Applied Chemistry). After qualifying all India CSIR-UGC National Eligibility Test (NET-JRF) examination, he joined Physical and Materials Chemistry Division, CSIR-National Chemical Laboratory, Pune, India to pursue his Ph.D. degree in July 2011 under the guidance of Prof. Dr. Rahul Banerjee. He has received the research fellowship (JRF and SRF) from Council of Scientific and Industrial Research (CSIR), New Delhi, India for the period of July 2011 - June 2016 to carry out the Ph.D. thesis work.

LIST OF PUBLICATIONS

1. ***Sharath Kandambeth***, *V. Venkatesh, Digambar B. Shinde, Sushma Kumari, Arjun Halder, Sandeep Verma, Rahul Banerjee*, Self-templated chemically stable hollow spherical covalent organic framework.* ***Nat. Commun. 2015, 6, 6786****.*

2. ***Sharath Kandambeth****, Digambar Balaji Shinde, Manas K. Panda, Binit Lukose, Thomas Heine and Rahul Banerjee "Enhancement of Chemical Stability and Crystallinity in Porphyrin Containing Covalent Organic Frameworks using Intra-molecular Hydrogen Bonding".* ***Angew. Chem. Int. Ed., 2013, 52, 13052–13056.***

3. ***Sharath Kandambeth****, Arijit Mallick, Binit Lukose, Manoj V. Mane, Thomas Heine, and Rahul Banerjee* "Construction of Crystalline 2D Covalent Organic Frameworks with Remarkable Chemical (Acid/Base) Stability via a Combined Reversible and Irreversible Route"* ***J. Am. Chem. Soc., 2012****, 134, 19524−19527.*

4. *Shouvik Mitra,* ***Sharath Kandambeth****, Bishnu P. Biswal, Abdul Khayum M., Chandan Kumar Choudhury, Mihir Mehta, Gagandeep Kaur, Subhrashis Banerjee, Asmita A. Prabhune, Sandeep Verma, Sudip Roy, Ulhas K. Kharul, Rahul Banerjee.* " Self-Exfoliated Guanidnium-Based Ionic Covalent Organic Nanosheets (iCONs)."* ***J. Am. Chem. Soc., 2016, 138, 2823-2828.***

5. *Suman Chandra,* ***Sharath Kandambeth****, Bishnu P. Biswal, Binit Lukose, Shrikant M. Kunjir, Minakshi Chaudhary, Ravichandar Babarao, Thomas Heine and Rahul Banerjee*, "Chemically Stable Multi-layered Covalent Organic Nanosheets from Covalent Organic Frameworks via Mechanical Delamination".* ***J. Am. Chem. Soc., 2013, 135, 17853–17861****.*

6. *Bishnu P. Biswal, Suman Chandra,* ***Sharath Kandambeth****, Binit Lukose, Thomas Heine and Rahul Banerjee* "Mechanochemical Synthesis of Chemically Stable Isoreticular Covalent Organic Frameworks".* ***J. Am. Chem. Soc., 2013, 135 , 5328–5331.***

7. *Suman Chandra, Tanay Kundu,* ***Sharath Kandambeth****, Ravichandar BabaRao, Yogesh Marathe, Shrikant M. Kunjir and Rahul Banerjee*, "Phosphoric acid Loaded Azo (-N=N-) based Covalent Organic Framework for Proton Conduction."* ***J. Am. Chem. Soc., 2014, 136, 6570–6573.***

8. *Gobinda Das, Bishnu P. Biswal,* ***Sharath Kandambeth****, V. Venkatesh, Gagandeep Kaur, Matthew Addicoat, Thomas Heine, Sandeep Verma, Rahul Banerjee*,Chemical Sensing in Two Dimensional Porous Covalent Organic Nanosheets.* ***Chem. Sci., 2015, 6, 3931-3939.***

9. *Pradip Pachfule, **Sharath Kandambeth**, David Díaz Díaz, and Rahul Banerjee* "Highly Stable Covalent Organic Framework-Au Nanoparticles Hybrids for Enhanced Activity for Nitrophenol Reduction"* ***Chem. Commun., 2014, 50, 3169-3172.***

10. *Digambar Balaji Shinde, **Sharath Kandambeth,** Pradip Pachfule, Raya Rahul Kumar and Rahul Banerjee*, Bifunctional Covalent Organic Frameworks with Two Dimensional Organocatalytic Micropores, **Chem Commun.**, **2014, 50, 310 - 313**.*

11. *Gobinda Das, Digambar Balaji Shinde, **Sharath Kandambeth**, Bishnu P. Biswal, and Rahul Banerjee*. Mechanosynthesis of Imine, β-Ketoenamine, and Hydrogen-Bonded Imine-Linked Covalent Organic Frameworks using Liquid- Assisted Grinding. **Chem Commun.**, **2014, 50, 12615-12618.***

12. *Pradip Pachfule, **Sharath Kandambeth**, Arijit Mallick, Rahul Banerjee, Hollow Tubular Porous Covalent Organic Framework (COF) Nanostructures, **Chem. Commun**., **2015, 51, 11717-11720.***

13. *Pradip Pachfule, Vishal M. Dhavale, **Sharath Kandambeth**, Sreekumar Kurungot* and Rahul Banerjee* "Porous Organic Framework Templated Nitrogen Rich Porous Carbon as Proficient Electrocatalyst than Pt/C for the Electrochemical Oxygen Reduction Activity". **Chem. Eur. J. 2013, 19, 974–980**.*

14. *Pradip Pachfule, Manas K. Panda, **Sharath Kandambeth**, S. M. Shivaprasad, David Díaz Díaz and Rahul Banerjee* "Multifunctional and Robust Covalent Organic Framework- Nanoparticles Hybrids." **J. Mater. Chem. A**, **2014**, **2**, **7944-7952.***

15. *Bishnu P. Biswal, **Sharath Kandambeth**, Suman Chandra, Digambar Balaji Shinde, Saibal Bera, Suvendu Karak, Bikash Garai, Ulhas K. Kharul, Rahul Banerjee*." Pore Surface Engineering in Porous, Chemically Stable Covalent Organic Frameworks for Water Adsorption. **J. Mater Chem. A, 2015, 3, 23664-23669.***

16. *Digambar Balaji Shinde, Harshitha Barike Aiyappa, Mohitosh Bhadra, Bishnu P. Biswal, Pritish Wadge, **Sharath Kandambeth**, Bikash Garai, Tanay Kundu, Sreekumar Kurungot, Rahul Banerjee*. "Mechanochemically Synthesized Covalent Organic Framework as Proton conducting Solid Electrolyte." **J. Mater Chem. A, 2016, 4, 2682-2690.***

17. ***Sharath Kandambeth**, Bishnu P. Biswal, Harshal D. Chaudhari, Kanhu Charan, Shebeeb Kunjattu H., Shouvik Mitra, Suvendu Karak, Anuja Das, Rabibrata*

Mukherjee, Ulhas K. Kharul and Rahul Banerjee. "Selective Molecular Sieving in Self-standing Porous Covalent Organic Framework Membranes." **Adv. Mater**., **2016**, DOI: 10.1002/adma.201603945.*

LIST OF PATENTS

1. Rahul Banerjee, **Sharath Kandambeth**, Suman Chandra, "*Chemically stable porous crystalline framework for gas purification and bio-application"* Publication number: EP2906565 A1 (Also published as US20150266885, WO2014057504A1).
2. Rahul Banerjee, **Sharath Kandambeth** "*Porphyrin containing covalent organic frameworks and process for the preparation thereof*" Publication number: WO2014203283 A4.
3. Rahul Banerjee, Suman Chandra, Tanay Kundu, **Sharath Kandambeth** "*Phosphoric Acid Loaded Covalent Organic Framework And A Process For The Preparation Thereof*" Publication number: US20150299147 A1.
4. Rahul Banerjee, Ulhas K. Kharul, **Sharath Kandambeth**, Bishnu P. Biswal, Harshal D. Chaudhari, Suvendu Karak *"Self Standing Crystalline, Porous Covalent Organic Membranes for Molecular Separation*" Provisional Filing No. 201611009671, Filing Date: 21th Mar. **2016**.

CONFERENCES AND PRESENTATIONS

1. Presented poster in "*9th CRSI-RSC and CRSI-NSC-17 symposia*" **2015**, Pune.
2. Presented poster in *International Conference on* "*Structural Chemistry of Molecules and Materials (SCOMM)*" **2014**, Kolkata.